Leibniz-Institut
für Festkörper- und
Werkstoffforschung
Dresden

Annual Report 2011

Contents

Flashback to 2011

2011 was the 20th year of the existence of the IFW Dresden. Like a human being at this tender age the IFW is grown-up already but still developing and expanding.

As for the growth the number of co-workers having a contract or being financed by scholarships achieved 560 persons during the last years. Additional about 100 guests are using the IFW's facilities for working and studying. The importance of third party projects becomes apparent from the considerable amount of coworkers that are financed by external funding via third party projects or scholarships. At the same time the amount of third party project funding is an important index of quality and competitiveness of the institute. The level of third party funding spent in 2011 amounts to 10 Mio. Euro – a level at the forefront of the Leibniz Association. Most of this project funding was acquired in a highly competitive mode from the German Science Foundation (DFG) and the European Union. In 2011 some new large projects have been launched, for example the EU network BioTiNet on innovative biocompatible Titanium-base structures for orthopedics, and two DFG priority programs – one on superconductivity in Fe pnictides and the other on ferroic cooling, both coordinated by IFW. A novelty in 2011 was a call for joint European and Japanese projects resulting in the funding of three such networks with European and Japanese consortia. The IFW is coordinating one of them and participating in a second one both of them dealing with Iron-based superconductors and its application. The IFW again was successful in applying for DFG means, many of them in the frame of larger networks like Collaborative Research Centres (SFB), Priority programs and Research Groups. So we are involved in the new DFG Graduate School on itinerant magnetism based at the Dresden University of Technology, in the new DFG Research Unit on sensoric micro- and nanosystems together with the Chemnitz University of Technology and in the new DFG Priority Program on spin caloric transport coordinated by the University Regensburg.

Young people completed their apprenticeship at IFW

The beginning of construction works in summer 2011

Kick-off meeting for the new EU network BioTiNet

In order to provide the growing number of co-workers with space for labs and desks for their research work we have planned and applied for a new annex building. After a long series of bothering for requirements, bans and rules the construction work for the new building could finally begin in August 2011. After the completion of the building in 2013 the expansion of the IFW will have reached the limits of our own territory. So we already reached out for the external research site Dresden-Niedersedlitz which was inaugurated in February 2011 in the presence of the State Minister for Sciences and fine Arts Prof. Sabine von Schorlemer. There the SupraTrans II facility was successfully put into operation. Being the next step towards the real superconducting transport system it consists of an 80-m-long circuit and a levitated vehicle for two persons. Meanwhile the research site Dresden-Niedersedlitz has developed into an information center on applied superconductivity eagerly asked for by various visitor groups, from industrial partners and politicians through students and school classes, up to interested laymen.

Expansion means also to reach further and deeper into new co-operative relationships and networks. On the local scale we intensified the close relationship to the Dresden University of Technology by large joint efforts to succeed in the second round of the German Universities Excellence Initiative of the German Federal Ministry of Education and Research and the German Research Foundation. The Dresden University of technology has set up an institutional strategy to promote top level research in a synergetic university. In this respect the IFW has been strongly involved in the creation of DRESDEN concept, DRESDEN standing for “Dresden Research and Education Synergies for the Development of Excellence and Novelty”. Together with all partners in DRESDEN concept, we believe in the abilities of this network to succeed also in the third line of funding – namely the institutional strategies required to promote top-level university research, the so-called future concepts. On a more regional scale the networking with Saxon universities received a fresh impetus by a number of joint projects, e.g. the DFG Research Group „Molecular Spintronics“ with all four Saxon Universities (TU Dresden, TU Chemnitz, Leipzig University and TU Bergakademie Freiberg). Among others, the “Center of

Soft skill workshop for our PhD students

Final workshop of the project of the gender project FINA

Final workshop of the project of the EU project DIVERSITY

Excellence for Nanosystem Integration" granted by the German Government and the proceeding of the joint International Graduate College „Materials and Concepts for Advanced Interconnects and Nanosystems " with TU Chemnitz and Fudan University Shanghai enhanced the cooperation with TU Chemnitz. In a similar way the relation between IFW and TU Bergakademie Freiberg has been further strengthened by the appointment of Prof. Knupfer as Honorary Professor at the TU Bergakademie Freiberg.

A crucial part of the IFW's identity is its vivid life including the cultivation of the scientific dialogue, family-friendly working conditions and the support of sportive, creative and cultural activities. The IFW organizes a series of workshops, colloquia and talks to foster the scientific dialogue and, along the way, allow for social and communication aspects of cooperation. An important meeting for all scientists of the IFW is the yearly two-day program session where all scientists discuss and adjust the research program for the following year. Also the annual IFW Winter School contributes to the scientific communication among all IFW groups and to the training of young scientists in special topics of the IFW research program.

The IFW continued its large efforts to make scientific work accessible for the general public and to inspire young people to study science or engineering also in 2011. The IFW took part in many joint actions like the lecture series "Physics on Saturday" or the Summer University of the TU Dresden. The Dresden Long Night of Sciences took place for the nineth time in 2011, and again, the IFW offered an ample program which attracted almost 6000 visitors. The greatest attraction in the IFW's program seemed to be the special offers "Chemistry for kids" and "Physics for kids" where the girls and boys could try experiments on their own. An equally large respond of young people as well as of their parents and grandparents was met in the one week event "Physik im Kaufpark" in advance of the conference of physicists in March 2011 in Dresden. Besides these big events we organize almost weekly lab-tours for various visitor groups, from school classes through official representatives to guests from foreign organizations.

Inauguration of the SupraTrans II facility

Presenting the SupraTrans II vehicle at the Hannovermesse 2011

Martin Knupfer becoming Honorary Professor at the TU BA Freiberg (Photo: TU Bergakademie Freiberg / Eckardt Mildner)



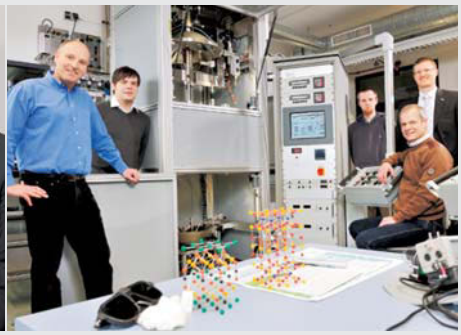

The training of students and young scientists remains a very important concern of the IFW work. PhD and diploma students are involved in nearly all scientific projects and in the resulting publications. The high level in terms of quality and quantity of PhD theses finished every year at the IFW was even enhanced in 2011. Altogether a record number of 39 PhD theses have been successfully completed, nine of them (also a record number) with the best grade possible – summa cum laude. From 2011 we introduced the Tschirnhaus-Medal to acknowledge these outstanding achievements of young scientist.

This Annual report addresses our cooperation partners worldwide, friends and all those who are interested in the Institute's life and progress within the international materials science community. We would like to thank all of you for your constructive cooperation and are looking forward to taking up future challenges together. Special tribute is paid to the members of the Scientific Advisory Board and of the Board of Trustees as well as the funding organizations that continuously support and foster the positive development of the IFW.

Dresden, January 2012

Prof. Dr. Ludwig Schultz
Scientific Director

Dr. h. c. Rolf Pfrengle
Administrative Director

Enlightened courtyard during the long night of sciences

Awardees at the Annual Reception: Dr. Annett Gebert, Dr. Petra Karl and Dr. Simon Pauly

Partners of the outsourced SciDre Scientific Instruments GmbH who received a special prize in the contest „wissen.schafft.arbeit"

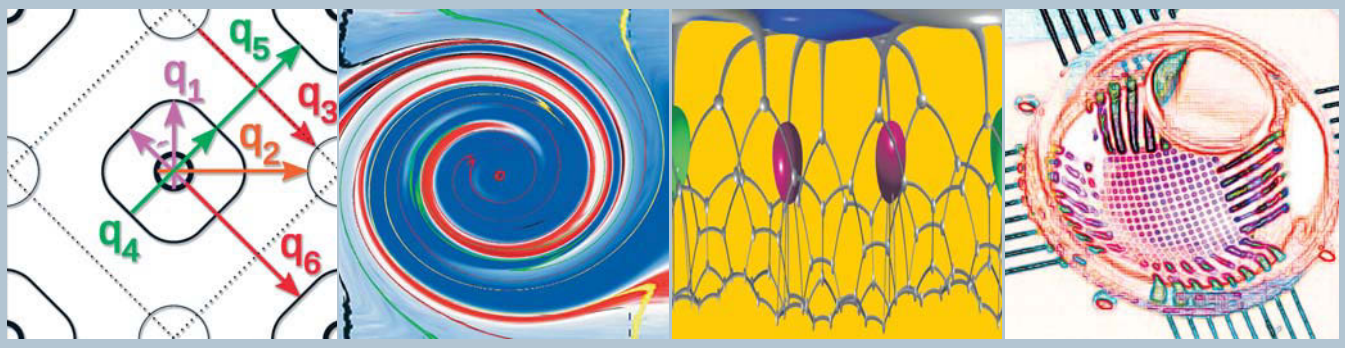

Highlights 2011

Highlights

Quasiparticle interference in LiFeAs

T. Hänke, S. Sykora, R. Schlegel, D. Baumann, L. Harnagea, S. Wurmehl,
M. Daghofer, B. Büchner, J. van den Brink, C. Hess

The quasiparticle interference (QPI) in a superconductor sensitively depends on the symmetry of its order parameter. To probe it, scanning tunneling spectroscopy has proven a powerful technique, in particular for revealing the nature of unconventional superconductivity. A very well suited material to apply this technique is the stoichiometric superconductor LiFeAs as it features clean, charge neutral cleaved surfaces without surface states and a relatively high $T_c \sim 18$ K. Our study revealed that a van-Hove singularity at the center of the Brillouin zone governs the quasiparticle scattering, in stark contrast with other pnictides where nesting is crucial for both scattering and $s_{\pm}$-superconductivity. Indeed, calculations of the QPI for the most elementary order parameters showed incompatibility of the LiFeAs data with singlet s- or *d*-wave pairing symmetry. Instead, an order parameter with chiral *p*-wave pairing provides optimal agreement between the experimental data and QPI simulations.

When an electron tunnels from a normal metal into a superconductor, it occupies a quasiparticle state which carries specific information about the superconducting order parameter. In particular, in the model of Bardeen, Cooper and Schrieffer (BCS) the energy $E_{\mathbf{k}}$ at a given momentum $\mathbf{k}$ is related via $E_{\mathbf{k}} = \pm(\xi_{\mathbf{k}}^2 + |\Delta_{\mathbf{k}}|^2)^{1/2}$ to the normal state band energy $\xi_{\mathbf{k}}$ and the gap function $\Delta_{\mathbf{k}}$ of the superconductor [1,2]. The scattering rate between quasiparticle states with momenta $\mathbf{k}$ and $\mathbf{k'}$ is proportional to *coherence factors* ($u_{\mathbf{k}}u_{\mathbf{k'}}^* \pm v_{\mathbf{k}}v_{\mathbf{k'}}^*$) which are sensitive to the phase of the superconducting order parameter via the Bogoliubov coefficients [1,2] $v_{\mathbf{k}}/u_{\mathbf{k}} = (E_{\mathbf{k}} - \xi_{\mathbf{k}})/\Delta_{\mathbf{k}}^*$, where the ± sign in the coherence factors is determined by the nature of the underlying scattering mechanism.

In tunneling experiments, the relation $\mathrm{DOS}(E) \propto dI/dV(V_{\mathrm{bias}})$ with tunneling voltage V and current I at given energy E and bias voltage V_{bias}, where $E = eV_{\mathrm{bias}}$, is exploited (DOS=density of states). In addition, the spatial dependence of the DOS is accessible in a scanning tunneling microscopy/spectroscopy (STM/STS) experiment. Such spatial dependence often arises from an impurity scattering of the quasiparticles. In this case the incident and scattered quasiparticle waves interfere and give rise to Friedel-like oscillations in the local DOS. The analysis of such quasiparticle interference (QPI) by means of STM/STS has proven an extremely powerful technique to investigate unconventional superconductors, in particular the symmetry of the superconducting gap, because the QPI pattern is decisively influenced by the coherence factors [3-6].

In a recent study [7], we have investigated the QPI of the *stoichiometric* superconductor LiFeAs with this technique. LiFeAs exhibits clean, charge neutral cleaved surfaces with a bulk-like electronic structure at the surface [8]. The critical temperature of LiFeAs is $T_c \sim 18$ K [9] and currently available LiFeAs single crystals are very pure [10]. For these reasons, the material is a promising candidate to probe the superconducting gap characteristics via QPI.

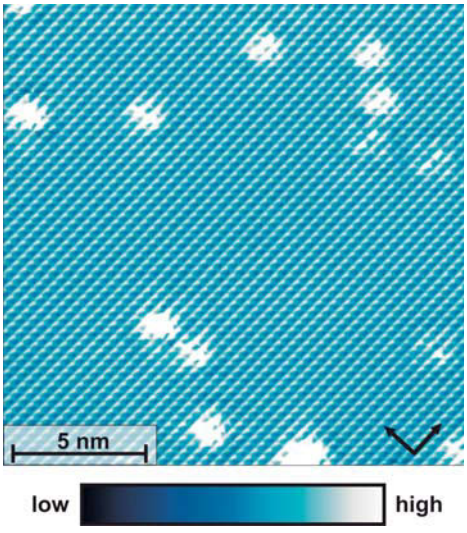

Fig.1: Surface topography of LiFeAs measured after cleaving in cryogenic vacuum in constant current mode (I = 600 pA, $V_{\mathrm{bias}} = -50$ mV) taken at $T \approx 5.8$ K with a field of view of about 18 nm × 18 nm. Black arrows indicate the direction of the lattice constants with $a = 3.7914$ Å [9]. The field of view exhibits a highly periodic atomic corrugation which corresponds to about 2000 atoms in the topmost layer. 14 defects are present in the field of view. This yields a defect concentration <1% and highlights the high purity of our samples. Image adapted from Ref. 7.

The pristine nature of the Li-terminated surface is evident in Fig. 1 which shows a representative surface topography of LiFeAs. The field of view exhibits a highly periodic atomic corrugation, where 14 defects appear as bright superimposed spots. In order to resolve the QPI, we have measured in the superconducting state the spatial- and energy resolved differential tunneling conductance, $dI/dV(\mathbf{r}, V_{\mathrm{bias}})$ in the energy window $E = -50$ meV…50 meV. Very clear QPI patterns have been observed which were particularly strong in the range of about –20 meV and the Fermi level. Selected dI/dV-maps at

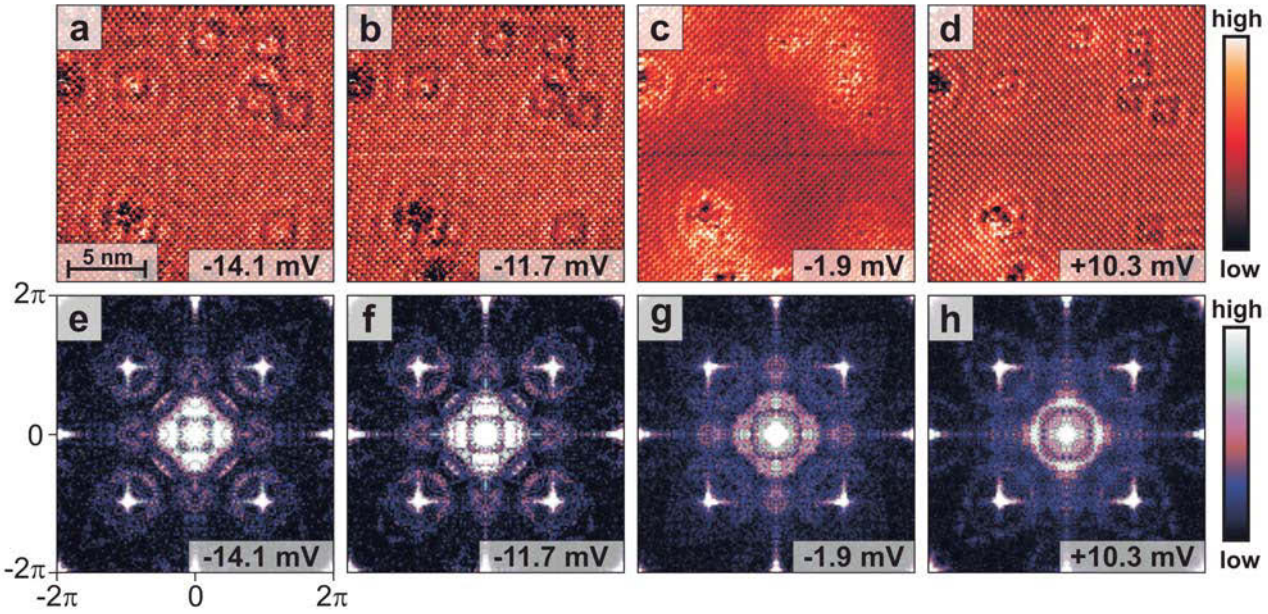

Fig. 2: a-d) *dI/dV*-maps of the region shown in Fig. 1 at selected representative bias voltages. **e-h)** Fourier transformed images of the maps shown in a-d. Bright spots at (π,π) and at higher **q** result from the atomic corrugation in the real space images. Image adapted from Ref. 7.

representative energies are shown in Fig. 2a. Here, the QPI is clearly not only visible as relatively strong modulations close to the defects but also appears as weak ripples (with a wavelength of a few lattice spacings) in the relatively large defect-free area in the center of the field of view.

Fig. 2b displays the Fourier transformation of the *dI/dV*-maps. The images reveal a very rich structure which directly accounts for the relevant scattering wave vectors. The most salient feature in the images is a bright structure distributed around $\mathbf{q}=(0,0)$, which attains a squarish shape with the corners pointing along the $(q_x,0)$ and $(0,q_y)$ directions. Further well resolved structures with significantly lower intensity are distributed around $(\pi/2, \pi/2)$, $(\pi,0)$ and (π,π). These structures again are most pronounced between −20 mV and the Fermi level. At positive bias voltage the main spot around (0,0) changes its shape towards an almost round structure while the others develop into a rather featureless diffuse background.

Already without considering a full calculation of the QPI in LiFeAs we can deduce important qualitative information from the data. The rather broad and intense distribution of scattering vectors around (0,0) and the rather weak intensity at $\mathbf{q}=(\pi,0)$ renders a strong nesting of hole and and electron Fermi surface sheets in LiFeAs very unlikely, because for such a scenario the highest QPI intensity would be expected at the nesting vectors $\mathbf{q}=(\pi,0)$ [6] which is clearly not confirmed by our data. In Fig. 3a and b we compare the electronic constant energy contour (CEC) of LiFeAs at E=-11.7 mV [11] with the observed QPI intensities in the Fourier transformed image. Most prominent is that the observed central squarish structure in Fig. 3b appears like a somewhat enlarged smeared replica of the large hole-like CEC around (0,0). This observation can directly be understood as stemming from scattering processes ($\mathbf{q}_1$) connecting the very small and the larger squarish-shaped hole-like CEC around (0,0). Furthermore, the much weaker structure at $\mathbf{q}=(\pi,0)$ in Fig. 3b, which resembles a smeared version of the electron-like CEC near $\mathbf{k}=(\pi,0)$, apparently results from scattering processes ($\mathbf{q}_2$) connecting this CEC with again the small hole-like CEC. Note that due to the presence of a van-Hove singularity [11] at $\mathbf{k}=(0,0)$ the DOS for momentum vectors on the small hole-like CEC is enhanced significantly. Thus, the QPI pattern in LiFeAs is dominated by scattering processes where one of the two momentum vectors involved in the scattering process is characterized by a very small absolute value. Consequently, the Fourier transformed QPI image essentially represents a 'map' of all CEC at a given energy.

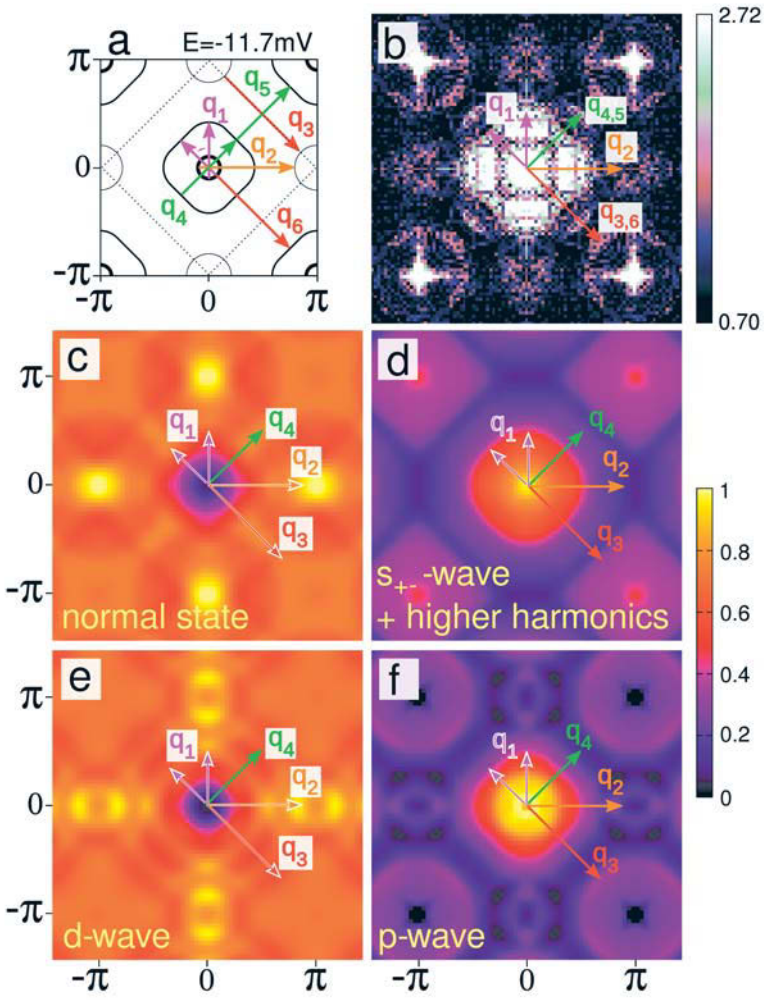

Fig. 3: a) Simplified CEC [11] at E = -11.7 meV in the periodic-zone scheme of the Brillouin Zone (BZ), where the first BZ (referring to the unit cell with two Fe atoms) is indicated by the dashed lines. The two pockets around (0,0) represent hole-like CEC while the pockets at the zone boundary are electron-like. $q_{1,2}$ represent scattering processes which connect states on the small hole-like CEC and on other CEC, $\mathbf{q}_3$ and $\mathbf{q}_4$ represent scattering between the electron-like and within the large hole-like CEC, respectively. $\mathbf{q}_{5,6}$ represent umklapp processes. Note that each scattering process $\mathbf{q}_{1...6}$ is described by a set of scattering vectors as is illustrated for $\mathbf{q}_1$.
b) Measured Fourier transformed image at the same energy (the same as Fig. 2b)} with $\mathbf{q}_{1...6}$ superimposed. The most salient QPI features around (0,0) and (π,0) match well with $\mathbf{q}_1$ and $\mathbf{q}_2$ (see text). The further observed but less prominent QPI intensities around (π,π) and at (π/2,π/2) are well described by $\mathbf{q}_3$ and $\mathbf{q}_4$, respectively. The umklapp scattering vectors $\mathbf{q}_5$ and $\mathbf{q}_6$ might also be of relevance here.
c-f) Calculated QPI in $\mathbf{q}$ space assuming the normal state and a superconducting order parameter with $s_\pm$, d- and p-wave symmetry. Note that Bragg intensity at the bright spots at (±π,±π) in panel b) is not taken into account in the calculation.

For a quantitative analysis of the experimental data, we calculated (see Ref.[7] for details) the QPI in the superconducting state using an appropriate BCS model for LiFeAs which can describe three cases of elementary singlet pairing (s_{++}, $s_\pm$, and d-wave) as well as a p-wave triplet pairing scenario. To ensure that our calculations are based on unbiased experimental findings, the electronic band structure of LiFeAs was modeled using tight-binding fits derived from recent ARPES experiments [11].

Fig. 3c-f shows the results of our calculations for the energy E=-11.7 V and assumed $s_\pm$ and d-wave singlet as well as p-wave triplet pairing. The calculated QPI pattern of the normal state shown in Fig. 3c exhibits an extended low-intensity region around (0,0), in stark contrast to the experimental data. However, the situation drastically changes if the superconducting state is taken into account (see Fig. 3d-f). The main feature, which now can be observed for two of the three superconducting cases is a wide high-intensity region centered at (0,0). This qualitative change clearly corroborates that the intense central structure observed in the experiment is characteristic of the superconducting state. A closer examination of the individual QPI patterns brings to light a very strong dependency of the pattern on the assumed pairing symmetry. Interestingly, we find a striking agreement between the experimentally observed QPI and the calculated image of Fig. 3f, which is based on a triplet paired superconducting state with a chiral p-wave gap function. The agreement is obviously much less pronounced for the three singlet pairing scenarios. Thus, among the considered order parameters the best agreement between experimental data and calculated QPI images is apparently obtained for a p-wave order parameter. We point out that this result is rather stable with respect to different types of electron-impurity interaction such as magnetic or resonant scattering [7].

In Fig. 4 we present a comparison between experimental results and calculated *p*-wave based QPI for another three energy values. We find an excellent agreement for the energy evolution of the three most intensive QPI structures (framed in Fig. 4). A closer inspection of the boundary of the central structure reveals a clear dispersive behavior of the high-intensity region within some finite energy range. As it is presented in Fig. 5 this energy dependence is confirmed very well within our model calculations.

Our main observation that the quasiparticle scattering is dominated by the van-Hove singularity at the center of the Brillouin zone fits in very well in recent experimental and theoretical findings. Angle resolved photo emission spectroscopy (ARPES) data provide clear-cut evidence for the absence of strong nesting in LiFeAs [11], consistent with our result. From these experiments an $s_{\pm}$ pairing scenario, which is believed to be nesting-driven by antiferromagnetic fluctuations [12], is not expected. In fact, a recent theoretical analysis based on a realistic band structure model with poor nesting yields a dominating role of the small hole-like Fermi surface for the scattering in LiFeAs, giving rise to ferromagnetic fluctuations which drive an instability towards triplet superconductivity [13]. It seems rather encouraging that our QPI calculations which are based on a quite simple model and very elementary assumptions are consistent with this finding. It is, however, thinkable that a more complex order parameter (such as *s+id* symmetry) would yield a similar convincing agreement.

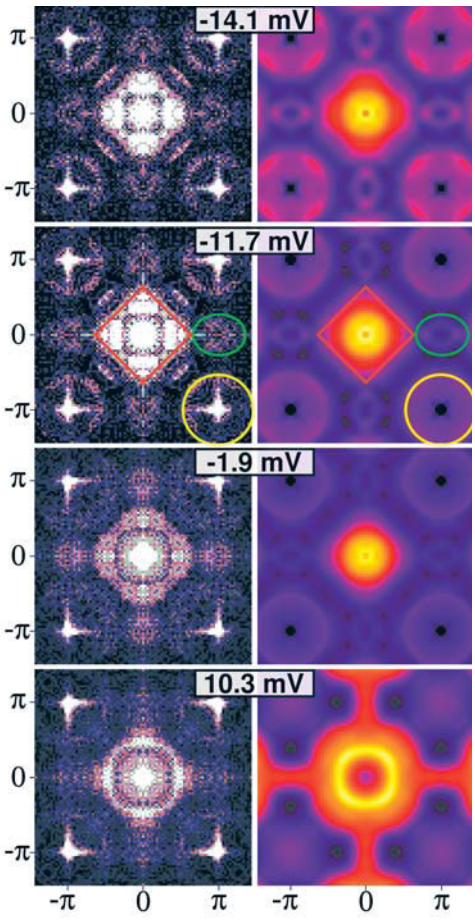

Fig. 4: Comparison of the measured QPI pattern and its calculated counterpart based on potential scattering and a chiral *p*-wave superconducting order parameter for various energies. The clearly observable dispersion unambiguously demonstrates that the observed structures result from QPI and not from non-dispersing modifications of the DOS around a defect. The experimentally observed strong intensity at $|\mathbf{q}| \leq 0.2\pi$ reflects a quasi-constant (i.e. constant plus very long wavelength modulations) background in the *dI/dV* maps which is not taken into account in our calculations. Thus, there is no enhanced intensity in the calculated Fourier transformed images at $\mathbf{q}=(0,0)$.

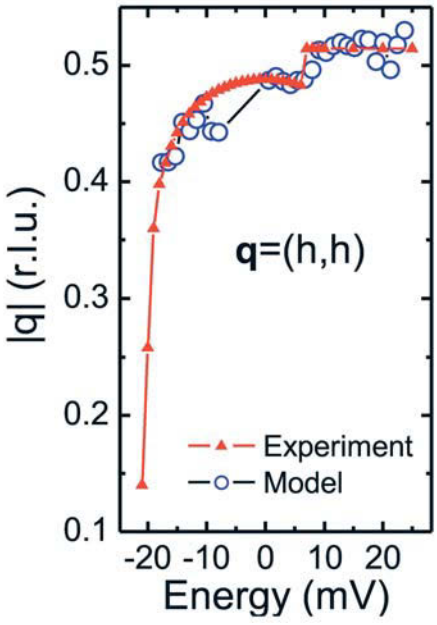

Fig. 5: Size of the measured and calculated central structure along $\mathbf{q}=(h,h)$.

[1] J. Bardeen, L. N. Cooper, J. R. Schrieffer, Phys. Rev. 108 (1957) 1175
[2] M. Tinkham, Introduction to Superconductivity (Dover Publications, 2004)
[3] J. E. Hoffman, et al., Science 297 (2002) 1148
[4] T. Hanaguri, et al., Nat Phys 3 (2007) 865
[5] T. Hanaguri, et al., Science 323 (2009) 923
[6] T. Hanaguri, et al., Science 328 (2010) 474
[7] T. Hänke et al., arXiv:1106.4217, accepted by Phys. Rev. Lett.
[8] A. Lankau, et al., Phys. Rev. B 82 (2010) 184518
[9] J. H. Tapp, et al., Phys. Rev. B 78 (2008) 060505
[10] I. Morozov, et al., Crystal Growth & Design 10 (2010) 4428
[11] S. V. Borisenko, et al., Phys. Rev. Lett. 105 (2010) 067002
[12] I. I. Mazin et al. Phys. Rev. Lett. 101 (2008) 057003
[13] P. M. R. Brydon et al. Phys. Rev. B 83 (2011) 060501

Funded by: DFG

Proximity effect superconductor/ferromagnet: A spin valve for the superconducting current

P. V. Leksin[1], N. N. Garifyanov[1], I. A. Garifullin[1], J. Schumann, H. Vinzelberg, V. Kataev, R. Klingeler, O. G. Schmidt, B. Büchner

It is well known that superconductivity and ferromagnetism are two antagonistic types of ordering of matter. In ferromagnetic metals the exchange field tends to align spins of conduction electrons parallel. In contrast, in conventional superconductors the electron spins in the Cooper pairs are aligned antiparallel. Therefore, when thin layers of a superconductor (S) and of a ferromagnet (F) are brought in a close contact, an interesting interplay between two competing ground states takes place [1]. Specifically, in our work [2,3] we have demonstrated experimentally that a thin multilayer F1/F2/S can be operational as a full spin valve for the superconducting current which can be completely switched off and on. Furthermore, we have observed a sign-changing oscillating behavior of this spin switch effect upon variation of the Fe2 layer thickness. Interference of Cooper pair wave functions reflected from both surfaces of the Fe2 layer appears to be the most probable reason for the observed phenomena.

In the artificially prepared thin film layered systems consisting of F and S layers the two conflicting types of ordering are separated in space [4-8]. In case of an S/F multilayered system this can lead to specific and intriguing effects which are called S/F proximity effects. Since the exchange field in a strong ferromagnet is much larger than the pairing energy in a superconductor, in an S/F multilayer the Cooper pair wave function penetrates into the F layer over a very small distance only. This value is usually defined as a ferromagnet coherence length ξ_f [9]. For pure Fe ξ_f is about 1 nm [10]. The penetration of the Cooper pair wave function from the S layer into the F layer has quite a complicated character. The conduction band of the F layer is split into spin up and spin down subbands due to the strong exchange interaction between the spins of conduction electrons and local magnetic moments. Hence in the F layer two Cooper electrons with antiparallel (AP) spins at the Fermi level have non equal wave vectors. Thus the total wave vector of the Cooper pair is a non-zero value inside the F layer. This means that the amplitude of the Cooper pair wave function not only decays but also oscillates over the penetration length ξ_f in the F layer (see, e.g. [6]). In case of the S/F and F/S/F structures these oscillations lead to quantum interference which modulates the value of the superconducting critical temperature T_c when the thickness of the F layer is varied [10,11].

The so-called superconducting (SC) spin valve effect, a complete switching on and off of the SC current flowing in complex S/F multilayers, gives another example of the fascinating interplay between superconductivity and ferromagnetism. Its theoretical concept developed in Refs. [12–14] is based on the S/F proximity phenomenon and relies on the idea to control the pair breaking and correspondingly the T_c by manipulating the mutual orientation of magnetizations of two F layers. This is because the mean exchange field from two F layers acting on the Cooper pairs is smaller for the AP orientation of magnetizations of these F layers compared to the parallel (P) case.

Historically, the first paper devoted to the realization of the spin switch effect has been published by Deutscher and Meunier in 1969 [15]. They studied a FeNi/In/Ni trilayer and obtained a surprisingly large difference in T_c between the AP and P orientations of the magnetizations $\Delta T_c = T_c^{AP} - T_c^{P}$. The reason for this effect has not been clarified up to now. Clinton and Johnson [16] have developed a SC valve which uses the magnetic fringe fields at the edges of the F film of a micrometer size. In this experiment a direct contact between F and S layers was absent similar to the case studied in Ref. [15]. The possibility to develop a real switch based on the S/F proximity effect has been theoretically substantiated in 1997 by Oh *et al* [12]. They proposed the F1/F2/S layer scheme where an S film is deposited on top of two F layers [see Fig. 1(a)]. Two years later a different

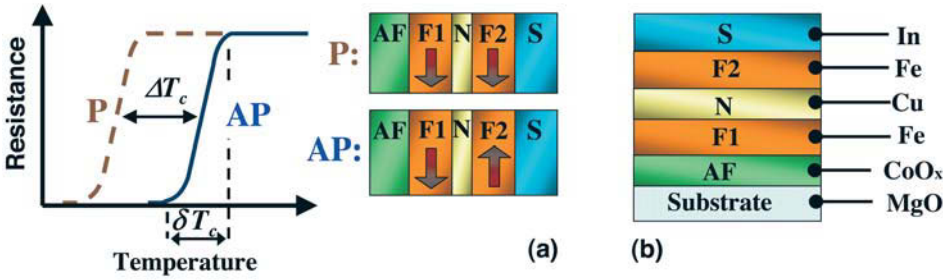

Fig. 1: (a) Scheme of the superconducting spin switch theoretically proposed by Oh *et al*. [12] and expected superconducting transition curves for the parallel (P) and antiparallel (AP) orientation of the magnetization in the ferromagnetic F1 and F2 layers. δT_c is the width of the transition curve and ΔT_c is the shift of the transition temperature T_c.
(b) Design of the studied samples.

construction based on an F/S/F trilayer was proposed theoretically by Tagirov [13] and Buzdin *et al.* [14]. Several experimental works confirmed the predicted effect in the F/S/F structure (see, e.g., Refs. [17–20]). However, ΔT_c turns out to be smaller than the width of the SC transition δT_c itself. Hence a full switching between the normal and SC state was not achieved. Implementation of a design similar to the F1/N/F2/S layer scheme by Oh *et al.* [12] with a $[Fe/V]_n$ antiferromagnetically coupled superlattice instead of a single F1/N/F2 trilayer [21] is not actually the spin switch device because the system cannot be switched from the AP to P orientations of the magnetizations instantaneously. But the analysis of the data revealed that the ΔT_c of this system can reach up to 200 mK with $\delta T_c \sim 100$ mK.

Theories [12–14] predict that the AP orientation is always more favorable for superconductivity than the P one, so that T_c^{AP} should be always larger than T_c^{P}. However, in case of the oscillating behavior of the Cooper pair wave function in the F layer possible interference effects in the spin valve cannot be ignored. This especially concerns the design F1/F2/S proposed by Oh *et al.* [12] whose functionality should obviously critically depend on the interference at the F2/S interface of the pair wave functions.

To realize experimentally the SC spin valve we have focused on the F1/F2/S layer sequence [Fig. 1(a)] [2,3]. The design of the samples is presented in Fig. 1(b). Here CoO_x/Fe1/Cu/Fe2 is the ferromagnetic part F1/F2 of the system. The CoO_x plays a role of the bias layer which pins the magnetization of the Fe1 layer while the magnetization of the Fe2 layer is free and can be varied using a small magnetic field. Cu is a normal metal layer (N) which decouples the magnetizations of the F layers. We used In as the superconducting S layer. With a standard molecular beam epitaxy we have prepared a set of spin valve samples CoOx(4 nm)/Fe1(3 nm)/Cu(4 nm)/Fe2(d_{Fe2})/In(230 nm) with different thickness d_{Fe2} of the F2 layer in the range 0.4 nm < d_{Fe2} < 5.2 nm.

The magnetic and superconducting characteristics of the samples were measured using a VSM SQUID magnetometer and a 4-contact method, respectively. Detailed presentation of the experimental technique and measurement protocols can be found in [2, 3].

Fig. 2(a) shows the major magnetic hysteresis loop for the sample with d_{Fe2} = 0.5 nm. The shape of this loop is similar for all studied samples. In the field range between -0.1 and -3.5 kOe the mutual orientation of the magnetization of the two F layers is antiparallel because the magnetization of the Fe1 layer is kept by the bias CoO_x layer. The minor hysteresis loop corresponding to the F2 layer is shown in Fig. 2(b).

Next, we have recorded the temperature dependence of the resistivity R for the P (H_0 = +110 Oe) and AP (H_0 = -110 Oe) orientation of the magnetization of the F layers. Notably, the critical temperature for the AP orientation T_c^{AP} is higher than that for the P orientation T_c^{P} [Fig. 3 (a)]. The SC valve effect $\Delta T_c = T_c^{AP} - T_c^{P}$ amounts to about 19 mK. The shift of the T_c is not of a record value [19] but, what is very important, the ΔT_c is

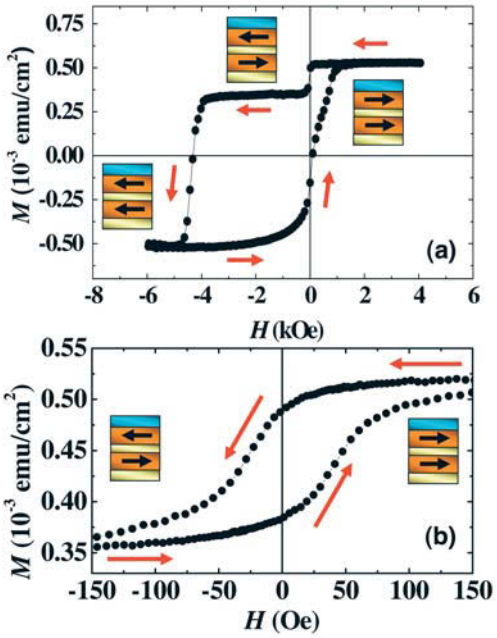

Fig. 2: Magnetic hysteresis loops for the sample CoOx/Fe1/Cu/Fe2(0.5nm)/In: **(a)** the major loop; **(b)** the minor loop corresponding to the free Fe2 layer.

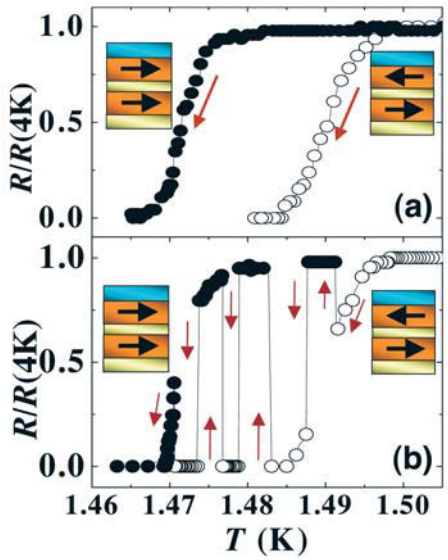

Fig. 3: (a) Resistivity curves for the spin valve sample CoO_x(3nm)/Fe1(3nm)/Cu(4nm)/Fe2(0.5nm)/In(230nm) for parallel and antiparallel orientations of the magnetizations of the F layers. The applied switching field is H_0 = ±110 Oe.
(b) Full switching between the normal and superconducting states for the spin valve sample CoO_x(3nm)/ Fe1(3nm)/Cu(4nm)/Fe2(0.5nm)/In(230nm) achieved by changing the mutual orientation of the magnetizations of the F layers. The applied switching field is H_0 = ±110 Oe.

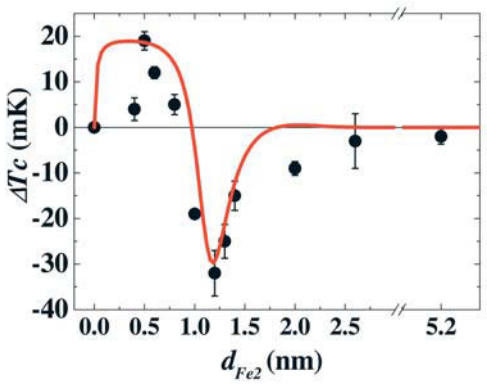

Fig. 4: The dependence of the T_c shift $\Delta T_c = T_c^{AP} - T_c^{P}$ on the Fe2-layer thickness d_{Fe2}. The applied switching field is $H_0 = \pm 110$ Oe. The solid line represents a result of the theoretical modeling in the framework of the S/F proximity theory (for details see Ref. [3]).

significantly larger than the SC transition width δT_c amounting to about ~ 7 mK only. This opens a possibility to switch the SC current on and off by changing the mutual orientation of the magnetizations of the F1 and F2 layers. To demonstrate this we have performed the measurements of the resistance R of this sample by sweeping slowly the temperature within the interval ΔT_c and switching the magnetic field between +110 and -110 Oe [Fig3. (b)]. Evidently, a *complete on/off switching of the SC current* flowing through the sample is achieved.

The second goal of our investigations was to study the dependence of the ΔT_c on the F2 layer thickness d_{Fe2}. The magnitude of the spin switch effect ΔT_c was measured in a similar way as described above. The results are shown in Fig. 4. Surprisingly, the $\Delta T_c(d_{Fe2})$ dependence exhibits a remarkable oscillating behavior in the thickness range $0.5\ \text{nm} \leq d_{Fe2} \leq 2.6\ \text{nm}$. For $d_{Fe2} \geq 1$ nm the critical temperature T_c for the parallel orientation of the magnetization is *higher* than for the antiparallel one. A detailed discussion of this, at first glance, counterintuitive result and an origin of the observed oscillating behavior of the $\Delta T_c(d_{Fe2})$ can be found in our recently published article [3]. We conclude that the most possible reason is a quantum interference mechanism arising due to the S/F proximity effect. In the F layer the Cooper pair acquires a nonzero momentum due to the Zeeman splitting of the electron levels in the presence of exchange field. Thus the wave function of the Cooper pair should oscillate in space (see, e.g., [6]). If the F layer is sufficiently thin, the wave function reflected from the surface of the F layer opposite to the S/F interface can interfere with the incoming one. Depending on the layer's thickness, the interference at the S/F interface may be constructive or destructive. This should lead to the enhancement of T_c or its decrease, respectively, thus naturally explaining our result (Fig. 4).

[1] A. I. Buzdin *et al.*, Adv. Phys. **34**, 175 (1985).
[2] P. V. Leksin *et al.*, Appl. Phys. Lett. **97**, 102505 (2010).
[3] P. V. Leksin *et al.*, Phys. Rev. Lett. **106**, 067005 (2011).
[4] I. A. Garifullin, J. M. M. M. **240**, 571 (2002).
[5] Yu. A. Izyumov *et al.*, Uspehi Fizicheskih Nauk, **172**, 113 (2002).
[6] A. I. Buzdin, Rev. Mod. Phys. **77**, 945 (2005).
[7] F. S. Bergeret *et al.*, Rev. Mod. Phys. **77**, 1321 (2005).
[8] K. B. Efetov *et al.*, *Magnetic Heterostructures. Advances and Perspectives in Spinstructures and Spintransport.* Series Springer Tracts in Modern Physics, Vol. **227**. Zabel H., bader S. D. (Eds.), 2007, p. 252.
[9] Z. Radovic *et al.*, Phys. Rev. B. **38**, 2388 (1988).
[10] L. Lazar *et al.*, Phys. Rev. B **61**, 3711 (2000).
[11] I. A. Garifullin et al., Phys. Rev. **66**, 020505R (2002).
[12] S. Oh *et al.*, Appl. Phys. Lett. 71, 2376 (1997).
[13] L. R. Tagirov, Phys. Rev. Lett. 83, 2058 (1999).
[14] A. I. Buzdin *et al.*, Europhys. Lett. **48**, 686 (1999).
[15] G. Deutscher and F. Meunier, Phys. Rev. Lett. **22**, 395 (1969).
[16] T. W. Clinton and M. Johnson, Appl. Phys. Lett. **70**, 1170 (1997).
[17] J. Y. Gu *et al.*, Phys. Rev. Lett. **89**, 267001 (2002).
[18] A. Potenza and C. H. Marrows, Phys. Rev. B **71**, 180503(R) (2005).
[19] I. C. Moraru *et al.*, Phys. Rev. Lett. **96**, 037004 (2006).
[20] G.-X. Miao *et al.*, Phys. Rev. Lett. **101**, 137001 (2008).
[21] K. Westerholt *et al.*, Phys. Rev. Lett. **95**, 097003 (2005).

Cooperation: [1]Zavoisky Physical-Technical Institute, Kazan Scientific Center of Russian Academy of Sciences, 420029 Kazan, Russia

Funded by: DFG, RFBR

Structured electrodeposition in inhomogeneous magnetic fields

K. Tschulik, F. Karnbach, R. Sueptitz, K. Hennig, V. Hoffmann, M. Uhlemann,
A. Gebert, L. Schultz

Electrochemical deposition of metals is a well-established technique for surface functionalization or decoration. However, when deposits of specific structures are desired, usually expensive templating- or masking-techniques are required.
In 2009 it was demonstrated that structured Cu layers may be electrodeposited in magnetic gradient fields [1]. Maxima of deposit thickness correlated with maxima of magnetic field gradients superimposed at the working electrode. Simple, i.e. additive-free, electrolytes containing paramagnetic Cu^{2+} ions were used in this study. In contrast, deposit structuring did not succeed using solutions of diamagnetic Bi^{3+} ions and homogeneous Bi layers were observed with and without superimposed magnetic gradient field. Due to this, the structuring effect was attributed to the magnetic field gradient force $\boldsymbol{F}_{\nabla B}$:

$$F_{\nabla B} = \frac{\chi_{sol}}{\mu_0} B\nabla B, \text{ with } \chi_{sol} = \sum_i \chi_{mol,i} c_i \quad (1)$$

This force is a function of the magnetic flux density ($\boldsymbol{B}$) and its gradient ($\nabla\boldsymbol{B}$). It also depends on the concentration (c) and the molar magnetic susceptibility (χ_{mol}) of all species (i) in the electrolyte. The constant μ_0 denotes the permeability of free space.
Values of the molar magnetic susceptibility of paramagnetic species exceed those of diamagnetic species by at least one order of magnitude [2]. Thus, effects of the magnetic field gradient force on electrolytes containing only diamagnetic species are almost negligible.
Heterogeneous magnetic fields of sufficient gradients need to be superimposed at the working electrode to enable magneto-electrochemical structuring. This may be realized by placing either NdFeB permanent magnets [3,4] or magnetized magnetic field gradient templates (∇B-templates) [1,5] behind the working electrode. ∇B-templates are arrangements of ferromagnetic building blocks of desired number and shape, fixed in a diamagnetic matrix (e.g. PVC or epoxy resin).
In Fig. 1 optical images of magnetic field gradient templates and the corresponding structured deposits are compared.

Fig. 1: Optical images of magnetic field gradient templates containing Fe wires or platelets as ferromagnetic building blocks and of deposits obtained in inhomogeneous magnetic fields generated by these templates.

This rather simple structuring technique is applicable for every metal or alloy that can be deposited from an electrolyte containing its paramagnetic ions. A structured Fe layer, obtained using a solution of paramagnetic Fe^{2+} ions as the electrolyte is depicted in Fig. 1 (left).
Although the resulting deposits appear as simple copies of the ∇B-templates, the structuring mechanism was found to base on a complex magnetic field gradient force induced convection in the electrolyte. This theoretically predicted convection was proved experimentally by Astigmnatism Particle Tracking Velocimetry (APTV) [5]. This in-situ measurement technique allowed three-dimensional analysis of the convection evolving during electrodeposition in magnetic field gradients. Indeed, the predicted magnetic field gradient force driven flow of electrolyte in electrode-normal direction was observed [3].
A jet-like stream of bulk-electrolyte is directed towards regions of maximum magnetic field gradients (indicated by a red arrow in Fig. 2). Thus, mass transport towards the electrode is locally enhanced and consequently, locally thicker deposits result.
For reasons of continuity, this stream has to be balanced by an upward flow (blue arrows) of fluid, which occurred at the edge of the electrochemical cell (Fig. 2).

Additionally, a rotational flow (indicated by a green arrow in Fig. 2) superimposed to the electrode-normal motion was detected. This convection was assumed to be induced

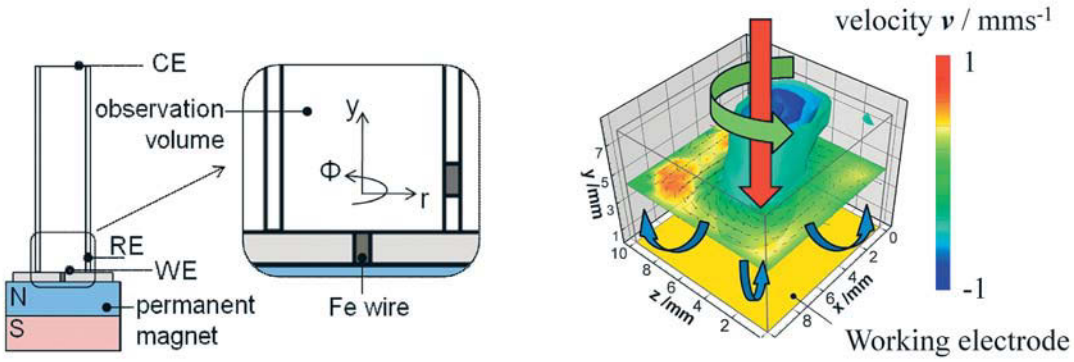

Fig. 2: Schematic illustration of the electrochemical setup for electrodeposition in magnetic gradient fields (left) and a plot of a volume representation of the measured velocity field in the electrolyte (right); WE: working electrode (Au), CE: counter electrode (Pt), RE: reference electrode (mercury sulfate electrode).

by the Lorentz force, which also acts on the ions during the movement towards the working electrode.

$$F_L = i \times B \quad (1)$$

However, this additional convection did not influence the deposit structuring, which is in very good agreement with results of numerical simulations.

Very recently, it was found that magneto-electrochemical structuring may even succeed when only diamagnetic species are involved in the deposition process [4,6]. For this purpose, electrochemically inert paramagnetic species have to be added to the electrolyte. Thus, structured Bi deposits were obtained using an electrolyte containing diamagnetic Bi^{3+} ions and electrochemically inert Mn^{2+} ions. Most interestingly, a reversal of the structuring effect – with respect to that previously described for Cu and Fe deposition, occurred (Fig. 3).

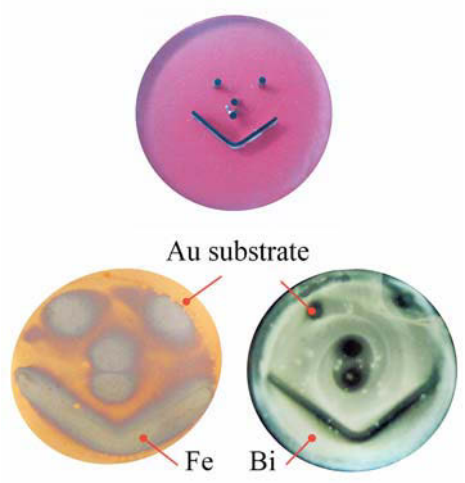

Fig. 3: Optical image of the ∇B-template (top) generating the magnetic field gradients during deposition of a structured Fe layer (left) and a reversely structured Bi layer (right).

A convincing explanation for this observation has not yet been published. It seems likely that although Mn^{2+} ions themselves are not involved in the deposition process, they might be enriched at the working electrode surface. Hence, a magnetic field gradient force driven convection may be induced. The fluid flowwould be directed away from the working electrode in regions of high magnetic field gradients, locally reducing the deposition rate there.

[1] K. Tschulik, J. A. Koza, M. Uhlemann, A. Gebert, L. Schultz, „Effects of well-defined magnetic field gradients on the electrodeposition of copper and bismuth," Electrochemistry Communications **11**, 2241-2244 (2009).
[2] S. R. Ragsdale, K. M. Grant, H. S. White, „Electrochemically Generated Magnetic Forces. Enhanced Transport of a Paramagnetic Redox Species in Large, Nonuniform Magnetic Fields," Journal of the American Chemical Society **120**, 13461-13468 (1998).
[3] G. Mutschke, K. Tschulik, T. Weier, M. Uhlemann, A. Bund, J. Fröhlich, „On the action of magnetic gradient forces in micro-structured copper deposition," Electrochimica Acta **55**, 9060-9066 (2010).
[4] P. Dunne, L. Mazza, J. M. D. Coey, „Magnetic Structuring of Electrodeposits," Phys. Rev. Lett. **107**, 024501 (2011).
[5] K. Tschulik, C. Cierpka, A. Gebert, L. Schultz, C. J. Kahler, M. Uhlemann, „In Situ Analysis of Three-Dimensional Electrolyte Convection Evolving during the Electrodeposition of Copper in Magnetic Gradient Fields," Analytical Chemistry **83**, 3275-3281 (2011).
[6] K. Tschulik, X. Yang, G. Mutschke, M. Uhlemann, K. Eckert, R. Sueptitz, L. Schultz, A. Gebert, „How to obtain structured metal deposits from diamagnetic ions in magnetic gradient fields?," Electrochemistry Communications **13**, 946-950 (2011).

Cooperation: Universität der Bundeswehr München – Institute of Fluid Dynamics and Aerodynamics; TU- Dresden – Institute for Fluid Dynamics; HZDR – Institute for Safety Research
Funded by: Studienstiftung des deutschen Volkes, DFG / SFB 609,

Fractional Quantum Hall states in strongly correlated multi-orbital systems

J. W. F. Venderbos, S. Kourtis, J. van den Brink and M. Daghofer

The past decade has spawned a remarkable surge in the quest for novel topological quantum states of matter. A fascinating aspect of this new field is the effect of (strong) electronic correlation in these materials. Recently, for topologically nontrivial and very narrow electronic bands, Coulomb repulsion between electrons has been predicted to give rise to a spontaneous fractional quantum-Hall (FQH) state – in absence of magnetic fields.

We predict that orbital degrees of freedom in frustrated lattice systems lead to a narrowing of topologically nontrivial bands. This robust effect does not rely on fine-tuned long-range hopping parameters and is directly relevant to a wide class of transition metal compounds. In addition, we show that strongly correlated electrons in a t_{2g}-orbital system on a triangular lattice self-organize into a spin-chiral magnetic order that induces precisely the required nontrivial and flat bands. An exact-diagonalization study has established the signatures of various spontaneous FQH states.

The Integer Quantum Hall (IQH) effect [1] is a prime example of an electronic state that cannot be classified within the traditional framework of symmetry breaking, but is instead characterized by a topological invariant [2]. In particular, the famous quantized Hall plateaus are directly related to this topological quantity, which forms an elegant explanation for its observed robustness. Even though the IQH effect is generally associated with a 2-dimensional electron gas in a magnetic field, it is by now well established – at least theoretically – that an external magnetic field is in principle not needed. Quantum states within the same topological class as the IQH states can be realized in lattice models, if time-reversal symmetry is broken by other mechanisms, e.g., by complex electron hoppings [3].

The past decade has witnessed the discovery that the classification of quantum states based on topological characteristics can be generalized to systems where time-reversal symmetry is not broken. While first suggested to occur in graphene [4], the Quantum Spin-Hall (QSH) state was soon after demonstrated to be a new topological quantum state [4], coming with its own topological index. The QSH effect was experimentally observed in 2007 [5], based on a proposal by Bernevig et al. [6] Both the IQH state and the QSH state live in two dimensions and their respective topological invariants are two-dimensional objects. Are topologically nontrivial states therefore restricted to two

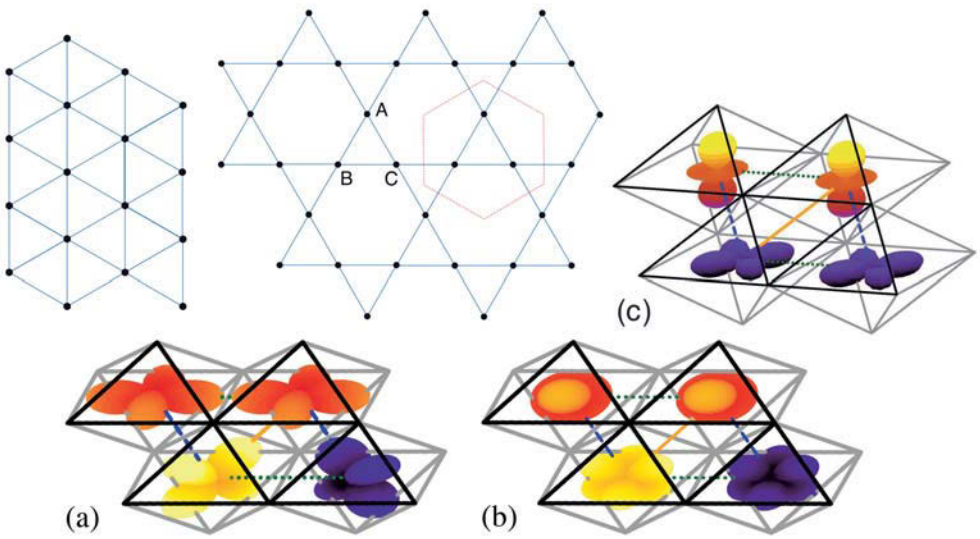

Fig. 1: The frustrated trinagular and kagome lattices. Plots of various d-orbitals surrounded by the oxygen octahedra; in **(a)** the so-called a1g and e'g orbitals that are split in a trigonal environment, **(b)** t2g xy, yz and xz orbitals, **(c)** e_g orbitals.

dimensions? No, they are not. The topological classification can be extended to arbitrary dimension, including the presently much studied 3-dimensional topological insulators that preserve time-reversal symmetry [7-9,10-12]. The hallmark of these peculiar materials, the 2D metallic Dirac cones at the surface, have been beautifully demonstrated in experiments [13-14].

As the search for novel topological states of matter continues – also superconductors allow for a distinction based on topology – a formidable and intriguing challenge is the investigation of electronic interactions in conjunction with topology. All the topological states mentioned above can be understood in terms of non-interacting fermionic band theory. Yet in real materials correlations are bound to play an important – and sometimes dominating – role. Establishing the fate of topological systems in the presence of strong electronic interactions is therefore both exciting and relevant. One very prominent example of such a system is the counterpart of the IQH state, the Fractional Quantum Hall (FQH) state, which can only arise due to electron-electron interaction. Already discovered in the 1980's [15], the FQH continues to fascinate and surprise to the present day.

Fractional Quantum Hall states are topological states that can be seen as composed of quasi-particles carrying an exact fraction of the elementary electronic charge [16]. Apart from the fundamental interest in observing a quasi-particle that behaves in many ways like a fraction of an electron, some FQH states also have properties relevant to fault-tolerant quantum computation [17]. Very recently [18-20], in the same spirit as the generalizations of the IQH effect, it was suggested that lattice-FQH states may similarly arise without a magnetic field, in fractionally filled topologically nontrivial bands.

In contrast to the IQH and QSH effects, interactions are an essential requirement for FQH states, which places demanding restrictions on candidate systems: One needs a topologically nontrivial band that must be nearly flat – similar to the highly degenerate Landau levels – so that the electron-electron interaction can at the same time be large compared to the band width and small compared to the gap separating it from other bands [18-20]. If the requirements can be fulfilled, however, the temperature scale of the FQH state is set by the energy scale of the interaction. This can allow temperatures considerably higher than the sub-Kelvin range of the conventional FQH effect, which would be extremely desirable in view of potential quantum-computing applications. Moreover, the lattice version of FQH states [21] may have unique and different properties [22].

Mimicking Landau level structure in lattice systems in the absence of fields thus requires very narrow nontrivial bands. For most recently proposed model Hamiltonians [18-20,23], the topological character of the bands was put in by hand and the flattening of these bands was achieved by incorporating longer-range hoppings in the tight-binding description. While providing an exciting proof of principle, these models typically require careful fune-tuning of hopping parameters, making experimental realization a daunting task. In our work, we establish an alternative route towards Landau level-like electronic bands, which relies on orbital degrees of freedom. Orbital degrees of freedom are generically relevant in many transition metal (TM) compounds, which at the same time feature strong electron-electron interactions [24,25]. When itinerant electrons are coupled to localized spins, it is known that geometric frustration can stabilize non-coplanar spin-chiral magnetic textures [26-29]. The Berry phase that electrons acquire in the background of this spin texture is indistinguishable from an Aharonov-Bohm phase and induces nontrivial topology in the electronic bands [27-28,30-32]. We have demonstrated that the bands are considerably flattened for d-orbital systems on a frustrated triangular and kagome lattice [33].

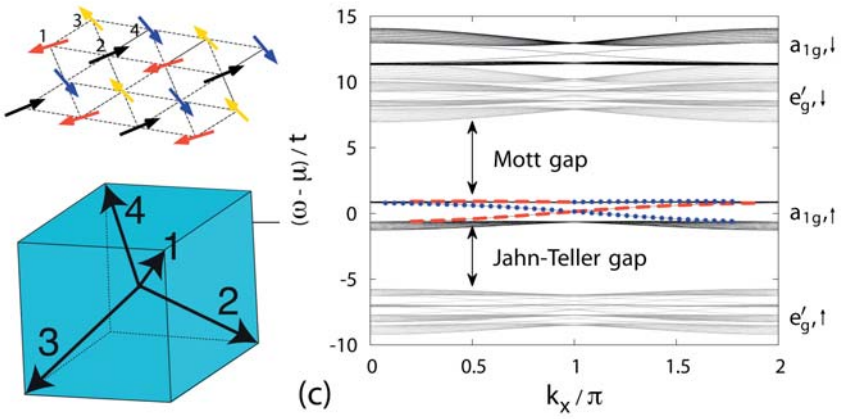

Fig. 2: (a) and **(b)** show the non-coplanar chiral spin texture on the triangular lattice. **(c)** shows the single-particle spectrum calculated in the mean-field solution on a strip geometry. The lower Hubbard-Kondo band is spin polarized in the direction of the chiral spin texture on every site. The half-filled a1g orbital level is shown to gapped as a consequence of the chiral spin pattern with chiral edge states traversing the gap.

In addition, we study a fully interacting model of t_{2g} orbitals on a triangular lattice with a mean-field treatment and find that the chiral spin texture, which carries the topologically nontrivial characteristics of the bands, spontaneously emerges as the ground state for a filling of 2.5 electrons per site. The t_{2g} orbital manifold consists of 3*d*-orbitals which are separated from the other two as a consequence of the local cubic crystal field. The overall triangular lattice symmetry splits this manifold further, leading to a nondegenerate level and a doubly degenerate level. In the mean-field ground state, two electrons occupy the lower lying doubly degenerate level at each site, having their spin arranged in the spin-chiral pattern. The single-orbital level is then half filled, with the restriction that all spins point in the direction of the chiral spin pattern. The resulting nontrivial electronic bands, one of them now being very flat, are shown in Fig. 2.

This situation is very reminiscent of the Kondo Lattice model (KLM), where itinerant electrons are coupled to localized spins by Hund's rule coupling. In fact, for large on-site Coulomb repulsion, Hund's rule coupling and crystal field splitting, we can map the fully interacting model (with three orbitals) onto a Kondo Lattice model, with a charge plus spin degree of freedom – hence a single orbital. The low energy configurations correspond to the mean-field solution as described above, with all spins aligned and arragned in the chiral ordering. In second order perturbation theory, we can include virtual processes via high-energy sectors. Working out these second order processes we find that they introduce next-nearest neighbor and nex-next-nearest neihbor hopping into the effective one-orbital KLM. This provides an explanation for the band-flattening in this particular case: orbitals induce effective longer-range hoppings.

We can take this simple one-orbital model and see whether nearest-neighbor Coulomb interactions indeed lead to a FQH state upon fractional filling of the nearly-flat band. This problem can be studied by exact diagonalization using Lanczos [20,34-35]. For several filling fractions we find clear signatures of a FQH state, as is presented in Fig. 3.

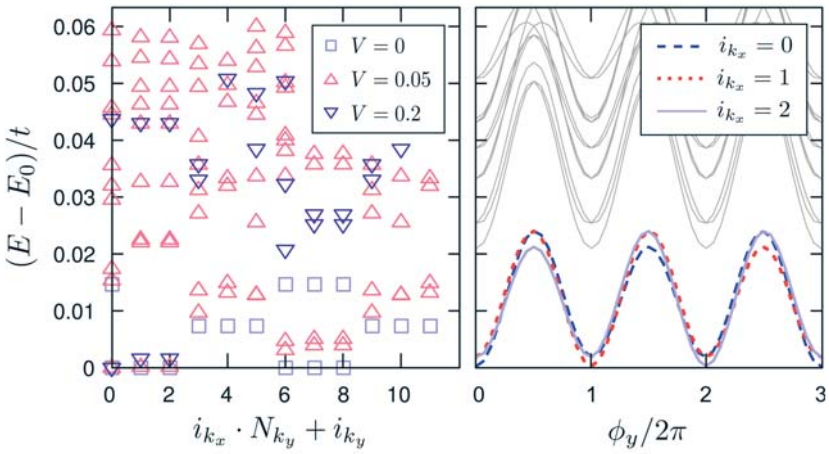

Fig. 3: (a) Energy spectrum obtained with exact diagonalization for the single-orbital effective model with nearest neighbor interaction, as function of interaction strength. The filling fraction here is 2/3.
(b) Spectral flow of the ground state manifold as function of adiabatic flux insertion.

Taking the filling of 2/3 as an example, we find the expected 3-fold topological ground state degeneracy. In addition, we calculated that upon adiabatic flux insertion, the ground state manifold exhibits spectral flow: they level-cross. A third key signature is Chern number, which is related to the fractionally quantized off-diagonal Hall conductivity and should equal the filling fraction. We find this to be case with an error margin smaller than 1% [36].

In conclusion, in our work we show that orbital degrees of freedom in transition metal oxides provide a route towards narrow topological bands. Second, we demonstrate the spontaneous formation of a nontrivial spin-chiral state for a t_{2g} orbital system on the triangular lattice, on the mean-field level for a interacting model with on-site interactions. And finally, we obtain signatures of a Fractional Quantum Hall state on a triangular lattice for a simple model derived from the strong coupling limit of the three-orbital model.

[1] K. v. Klitzing *et al.*, Phys. Rev. Lett. **45**, 494 (1980).
[2] D. J. Thouless *et al.*, Phys. Rev. Lett. **49**, 405 (1982).
[3] F. D. M. Haldane, Phys. Rev. Lett. **61**, 2015 (1988).
[4] C. L. Kane *et al.*, Phys. Rev. Lett. **95**, 226801 (2005); ibid. 146802 (2005).
[5] M. König *et al.*, Science **318**, 766 (2007).
[6] B. A. Bernevig *et al.*, Science **314**, 1757 (2006).
[7] L. Fu *et al.*, Phys. Rev. Lett. **98**, 106803 (2007).
[8] R. Roy, Phys. Rev. B **79**, 195322 (2009).
[9] J. E. Moore and L. Balents, Phys. Rev. B **75**, 121306 (2007).
[10] A.P. Schnyder et al., Phys. Rev. B **78**, 195125(2008)
[11] M. Hasan and C. Kane, Rev. Mod. Phys. **82**, 3045 (2010).
[12] X.-L. Qi and S.-C. Zhang, Rev. Mod. Phys. **83**, 1057 (2011).
[13] H. Zhang *et al.*, Nature Phys. **5**, 438 (2009).
[14] Y. Xia *et al.*, Nature Phys. **5**, 398 (2009).
[15] D. C. Tsui *et al.*, Phys. Rev. Lett. **48**, 1559 (1982).
[16] R. B. Laughlin, Phys. Rev. Lett. **50**, 1395 (1983).
[17] C. Nayak *et al.*, Rev. Mod. Phys. **80**, 1083 (2008).
[18] E. Tang *et al.*, Phys. Rev. Lett. **106**, 236802 (2011).
[19] K. Sun *et al.*, Phys. Rev. Lett. **106**, 236803 (2011).
[20] T. Neupert *et al.*, Phys. Rev. Lett. **106**, 236804 (2011).
[21] X.-L. Qi, Phys. Rev. Lett. **107**, 126803 (2011).
[22] M. Barkeshli and X.-L. Qi, arXiv:1112.3311.
[23] X. Hu, M. Kargarian and G. A. Fiete, Phys. Rev. B **8**4, 155116 (2011).
[24] K. I. Kugel and D. I. Khomski, Physics Uspekhi **25**, 231 (1982).
[25] Y. Tokura and N. Nagaosa, Science **288**, 462 (2000) .
[26] R. Shindou and N. Nagaosa, Phys. Rev. Lett. **87**, 116801 (2001).
[27] I. Martin and C. D. Batista, Phys. Rev. Lett. **101**, 156402 (2008).
[28] Y. Akagi and Y. Motome,J. Phys. Soc. Jpn. **79**, 083711 (2010).
[29] G.-W. Chern, Phys. Rev. Lett. **105**, 226403 (2010).
[30] K. Ohgushi *et al.*, Phys. Rev. B **62**, 6065 (2000).
[31] Y. Taguchi *et al.*, Science **291**, 2573 (2001).
[32] X. Chen *et al.*, Phys. Rev. B **81**, 064420 (2010).
[33] J. W. F. Venderbos *et al*, Phys. Rev. Lett. **107**, 116401 (2011).
[34] D. N. Sheng *et al.*, Nature Comm. **2**, 389 (2011).
[35] N. Regnault and B. A. Bernevig, Phys. Rev. X **1**, 021014 (2011)
[36] J.W.F. Venderbos *et al.*, arXiv:1109.5955 (2011)

β-HgS: A Strong 3D Topological Insulator with Anisotropic Surface States

F. Virot, R. Hayn, M. Richter, J. van den Brink

We establish the presence of topologically protected edge states on the (001) surface of metacinnabar (HgS in the zincblende structure) using density-functional electronic structure calculations. The Dirac point of the edge state cone is very close to the bulk valence band maximum. The Dirac cone is anisotropic with a large electron velocity along one diagonal of the surface elementary cell and a nearly flat dispersion in the perpendicular direction. The strong anisotropy originates from a broken fourfold rotoinversion symmetry at the surface.

Topological insulators (TI) distinguish themselves from ordinary insulators due to the presence of a nontrivial topological invariant in the bulk band structure. Although there is an excitation gap in the bulk as in conventional band insulators, the topological properties of the bulk band structure dictate that there be gapless modes at the surface. These surface states of a threedimensional (3D) TI form massless Dirac cones. Potential applicability for spintronics arises because the surface states of such a 3D TI appear in time-reversed pairs in which the two electrons have both opposite spin and velocity.

From the material's viewpoint, 3D TI's discovered so far are the binary compounds Bi_2Se_3, Sb_2Te_3, Sb_2Te_3, and the alloy $Bi_{1-x}Sb_x$. The presence of Dirac cones has been established by photoemission, but direct electronic transport evidence for metallic surface states on top of an insulating bulk is lacking, mainly because of the small bulk band gaps. Also, 3D-TI behavior was proposed in certain ternary Heusler compounds, in β-Ag_2Te and other systems. We recently predicted that metacinnabar, the binary compound β-HgS, is a strong 3D topological insulator [1]. As opposed to other TI's discovered to date, the topologically protected Dirac cone on the (001) surface of HgS in the zinc-blende structure is very anisotropic.

Metacinnabar is a gray-black natural mineral, found in mercury deposits that are formed near-surface, under low-temperature conditions. The bulk electronic structure of HgS in the zinc-blende structure has been considered before. Delin [2] found HgS to be insulating with an unconventional band order due to spin-orbit coupling: At the Γ-point the conduction band minimum has p-character and the s-band, which usually builds the conduction band minimum, is about one eV below the Fermi level. For lattice structures with inversion symmetry the parity criteria of Fu and Kane [3] guarantee that an inverted semiconductor is a topological insulator, but owing to the lack of inversion symmetry of the zinc-blende crystal structure of β-HgS these criteria do not apply. We therefore established the TI nature of β-HgS by explicitly calculating its surface states.

To this end we performed high precision, all electron, full potential and fully relativistic electronic structure calculations using the FPLO code developed at IFW [4]. We systematically studied slabs containing a stack of n elementary cells with n ranging from 3 to 8. With increasing slab thickness the gap caused by the coupling of the surface states at opposite sides of the stack gradually closes (see Fig. 2a) and a band crossing appears which is most clearly seen for the 8-layer slab the band structure of which is shown in Fig. 1. In this figure the band structure of the slab calculation is superimposed with the bulk band structure projected onto the surface. There are four bands crossing the Fermi level at the Γ-point. Two of them belong to the top and two of them to the bottom layer, i.e. there is one Dirac cone per surface layer. The calculated weights of these bands clearly show that they are surface bands with predominantly 3p character from the sulfur atoms in the sub-surface atomic layer. It is remarkable that these surface states decay rather slowly into the bulk (see Fig. 2b), which explains the remaining (tiny) gap for finite layer thickness.

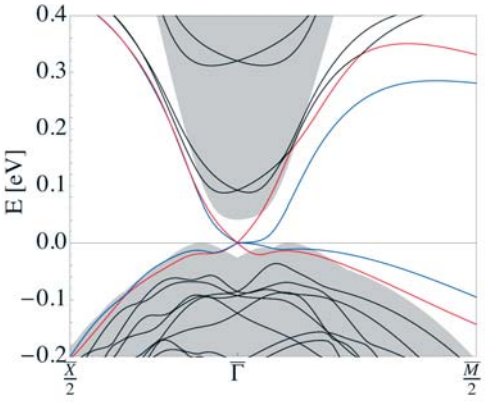

Fig. 1: Band structure of the 8-layer slab (lines) superimposed with the bulk band structure projected onto the surface (shaded area). The relevant surface bands are indicated in red (top surface) and blue (bottom surface).

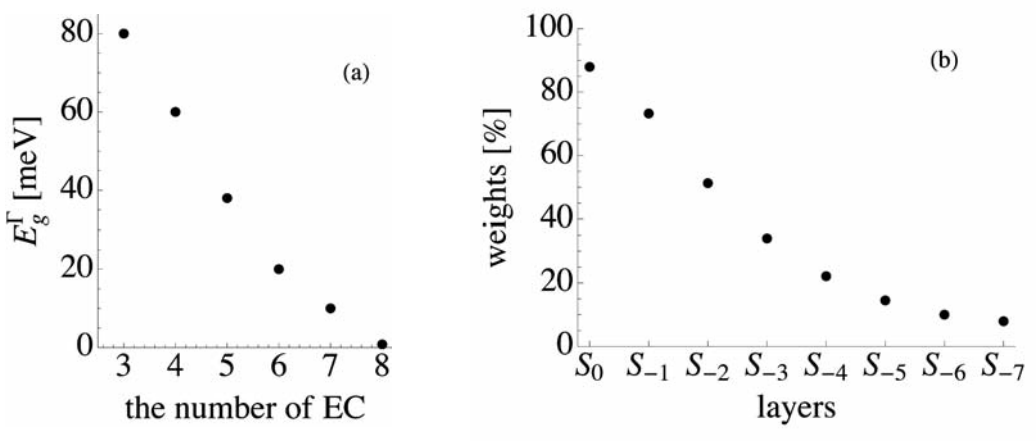

Fig. 2: (a) Width of the gap as function of the number of elementary cells (EC) and **(b)** sum of 3p weights over the four surface states at Γ, resolved for each sulfur layer in the slab of 8 EC. S_0 denotes the sulfur layer(s) next to the surface and S_{-7} denotes the innermost sulfur layer(s).

The two resulting Dirac cones are almost degenerate in the direction Γ-X but in the direction Γ-M they split up because of the broken fourfold rotoinversion symmetry at the (001) surface of the zincblende structure. The direction Γ-M corresponds to the diagonal [110] which is identical to the other diagonal [1-10] in the tetragonal, rotoinversion symmetric electronic structure of the slab (space group 111), but not at either of the surfaces. In fact, the Dirac cone with the large dispersion along [110] belongs to the top surface and the other one with two nearly flat bands above and below the crossing point corresponds to the bottom surface. Along the other diagonal, these roles are interchanged. The anisotropy can effectively be described by a crystal field splitting of p-orbitals that build the Dirac cone of the surface [1].

To summarize, our density-functional calculations prove that β-HgS is a topological insulator. A detailed study of the (001) surface reveals that its Dirac cone is very anisotropic. This quasi one-dimensionality of the topological electronic surface states arises from a broken fourfold rotoinversion symmetry and contrasts the perfectly isotropic bulk band structure. From this observation we expect instead an *isotropic* Dirac cone at the (111) surface since the threefold rotation axis along the (111) direction of the bulk remains unbroken at the (111) surface. These predictions can directly be tested by experimental techniques that probe surfaces states, for instance high precision photo-emission experiments. In particular spin and charge transport at the (001) surface will be very sensitive to the anisotropy of the electronic structure.

[1] François Virot, Roland Hayn, Manuel Richter, and Jeroen van den Brink, Phys. Rev. Lett. **106** (2011) 236806.
[2] A. Delin, Phys. Rev. B **65**, (2002) 153205.
[3] L. Fu and C. L. Kane, Phys. Rev. B **76**, (2007) 045302.
[4] http://www.fplo.de/

Cooperation: Institut de Matériaux, Microélectronique et Nanosciences de Provence, Univ. Aix-Marseille, France

Three-dimensional hybrid organic/inorganic heterojunctions based on rolled-up nanomembranes

C. C. Bof Bufon, J. A. Espinoza, D. J. Thurmer, Ch. Deneke, O. G. Schmidt

In this work we fabricate and characterize novel three-dimensional electronic devices based on strained hybrid organic/inorganic nanomembranes. By combining bottom-up with top-down approaches, we are able to prepare heterojunctions consisting of single organic molecular monolayers sandwiched between metal and/or single-crystalline semiconductor nanomembrane contacts. This particular heterojunction layout has not been realised to date by any other fabrication method such as conventional layer-by-layer deposition. One of the device architectures we pioneer here is a semiconductor/molecule/semiconductor tunneling diode consisting of epitaxially grown III-V nanomembrane contacts and a single organic monolayer. This combination gives rise to a device with completely new electrical characteristics which are not expected or possible to be demonstrated by either element separately. Furthermore, the structures can be patterned on a chip with a yield loss of less than 5%.

The investigation of the electronic properties of molecular systems as well as their potential use for future device applications is strongly correlated with the way they are connected to the external world [1]. Nowadays, self-assembly is widely accepted as a standard technique to generate complex structures on many length scales [2]. One of these self-assembly processes consists of strained metal layers which spontaneously "curl up into close rolls" once they detach from their host substrate [3, 4]. Here we present a method based on self-released strained nanomembranes (metallic and/or semiconducting) for electrically contacting single molecular layers. During release of the nanomembrane, the strain relaxation gives rise to a self-rolling process in which the membrane bonds back to the substrate top surface where the thin organic layer was previously deposited. By this means, we are able to fabricate not only standard metal-molecule-metal and metal-molecule-semiconductor structure configuration but also unique semiconductor-molecule-semiconductor heterojunctions. In this latter case, the type of doping and its concentration can be independently and precisely set for each electrode in order to tune the devices electronic properties. Such a novel hybrid device was observed to display completely different electric characteristics which are not expected or possible to be demonstrated by using their elements separately. In addition, the strained nanomembrane based electrodes provide a soft and robust contact on top of the organic film. Consequently, no damage to the organic layer and short circuits via pinholes, which is commonly observed in SAMs has been observed. Since the contacting process takes place at room temperature, the metallic diffusion into the organic

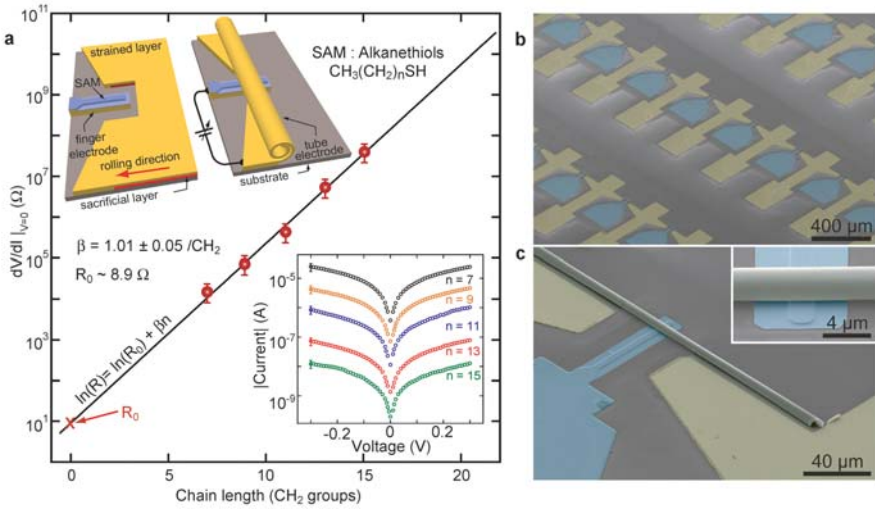

Fig. 1: (a) Differential resistance at zero bias condition ($R = dV/dI|_{V=0}$) as a function of the number of CH_2 groups (obtained from the *i-v* characteristics displayed in the bottom inset) for Au-alkanethiol SAM/Au heterojunctions. The uppers inset shows (left) the device structure before rolling and (right) after rolling. **(b)** Scanning electron microscope (SEM) image of an array of devices highlighting the excellent reproducibility and parallelism of the fabrication process with a yield of at least 95%. **(c)** SEM image of a single element. The inset highlights the overlap of the tube and metallic finger electrode. (after [5]).

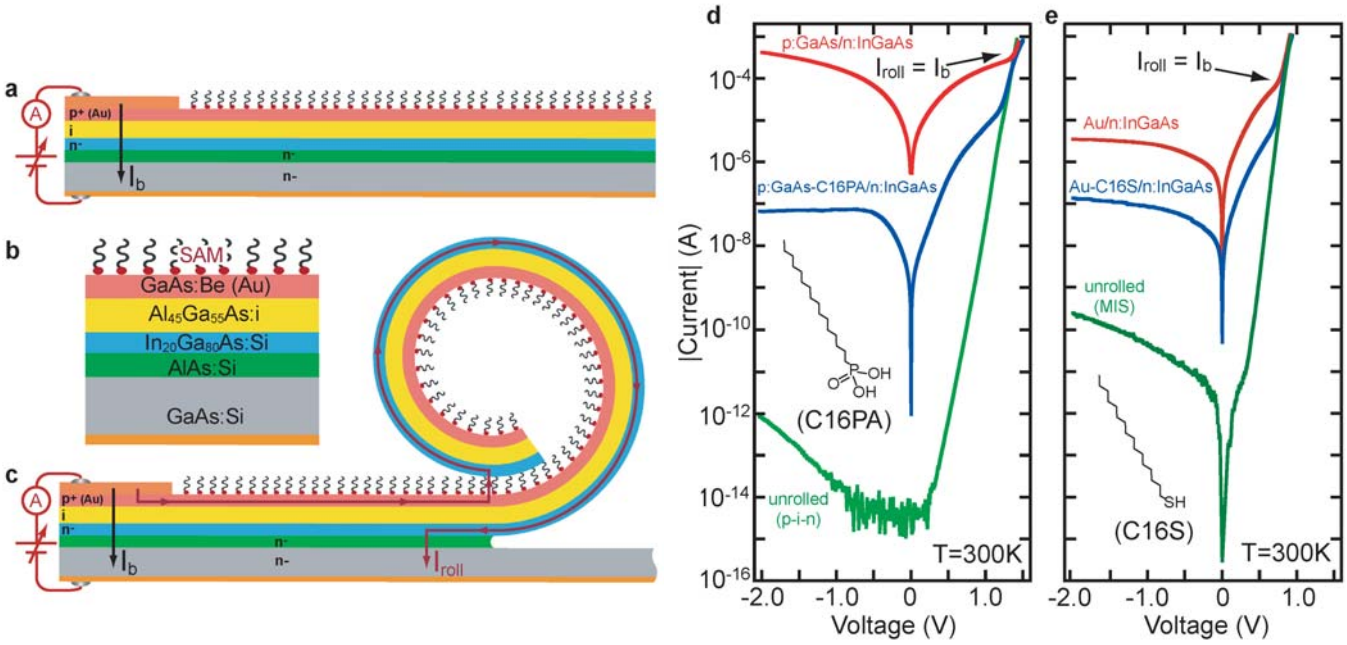

Fig. 2: (a) Schematic of a multi-layer semiconductor device before rolling. The detailed layer structure for the unrolled devices, including the SAM, is revealed in **(b)**. The rolled-up device **(c)** is formed after the selective removal of the sacrificial layer. The *i-v* characteristics for the heterojunctions having p-doped GaAs as a top layer, before and after rolling, with and without the SAM incorporation are shown in **(d)**. Similarly the traces for heterojunctions incorporating Au as a top layer are shown in **(e)**. The molecular structure of the hexadecylphosphonic acid (C16PA) and hexadecylthiol (C16S) are also shown in the inset of (d) and (e), respectively. (after [5]).

layer is suppressed. Furthermore, applying the self-rolling phenomenon, we achieve an approach that is fully integrative on-chip, and several components can be fabricated in parallel using well-established semiconductor processing technologies. Additionally, all the procedures adopted here can be employed to create even more complex heterojunctions based on a variety of different inorganic and organic materials.

As a first example, self-assembled monolayers (SAM) of alkanethiols with chain lengths varying from 6 to 16 carbon atoms are connected between bottom finger-like electrode and a top rolled-up metallic tube (inset of Fig. 1a). The *i-v* characteristics indicate that the current is strongly dependent on the SAM chain length and the systematic change of the chain length furthermore reveals direct tunneling as the dominant transport mechanism. As expected for coherent and nonresonant tunneling, the differential resistance ($R = dV/dI|_{V=0}$) exhibits an exponential dependence on the chain length.

In addition to contacting molecules with metallic electrodes, we also demonstrate an approach where semiconductor layers are used to inject charge into, and through, the molecular layers. Fig. 2a is a sketch of the layer structure before the release of the semiconducting nanomembrane. In the rolled-up architecture (Fig. 2c), a voltage bias applied between the top and back contacts creates a current that can flow into the top p:GaAs electrode. Subsequently it is radially injected across the hexadecylphosphonic acid (C16PA) layer and then into the n:InGaAs nanomembrane. The current flows tangentially around the n:InGaAs tube wall and is then collected via the back contact. A similar concept is still valid if the p:GaAs layer is replaced by an Au film.

In the *unrolled* device, the measured current (I_M) originates solely from the leakage through the AlGaAs barrier (I_b). In the *rolled-up* device however, I_M becomes a combination of the tangential current around the n:InGaAs nanomembrane (I_{roll}) and I_b (Fig. 2c). The comparison between rolled and unrolled devices is shown in Fig. 2d. At reverse bias I_M is below 1 pA ($I_M = I_b$) in the unrolled device. At the same bias conditions, an increase of at least 8 orders of magnitude is observed after the formation of the p:GaAs/n:InGaAs heterojunction ($I_M = I_b + I_{roll}$). This observation is a clear evidence of the radial injection and tangential transport across the rolled-up semiconductor nanomembrane. At high forward bias, I_b increases exponentially and dominates for $V > 1V$ ($I_b > I_{roll}$). Here all *i-v* curves merge into a single trace and the maximum allowed forward bias in the rolled-up junction can be defined as the point at which $I_b = 0.1 I_{roll}$. As shown in Fig. 2e, the behaviour of the metal-insulator-semiconductor (MIS) structure after rolling is qualitatively similar to the *p-i-n* device. In both examples (MIS and p-i-n) the insulating layer behaves as an ultra-thin organic insulator.

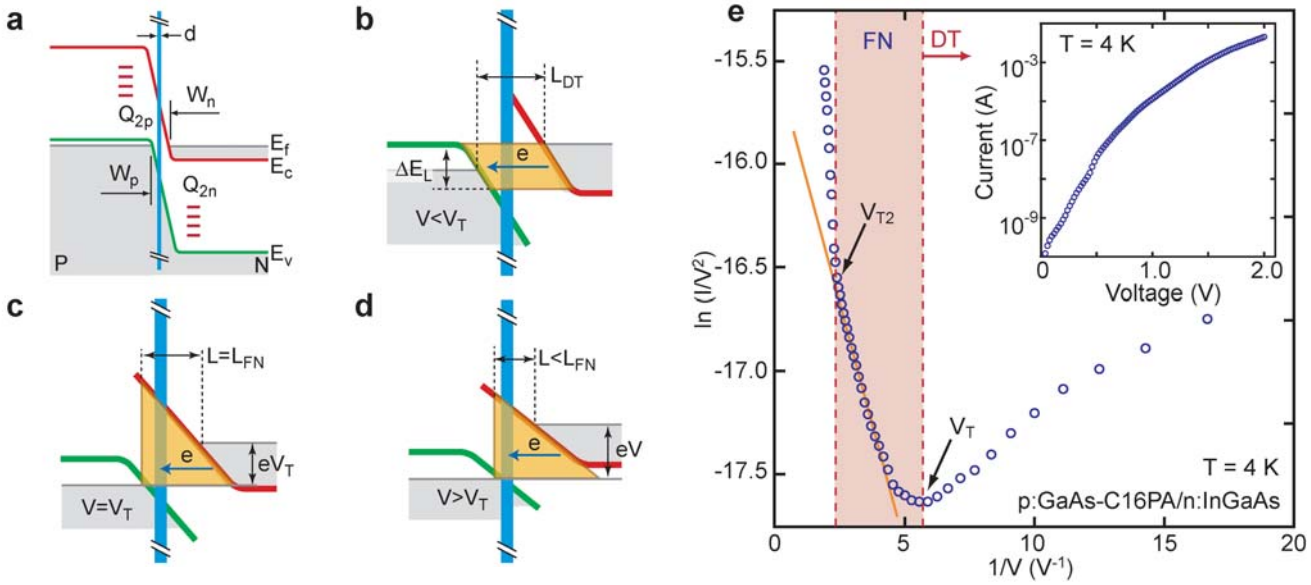

Fig. 3: (a - d) Band diagram schematics (not to scale) for the p:GaAs-C16PA/n:InGaAs heterojunction under different bias condition. a, In equilibrium the Fermi level in the *p*-side of the junction, which is below the top of the valence band (VB), is aligned to the Fermi level at the *n*-side, which sits above the bottom of the conduction band (CB). b, A zoom of the central region of the band structure shows a rectangular-like barrier that is present at low bias condition ($V < V_T$). As the voltage bias increases, the hybrid barrier shape changes from rectangular (b) to triangular (c) at $V = V_T$. At this point a transition from DT to FN is observed (e). For $V > V_T$, FN dominates (d) until the both W_p and W_n become field independent. In **(e)** the clear transition from DT to FN to DT is shown, indicated by the linear fit for FN tunneling in the intermediate region (the inset highlights the measured *i-v* trace). (after [5]).

In Fig. 3a a simple band structure model (not to scale) is proposed for such a junction at zero bias condition. The hybrid barrier is assumed to be a combination of the C16PA molecular barrier (d) with the potential barriers at the chemisorbed p:GaAs-C16PA (W_p) and physisorbed C16PA/n:InGaAs (W_n) interfaces of the junction. Due to the high density of charges in the semiconducting layers, the Fermi level on the *p*-doped interface is below the top of the valence band (VB) while the *n*-doped interface sits above the bottom of the conduction band (CB). By comparing the value of barrier height (Φ) reported for alkyl chains bonded to p:GaAs (1.1 ± 0.3 eV) with the maximum applied voltage used to characterize the junctions, we assume that most changes in the total width/shape of the hybrid tunneling barrier ($L = W_p + W_n + d$) can be attributed to W_p and W_n, which are sandwiching the molecular layer. Due to the asymmetric nature of both semiconducting electrodes, the changes of W_p and W_n as the voltage bias increases are expected to be different. Fig. 3e shows the field emission plot according to the equation [6]:

$$I \propto V^2 exp\left(-\frac{4W\sqrt{2m_e\phi^3}}{3\hbar qV}\right)$$

As illustrated in Fig. 3b, for low forward bias, direct tunneling (DT) occurs across the rectangular-like potential barrier (with $L = L_{DT}$) since the band bending is not very pronounced and an overlap between the filled levels in the CB and the empty levels in the VB is expected. Once the potential increases (Fig. 3c), this overlap decreases and, associated with an asymmetric change of W_p and W_n, the tunneling probably becomes strongly voltage-dependent. At the transition voltage V_T, the hybrid barrier assumes a triangular-like shape (with $L = L_{FN}$) and the transition from DT to field emission (FN) occurs. For $V > V_T$, the transport is mainly field-dependent with a systematic decrease of the tunneling distance as the voltage increases (Fig. 3d). For $V >> V_T$, we expect that both W_p and W_n reaches their minimum width and becomes bias independent. Consequently, DT once more becomes the dominant transport mechanism with tunneling occurring from

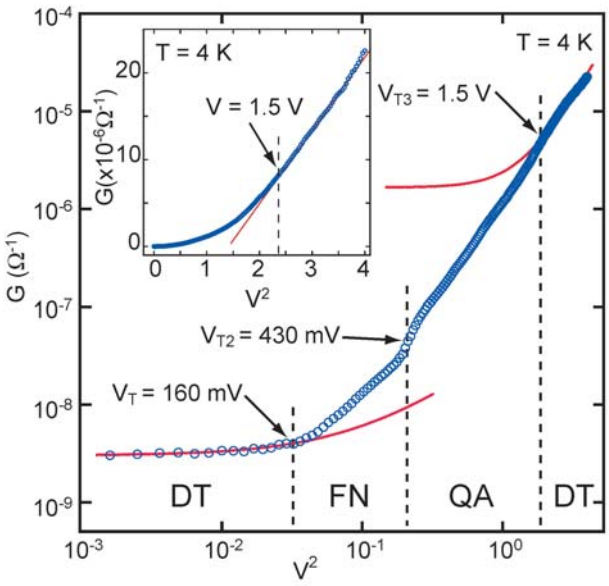

Fig. 4: All transitions observed for the p:GaAs-C16PA/n:InGaAs heterojunction at 4 K. The fitting lines represent the agreement with the Simmons model and define the region where DT takes place. In the intermediate region, both FN and surface state-enhanced tunneling (QA) takes place. For $V > 1.5$ V DT is once again recovered (after [5]).

the CB to VB across the rectangular-like potential barrier. This second transition (FN to DT) however, is clearly observed only at low temperatures (Fig. 4).

In conclusion, we have demonstrated a reliable approach to contact molecular layers with a contact area much smaller than 1μm^2 using conventional semiconductor processing methods. The fabrication process is highly integrative and several devices can be processed in parallel with a yield higher than 95%. We have shown the assembly and characterization of a hybrid semiconductor/SML/semiconductor heterojunction, where epitaxially grown III-V nanomembranes are used as charge injectors in self-assembled organic monolayers. This system displays unique transport characteristics, namely, the sequential transition from direct tunneling to field-emission and then returning to direct tunneling. Consequently, by connecting molecular layers with semiconducting contacts, devices with completely different electronic characteristics are created where such characteristics are not expected, or possible, using either element separately. Furthermore, we have shown that it is possible to use Au as an electrode material in order to create new MIS structures.

[1] H. Haick et al. Accounts of Chemical Research **41**, (2008).359.
[2] G. M. Whitesides et al. Science **295**, (2002). 2418
[3] O. G. Schmidt et al. Nature **410**, (2001).168.
[4] C.C. Bof Bufon et al. Nano Letters **10**, (2010) 2506.
[5] C.C. Bof Bufon et al. Nano Letters **11**, (2011) 3727.
[6] S. M. Sze *Physics of Semiconductor Devices*; Wiley: New York, 1981.

Cooperation: H. Klauk, Max Planck Institute for Solid State Research, Stuttgart, Germany.
Funded by: DFG FOR 1154 "Towards Molecular Spintronics".

Looking at the Nut inside a Shell: NMR Spectroscopic Studies of Nitride Clusterfullerenes

Y. Zhang, L. Zhang, S. Schiemenz, S. Klod, S. Avdoshenko,[1] G. Cuniberti,[1] A. Popov, L. Dunsch

Recent developments in the NMR spectroscopic studies of endohedral metallofullerenes establish important role of NMR spectroscopy in the fullerene science. Molecular structure, dynamics, magnetic state and chemical environment of all kinds of atoms in the endohedral fullerene molecule both in the diamagnetic and paramagnetic state can be now directly addressed by multinuclear NMR spectroscopy.

Among the endohedral metallofullerenes (EMFs) encapsulating one or more metal atoms or a cluster in their inner space, the nitride clusterfullerenes (NCFs) of the general formulae $M_3N@C_{2n}$ stand out for their enhanced yield, stability and the largest variety of structures both for the cage and the cluster. From the structural point of view, the molecule of NCF consists of three key „shells": the outer carbon cage, the central nitrogen atom, and three metal atoms in between. An extent and the nature of interactions between these shells determines electronic and magnetic properties of NCFs. Description of the valence state and dynamics of all shells is thus of paramount importance for the understanding of their mutual influence.

In the spectroscopic studies of EMFs, the carbon cages have by far the highest impact. For instance, absorption spectra are dominated by $\pi \rightarrow \pi^*$ excitations of the fullerene; likewise, vibrational spectra of EMFs are dominated by their carbon cage. ^{13}C NMR has been a standard tool in the structural studies of fullerenes and diamagnetic EMFs for two decades. For instance, even subtle changes in the local pyramidalization angles of the metal-bonded carbon atoms induced by the increase of the cluster size in the series of $Lu_xSc_{3-x}N@C_{80}$ and $Lu_xY_{3-x}N@C_{80}$ ($x = 0-3$) NCFs can be revealed with the use of ^{13}C NMR spectroscopy.[1] However, addressing paramagnetic NCFs (for instance, encapsulating lanthanides) by ^{13}C NMR spectroscopy still remains a challenge because of the fast nuclear spin relaxation which severely broadens the signals. On the other hand, when accessible, such spectroscopic data would provide additional information on the magnetic state of the endohedral cluster.

Fig. 1 shows ^{13}C NMR spectrum of $CeLu_2N@C_{80}$ NCFs in comparison to the spectrum of diamagnetic $Lu_3N@C_{80}$.[2] High symmetry of the carbon cage and fast rotation of the nitride cluster at the room temperature results in only two narrow ^{13}C signals in 3:1 ratio

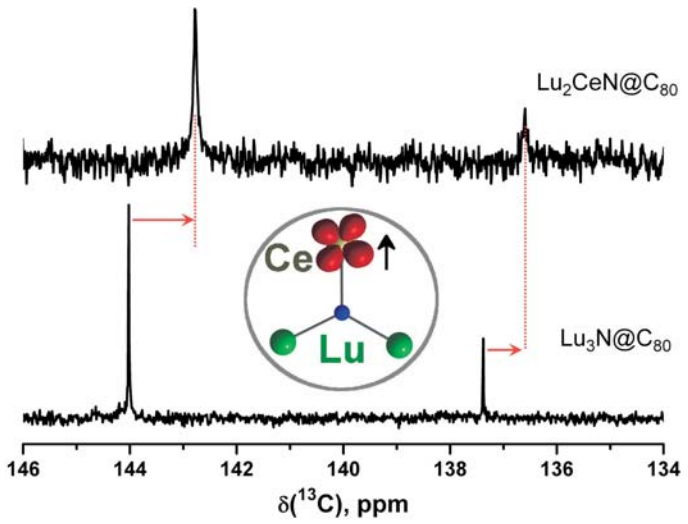

Fig. 1: Room temperature ^{13}C NMR spectra of $Lu_2CeN@C_{80}$ and $Lu_3N@C_{80}$, and schematic description of the $CeLu_2N@C_{80}$ with unpaired electron and spin density localized on Ce. Paramagnetic shifts are indicated by red arrows.

in the spectrum of $Lu_3N@C_{80}$. Similar two signals are also detected in the spectrum of $CeLu_2N@C_{80}$, but they are ca 10-fold broadened and significantly shifted. Besides, ^{13}C chemical shifts (δ) of $CeLu_2N@C_{80}$ exhibited noticeable temperature dependence (whereas the signals of the diamagnetic $Lu_3N@C_{80}$, δ_{dia}, are virtually temperature-independent). These phenomena originate from the influence of the paramagnetic metal ion (Ce^{3+} with localized 4f-electron) on the magnetic state of the carbon atoms. The paramagnetic contribution to the chemical shift has two major contributions: $\delta = \delta_{dia} + c_{Fc}/T + c_{pc}/T^2$, where c_{Fc}/T is the Fermi contact term („through bond", describes transfer of the spin density to the carbon atoms) and c_{pc}/T^2 is the pseudocontact term („through space", determined by effective magnetic moment of the metal ion). Extrapolation of the temperature-dependent chemical shifts to the diamagnetic limit (i.e. $1/T^2 = 0$ and $1/T = 0$) should yield the δ_{dia} value close to the diamagnetic analogues, which allows one to determine which term is the dominant. For $CeLu_2N@C_{80}$ this analysis shows that the contribution of Fermi contact term is negligible, in line with localization of the whole spin density on Ce^{3+}. Hence, paramagnetic chemical shift in $CeLu_2N@C_{80}$ reflects the magnetic state of Ce^{3+} ion inside the carbon cage.[2]

Ce^{3+} has only one unpaired electron and the smallest magnetic moment in the lanthanide series (2.5 μ_B). With the increase of the number of electrons in the 4f-shell, the measurement of the ^{13}C NMR spectra becomes more complicated due to the increased line width. Yet, successful measurement of the ^{13}C NMR spectra was accomplished in our group even for NCFs with such lanthanides as Dy, Tb, Ho, and Tm. As an example, Fig. 2 compares ^{13}C NMR spectra of $HoSc_2N@C_{80}$ and $Ho_2ScN@C_{80}$ to that of the diamagnetic $Sc_3N@C_{80}$. In line with much higher magnetic moment of Ho^{3+} (10.6 μ_B), paramagnetic shift in $HoSc_2N@C_{80}$ is an order of magnitude large than in $CeLu_2N@C_{80}$, and is increased almost twice in $Ho_2ScN@C_{80}$, *i.e.* when one more Sc atom is substituted by Ho. Thus, paramagnetic ^{13}C NMR spectroscopy appears to be an efficient probe of the magnetic state of endohedral metal atoms and their interaction with the carbon cage.

NMR spectroscopic studies of NCFs are not limited to the ^{13}C NMR. ^{45}Sc has nuclear spin 7/2 and hence allows for Sc-NMR measurements, although the signal in the ^{45}Sc-NMR is broadened due to quadrupole moment of Sc. The method has been successfully employed in the studies of the structure and dynamics of endohedral Sc clusters, but such studies were limited so far to diamagnetic EMFs.[3-5] Fig. 3 shows ^{45}Sc-NMR spectra of $HoSc_2N@C_{80}$ measured at different temperatures. At the room temperature the signal is ca 3 times broadened and shifted by 900 ppm compared to the ^{45}Sc chemical shift in $Sc_3N@C_{80}$. Importantly, for the same compound, paramagnetic shift of the ^{45}Sc signal is much

Fig. 2: Room temperature ^{13}C NMR spectra of $Sc_3N@C_{80}$, $HoSc_2N@C_{80}$, and $Ho_2ScN@C_{80}$. The asterisk marks the solvent's signal. Paramagnetic shifts are indicated by red and blue arrows.

Fig. 3: Variable-temperature ^{45}Sc NMR spectra of $HoSc_2N@C_{80}$.

Fig. 2

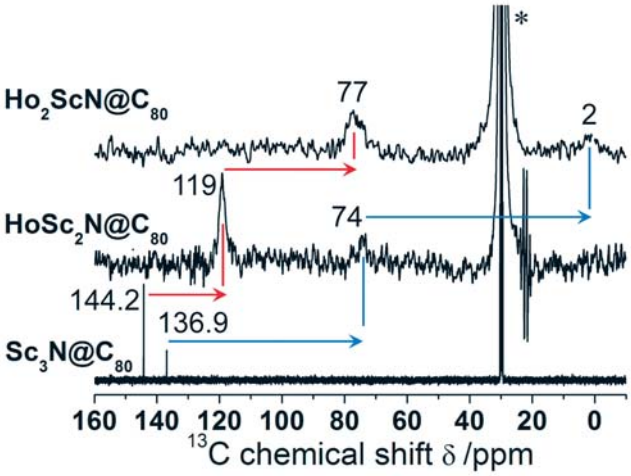

Fig. 3

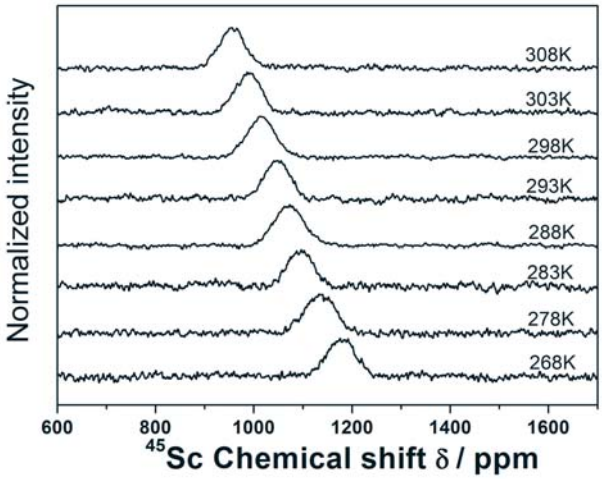

higher than that in the ^{13}C NMR spectrum, which can be explained by a dynamic nature of the ^{13}C NMR. In ^{13}C NMR, the measured signal is averaged for all carbon atoms of a given type (and hence it has contribution both from the atoms which are far away from the Ho ion and have small instant paramagnetic contribution and from those which are close to Ho). On the contrary, the $HoSc_2N$ cluster has rigid geometry with constant Sc-Ho distances. As a result, ^{45}Sc NMR is a more sensitive probe of the paramagnetic effect of Ho atom. Analysis of the temperature dependence of the ^{45}Sc chemical shift shows that pseudocontact term is dominating here as well, which indicates that there is no "leakage" of the spin density from the Ho-4f shell to Sc atoms.

Direct observations of the spectroscopic response of the central nitrogen atom in NCFs are rather rare and are limited so far to only one work reporting the 1s(N) PES of nitrogen in $Sc_3N@C_{80}$.[6] Till recently, IR spectroscopy has been the most informative technique in the studies of the central nitrogen atom state in NCFs due to the high intensity of the antisymmetric metal–nitrogen stretching. Although nitrogen has non-zero nuclear spin, the use of NMR spectroscopy is mostly focused on the low-abundant ^{15}N isotope, because it is believed that the quadrupolar moment of ^{14}N nuclei severely broadens the signal and makes ^{14}N NMR studies hardly useful. However, the recent studies showed that NCFs exhibit surprisingly narrow ^{14}NMR peaks which makes ^{14}N NMR spectroscopy the method of choice in addressing the valence state of the nitrogen atom in NCFs.[4,7] Fig. 4 shows ^{14}N NMR spectra of $Lu_xSc_{3-x}N@C_{80}$ and $Lu_xY_{3-x}N@C_{80}$ ($x = 0–3$) mixed-metal NCFs. ^{14}N chemical shift appears to be very sensitive to the chemical environment of the nitrogen atom and exhibits linear dependence on x, i.e. on the composition of the cluster in each series of mixed clusterfullerenes.

To reveal the main factors affecting ^{14}N chemical shifts in nitride clusterfullerenes, shielding tensor components are analyzed in terms of Ramsey theory both in localized and canonical molecular orbitals.[7] ^{14}N chemical shifts in $M_3N@C_{80}$ and related systems are shown to be determined solely by nitrogen-localized orbitals, and in particular by N-$p_{x,y,z}$ atomic orbitals. As a result, the peculiarities of the nitrogen shielding in nitride clusterfullerenes can be interpreted by the simple analysis of the nitrogen-projected density of states and its variation in different chemical environments. Significant difference of the chemical shifts of $Lu_3N@C_{80}$ compared to $Sc_3N@C_{80}$ and $Y_3N@C_{80}$ is explained by relativistic effects.

In summary, multinuclear NMR spectroscopy has been found to be a particular important tool in the studies of nitride clusterfullerenes. By this approach it is now possible to address structural, magnetic, and electronic states of all structural "shells" comprising the endohedral fullerene molecule.

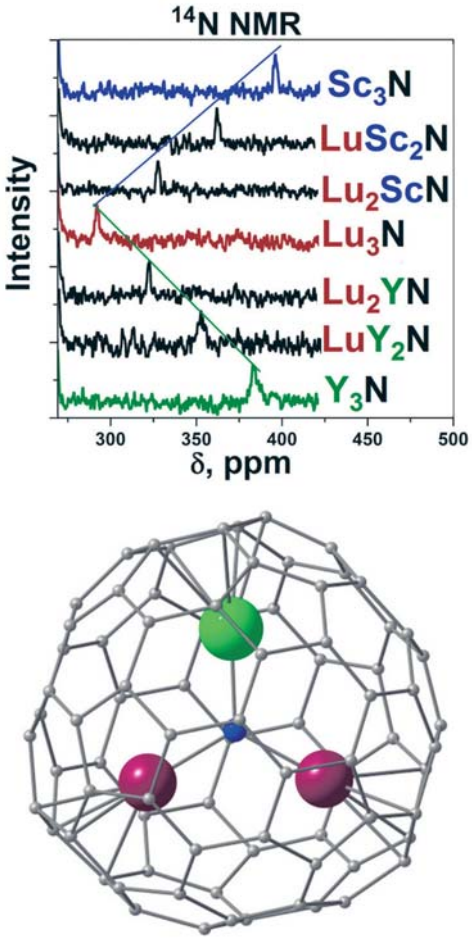

Fig. 4: ^{14}N NMR spectra of $Lu_xSc_{3-x}N@C_{80}$ and $Lu_xY_{3-x}N@C_{80}$ ($x = 0 – 3$) in CS_2 solution at room temperature. The structure of the $Lu_2YN@C_{80}$ molecule is shown on the left.

[1] S. Yang et al., Angew. Chem.-Int. Edit. Engl. **47** (2008) 8196.
[2] L. Zhang et al., Phys. Chem. Chem. Phys. **12** (2010) 7840.
[3] L. Dunsch et al., J. Am. Chem. Soc. **132** (2010) 5413.
[4] W. Fu et al., Chem. Commun. **47** (2011) 3858.
[5] S. Yang et al., J. Phys. Chem. C **113** (2009) 7616.
[6] L. Alvarez et al., Phys. Rev. B **66** (2002) 035107.
[7] A. A. Popov et al., J. Phys. Chem. C **115** (2011) 15257.

Cooperation: [1]TU Dresden
Funded by: DFG, AvH, Chinese Scholar Council

Direct imaging and analysis of the internal interfaces between carbon nanotubes and their catalyst particles

D. Pohl[1], F. Schäffel[1], C. Täschner[2], M. H. Rümmeli[2], C. Kisielowski[3], L. Schultz[1], and B. Rellinghaus[1]

Any functionalisation of carbon nanotubes, for which the relative orientation between their (metallic) catalyst particle and the tube axis is essential, requires a detailed knowledge on the nature of the internal interface between the particle and the outgrown tube. In the present work, this interface is characterized with atomic precision using state-of-the-art low voltage aberration-corrected transmission electron microscopy in combination with molecular dynamics simulations for the case of hard-magnetically terminated carbon nanotubes. Our results reveal the reduction of the carbon desorption energy as a physical guiding principle that determines the choice of the metal facets from which the carbon nanotubes are grown.

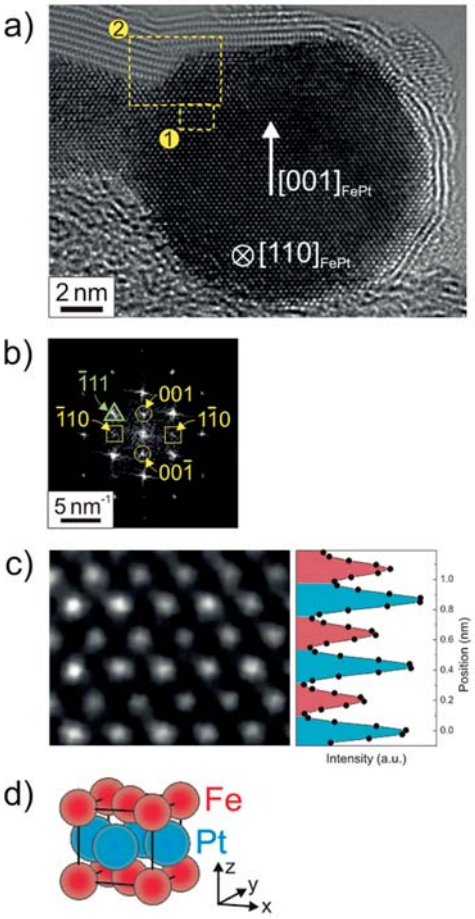

Fig. 1: Monochromised and aberration-corrected low-voltage HRTEM image of the tip section of a multi-wall CNT terminated with a FePt catalyst particle. **a)** HRTEM image. The [001] easy axis of magnetisation and the [110] zone axis orientation are indicated by an arrow and an encircled cross, respectively. Two regions #1 and #2 are marked for subsequent analysis. **b)** Fourier transform of the particle section in fig. a. Super structure reflections indicating the ordered $L1_0$ phase and the (regular) [111] reflection are labelled with yellow and green symbols, respectively. **c)** Magnification of region #1 in fig. a together with an intensity profile of this section as obtained along [001]. **d)** Schematic representation of the crystallographic cell of $L1_0$-ordered FePt.

For the application of carbon nanotubes (CNT) in electronic devices as well as in novel composite materials a detailed understanding of both their structure and growth mechanism at the atomistic level are required [1]. The functionalization of the ends of the CNT has become an important research field due to the potential to hereby modify their electronic and magnetic properties [2,3]. Functionalized CNT can thus be used to build up new functional micro-scaled structures with high performance.

Owing to its large magneto-crystalline anisotropy energy, $L1_0$ ordered tetragonal FePt is among the most intensively discussed materials when it comes to pushing the superparamagnetic limit towards minimum particle sizes [4]. As a consequence, this material is of particular interest for the realisation of a hard-magnetic termination of the CNT. In the present study, plasma-enhanced chemical vapour deposition (PE-CVD) is used to synthesize CNT from a Fe-Pt multilayer catalyst thin film stack [5] with the aim to implement hard-magnetic FePt nanoparticles at the end of the CNT. However, the orientation of the easy axes of magnetisation ([001] in $L1_0$-FePt) was random in these samples, whereas a controlled alignment of this (crystallographic) axis with respect to the CNT axis is desired for applications. Only if accomplished, magnetic functionalization can be effectively exploited.

Likewise prepared CNT are characterized by means of monochromated aberration-corrected HRTEM. In order to gain a deeper insight into the growth mechanism these structural investigations are focused on the atomically resolved characterisation of the inner FePt-CNT interface. This helps to (i) understand and (ii) control the relative orientation of the crystal lattice of the catalyst particle with respect to the CNT axis. Also unknown are the physical principles which rule the choice of a particular facet that then forms the metal-carbon interface. Consequently, the interface between the catalyst particle and the CNT is considered to play a key role for the CNT growth [6-9].

CNT are extremely susceptible to radiation damage. Therefore, HRTEM investigations are to be conducted at acceleration voltages as low as 80 kV. Furthermore, since the interatomic distances at the particle-CNT interface may vary over a wide range, high spatial frequencies are required to atomically image these interfacial layers. In this study, the structure of the internal metal-carbon interface of $L1_0$-FePt-terminated CNT is characterised by means of monochromated, aberration-corrected "Team 0.5" microscope at the NCEM in Berkeley.

Fig. 1a shows exemplarily a HRTEM image of the tip section of a multi-wall CNT (MWCNT) terminated with a FePt catalyst particle. The attachment of the CNT to the amorphous carbon film (see bottom part of the image) provides the necessary mechanical stability in order to obtain atomically resolved images. The Fourier transform of the particle (Fig. 1b) reveals that the particle exhibits the ordered $L1_0$ structure (cf. Fig. 1d) and is

oriented with its [110] zone axis parallel to the electron beam (i.e., perpendicular to the image plane). The [001] easy axis of magnetisation lies within the image plane as indicated by the white arrow. Fig. 1c shows a magnification of region #1 as marked in the original HRTEM image. Here, owing to the different scattering strengths of Fe and Pt atoms, the layered $L1_0$ structure manifests itself by an oscillation in the intensity profile obtained along the [001] direction in this region.

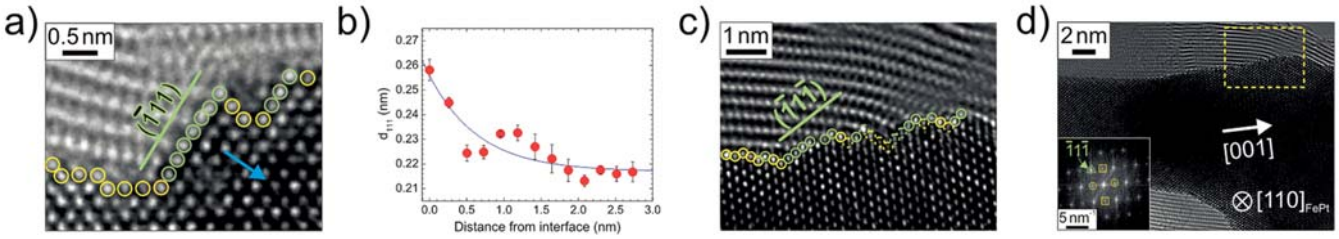

Fig. 2a shows a magnification of region #2 in Fig. 1a. In this region at the very metal-carbon interface, where the particle is only a few atoms thick, the strong differences between the scattering strengths of the heavy Fe and Pt atoms and the light C atoms provide a criterion based on which the atomic columns may be clearly attributed to either C or Fe/Pt from merely analyzing the image intensity (i.e., the grey value). As a result of this interface analysis, the edge atoms of the FePt particle are identified and labelled with circles. Here, those atom columns which belong to {111} type facets are labelled in green, whereas all others are labelled in yellow. From Fig. 2a and the Fourier transform in Fig. 1b it becomes evident that the four bottom-most concentric graphene sheets emanate from a (-111) facet. In order to show that this observation is not singular, a second HRTEM micrograph of such an internal metal-carbon interface is depicted in Figs. 2c and d. Again, the graphene sheets are found to originate from a {111} facet. Thus our experiments reveal that the carbon atom columns are predominantly emerge from {111} facets (in total more than 75% [14]). Fig. 2c furthermore reveals a frequently observed and pronounced bending of the graphene layers toward the {111} facets, which again confirms the rooting of the CNT on these particular facets. In Fig. 2b, another characteristic feature of these internal metal-carbon interface is presented. Here, the inter-planar {111} lattice spacing, d_{111}, is plotted as function of the distance from the interface. It can be seen that there is a significant increase of the lattice spacing upon approaching the interface which can even exceed 10% (as is the case in the depicted example). This dilation of the surface-near lattice is known as an enrichment of Pt at the surface of binary FePt particles and is considered to be the origin of a frequently observed reduction of the degree of $L1_0$ order in such particles [10-13]. Also the (surface-near) dissolution of C in the FePt catalyst particle and the interface itself can be ruled out as a possible origin for the observed lattice expansion close to the metal-carbon interface [14]. Molecular dynamic simulations are conducted to investigate why carbon preferentially emerges from the Pt-rich {111} facets of the FePt catalyst particle. Therefore, the changes of the desorption (or adsorption) energy of carbon atoms from various surfaces is calculated. Single carbon atoms were randomly positioned onto different surfaces, and the desorption energy was then estimated from the maximum energy difference between the substrate crystal with and without carbon (represented in Fig. 3a). For the {111}, {110}, and {100} surfaces of fcc Fe, the obtained adsorption energies are $E^{111} = -6.7$ eV, $E^{110} = -7.2$ eV, $E^{100} = -7.9$ eV respectively, whereas for Pt, $E^{111} = -3.8$ eV, $E^{110} = -5.1$ eV, $E^{100} = -5.0$ eV are clearly smaller. This reflects the stronger chemical binding between Fe and C and is in accordance with the fact that the chemical affinity of an element to

Fig. 2: Close-ups of the internal metal-carbon interface in FePt-terminated CNTs. **a)** Magnification of region #2 in Fig. 1a. Atoms which belong to {111} facets are labelled with green circles, others with yellow ones. **b)** Variation of the {111} inter-planar spacings, d_{111}, with the distance from the interface. The red symbols and blue line represent the experimental data as obtained applying Gaussian fits to the intensity profile along [111] and a fitted exponential decay function, respectively. Error bars represent the 2δ errors of the Gauss fit. **c)** Magnification of the marked region in fig. d. **d)** Tip-region of a second FePt-terminated CNT. The [001] easy axis of magnetisation and the [110] zone axis orientation are indicated by an arrow and an encircled cross, respectively. The insert shows the Fourier transform of the particle section. Super structure reflections indicating the ordered $L1_0$ phase (c.f. Fig. 1b) and the (regular) <111> reflections are labelled with yellow and green symbols, respectively.

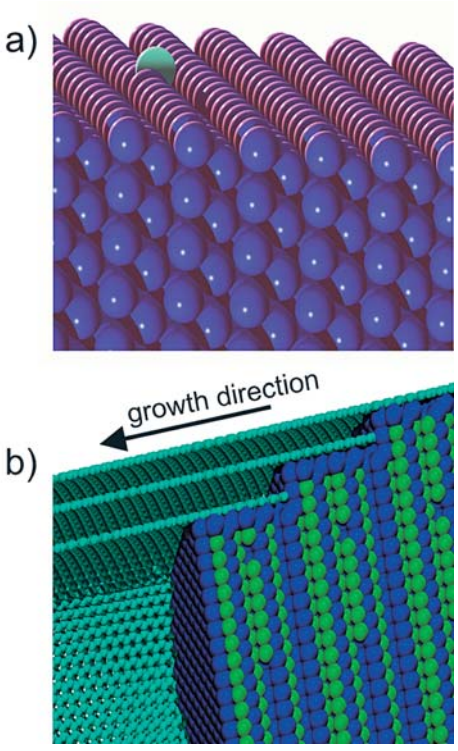

Fig. 3: Structural model. **a)** Calculation of adsorption energies: a carbon atom is placed randomly at the surface of the crystal. **b)** (Simplified) atomic structure model of the metal-carbon interface: the concentric graphene sheets emanate mainly from the Pt-rich {111} catalyst particle facets.

carbon is higher the larger its number of unfilled d orbitals is. For surfaces of a FePt alloy the calculated desorption energies lie between those for elemental Fe and Pt and vary with the local chemical environment (i.e., the number of Fe and Pt bonds). Within the framework of our MD simulations, Pt {111} surfaces provides the lowest desorption energy of carbon. This means, that carbon atoms are easiest released from Pt covered {111} facets of the catalyst particle which is in good agreement with the experimental findings.

The present study shows that the combination of state-of-the-art structural characterisation by means of monochromated aberration-corrected low-voltage HRTEM in combination with model calculations provides a powerful and effective tool to (i) resolve interfacial structures within carbon nanotubes at minimum impact and with atomic precision and (ii) gain valuable insight into the construction principles behind such structures.

It has been found, that for the here investigated internal metal-carbon interface in hard-magnetically terminated CNT the onset of the graphene sheets is at the {111} facets of the catalyst particle. Fig. 3b) shows the final growth model, where the concentric graphene layers of the outgrowing CNT preferentially emanate from Pt-enriched {111} facets of the FePt catalyst particles. The physical principle behind this preference appears to be of kinetic rather than of thermodynamic nature, as the chosen facets provide the lowest desorption energy to be paid in order to release carbon from the metal particle during the growth process.

This new insight into the formation of the metal-carbon interface in CNTs may nourish future efforts to control and tailor the relation between the CNT axis and the orientation of the catalyst particle more precisely in order to provide new opportunities for the construction of novel nanoscale devices.

[1] J. A. Rodriguez-Manzo et al., Nature Nanotech. **2** (2007) 307.
[2] S. S. Wong et al., Nature **394** (1998) 52.
[3] P. Avouris, Acc. Chem. Res. **35** (2002) p1026.
[4] D. Weller et al., IEEE Trans. Magn. **36** (2000) 10.
[5] F. Schäffel et al., Appl. Phys. Lett. **94** (2009) 193107.
[6] S. Hofmann et al., Phys. Rev. Lett. **95** (2005) 036101.
[7] W. Xiao et al., Surf. Sci. **603** (2009) 1985–1998.
[8] F. Ding et al., Nano Lett. **8** (2008) 463–468.
[9] F. Banhart, Nanoscale **1** (2009) 201–213.
[10] R. M. Wang et al., PRL **100** (2008) 17205.
[11] C. Antoniak et al., J. Phys. Condens. Matter **21** (2009) 336002.
[12] M. Müller and K. Albe, Phys. Rev. B **72** (2005) 094203.
[13] B. Rellinghaus et al., J. Magn. Magn. Mater. **266** (2003) 142.
[14] D. Pohl et al., Phys. Rev. Lett. **107** (2011) 185501.

Cooperations: R. Erni (EMPA, Zurich); K. Albe (Darmstadt); [1]IFW Dresden, Institute for Metallic Materials; [2]IFW Dresden, Institute for Solid State Research; [3]National Center for Electron Microscopy, Lawrence Berkeley National Laboratory, USA

Developments in the Synthesis, Structuring and Characterization of Graphene

M. H. Rümmeli, A. Bachmatiuk, J. Warner, F. Schaeffel, D. Makarov,
C. Yan, L. Fu, G. Cuniberti, O. Schmidt, B. Büchner

Graphene has many striking properties that make it an exceedingly attractive material for a variety of applications. It is very likely that many will emerge over the next decade. However, one of the more promising applications lies in exploiting its peculiar electronic properties which are governed by its electrons which obey a linear dispersion relation, *viz*. the electrons interact with the carbon atoms in the graphene lattice in such a way as to create a system that acts like a single mobile charge carrier. This leads to the existence of a half integer quantum hall effect and the absence of localization. The absence of localization is useful for graphene-based field effect transistors. However, if graphene is to be the material for future electronics significant hurdles in its fabrication need to be surmounted, namely, it needs to be mass produced in an economically viable manner and be of high crystalline quality with no or virtually no defects or grains boundaries [2]. Moreover, it will have to be processable with atomic precision. Here at the IFW along with several collaborators we are adopting multi-lateral strategies to develop suitable synthesis routes for large area, high quality and uniform graphene as well as graphene fabrication directly over dielectrics without the use of metal catalysts. We are also developing rapid and efficient characterisation routes based around low voltage aberration corrected transmission electron microscopy that allow easy, clear and fast determination of the homogeneity and quality graphene. In addition, we are extending the potential of low voltage aberration corrected transmission electron microscopy to actually structure freestanding graphene with remarkably high precision.

Large Area homogeneous single layer graphene synthesis:

This novel technique developed by Prof. Lei Fu [2] is now being optimized to yield highly crystalline (minimal grain boundary formation). The technique is exciting because it overcomes a key difficulty encountered when using Ni as a catalyst for CVD grown graphene. Graphene formation over nickel is attractive because the surface planar (111) surface is commensurate with graphene i.e. it has the same hexagonal cell symmetry and similar lattice constants. However, Ni has a high carbon solubility which causes difficulties because CVD grown graphene over Ni involves the catalytic decomposition of the hydrocarbon feedstock at its surface and subsequent absorption of carbon in to the Ni bulk. Upon cooling the absorbed carbon diffuses out to the surface. This carbon segregation process is difficult to control to ultimately yield a single homogenous graphene layer, particularly because the solubility of carbon in Ni is rather high. A rather ingenious ploy to overcome this is involve Mo in the process. Mo_2C remains as a stable carbide at high temperature and also during cooling. Thus, in essence the Mo serves as a sponge for excess carbon species and enables the formation of large area homogeneous single layer graphene. However, further studies show significant grain boundaries exist and currently we are developing improved routes to minimize grain boundary formation as well as conducting studies to better comprehend the growth processes itself.

Graphene formation over non-metals.

Whilst metal catalyst systems (e.g. Ni, Ni-Mo alloys, and Cu) are enormously successful for routine large area graphene synthesis they suffer from a rather important problem. Namely, if graphene is to be used as a future material for high speed electronics it needs to be placed on a semiconducting material. One possible route is the synthesis of graphene on SiC [3]. The synthesis of graphene over oxides, in particular oxides typically used as gate materials in field effect transistors is attractive. To this end we are exploring the used of chemical vapour deposition and thermal processes as techniques

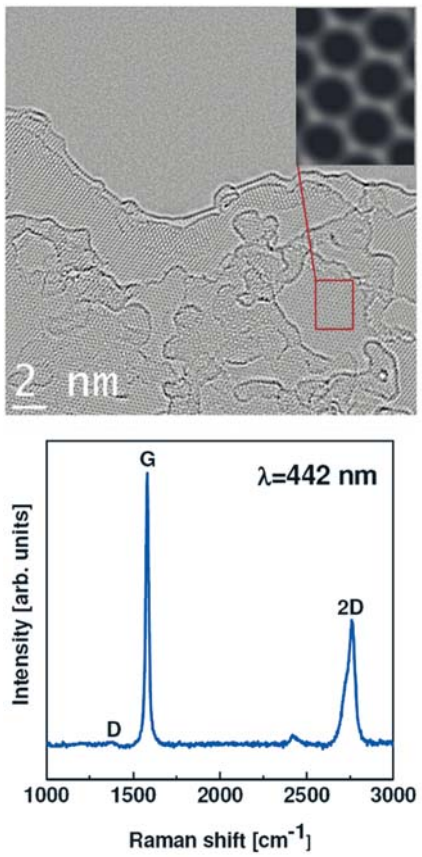

Fig.: Top: Micrograph of few-layer graphene grown by the carbothermal reduction of SiO_2. *Inset:* Fourier filtered image from a small section of the micrograph that highlights the honeycomb lattice. **Bottom:** Raman spectrum of the few-layer graphene.

for the synthesis of graphene over oxides. The investigated oxides are categorized into irreducible oxides (they remain in their oxide phase in the reaction) and reducible oxides (they reduce to a carbide phase). Magnesia and Zirconia are two examples of irreducible oxides that were investigated. For the studies, powdered forms of the oxides were used as this is ideal for fundamental investigations in transmission electron microscopes. To grow the graphene the powdered oxides were exposed to CVD reactions. The samples were grown from cyclohexane at 775 °C and 100 mbar. Under these conditions, the reaction stops when the catalyst is fully encapsulated by graphitic layers. We observed that the number of layers can increase up to nine and can be tuned via the reaction time. The multilayers are ubiquitously anchored into step edges on the [100] surfaces. This suggests that these step sites initiate the growth of graphitic layers. Moreover it seems that these step sites are not only nucleation sites, but also growth sites because growth appears to stop once the particle is fully encapsulated.

The importance of step sites to the growth of carbon nanotubes is already well established for some metal catalysts. The surface growth processes over metals can divided into four distinct subprocesses — the adsorbtion of carbon feedstock molecules on the catalyst, dissociation of hydrogen from the precursor, surface diffusion, and addition of carbon atoms to the network.

We conducted initial theoretical investigations for graphene over MgO, which, while still preliminary, clearly show each of these sub-processes on MgO [100] [4].

In the case of a reducible oxide catalyst silicon dioxide is naturally of interest. Previous studies of ours showed silica can be reduced to SiC via a carbothermal reduction process and that this SiC can graphitize carbon to for carbon nanotubes and can be tailored to produce exotic structures like helical carbon nanostructures [5]. Currently we are developing a modified technique in which (solid) amorphous carbon serves as the carbon source for the carbothermal reduction of silica and subsequent graphene formation. Initial studies look promising as shown in figure.

Graphene Characterisation

The promise afforded by graphene is huge. However, as already mentioned, in order for much of its promise to be fulfilled we need to be able to structure it with atomic precision. Inherently this requires the means with which to characterize it easily and with atomic precision. Whilst scanning probe methods (e.g. scanning tunnelling microscopy) offer atomic resolution, the technique is cumbersome and does not allow rapid and efficient sample turnover. Aberration corrected transmission electron microscopy (ACTEM) provides atomic resolution at operating conditions that do not damage graphene (i.e. acceleration voltages of 80 kV or below can be used). Moreover sample turnover is efficient. Thus we are developing ACTEM characterisation techniques for graphene. We are able to investigate graphene edges with immense precision. For example, a technique has been developed enable the edges of graphene formed from catalytic hydrogenation to be investigated [6]. Catalytic hydrogenation is a process in which metal catalyst particles on graphene are exposed to pure hydrogen at elevated temperatures. The catalytic particles etch or eat away carbon at the particle/graphene interface producing CH_4 in the process. The technique is of interest for the possible production of parallel arrays of graphene nanoribbons. An important question regards this catalytic hydrogenation technique is how precisely are the edges formed? To this end sample preparation routes which avoid the use of solvents was developed since solvent molecules can easily attach to unsaturated bonds at the edges of graphene which then react with the electron beam when under TEM investigation and so provide unclear edge information. In essence graphene and the catalytic particles were prepared directly on TEM sample grids and the hydrogenation reaction run. Afterwards the sample can be directly placed in a TEM for direct observation eliminating the need to use solvents or any additional sample preparation steps. This allowed precision examination of the freshly etched edges formed by the

hydrogenation procedure. The ACTEM studies showed that the hydrogenation process can form edges with sub-nanometer precision highlighting the degree of edge control that can be achieved by means of catalytic hydrogenation.

Another important aspect of graphene characterisation is determining grain boundary presence understanding the type grain boundary formation. This is particularly pertinent to CVD grown graphene over large areas where poly crystalline supports/catalysts are used. For example graphene formation using CVD over Cu foils. The technique is very successful for large are graphene formation, but inherently the Cu foil is poly crystalline and this can lead to defects and grain formation in the surface formed graphene during CVD growth. Hence, in order to improve the CVD process (and graphene synthesis routes in general) there is a need for rapid and efficient boundary detection and type determination. In this study few layer graphene (FLG) domains are shown to interconnect via two principle processes: graphene sheets from one domain grow over the top of a neighbouring domain, while in other graphene domains the interconnection occurs by direct atomic bonding. Differentiating between these two types of interconnects is possible by examining the HRTEM contrast profiles produced at the interface. Graphene boundary sheets that terminate without bonding but simply overlap a neighbouring sheet produce strong edge contrast with increasing defocus values, as well as a broader edge cross section. Atomically bonded interfaces do not exhibit any contrast, even under large defocus values. The findings were reinforced by correlating the experimental data with multi-slice TEM image simulations of appropriate structures. The developed technique is simple and allows easy and rapid grain boundary detection and boundary type [7].

[1] *M.H. Rümmeli, C.G. Rocha, F. Ortmann, I. Ibrahim, H. Sevincli, F. Börrnert, J. Kunstmann, A. Bachmatiuk, M. Poetschke, M. Shiraishi, M. Meyyappan, B. Büchner, S. Roche, G. Cuniberti* Graphene: Piecing it together, Advanced Materials 23 (2011), S. 4471-4490.

[2] *B. Dai, L. Fu, Z. Zou, M. Wang, H. Xu, S. Wang, Z. Liu,* Rational design of a binary metal alloy for chemical vapour deposition growth of uniform single-layer graphene, Nature Communications 2, 541 doi:10.1038/ncomms1545

[3] *V.Y. Aristov, G. Urbanik, K. Kummer, D.V. Vyalikh, O.V. Molodtsova, A.B. Preobrajenski, A.A. Zakharov, C. Hess, T. Haenke, B. Buechner, I. Vobornik, J. Fujii, G. Panaccione, Y.A. Ossipyan, M. Knupfer* Graphene synthesis on cubic SiC/Si Wafers. Perspectives for mass production of graphene-based electronic devices, Nano Letters 10 (2010), S. 992-995

[4] *A. Scott, A. Dianat, F. Boerrnert, A. Bachmatiuk, S. Zhang, J.H. Warner, E. Borowiak-Palen, M. Knupfer, B. Buechner, G. Cuniberti, M.H. Ruemmeli* The catalytic potential of high-K dielectrics for graphene formation, Applied Physics Letters 98 (2011) Nr. 7, S. 73110/1-3

[5] *A. Bachmatiuk, F. Boerrnert, V. Hoffmann, D. Lindackers, J.-H. Lin, B. Buechner, M.H. Ruemmeli* Hydrogen-induced self-assembly of helical carbon nanostructures from ethanol over SiO2 catalysts, Journal of Applied Physics 109 (2011) Nr. 9, S. 94317/1-4

[6] *F. Schaeffel, M. Wilson, A. Bachmatiuk, M.H. Ruemmeli, U. Queitsch, B. Rellinghaus, G.A.D. Briggs, J.W. Warner* Atomic resolution imaging of the edges of catalytically etched suspended few-layer graphene, ACS nano 5 (2011) Nr. 3, S. 1975-1983

[7] *A.W. Robertson, A. Bachmatiuk, Y.A. Wu, F. Schaeffel, B. Rellinghaus, B. Buechner, M.H. Ruemmeli, J.H. Warner* Atomic structure of interconnected few-layer graphene domains, ACS nano 5 (2011) Nr. 8, S. 6610-6618

Cooperation: The Univ. of Oxford, Beijing Univ

Complex hydrides and composites for H_2 storage

I. Lindemann, C. Bonatto Minella, L. Schultz, O. Gutfleisch

Complex hydrides and, in particular, tetrahydroborates (borohydrides) of the alkali and alkali earth metals are considered ideal candidates for solid state hydrogen storage due to their high hydrogen content both in volume and weight.
The mixed metal Al-Li-borohydride combines high H_2 density (17.2 wt.%) with a desorption temperature at about 60°C which is compatible with PEM fuel cells. In this work, the decomposition behaviour of Al-Li-borohydride is clarified by the combination of thermogravimetry (TG) coupled with infrared spectroscopic (FT-IR) and mass spectrometric (MS) analysis of the gas phase.
The results evidence that, upon decomposition, the mixed metal borohydride transforms into its pristine borohydride components $Al(BH_4)_3$ and $LiBH_4$.

Material innovations are needed solving the issues related to energy conversion, storage and transport in order to find alternatives to fossil fuels. Hydrogen represents a promising solution because of its high energy density per mass (142 MJ kg^{-1}) which is about three times higher than the one of liquid hydrocarbons (47 MJ kg^{-1}). Hydrogen is regarded as a suitable energy carrier due to its high abundance and low weight. Unlike fossil fuels, it needs to be synthesised. Only when hydrogen is produced by renewable energy sources (solar, wind, water) the hydrogen cycle is sustainable. During the conversion in the fuel cell from chemical energy to electric energy the oxidation product from hydrogen is just water.
The bottleneck for a large scale hydrogen technology is the storage of this extremely light gas. Compression is one option but especially for mobile applications only high pressure tanks with about 700 bar are efficient enough. This technology still suffers from a comparably low volumetric H_2 density, high cost of gas compression and safety issues. Another option of volume reduction is the liquefaction, however the boiling point of hydrogen (23 K) is so low that this is no alternative due to high energy consumption during liquefaction and boil off phenomenon. Solid state hydrogen storage provides the highest volumetric H_2 density among the aforementioned technologies. In addition, due to the low pressures involved and the endothermic desorption process, it represents the safest technology. Generally, a desirable hydrogen storage material should possess high storage capacity, mild operating temperatures, fast kinetics, low cost, excellent reversibility and low or, even no, toxicity. So far, there is not a single material fulfilling all of these requirements simultaneously.[1-3]
It is well known that hydrogen reacts in combination with several metallic elements to form metal hydrides. Conventional metal hydrides which store hydrogen interstitially (e.g. $LaNi_5$) possess only low hydrogen capacity (~1wt.% H_2) although at moderate storage temperatures and pressures. For economic mobile applications a material with a hydrogen capacity of at least 6 wt.% is needed. Furthermore, the hydrogen uptake and release should meet the working temperatures provided by the fuel cell technology: between 60 and 120 °C with an equilibrium pressure in the range of 1-10 bar H_2.[3] Additionally, the air- and moisture sensitivity of most hydrides need to be addressed.

Complex hydrides such as tetrahydroaluminates (or alanates AlH_4^-) and tetrahydroborates (or borohydrides BH_4^-) show much higher H_2 densities than conventional metal hydrides. Hydrogen is bonded covalently within the respective tetrahedron (AlH_4^- or BH_4^-) which is counteracting with a cation. The prototype compound $NaAlH_4$ can store practically about 5 wt.% H_2 and is reversible for many cycles.[4] However, its H_2 density is still too low for practical applications. Therefore, research moved towards complex hydrides [5-7] in particular borohydrides which can offer hydrogen densities up to 18.5 wt.%. But, their thermodynamic stability is either to high or too low which is directely connected to their hydrogen desorption temperature. A recent study showed

that the stability of boroyhydrides scales with the electronegativity of the cation within the borohydride.[8] Therefore mixed metal borohydrides should exhibit intermediate stability.

$AlCl_3$ and $LiBH_4$ was ball milled together for 5h in Ar atmosphere to initiate the metathesis reaction according to equation (1). The novel mixed metal borohydride $Al_3Li_4(BH_4)_{13}$ and LiCl as a side product were evidenced by XRD analysis. Furthermore, structure determination was carried out from powder diffraction data collected at the synchrotron source. As a result $Al_3Li_4(BH_4)_{13}$ forms a primitive cubic unit cell containing complex cations $[Li_4(BH_4)]^{3+}$ and anions $[Al(BH_4)_4]^-$.[5]

$$3\ AlCl_3 + 13\ LiBH_4 \rightarrow Al_3Li_4(BH_4)_{13} + 9\ LiCl \qquad (1)$$

Indeed, the combination of Al-Li-borohydride showed desorption at moderate temperatures at about 60°C. The component borohydride $LiBH_4$ (18.5 wt.% H_2) desorbs considerable amounts of H_2 only above 300°C. [9] In contrast, the other component borohydride $Al(BH_4)_3$ (16.8 wt.% H_2) is an extremely volatile liquid (T_m = -40°C) which desorbs at about 50°C. [10] However, thermogravimetric analysis of the milled sample showed a very high mass loss of 25 % upon decomposition. This cannot be explained by desorption of only H_2. Al-Li-borohydride contains 17.2 wt. % H_2 but just 44 wt. % of the sample correspond to the mixed metal borohydride. Therefore the decomposition pathway of the compound needs to be clarified.

In-situ Raman measurements [11] were carried out in order to analyse the decomposition product in the solid (see Fig. 1). Raman spectroscopy is a superior method for structural analysis of these very light and often amorphous materials. At room temperature (RT), the Raman spectra corresponds to that of $Al_3Li_4(BH_4)_{13}$. The spectrum of the sample obtained after heating the powder above the decomposition temperature (90°C) and after cooling to RT, shows the formation of orthorhombic $LiBH_4$. This is the decomposition product in the solid phase.

The gas phase analysis is another challenge which was only possible with a special setup.[12] TG measurement was carried out in combination with infrared spectroscopic analysis (FT-IR) on the released gas. In addition, a mass spectrometer (MS) was coupled to the setup since H_2 is not IR active. But IR helps to detect unstable species which are often desorbed from borohydrides. Therefore a combination of the FT-IR and MS method for gas phase analysis was used. The coupled TG and FT-IR measurements in Ar and H_2 atmosphere are shown in Fig. 2a. Both signals are displayed as a rate of mass change for better comparison. In both atmospheres, the measurement evidences mainly $Al(BH_4)_3$

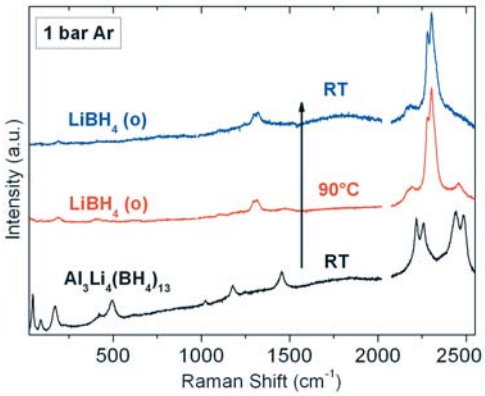

Fig. 1: In-situ Raman spectroscopy of the milled sample $AlCl_3$ + 4.33 $LiBH_4$ at room temperature (black curve), 90°C (red curve) and again after cooling in Ar atmosphere (blu curve).

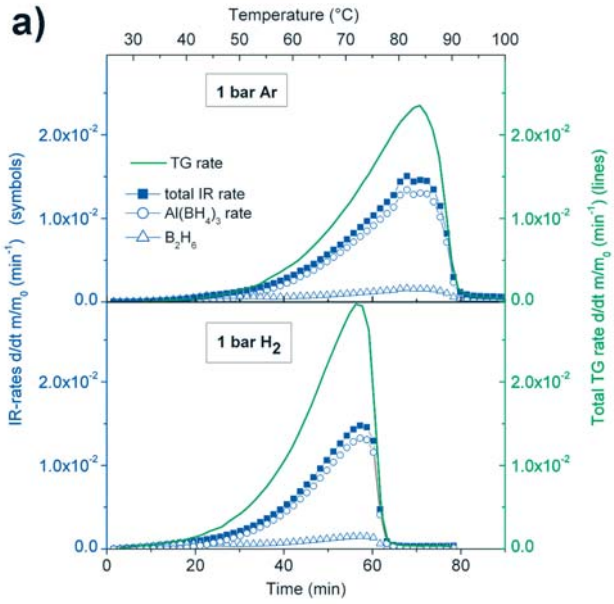

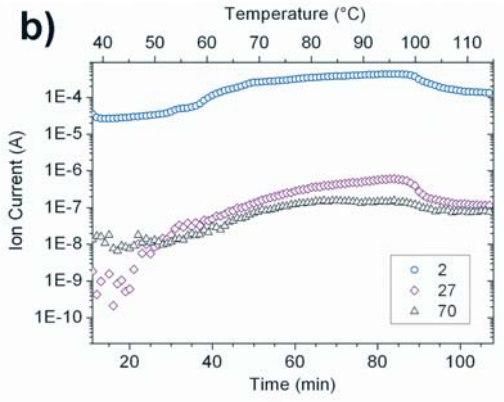

Fig. 2: a) IR and TG rates vs. time and temperature in Ar (top panel) and in hydrogen atmosphere (bottom panel). **b)** Evolution of selected masses vs. time and temperature measured by mass spectrometry in Ar atmosphere (2-H_2, 27-B_2H_6, 70-$Al(BH_4)_3$).

beside lower amounts of B_2H_6. The overall FT-IR rate does not match the TG rate. This is due to the desorbed H_2 which is not detected by IR. The MS measurement, carried out simultaneously to the IR measurement in Ar, is shown in Fig. 2b. This experiment confirms the results obtained from the IR measurement: H_2, B_2H_6 and $Al(BH_4)_3$ evolve during decomposition of $Al_3Li_4(BH_4)_{13}$. Therefore, the $Al_3Li_4(BH_4)_{13}$ decomposes into its component borohydrides since H_2 and B_2H_6 are only desorption products of $Al(BH_4)_3$. The overall decomposition reaction is shown in Fig. 3. It is noteworthy that the decomposition temperature is as always depending on the atmosphere. But in this case it is lower in 1 bar H_2 than in 1 bar Ar only due to better heat conductivity and equals the boiling point of $Al(BH_4)_3$.

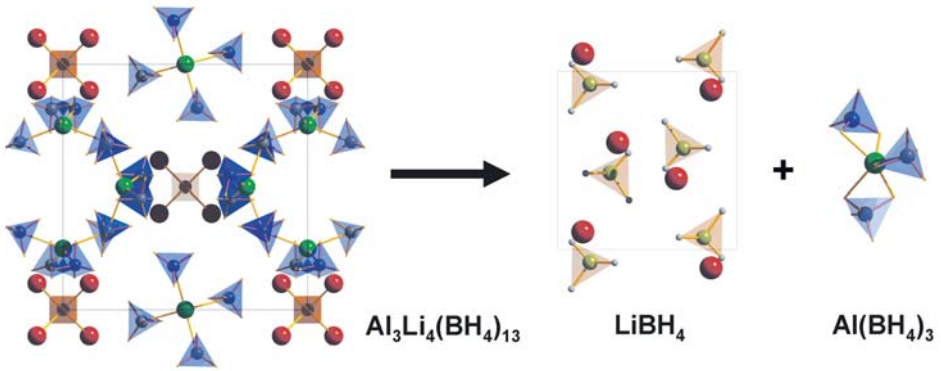

Fig. 3: Schematic decomposition reaction of $Al_3Li_4(BH_4)_{13}$. Al^{3+} cations (green) are surrounded by blue $(BH_4)^-$ groups and Li^+ cations (red) by brown $(BH_4)^-$ tetrahedrons, respectively.

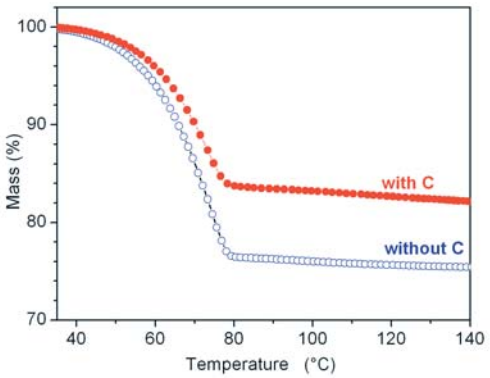

Fig. 4: Weight vs. temperature of TG measurements in Ar atmosphere (heating rate 5 K/min) for the sample with and without carbon addition.

In order to achieve reversibility the evaporation of $Al(BH_4)_3$ from the powder should be hindered. This is possible by the addition of porous carbon as shown in the TG measurement in Fig.4. Only 10 wt.% porous carbon was added prior the milling process. Due to the reduced vapour pressure the mass loss reduces by 6 %.

Therefore an advanced sample design which includes 3D "architecture" and the addition of suitable decomposition catalyst for B_2H_6 desorption can improve H_2 desorption while avoiding unwanted products. Further improvements in such advanced materials have to be performed when only hydrogen should to be cycled at moderate conditions.[13,14]

[1] L. Schlapbach, A. Züttel, Nature **414** (2001) 353.
[2] A. Züttel, A. Borgschulte, L. Schlapbach, Hydrogen as a Future Energy Carrier (2008).
[3] U. Eberle, M. Felderhoff, F. Schüth, Angew. Chem. **48** (2009) 6608.
[4] B. Sakintuna et al., Int. J. Hydrogen Energy **32** (2007) 1121.
[5] I. Lindemann et al., Chem. Eur. J. **16** (2010) 8707.
[6] I. Lindemann et al., Faraday Discuss. 151 (2011) 231.
[7] C. Bonatto Minella et al., Faraday Discuss. **151** (2011) 253.
[8] Y. Nakamori et al., J. Phys. Chem. Solids **69** (2008) 2292.
[9] A. Züttel et al., J. Power Sources **118** (2003) 1.
[10] H. Schlesinger et al., J. Am. Chem. Soc. **62** (1940) 3273.
[11] R. Domènech-Ferrer et al., Anal. Chem. **83** (2011) 3199.
[12] A. Borgschulte et al., J. Phys. Chem. C **115** (2011) 17220.
[13] P. Adelhelm et al., Chem. Mater. **22** (2010) 2233.
[14] J. Gao et al., J. Phys. Chem. C **114** (2010) 4675.

Cooperation: Empa Dübendorf, Switzerland; TU Dresden, Germany; University of Geneva, Switzerland; Helmholtz-Zentrum Geesthacht, Germany; University of Utrecht, Netherlands; University of Glasgow, United Kingdom; Swiss-Norwegian Beam Line at ESRF, France
Funded by: EU and Free State of Saxony (ECEMP 13853/2379).

Magnetic Microhelix Coils

E. J. Smith, D. Makarov, S. Sanchez, V. M. Fomin and O. G. Schmidt

The creation of magnetic microhelix coil structures is made possible through an innovative fabrication approach known as polymer delamination. The delamination of strips of a polymer, which have an "active" magnetic nanomembrane sputtered onto them, allows for the creation of architectures which can exhibit one of three unique magnetic configurations: Hollow-bar-, Corkscrew- and Radial-magnetization. These scaled-up microstructures are helimagnetic-like in configuration, mimicking those found naturally on the nanoscale, and may allow for a better understanding and more detailed probing of such magnetic arrangements.

The effect of topology plays an important role in the electromagnetic properties of architectures which have complex magnetic configurations and often allows for the discovery of new phenomena. These complex systems include helimagnetic materials which are characterized by a gradual tilting of adjacent spins. These types of materials reveal metamagnetic transitions, which make them of high interest, and have been recently explored theoretically. The number of experimental investigations however, is minimal due to the extraordinary properties required of a material in order to support helimagnetism.

Rather than depending on nature to produce such structures, there is another approach which relies on a continuous distribution of the magnetic moment through intelligent design, realised with micro-/nanofabrication techniques. One example is designing magnetic disk-shaped structures, allowing for the formation and investigation of magnetic vortices [1]. In spirit of this exciting opportunity, we set out to create and investigate helimagnetic-like configurations on the microscale, namely, Hollow-bar-, Corkscrew-, and Radial-magnetized microhelix coils [2].

The fabrication approach that was utilized for these experiments is based on the self-assembly of strained polymeric structures [3] which delaminate from the host substrate to form microhelix coils [4]. The process is as follows: First, a thick photosensitive polymer (2 – 10 μm), SU8, is spin-coated onto a cleaned Si substrate. Narrow strips (1 mm × 7 μm) are then defined through a photolithography step. An "active" magnetic layer is then sputtered onto the polymer. This magnetic layer can have either an in-plane easy axis magnetization (20 nm Co) or an out-of-plane easy axis magnetization ($[(0.4\ \text{nm})\text{Co}/(0.6\ \text{nm})\text{Pt}]_5$). Next, the samples are placed into the delamination medium, *N*-Methyl-2-pyrrolidone (NMP), at an initial time t_i. The polymer absorbs the NMP, causing it to swell, which in turn, increases the differential strain in the structure. At some point the strain becomes so great that the structure delaminates and curls-up in order to relax [5]. This curl-up turns into a full coil-up, as the structure completely delaminates from the substrate, forming compact microhelix structures at a final time t_f, Fig. 1. If an SU-8 layer that is 6.2 μm is used, the resulting helices are 50 μm in length with a radius of 35 μm, the dimensions of the helices further investigated in these experiments.

This coil-up can lead to structures exhibiting one of three magnetic configurations. The first structure is created by using an in-plane easy axis magnetic film, and saturating the film perpendicular to the strip prior to coil-up. Upon coil-up, a Hollow-bar-magnetized

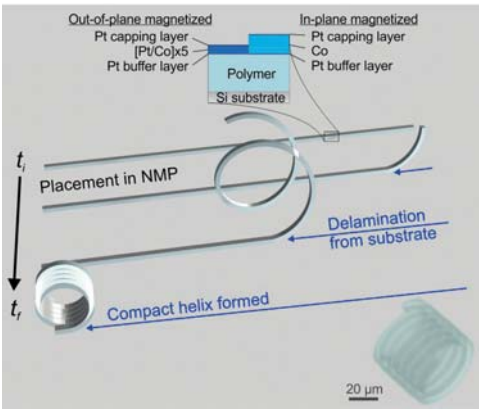

Fig. 1: Microhelix coil fabrication. First polymer strips are defined through a photolithographic step and then an "active" nanomembrane is sputtered onto the strips. This active layer has an easy axis out-of-plane magnetization or an easy axis in-plane magnetization. The strips are then placed in a delamination medium, *N*-Methyl-2-pyrrolidone (NMP), at an initial time t_i, in which the polymer swells, increasing the deferential strain in the structure, which leads to a coil-up (due to a relaxation of the structure). The coil-up results in the creation of compact microhelix coils, at the final time t_f, as seen in the optical image, bottom right.

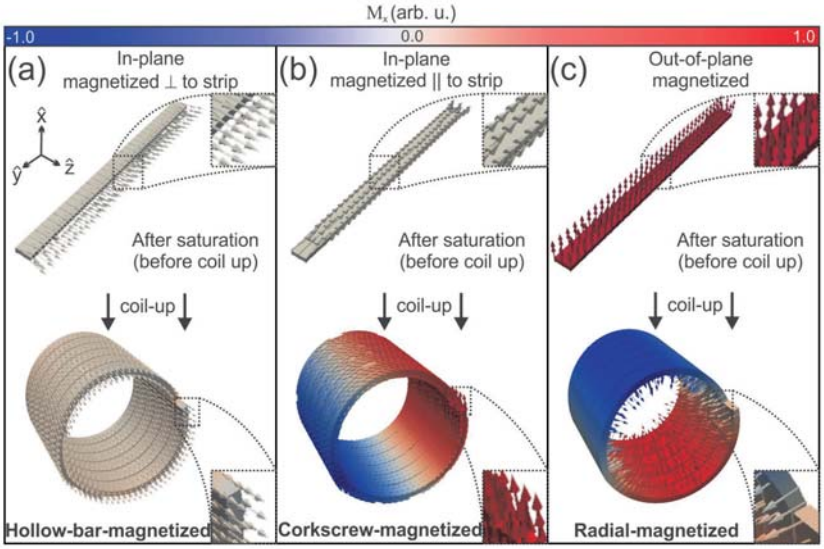

Fig. 2: Unique magnetic configurations. Coil-up allows for the creation of three unique magnetic configurations by utilizing one of two magnetic films which have either an in-plane magnetic easy axis or out-of-plane magnetic easy axis. If an in-plane magnetic film is used, and the strip is saturated **(a)** perpendicular to its length prior to coil-up, upon coil-up the helix coil has a Hollow-bar-magnetized configuration. **(b)** If instead the strip is saturated parallel to its length, the result of coil-up is a helix coil which is Corkscrew-magnetized. **(c)** If rather a out-of-plane easy axis film is used, once the strip is coiled-up, the helix coil will be Radial-magnetized.

helix coil is formed, Fig. 2(a), named due to its similarity to the magnetic orientation which would be obtained by drilling out the core of a cylindrical permanent magnet. The second structure can be created again by using an in-plane easy axis magnetic film, however this time the film is saturated parallel to the strip before coil-up. The magnetic configuration of the helix coil which is formed is Corkscrew-magnetized, Fig. 2(b), and has a micron-scaled helimagnetic-like orientation. The third unique structure which can be created begins with an out-of-plane easy axis film, saturated out-of-plane. After coil-up, a Radial-magnetized coil is created, a magnetic configuration with is unobtainable by any other technique and does not exist naturally, Fig. 2(c).

In order to verify the magnetic configurations of the constructed microhelix coils we investigated their dynamics in response to an oscillating magnetic field. This allows for a probing of the structures without destroying their magnetic state. The different structures responded to the oscillating field via diverse rotating motion, due to an alignment of the magnetic moment of the particularly-magnetized structures, to that of the external field. The magnetic moment of the Hollow-bar-magnetized coils points along the axis of the coils which leads to an end-over-end tumbling motion through the medium, Fig. 3(a). The Corkscrew-magnetized coil has a magnetic moment that spirals itself along the length of the structure. This leads a forward dancing motion in response to the alternating field, Fig. 3(b). The Radial-magnetized structure responds with a directionally-deterministic forward rotation, Fig. 3(c). This can be explained by an uncompensated magnetic moment that is present at the ends of the helix windings which point inward.

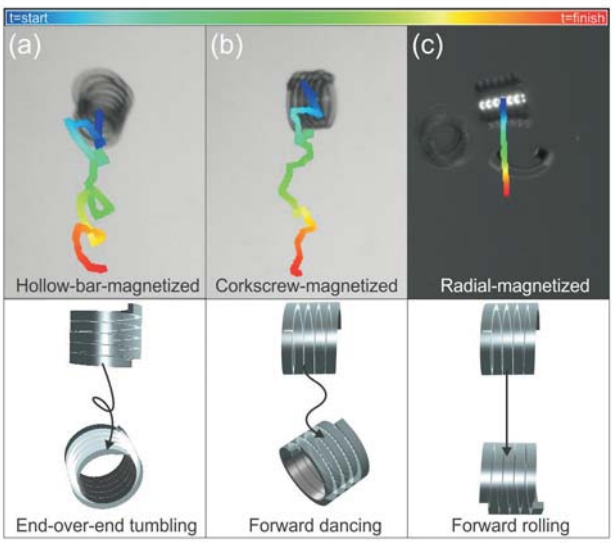

Fig. 3: Magnetic configuration probed through investigation of coils in an alternating magnetic field. The probing of the microhelix coils revealed different dynamics for the different magnetic orientation of the structures. **(a)** The Hollow-bar-magnetized coils responded in an end-over-end tumbling motion. **(b)** The Corkscrew-magnetized coils responded in a forward dancing motion through the liquid. **(c)** A probing of the Radial-magnetized coils resulted in a directionally-deterministic forward rolling.

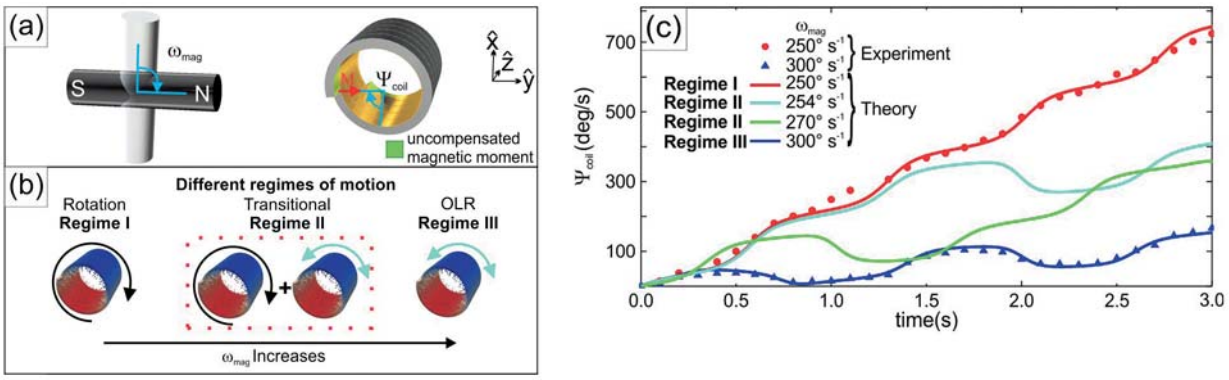

Fig. 4: Trajectories of Radial-magnetized coils. **(a)** The coil's uncompensated magnetic moment aligns itself with the rotating external magnetic field through a rotation about the z-axis. **(b)** The coils can move in one of three regimes of motion: (Regime I) rotational and (Regime III) oscillatory-like-rotative (OLR), as seen in experiment, as well as a (Regime II) transitional regime in between, predicted theoretically. **(c)** The trajectories of motion observed experimentally can be recreated theoretically [6].

We focused on an analysis of the Radial-magnetized microhelix coils due to their single axis of rotation around the *z*-axis. The oscillating magnetic field was provided by the end-over-end rotation of an external magnet that rotated at various velocities ω_{mag}, resulting in the angular rotation of the coil Ψ_{coil}. This coil rotation can be mapped out, Fig. 4(a). At low excitation frequencies the coils respond with rotative motion, Regime I [Fig. 4(b)]. As the speed is increased, the coils continue to rotate, but due to friction, their average angular velocity begins to lag behind and drops off at a certain frequency $\omega_{mag}^{transition}$. At higher frequencies the dynamics transits into a different regime known as oscillatory-like-rotative motion, Regime III [Fig. 4(b)]. This regime is characterized by oscillations superimposed over the rotative motion, Fig. 4(c). A theoretically predicted transition regime [6], Regime II, is composed of rotative motion, interrupted by hiccups of oscillation. This transition regime has most recently been observed by us in the rotative dynamics of a similar system. A theoretical model (Ref. [6]) was developed that provided an insight into the experimentally observed rich dynamics of the Radial-magnetized microhelix coils, Fig 4(c).

In conclusion, we have created unique magnetic configurations on the micron-scale in the form of microhelix coils which are helimagnetic-like in orientation. In order to design such structures, we developed an alternate approach to rolled-up technology which relied on a polymer system requiring no sacrificial layer. Polymer strips, with an active magnetic layer sputtered on top, delaminated from the substrate and self-assembled into microhelix coil structures. Depending on the alignment of the magnetic films prior to coil-up, three unique magnetic configurations could be created, namely: Hollow-bar-, Corkscrew-, and Radial-magnetized. The magnetic configurations of these complex structures were probed by following their orientation-dependent dynamics in an alternating magnetic field. Further in-depth study was made on the Radial-magnetized coils which revealed two regimes of motion, rotative and oscillatory-like-rotative. The new fabrication approach, the unique magnetic structures, and the rich dynamics discussed in this work are surely to motivate novel, interesting scientific studies in numerous fields, including but not limited to: M icro/nanofabrication, magnetics, hydrodynamics and chaotic systems.

Acknowledgements: We would like to thank Daniel Grimm for maintenance of the cleanroom and Cornelia Krien for magnetic layer sputtering.

[1] B. Pigeau et al., Nature Phys., **7**, (2010) 26.
[2] E. J. Smith, D. Makarov, S. Sanchez, V. M. Fomin and O. G. Schmidt, Phys. Rev. Lett., **107**, (2011) 097204.
[3] V. Luchnikov et al., Adv. Mater., **17**, (2005) 1177.
[4] E. J. Smith, D. Makarov and O. G. Schmidt, Soft Matter, **7**, (2011) 11309.
[5] O. G. Schmidt and K. Eberl, Nature, **410**, (2001) 168
[6] V. M. Fomin, E. J. Smith, D. Makarov, S. Sanchez and O. G. Schmidt, Phys. Rev. B, **84**, (2011) 174303.

Funded by: Volkswagen Foundation (I/84 072), MURI through the AFOSR (FA9550-09-1-0550).

Spin-selective tunnel rates in SiGe self-assembled quantum dots

G. Katsaros, V. N. Golovach, P. Spathis[1], N. Ares[1], M. Stoffel, F. Fournel[2], L. I. Glazman[3], S. De Franceschi[1], O. G. Schmidt

The field of metallic spin electronics has been a very active field since injection of spin-polarized electrons from a ferromagnet into a metal was observed. Various discoveries were made in the past few decades, with that of the giant magnetoresistance effect, now widely used in hard disks, being the most striking example. While metallic spintronics is a rather mature field, the field of semiconductor spintronics is still not fully developed. The main reason for this is the poor spin injection efficiency from a ferromagnetic metal into a semiconductor. Despite recent progress in bulk semiconductors, there exist substantial problems for semiconductor nanostructures. In our study we have observed that spin-selective tunnel rates to individual SiGe semiconductor nanocrystals can be achieve with *normal metallic contacts*. The surprising spin selectivity arises from the interplay of the orbital effect of the magnetic field with the strong spin-orbit interaction present in the valence band of the semiconductor.

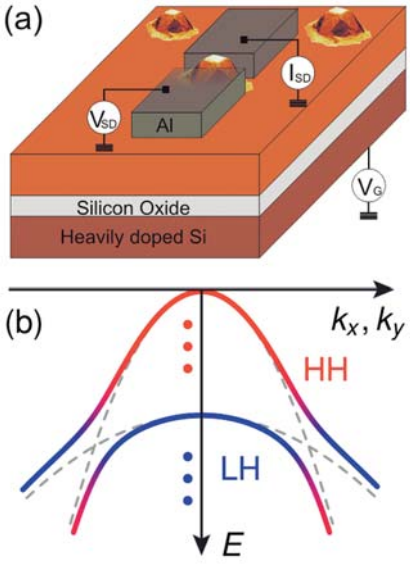

Fig. 1: Schematic of a QD device fabricated from a SiGe self-assembled nanocrystal grown on a silicon-on-insulator substrate having a heavily doped handle wafer which is used as a back gate. **(b)** Qualitative band diagram of a Ge-rich SiGe quantum well illustrating the effect of quantum confinement along the growth (z) direction: HH and LH branches are split at $k_x = k_y = 0$ and anti-cross at finite k_x or k_y. The red dots indicate that many other HH subbands exist before the first LH subband is encountered.

The spin-orbit interaction (SOI) has become of central interest in the past years, because it enables an all-electrical manipulation of the spin. In the field of spin qubits, the electrical control of localized spins by means of the electric-dipole spin resonance [1] has been used for rotating confined electrons in quantum dots (QDs) [2,3]. Already much earlier, Datta and Das proposed a semiconductor transistor that would operate through a gate-controlled spin precession, mediated by the SOI [4]. In this type of spin transistor, spin-polarized electrons are injected into the semiconductor from a ferromagnetic (FM) contact. However, the realization of an efficient spin injection has proven to be a difficult task. Only recently, high spin-injection efficiencies were reported for FM contacts to semiconductors [5,6]. Still for nanostructures, experimental evidence of spin injection is not as strong and clear. Our measurements show that the SOI in the valence band, quantified by the spin-orbital splitting Δ_{SO}, provides an alternative way to obtain spin-selective tunnelling into nanostructures without requiring FM electrodes.

We have studied the low-temperature magneto-transport properties of individual SiGe self-assembled QDs with a base diameter $d \approx 80$ nm and a height $w \approx 20$ nm. The hole motion is strongly quantized along the growth direction [001]. A schematic of a typical QD contacted with Al electrodes is shown in Fig. 1(a). For such QDs, the hole wave function is generally composed of both heavy holes (HHs) and light holes (LHs). Due to the confinement and compressive strain, the degeneracy between the HH and LH branches, present in bulk at the Γ-point, is lifted. The HHs become energetically favorable. However, the QD wave-function is composed both of HH and LH states. In Fig. 1(b), we illustrate the interaction between a HH and a LH branch in the two-dimensional (2D) case.

At cryogenic temperatures, transport through QDs is dominated by the Coulomb blockade (CB) effect. In the CB regime, single-hole sequential transport is suppressed and electrical conduction is due to second-order co-tunnelling (CT) processes [7]. We consider here the case of a QD with an odd number of holes and a spin-doublet ground state. A magnetic field, B, lifts the spin degeneracy by the Zeeman energy $E_Z = g\mu_B B$, where g and μ_B are the hole g-factor and Bohr magneton, respectively. Once the bias voltage across the QD exceeds the Zeeman energy, $|eV| > E_Z$, the inelastic CT processes can flip the QD spin, leaving the QD in the excited spin state [Fig. 2(a)]. The onset of

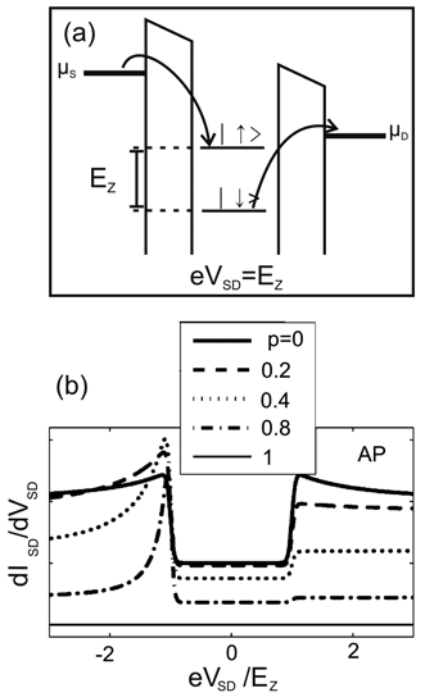

Fig. 2: (a) Schematic energy diagram showing the onset condition ($eV_{SD} = E_Z$) for spin-flip inelastic cotunneling. **(b)** Theoretical curve for G in a case of a QD contacted by ferromagnetic contacts with antiparallel magnetization. The case p = 0 corresponds to non-magnetic leads. Adapted from Ref. 9.

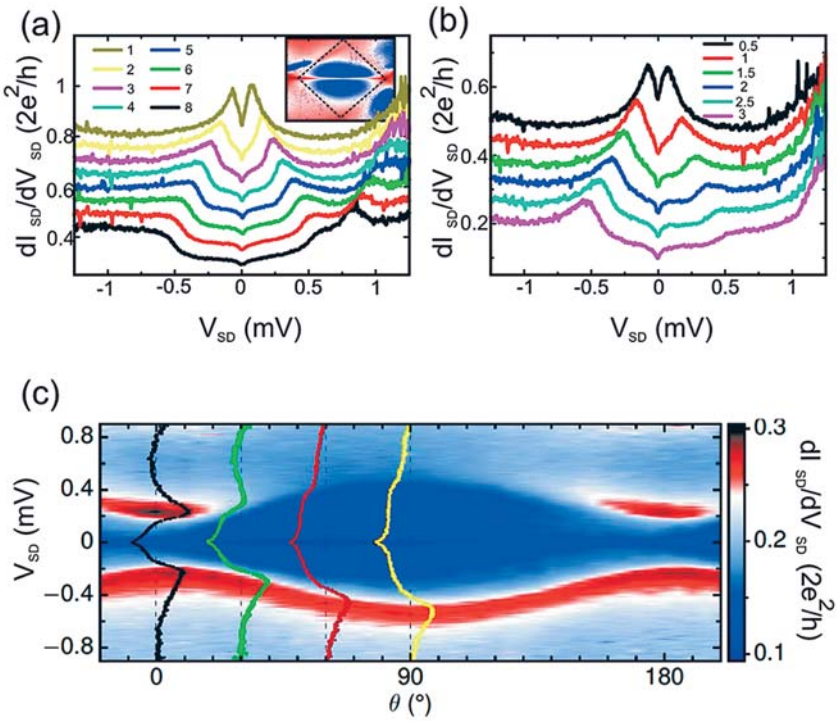

Fig. 3: (a) $G(V_{SD})$ for different parallel fields from 1 to 8 T. The traces have been shifted by 0,06 × $2e^2/h$ for clarity. Inset: $G(V_G,V_{SD})$ for a 75-mT perpendicular field needed to suppress the superconductivity of the Al electrodes. (V_G spans a range of 850mV and V_{SD} ranges from -3.5 to 3.5 mV). **(b)** $G(V_{SD})$ for different perpendicular B-fields from 0.5 to 3 T. The traces have been shifted by 0,06 × $2e^2/h$ for clarity. The Zeeman splitting of the Kondo peak is symmetric in (a) and asymmetric in (b). **(c)** Angular dependence of the split Kondo peak for a fixed V_G and B = 3 T. Superimposed $G(V_{SD})$ traces for θ = 0, 30, 60, and 90 degrees. The V-shape dip of G at zero bias observed in (a)-(c) is caused by electron-electron interactions in disordered leads.

spin-flip inelastic CT manifests itself as a step in the differential conductance, $G = dI/dV$, at $eV = \pm E_Z$ [8]. The values of G at $eV = \pm E_Z$ are equal when the QD is contacted by normal-metal leads. Theoretical calculations have revealed, that contacting a QD by ferromagnetic contacts with antiparallel magnetization leads to a pronounced asymmetry in the step height of G with respect to the polarity of V [9]. This asymmetry is induced by the spin-dependent tunnel rates.

The stability diagram, $G(V_G, V_{SD})$, of a QD device with an odd number of holes and a spin-doublet ground state is shown in the inset of Fig. 3(a). The diamond-shape region delimited by dashed lines highlights the CB regime for an odd number of confined holes. While G is generally suppressed within this CB diamond, a G resonance can be identified at V = 0, providing a clear signature of a Kondo effect. At finite B, the Kondo resonance is split by the Zeeman effect as shown in Figs. 3 (a) and (b) for parallel and perpendicular B, respectively (all $G(V_{SD})$ traces were taken at the same V_G). For parallel B, no asymmetry is observed, which is in line with the fact that our QD is contacted by normal metallic leads (aluminium leads). However, for perpendicular B [Fig. 3(b)], the splitting of the Kondo peak is clearly asymmetric with respect to a sign change in V. This is very similar to the theoretically investigated case where ferromagnetic contacts are used to contact the QD. To further investigate this anisotropy, a sequence of $G(V_{SD})$ traces was taken while rotating a 3T field in a plane perpendicular to the substrate. The resulting data, $G(\theta,V_{SD})$, are shown in Fig. 3(c), with θ being the angle between the field and the substrate plane. Along with a variation in the Zeeman splitting of the Kondo peak, caused by the angle-dependent hole g-factor [10], the asymmetry becomes progressively more pronounced when going from $\theta = 0$ (or 180°) towards $\theta = 90°$.

The asymmetries observed in our measurements indicate that the tunnel rate is spin-selective, i.e. the QD's level couples preferentially to one of the two spin species in the lead. Such an effect is well expected in a setup with ferromagnetic contacts. However, no ferromagnetic contacts were used in our experiment. To understand this result, consider the rate to tunnel from the QD into the lead in the usual setup without spin-selective tunnelling. The rate is given by $\Gamma = \pi\nu|t|2$, where t is the tunnelling amplitude and ν the density of states in the lead. For a QD contacted by ferromagnetic leads with antiparallel magnetization it is the density of states that brings about the spin selectivity of the tunnelling. For normal-metal leads the spin selectivity is caused by the tunnelling amplitude t. Indeed, by analysing the Luttinger Hamiltonian in the two-

dimensional limit, we have found that the combination spin orbit coupling and an orbital magnetic field leads to spin-selective tunnel rates (for a rigorous derivation see Ref. [11]).

A natural question arises: What is the physical picture behind this mechanism of spin-selective tunnelling? As mentioned above, in the QD, the states consist of a mixture of HH and LH states. In spite of a predominant HH character, since the measured QDs are rather shallow and the metallic contacts are positioned on top, we can assume that tunnelling takes preferentially place via the Z Bloch amplitude. This fact has an important consequence on tunnelling, since among HH and LH, just LH states include the Z Bloch amplitude. Therefore, tunnelling into QD states takes place predominantly via the LH component of the wave-function, even though the state might have a mainly HH character. However, LH states are not factorizable, i.e. the spin and orbital part of the wave-function are entangled. This is the consequence of the strong spin-orbit interaction present in the valence band of Ge. At zero magnetic field, the tunnel rate for the spin-up and spin-down states is the same. Once a perpendicular magnetic field is switched on, it couples to the orbital part of the envelope function and induces a spatial variation in the relative orbital "weights" of the two spins, i.e. to a difference for the spin-up and spin-down tunnel rates. This effect is highly anisotropic since the studied QDs are rather flat and thus just a perpendicular field has an effect on the orbital motion, leading to spin-selective tunnelling.

While this effect is interesting from a fundamental point of view it might open up new ways to observe Rabi oscillations in single QD devices and allow the realization of novel hybrid spin valve-like devices.

[1] V. N. Golovach et al, Phys. Rev. B 74, 165319 (2006).
[2] K. C. Nowack *et al.*, Science **318**, 1430, (2007).
[3] S. Nadj-Perge *et al.*, Nature **468**, 1084 (2010).
[4] S. Datta, and B. Das, Appl. Phys. Lett. 56, 665 (1990).
[5] I. Appelbaum *et al.*, Nature **447**, 295 (2007).
[6] C. H. Li *et al.*, *Nature Communications*, DOI: 10.1038/ncomms1256, (2011).
[7] S. De Franceschi *et al.*, Phys. Rev. Lett. **86**, 878 (2001).
[8] A. Kogan et al., Phys. Rev. Lett. 93, 166602 (2004).
[9] D. Bing et al., Commun. Theor. Phys 48, 1099 (2007).
[10] G. Katsaros *et al.*, Nature Nanotechnology **5**, 458, (2010).
[11] G. Katsaros et al., Phys. Rev. Lett. 107, 246601, (2011).

Cooperation: [1]SPSMS, CEA-INAC/UJF-Grenoble 1, France
[2]CEA, LETI, MINATEC, F38054 Grenoble, France
[3]Department of Physics, Yale Univ. New Haven, Connecticut, USA

Funded by: Agence Nationale de la Recherche (through the ACCESS and COHESION projects), US DOE Contract No. DE- FG02-08ER46482 (Yale); Nanosciences Foundation at Grenoble, France. Georgios Katsaros was partially supported by the DFG via a research scholarship.

Technological impact

"SupraTrans II" – large scale test-platform for railway-systems with superconductor bearings

D. Berger, O. de Haas, L. Kühn, L. Schultz

In 2011 the full scale R&D-facility for a transportation system with superconducting bearings – SupraTrans II - has been put into operation at the IFW research site in Dresden-Niedersedlitz. SupraTrans II is a research investment of IFW Dresden and has been realized by evico GmbH as system supplier in cooperation with regional partners.

SupraTrans II was officially inaugurated in February 2011 in presence of the Saxon Minister for Science and Art, Prof. Schorlemer, and other guests from politics, industry, research and public transport companies (Fig. 1). Since then several newspapers and TV-journalists like CNN, Spiegel Online, sz-online and many more were visiting the test-facility in Dresden. The new vehicle including a beautiful and dynamic car body was the hot-spot and visitors attraction at the Superconducting City at Hannover Messe 2011.

Fig. 1: Saxon Minister for Science and Art, Prof. Schorlemer taken for a ride on Supratrans II by Prof. Schultz

SupraTrans II is a research platform for superconducting levitation. The main advantage of the system is the possibility of implementing electromagnetic guideway-switches with switching times of a fraction of a second, allowing highly branched railroad systems. Further, there is no electric control system needed and no power consumption (besides a little for cooling of the superconductors) for the levitation and guiding of the vehicle.

Driveway

4.8 tons of NdFeB magnets have been mounted into iron-yokes for the 80 m long magnetic track with curved sections. A new track-design has been developed together with a semi automatic mounting tool for the efficient manufacturing of the magnetic driveway. In addition a passive reaction rail of the linear drive as well as cables and converters for the inductive energy supply have been installed (Fig. 2). For the first time a turnout switch has been implemented using the concept of a mechanical gliding switch.

Fig. 2: Driveway: 80 m long magnetic track with curved sections

Vehicle

The vehicle for two passengers is carried by four cryostats with YBCO bulk superconductors. Only 0.1 l/h of liquid nitrogen is necessary to keep the superconductors cool. Two cryostats are mounted on each, front and back axle. The main frame in between carries the three-phase asynchronous linear motor, the inductive power collector, the entire

Fig. 3: The vehicle for two passengers is carried by four cryostats with YBCO bulk superconductors.

electrical equipment as well as two racing seats. The vehicle design motivates an application as a gate to gate shuttle for airline passengers in modern hubs (Fig. 3). It was evolved in cooperation with the University of Applied Science Dresden.

Control and communication system

In addition to the drive control, systems for positioning and automatic train control have been implemented. The vehicle can be driven by remote control from the control center as well as directly by the driver. Large displays provide on the current operation status. Measurement signals of various vehicle-sensors are transmitted wireless in real-time to the control panel for their scientific analysis.

Specifications of the Test Drive Facility

Rail	gauge of the track	1000 mm
	track length	80 m
	average radius of the bending	6,5 m
	average flux density in the air-space	0,6 T
	distance superconductor - rail	13 mm
	effective airspace under Cryostate	10 mm
Vehicle	Length	2500 mm
	Width	1200 mm
	Mass with rated load (2 persons)	600 kg
	Superconducting material	YBCO
	maximum propulsion power	3,4 kW
	maximum thrust	600 N
	maximum accleration	1 m/s^2
	maximum speed	20 km/h

Cooperation: evico Gmbh, Oswald Elektromotoren GmbH, ELBAS, Conductix-Wampfler AG, University of Applied Science Dresden, Adelwitz Technologiezentrum GmbH
Funding by: Free State of Saxony

Stretchable magnetoelectronics

M. Melzer, D. Makarov, D. Karnaushenko, L. Baraban,
I. Mönch, S. Baunack, R. Kaltofen, and O. G. Schmidt

We fabricated magnetic multilayers ([Co/Cu] and [Py/Cu]) revealing giant magnetoresistance (GMR) effect on free-standing elastic Poly(dimethylsiloxane) (PDMS) membranes. The GMR performance of [Co/Cu] multilayers on rigid silicon and on free-standing PDMS is similar and does not change with tensile deformations up to 4.5%. Mechanical deformations imposed on the sensor are totally reversible, due to the elasticity of the PDMS membranes. This remarkable performance upon stretching relies on a wrinkling of GMR layers on top of the PDMS. A conceptually new approach for the detection of magnetic objects flowing through a fluidic channel was introduced relying on stretchable magnetic sensor wrapped around a capillary tubing. Thus, the stray fields induced by the flowing magnetic objects can be detected virtually in all directions (isotropic sensitivity), which is unique for the elastic sensor compared to rigid planar counterparts.

Research on non-rigid electronics started almost 20 years ago originally motivated by interest in flexible, paper-like displays [1]. There are several ways to achieve non-rigid electronics. One is related to the development of organic electronics [2], which is flexible but slow. A good alternative to this approach is stretchable inorganic electronics, which combines advantages of being flexible with the speed and performance of conventional semiconductor-based electronics. Since being first introduced, stretchable electronics has become a dynamically developing research area which is of strong application interest due to the possibility to reshape the functional element on demand after its fabrication. There are already a variety of flexible devices commercially available and even some of them are implemented in medicine (Fig. 1).
Until recently, the main focus was on fabrication of stretchable high-speed electronics [5] and optoelectronics [6] (Fig. 2). However, the family of shapeable electronics is not limited to these two members. As was mentioned by Prof. M. G. Lagally (University of Wisconsin-Madison), flexibility enables new directions in photonics, thermoelectrics, and integration with magnetic and ferroic materials. Only very recently, we reported for the first time the fabrication of stretchable magnetoelectronics [7]. Magnetic sensor

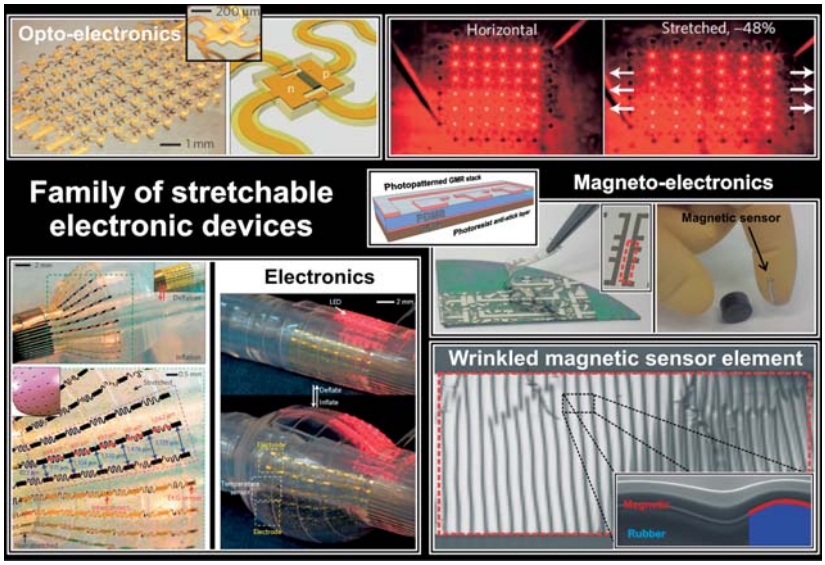

Fig. 2: Family of stretchable electronic devices: (Top panel) Stretchable opto-electronics [5]: array of light emitting diodes (LEDs). (Bottom left) Stretchable electronics [6]: Multifunctional inflatable balloon catheters. (Bottom right) New member of the family – stretchable magneto-electronics: giant magnetoresistive (GMR) sensor element on a free-standing PDMS membrane [7]. Stretchability of the magnetic sensor element is due to wrinkle formation.

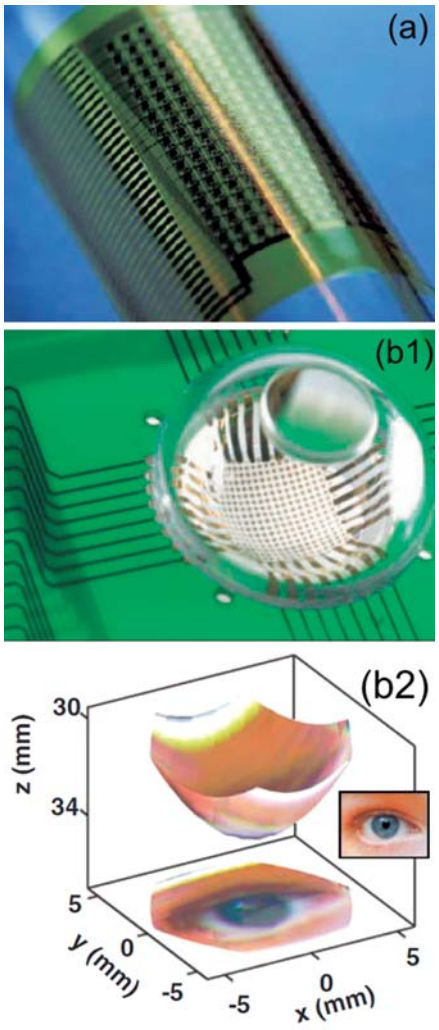

Fig. 1: Stretchable electronics for biomedical applications: **(a)** Implantable device for measuring the heart's electrical output with a vast improvement over conventional devices [3]. **(b)** Towards artificial retina: Electronic eyeball camera (b1) that uses a hemispherically curved array of silicon photodetectors and picture collected with a similar camera that uses a paraboloid design (b2). The image in the top is rendered in a form consistent with the curvature of the detector. A planar projection appears on the bottom, with the actual object in the centre right inset. The image is adopted from [4].

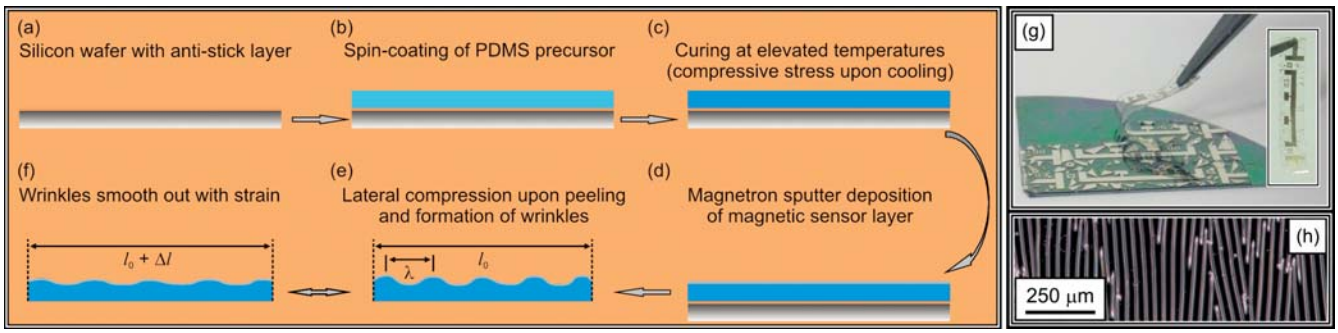

Fig. 3: Fabrication of the stretchable GMR multilayer stack: **(a)** SiOx wafer coated with photoresist as anti-stick layer. **(b)** The PDMS precursor blend is spin-coated on top. **(c)** The precursor is cured at elevated temperatures to form a rubber film. **(d)** Deposition of the magnetic sensor layer. **(e)** The metal coated rubber film is peeled from the SiOx wafer. By peeling off the PDMS from the rigid support, wrinkling of the GMR multilayer stack takes place. **(f)** Upon stretching the wrinkles are smoothened out and prevent the sensor from cracking, allowing for superior stretchability. **(g)** Peeling of the magnetic coated rubber from the rigid silicon. **(h)** For the metal film on free-standing rubber the formation of wrinkles is observed.

devices on elastic substrates could enable fabrication of smart biomedical systems, where large-angle folding of the micrometer-sized functional elements is a crucial prerequisite for a successful implementation. Furthermore, flexible magnetic sensors can be directly integrated into already existing stretchable electronic systems to realize smart hybrid magneto-electronic devices with the functionality to sense and to respond to a magnetic field.

Layered magnetic structures revealing a giant magnetoresistance (GMR) effect are crucial components of magnetic sensor devices. Currently, GMR sensors are fabricated on rigid inorganic substrates. Here, we demonstrate functional stretchable magnetic sensor based on [Co/Cu] and [Py/Cu] GMR multilayers prepared on free-standing elastic PDMS membranes. In order to produce magnetic layer stacks on a free-standing rubber membrane, PDMS (Sylgard® 184) was first spin-coated onto silicon wafers. An anti-stick photoresist layer is introduced to assist peeling the PDMS film from the rigid silicon support (Fig. 3(a, b)). The PDMS precursor blend was cured in an oven under continuous nitrogen flow, resulting in a rubber film (Fig. 3(c)). To provide the possibility of electrical resistance measurements of the magnetic sensor device on the rubber substrate, the PDMS surface was patterned by means of photolithography before metal deposition (Fig. 3(g)). This renders the fabrication process compatible to current microelectronic structuring procedures. The magnetic sensor layer was grown onto the elastic PDMS surface (Fig. 3(d)) using magnetron sputter deposition. Afterwards, the PDMS film was peeled from the rigid silicon wafer leading to a free-standing elastic membrane covered with magnetic layer (Fig. 3(e)).

The GMR ratio is defined as the magnetic field dependent change of the sample's resistance, $R(H_{ext})$, normalized to the value of resistance when the sample is magnetically saturated, R_{sat}: $GMR(H_{ext}) = [R(H_{ext}) - R_{sat}] / R_{sat}$. Fig. 4(left panel, top) shows the GMR ratio measured for $[Co/Cu]_{50}$ multilayers grown on different substrates. The GMR curves obtained from the samples prepared in the same deposition run on a rigid silicon wafer without (open square symbols) and with PDMS coating (open circle symbols) are very similar. A maximum GMR value of more than 50% is obtained on both substrates. Furthermore, the GMR signal does not change after the PDMS is peeled off the silicon wafer (compare curves with open and close circle symbols). Although the GMR performance of the devices on free-standing PDMS membranes and on PDMS-coated silicon wafers is similar, the morphology of the samples is found to be substantially different due to appearance of thermally induced wrinkles (Fig. 4(left panel, middle)). The height profile of the sample reveals a wrinkling period of about 17 µm and a mean amplitude of about 0.5 µm. Upon stretching the wrinkles are smoothened out and prevent the sensor from

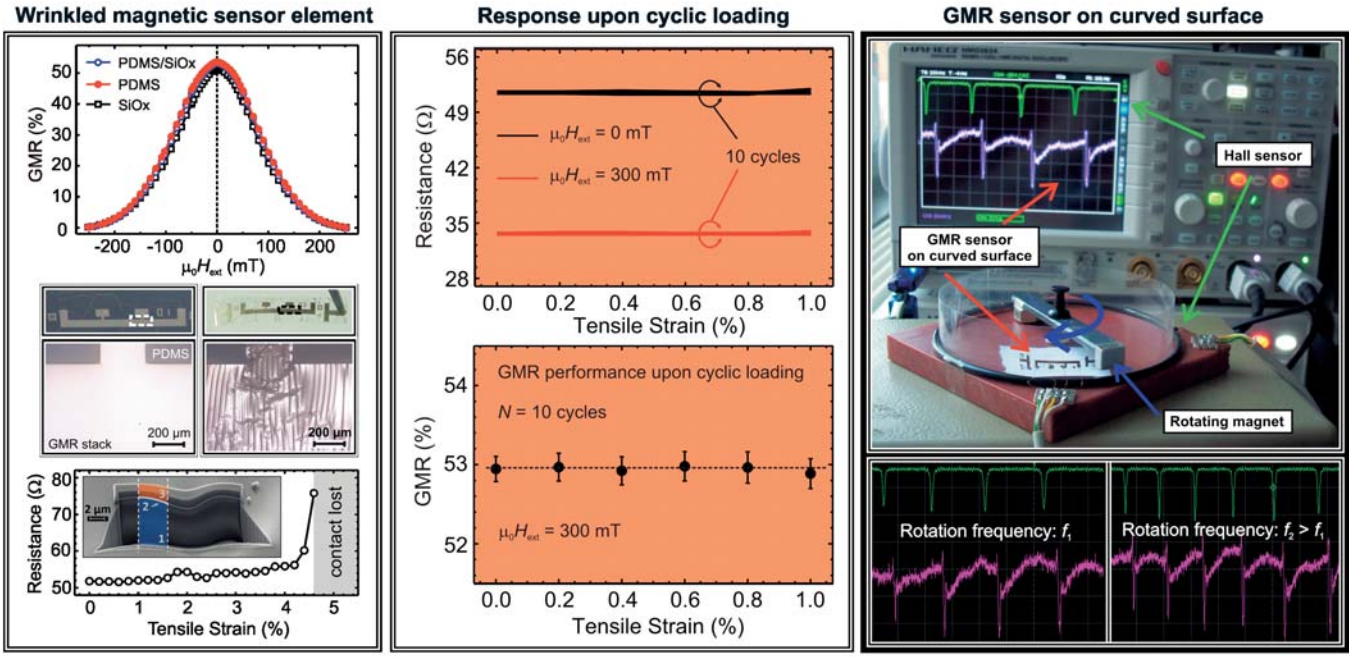

Fig. 4: (Left panel) Stretchable magnetoelectronics: giant magnetoresistive (GMR) sensor element on a free-standing PDMS membrane. Even after the sample is peeled from the SiOx wafer, the GMR performance remains unchanged. Optical microscopy images taken from the photolithographically patterned GMR multilayers on PDMS/SiOx and free-standing PDMS membrane revealing wrinkle formation. Electrical resistance of the wrinkled GMR multilayer upon tensile strain. Only gradual increase in the sample resistance is observed up to 4.5% strain. The inset shows SEM image of a FIB cut through the sample (1: PDMS; 2: [Co/Cu] multilayers; 3: carbon protective layer). (**Middle panel**) Response of the GMR sensor to cyclic loading. (**Right panel**) Measurement of the magnetic field of a rotating magnet using an elastic GMR sensor attached to the curved surface of a plastic foil. The figure is adopted from [7].

cracking, allowing for superior stretchability. Fig. 4(left panel, bottom) shows the measured electrical resistance while the sample was stretched. For strains of up to about 4% only a slight increase of the samples resistance is observed. For higher strains the resistance abruptly increases and finally the electrical contact is lost at a strain of about 4.5% (gray-shaded area). Please note that flat metal films on top of a rubber substrate without surface wrinkling withstand tensile strains of only below 1% [8].

The GMR sensor element is remarkably stable against cyclic loading. Fig. 4(middle panel) shows the resistance of a GMR multilayer on a rubber membrane during 10 stretching cycles from 0 to 1% and back. A permanent magnet was employed to measure the GMR performance. The magnetic field was chosen to be 300 mT to assure that the sample is magnetically saturated. When the magnetic field is applied, the resistance of the sample drops (Fig. 4(middle panel, top), red curve) as expected for [Co/Cu] multilayers. The resistance of the sample (with and without applied magnetic field) remains unchanged even after the sample was reversibly stretched and relaxed for 10 times. Fig. 4(middle panel, bottom) shows the GMR ratio in dependence of the tensile strain for the cyclic loading measurements. The GMR ratio remains at a constant value of ≈ 53% with low deviations (±0.2%) for tensile strains up to 1% and therefore is well-suited for magnetic sensor applications in environments where deviations from a flat geometry are required.

To demonstrate the performance of the elastic GMR sensor element, the sensor was attached to a plastic foil shaped into a ring geometry to track the magnetic field of a rotating permanent magnet (Fig. 4(right panel, top)). The change of the resistance of the GMR multilayer was recorded versus time: When the magnet is in the proximity of the GMR sensor, a clear decrease of the sample resistance is detected. The dynamic response is illustrated by sensing the rotating magnetic field at higher frequency, which is easily traced with the GMR sensor (Fig. 4(right panel, bottom)).

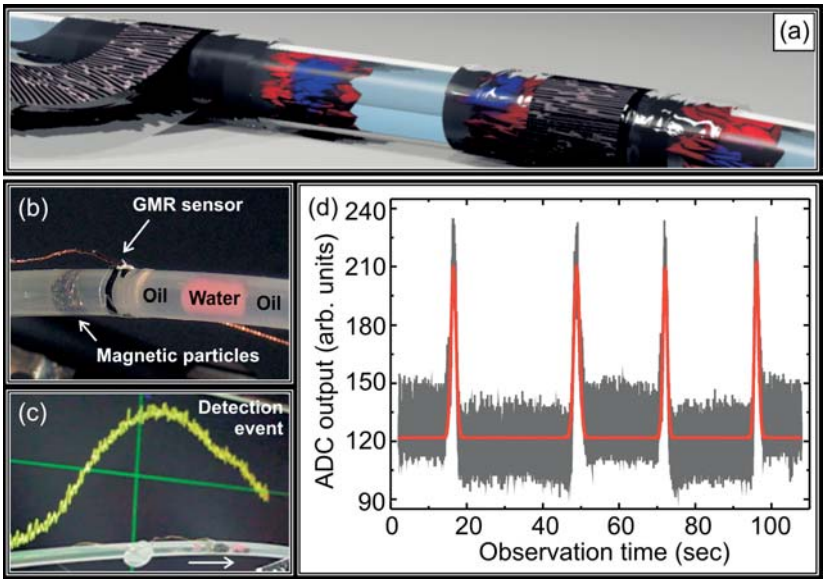

Fig. 5: (a) Sketch demonstrating the application of stretchable magnetic sensors for in-flow detection of magnetic objects in fluidics: the elastic sensor can be tightly wrapped around a fluidic channel allowing for an enhanced and isotropic sensitivity. Detection of magnetic particles in a fluidic channel: **(b)** optimized $[Py/Cu]_{30}$ elastic GMR sensor wrapped around the circumference of a Teflon tube. Agglomerate of FeNdB particles suspended in oil and separated by colored water droplets inside the tubing is shown. The magnetic particles are approaching the GMR sensor. **(c)** Signal of the elastic GMR sensor on a screen (background) as the magnetic cluster is passing the sensor (foreground). **(d)** Several consecutive detection events of particles passing the elastic GMR sensor.

Furthermore, we proposed a new concept for in-flow detection of magnetic particles in millifluidics using elastic GMR sensors. Due to their stretchability, GMR sensors can be wrapped tightly around a fluidic channel (Fig. 5(a, b)). This strategy offers the following advantages: (i) sensing of the magnetic stray fields in virtually all directions (isotropic sensitivity), which is unique compared to the rigid planar counterparts; (ii) simplicity of the sensor integration into a fluidic circuit; (iii) possibility of being reused. As magnetic stray fields to be detected in fluidics are small, the strong emphasis was on the enhancement of the sensitivity of the sensor on elastic membranes to small magnetic fields. For this purpose, we fabricated different GMR multilayer systems, including [Co/Cu] and [Py/Cu] stacks coupled in the 1^{st} or 2^{nd} antiferromagnetic (AF) maximum. Even when prepared on elastic 40-µm-thick free-standing rubber membranes, [Py/Cu] multilayers coupled in the 2^{nd} AF maximum reveal a remarkable sensitivity of 106 T^{-1} (magnetic field: 0.8 mT); this value is almost 30 times larger than for the [Co/Cu] stack coupled in the 1^{st} AF maximum. We successfully demonstrate the performance of this elastic sensor wrapped around a fluidic channel (diameter of 3 mm) for in-flow detection of assemblies of magnetic FeNdB particles (Fig. 5(c, d)). Our approach potentially opens an exciting possibility for stretchable magnetoelectronics to be applied in the field of biology and chemistry. Indeed, in combination with magnetic particles as biomarkers, this elastic magnetic sensor can be considered as a new generation of biosensors for cells or even biomolecules evading many difficulties of traditional optical detection methods like low speed, excitation, bulky and expensive equipment, biomolecular amplification and the need for transparent packaging.

[1] D. H. Kim et al., Adv. Mater.22, 2108 (2010).
[2] T. Sekitani et al., Adv. Mater. 22, 2228 (2010).
[3] J. Viventi et al., Science Transl. Med. 2, 24ra22 (2010).
[4] J. A. Rogers et al., Science 327, 1603 (2010).
[5] D. H. Kim et al., Nature Mater. 10, 316 (2011).
[6] R. H. Kim et al., Nature Mater. 9, 929 (2010).
[7] M. Melzer et al., Nano Letters 11, 2522 (2011).
[8] S. P. Lacour et al., Appl. Phys. Lett. 82, 2404 (2003).

Cooperation: Leibniz Institute of Polymer Research Dresden, Dresden, Germany; Department of Materials Science, Fudan University, China
Funded by: BMBF project Nanett (federal research funding of Germany FKZ: 03IS2011F).

High-strength iron-based alloys with an outstanding range of properties

J. Hufenbach, U. Kühn, L. Giebeler, H. Wendrock, T. Gemming, S. Oswald,
M. Hoffmann, L. Schultz and J. Eckert

The present work describes the correlation between microstructure and mechanical properties of high-strength iron-based alloys manufactured under preparation conditions similar to that of bulk metallic glasses. The applied process parameters promote the formation of non-equilibrium phases such as martensite, retained austenite and special carbides already in the as-cast state. By varying the composition and preparation conditions of the iron-based alloys, a wide range of mechanical properties can be adjusted. Thus extreme engineering compression strength of almost 5500 MPa combined with a large compression strain of about 23 % may arise. By an appropriate short-term tempering process, it is furthermore possible to adjust a high hardness, compressive and tensile strength simultaneously. This range of mechanical properties leads to outstanding engineering materials for a variety of structural applications.

The increasing demand of industry for high-performance steels with excellent durability under extreme loading conditions promotes the development of novel iron-based alloys possessing high strength, hardness, wear resistance and ductility. Therefore, a manufacturing process was developed, which leads to superior mechanical properties for tailored iron-based alloys already in the as-cast state [1,2]. The composition of the manufactured high-strength alloys is based on the Fe-Cr-Mo-V-(W)-C system and similar to a commercial tool steel, but the applied casting conditions resemble those of bulk metallic glasses implying relatively high cooling rates and pure preparation conditions. Thereby a microstructure composed of martensite, retained austenite and a complex network of special carbides can be obtained already in the as-cast state. Depending on the composition and preparation conditions of the iron-based alloys (especially the solidification rate and subsequent heat treatment) a wide range of mechanical properties is adjustable. Here, the high-strength iron-based alloys $Fe_{86.7}Cr_{4.4}Mo_{0.6}V_{1.1}W_{2.5}C_{4.7}$ (at.%) and $Fe_{84.3}Cr_{4.3}Mo_{4.6}V_{2.2}C_{4.6}$ (at.%) are presented as examples, which were tailored for different loading conditions and applications [2,3].

For the preparation of the alloys, pure elements were inductively melted in a ceramic crucible under argon atmosphere. Afterwards the melt was cast into a copper mould and the resulting ingot had dimensions of 70 x 120 x 15 mm^3. To achieve a microstructure with the desired phase fractions of martensite, retained austenite and complex carbides an average cooling rate of about 10 to 70 K/s has to be achieved.

For a certain group of the developed iron-based alloys (including $Fe_{84.3}Cr_{4.3}Mo_{4.6}V_{2.2}C_{4.6}$) additional short-term tempering in the temperature range of the secondary hardening maximum and stress free annealing further increases the mechanical properties and enables their load-adapted adjustment. Originally, this heat treatment method was described for rolling bearing steels [4] or heat-resistant steels [5], but not in combination with accelerated cooled iron-based alloys. The adapted tempering process for the high-strength alloys was realised in a muffle furnace under argon atmosphere. Previous investigations of the $Fe_{84.3}Cr_{4.3}Mo_{4.6}V_{2.2}C_{4.6}$ alloy showed a typical secondary hardness maximum at a temperature of 833 K. To adjust the properties occurring at this temperature, the ingots were once or twice heated up with approximately 25 K/min to 833 K, held for one minute and cooled down to room temperature with an average rate of 25 K/min [6].

The dendritic microstructure of the as-cast $Fe_{84.3}Cr_{4.3}Mo_{4.6}V_{2.2}C_{4.6}$ after etching with Beraha I is shown in Fig. 1a. The dendrites are mainly composed of martensite (dark

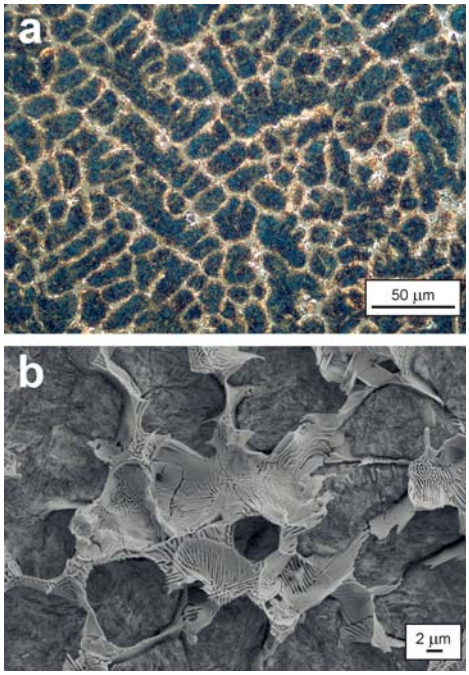

Fig. 1: a) Optical micrograph of the dendritic structure of the as-cast $Fe_{84.3}Cr_{4.3}Mo_{4.6}V_{2.2}C_{4.6}$ alloy (etched with Beraha I) showing the distribution of the present phases; **b)** SEM image of the deep etched $Fe_{84.3}Cr_{4.3}Mo_{4.6}V_{2.2}C_{4.6}$ alloy revealing the fine network-like structure formed by complex carbides and its arrangement within the material.

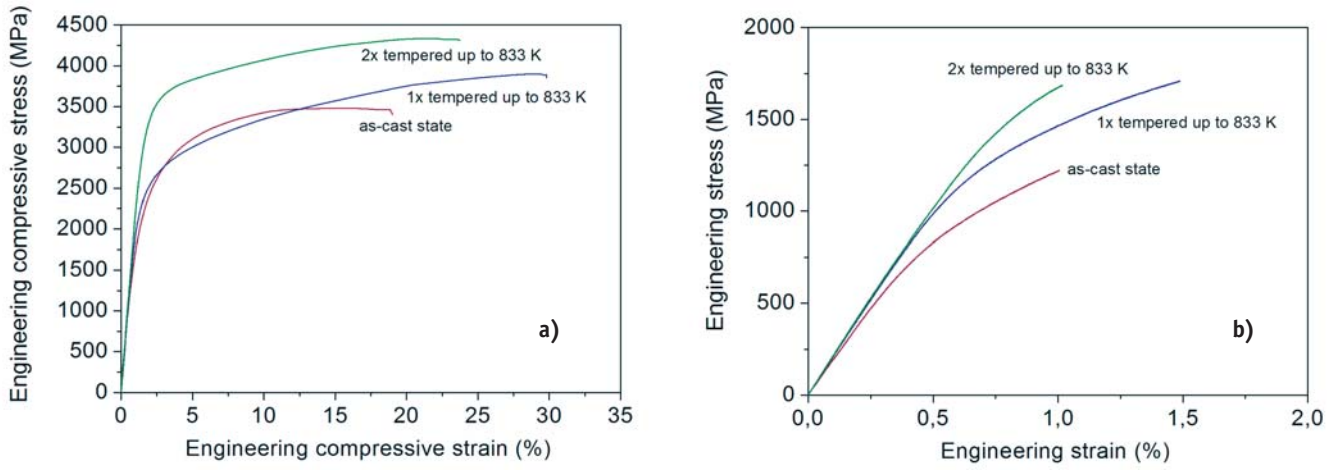

Fig. 2: a) Engineering compressive stress as a function of the engineering strain for the as-cast and tempered samples; **b)** Engineering tensile stress-strain curves of the as-cast and tempered samples.

phase) as well as fine carbides, whereas the interdendritic area is composed of retained austenite and coarse primary Mo_2C and VC type carbides (light phases). The carbides form a fine skeleton-like structure around the dendrites, which is illustrated in Fig. 1b for a deep etched as-cast sample. The effect of this one- or two-stage heat treatment on the mechanical properties of the as-cast $Fe_{84.3}Cr_{4.3}Mo_{4.6}V_{2.2}C_{4.6}$ alloy is shown in Fig. 2a and b. In these graphs the engineering compressive stress as a function of the engineering strain (Fig. 2a) and the engineering tensile stress-strain curves are presented (Fig. 2b). Apparently, short-term tempering has a significant influence on the mechanical behaviour of the investigated alloy. The ultimate and yield strengths as well as the strains of the tempered samples increase in comparison to the as-cast state. The one-stage tempered sample shows the highest engineering strain under compressive and tensile loading, while the two-stage tempered samples possess the highest strength of about 4408 MPa under compression.

Fig. 3: XRD patterns of the as-cast, one-stage and two-stage tempered samples of the $Fe_{84.3}Cr_{4.3}Mo_{4.6}V_{2.2}C_{4.6}$ alloy with indexed martensitic (m) and austenitic (a) phases as well as carbides.

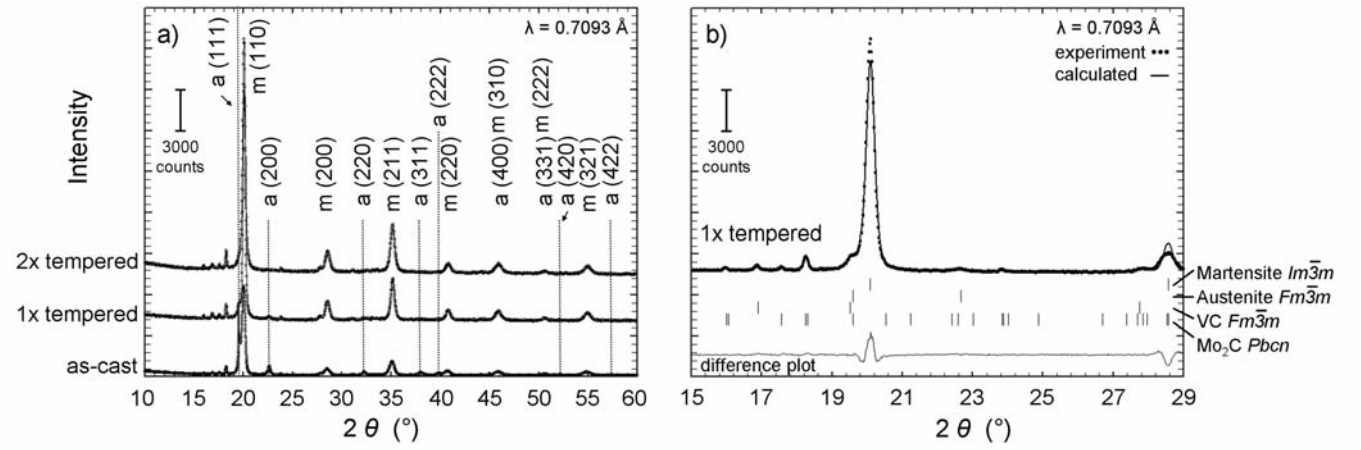

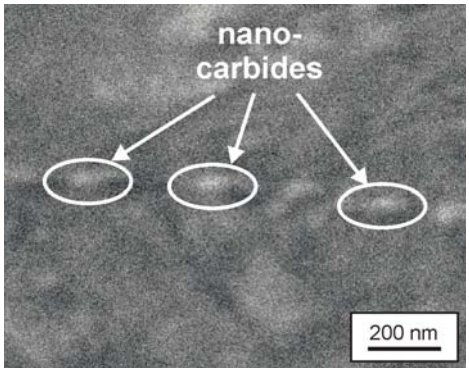

Fig. 4: SEM image of nano-precipitates in the martensitic matrix of a two-stage short-term tempered sample.

This behaviour is a result of the competing mechanisms increasing the ductility and strength of the alloy. The ductility is enhanced by residual stress relaxation and the diffusion of carbon atoms as well as substitutional alloying elements (such as Cr) from the martensite. In contrast, the strength is increased by the transformation of retained austenite into martensite (see Fig. 3), the associated elastic distortion as well as the precipitation of chain-like arranged nano-carbides due to tempering (Fig. 4). To determine the contents of phases in the as-cast and tempered states, X-ray diffraction in combination with Rietveld analysis was applied. Due to the heat treatment the fraction of martensite increases, whereas the austenite content drops (see Fig. 3) from about 24 wt.% to 4 wt.% after one-stage tempering and after two-stage tempering austenite can no longer be detected. Thereby the fraction of the primary carbides does not significantly change due to the heat treatment. The reason for the decreasing ultimate tensile strength and strain after two-stage tempering is an early failure at the interface between carbides and dendrites and the absence of the damage-tolerant austenitic phase.

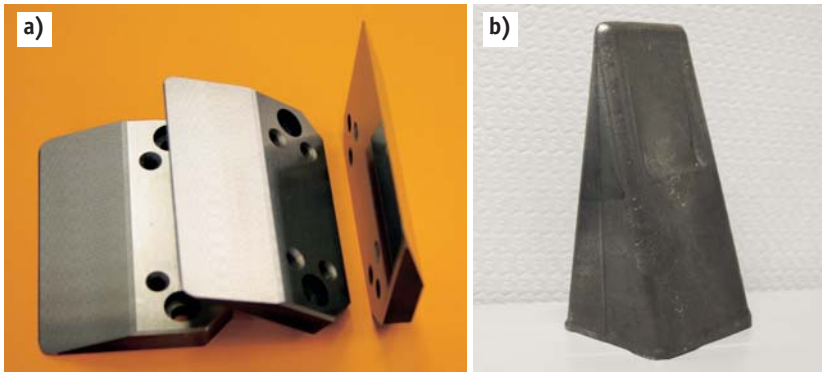

Fig. 5: Knife for packaging machine (Rohrer AG) and digging tooth made of developed high-strength iron-based alloy.

In any case, the strength values achieved by short-term tempering are significantly higher than the tensile strength [7] and the compressive strengths [8] of commercial tool steels. This opens up new possibilities to replace these steels for appropriate application in tool making. Alloys with the described properties are already engaged in packaging machines of the Rohrer AG and were successfully tested as tool material for precision cutting of medical filters by Alpha Plan GmbH and as digging teeth (Fig. 5).

The second remarkable group of developed iron-based alloys shows ultra-high compressive strength already in the as-cast state. In Fig. 6a and b the microstructure of an as-cast $Fe_{86.7}Cr_{4.4}Mo_{0.6}V_{1.1}W_{2.5}C_{4.7}$ ingot is displayed. The optical microscope image obtained after etching with Beraha I (Fig. 6a) reveals that the material is composed of martensite, austenite and a complex 3-dimensional network of fine structured carbides (Fig. 6b), which are mainly $(Mo,W)_2C$ compounds.

Fig. 7 shows the engineering compressive stress and the volume fraction of martensite as a function of the engineering strain for the as-cast material. The most significant mechanical property of the present $Fe_{86.7}Cr_{4.4}Mo_{0.6}V_{1.1}W_{2.5}C_{4.7}$ alloy is its very pronounced work-hardening behaviour. The material starts to deform plastically at a 0.2-offset yield strength of about 1296 MPa and fails at an outstanding engineering compression ultimate strength of about 5439 MPa at a compressive strain of almost 24% [3], which is much superior compared with commercial high-duty tool steels [8]. In order to clarify the reason for this special deformation behaviour, the volume fraction of martensite at different strain levels (0, 4, 9, 14, and 24%) was determined by vibrating sample magnetometer. The volume fraction of martensite in the examined iron-based alloy clearly increases with increasing strain. The metastable austenite in the as-cast material, which amounts to about 30 vol.% (when the volume fraction of carbides is neglected), transforms into martensite because of the imposed external stress during deformation. Therefore, the reason for the large work hardening is, besides conventional dislocation

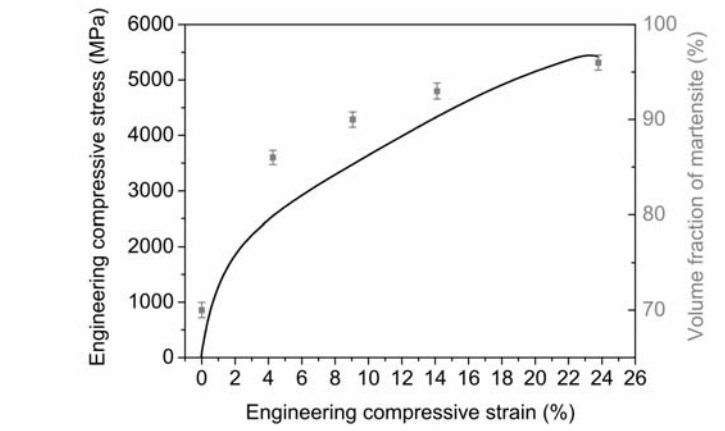

Fig. 7: Engineering compressive stress and volume fraction of martensite as a function of the engineering strain for the as-cast $Fe_{86.7}Cr_{4.4}Mo_{0.6}V_{1.1}W_{2.5}C_{4.7}$ alloy.

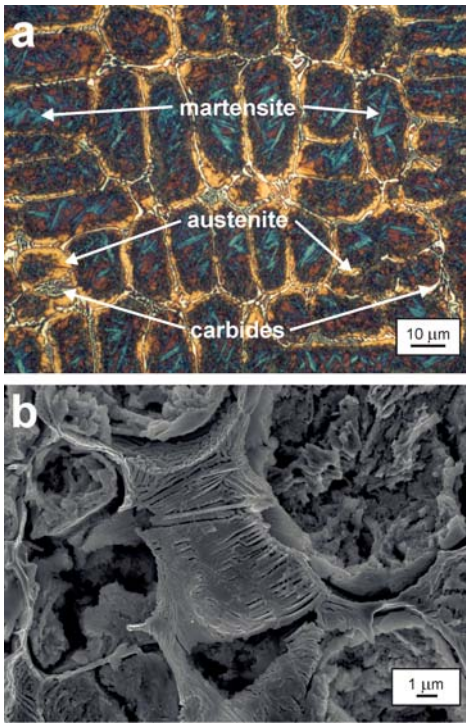

Fig. 6: a) Optical micrograph of the dendritic structure of the as-cast $Fe_{86.7}Cr_{4.4}Mo_{0.6}V_{1.1}W_{2.5}C_{4.7}$ alloy showing the distribution of the present phases; **b)** SEM images of the $Fe_{86.7}Cr_{4.4}Mo_{0.6}V_{1.1}W_{2.5}C_{4.7}$ alloy illustrating the fine network-like structure formed by complex carbides and its arrangement within the material.

mechanisms, linked with the transformation-induced plasticity (TRIP) effect caused by the deformation-induced transformation of metastable austenite into martensite [3,9]. The $Fe_{86.7}Cr_{4.4}Mo_{0.6}V_{1.1}W_{2.5}C_{4.7}$ alloy is, therefore among others, a promising engineering material for energy absorbing parts, e.g. in vehicles.

In conclusion, applying preparation conditions similar to those of bulk metallic glasses to the presented iron-based alloys promotes the formation of martensite, retained austenite and special carbides already in the as-cast state. The combination of these phases yields alloys with outstanding mechanical properties exhibiting high hardness, good tensile strength as well as extremely high engineering compression strength together with large compression strain. By utilising a novel manufacturing technology employed for the $Fe_{84.3}Cr_{4.3}Mo_{4.6}V_{2.2}C_{4.6}$ alloy combining accelerated solidification under pure preparation conditions and subsequent short-term tempering, a fast and energy efficient possibility for load-adapted adjustment of hardness, strength and ductility under compressive and tensile load was developed.
In the future, the range of mechanical properties of the high-strength iron-based alloys shall be further increased for applying the large potential of this group of materials for high performance demands e.g. in the automotive and tool manufacturing industry.

[1] K. Werniewicz et al. Acta. Mater. **55** (2007) 3513
[2] U. Kühn et al. Appl. Phys. Lett. **90** (2007) 261901
[3] J. Hufenbach et al. J. Mater. Sci. **47** (2012) 267
[4] H. Scheerer et al. Matwiss. Werkstofftech. **37** (2006)183
[5] K. Tamakia et al. Welding Int. **10** (1996) 971
[6] J. Hufenbach, J. Eckert, U. Kühn, S. Kohlar: Verfahren zur Wärmebehandlung von hochfesten Eisenlegierungen. German patent application deposited
[7] A. Benazza et al. J. Mater. Sci. **42** (2007) 834
[8] J. R. Davis ASM Specialty Handbook Tool Materials, ASM International, Materials Park
[9] U. Kühn et al. J. Mater. Res. **25** (2010) 368

Cooperation: University of Oxford (Great Britain), Foundry Research Institute Cracow (Poland), Korea Institute of Industrial Technology / Institute for Rare Metals (Korea), Freiberg University of Technology (Germany), Karlsruhe Institute of Technology (Germany)
Funding by: European Union and the Free State of Saxony, WIWeB Erding

Innovations for Surface Acoustic Wave Devices

S. V. Biryukov, G. Martin, H. Schmidt, S. Menzel, A. Winkler,
M. Spindler, T. Gemming, H. Wendrock, H. Turnow

The design and fabrication of interdigital transducers (IDT) are of outstanding relevance for modern surface acoustic wave (SAW) devices in their application as electric frequency filters, resonators, sensors and actuators. Such devices are increasingly used at operation frequencies reaching into the GHz range as well as under extremely high input power levels. In the following examples for new design principles for GHz range SAW devices as well as for advanced SAW device material systems will be given.

SAW-based ID tags operating in GHz range

An important challenge in recent surface acoustic wave (SAW) device design is to develop low-loss identification devices (ID tags) which are insensitive to fluctuations of technological production parameters. Such ID tags are frequently carried out as reflective delay lines consisting of an interdigital transducer (IDT) and differently coded reflectors on the surface of the piezoelectric chip. The IDTs have previously been implemented as bidirectional transducers. However, it is advantageous to use single phase unidirectional transducers (SPUDT) in order to reduce the loss of these tag devices.

There are numerous solutions for such unidirectional transducers, however, usual SPUDT designs have strong disadvantages making their application to GHz range devices impossible:

- Previous solutions include very narrow finger electrodes. These exceed the critical dimensions of available technology and, therefore, they can hardly be realized with sufficient quality for the GHz range.
- All known SPUDT cells include finger electrodes and gaps of different width, resulting in high losses due to acoustic bulk wave generation.

As an alternative, new solutions for unidirectional transducers were developed at IFW implementing finger electrodes and gaps of equal width where the finger electrodes form a regular grating in wave propagation direction. For these designs fingers and gaps have at least a width of a quarter of the wavelength. Two new approaches for transducers meeting these conditions are presented here.

(1) Natural single phase interdigital transducers (NSPUDT): The Y cut of $LiNbO_3$ (YZ $LiNbO_3$) with Rayleigh wave propagation direction along Z is a candidate for NSPUDT behavior because the Z axis is parallel to the threefold rotation crystal axis. According to the definition applied here the unidirectional behavior is characterized by a phase of the reflection factor (with respect to the transduction center) φ_r equal to $\pm 45°$. As Fig. 1 demonstrates, there is no chance to achieve any NSPUDT behavior by using Al electrodes of reasonable normalized layer thickness (absolute layer thickness h normalized to IDT period p, i.e. h/p). In contrast, three different layer thickness values meeting the unidirectionality condition of $\varphi_r = \pm 45°$ are found below a normalized electrode thickness of 0.06 if aluminum is replaced by platinum. Similar results could be obtained for gold as electrode material. The NSPUDT case with Pt electrodes with $h/p = 0.048$ was confirmed experimentally and a strong unidirectionality could be stated (Fig. 2). The frequency dependencies of forward and backward directions show the characteristic shapes for unidirectional behavior. A SPUDT setup including a Pt-IDT and Al-reflectors was applied to an ID-tag design as presented in Fig. 3. The time domain S_{11} behavior of this reflective

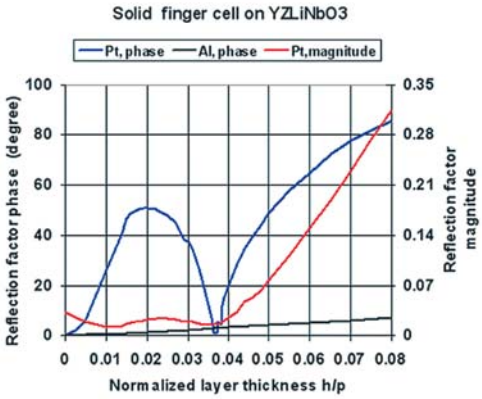

Fig. 1: Reflection factor of a platinum solid finger cell (magnitude and phase) in comparison to reflection factor of an aluminium solid finger cell (magnitude).

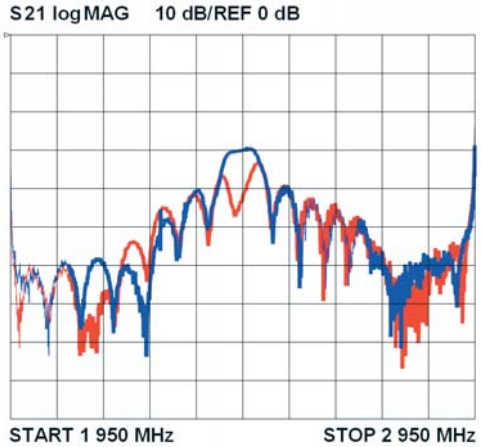

Fig. 2: NSPUDT behavior of a platinum solid finger cell (blue: forward; red: backward direction).

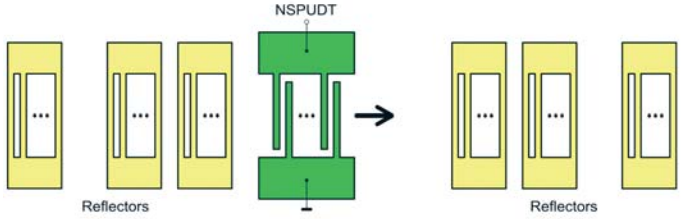

Fig. 3: Layout of a reflective delay line operating as an ID tag. The arrow marks the forward direction of the unidirectional transducer.

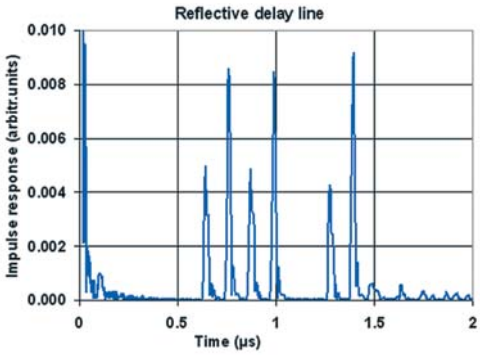

Fig. 4: Impulse response of reflective delay line of Fig. 3

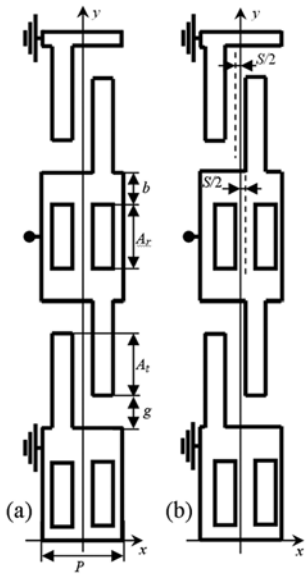

Fig. 5: APTUDT cell, **(a)** bidirectional, **(b)** unidirectional setup

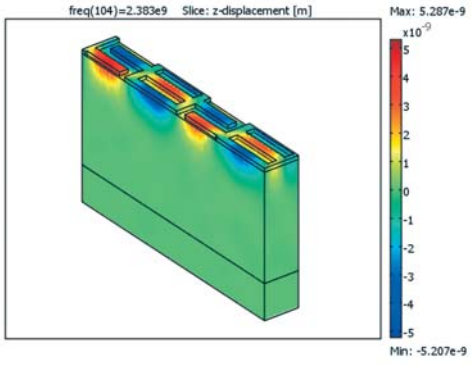

Fig. 6: SAW amplitude distribution within an APTUDT cell (FEM simulation)

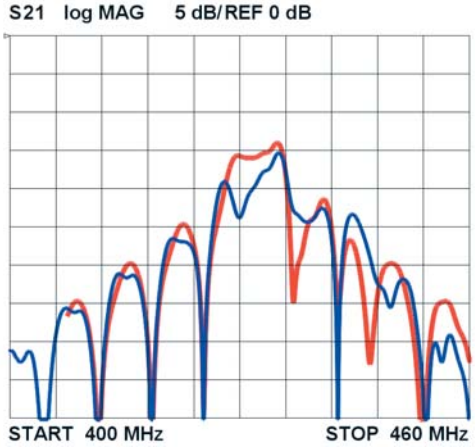

Fig. 7: Unidirectional behavior of an APTUDT (blue: forward; red: backward direction).

delay line is depicted in Fig. 4. As can be seen clearly, the (delayed) pulses resulting from the right-side reflectors are larger as compared to those from the left what gives clear evidence for the unidirectionality. According to Fig. 3 the individual distance of each single reflector to the transmitter IDT is smaller for those reflectors arranged on the left than for those on the right side, resulting in shorter delay times. With a platinum finger electrode width of 0.3 µm this design is still clearly within the limits of today's SAW patterning technology.

(2) Multi-track single phase interdigital transducers (Multi-track SPUDTs): Designs of this type are a second option for unidirectional transducers comprising finger electrodes and gaps with a width of at least a quarter of the wavelength. Such a transducer consists of two types of alternating tracks: the active tracks which excite and reflect the surface waves at the same time and the passive tracks which are non-exciting and only reflect the waves. To achieve unidirectionality the phase of the total reflection factor of the setup has to be ±45° what can be adjusted by a shift of passive tracks with respect to active ones along the wave propagation direction. Fig. 5 shows two cells of this transducer type continuing periodically in parallel as well as perpendicularly to the direction of finger electrodes. This new transducer type with two-dimensional periodicity is called active-passive track unidirectional transducer (APTUDT). The characteristic shift between active and passive tracks is denominated by S in Fig. 5. For comparison, Fig. 5a describes a bidirectional cell with S = 0, whereas the shift $S \neq 0$ in Fig. 5b leads to a unidirectional SAW radiation. The wave field of an APTUDT cell on 128°YX $LiNbO_3$ with Al electrodes (h/p = 0.06) was calculated by finite element method. Due to strong diffraction effects a comparable wave field exists in the passive tracks as well as in the active tracks (Fig. 6). The unidirectional behavior of such an APTUDT was verified experimentally, as depicted in Fig. 7 in analogy to Fig. 2. As expected, the curves for forward and backward direction differ considerably. The first proof of principle was realized at 430 MHz. Scaling down to GHz range will result in electrode widths of 0.39 µm and still meet the limits of available technologies.

Advanced materials for innovative SAW devices

High power load limits performance and lifetime of SAW devices due to damaging of IDT finger electrodes. Both, thermal and stress induced material transport can result in thermal grooving, void and hillock formation, or even delamination effects of the metal electrodes resulting in frequency shift and failure of the device. But also crack initiation and growth in the piezoelectric substrate is possible at extremely high power load.

The IFW has a long-time experience in theory, design, fabrication and characterization of SAW devices of high performance and for high power applications. This includes general work to the physics of surface dynamics and structure design, the development of thin film materials for IDT electrodes with high power durability and lifetime, the study of damaging and failure mechanisms under SAW load (acoustomigration) as well as relevant technological and measurement aspects.

Several power durable metallization systems were developed in specifically targeted projects. Especially aluminum or copper based alloys and multilayers or graduated layer stacks have been developed combining high electrical conductivity and high acoustomigration resistance. Also high texture (htx) metallic films avoiding transport paths of high diffusivity highlight the activities in electrode material development. It has been

shown that lifetime of SAW structures can be increased by several orders of magnitude by using htx Al-based materials in comparison to polycrystalline films as well as by a specific copper technology. This fact correlates with a significant increase in power durability (Fig. 8).

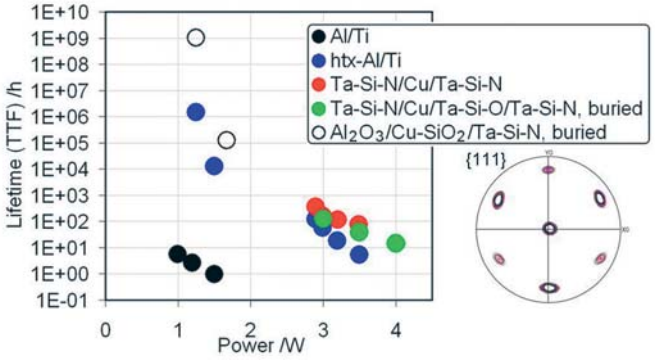

Fig. 8: Lifetime of SAW test structures with different finger metallizations and a typical EBSD pattern of htx-Al films

Contrary to a conventional design principle where the IDTs are arranged on top of the substrate a novel technology was developed where the copper finger electrodes are buried in the substrate material or in an additional magnetron sputtered SiO_2 layer. This so-called damascene technology enables to build up a technological platform of high flexibility especially suited for SAW-driven microfluidic actuators at low costs in combination with other functional layers that can be adapted to different applications and other custom-designed modules (Fig. 9). Such a setup offers a wide range of applications, e.g. in medical science, chemistry or analytics. For this purpose a variety of chip layouts was designed for different applications including microfluidic manipulation, droplet transport, atomization of fluids and others (Fig. 10).

In this context the IFW built up a special cluster tool (Fig. 11) which enables to develop and deposit dedicated and advanced thin films on piezoelectric or pyroelectric substrates by dc and rf magnetron sputtering (e.g. SiO_2, Ta-Si, Ru, Ti, W, Mo, Cu, Zr, Ni) as well as electron beam evaporation (e.g. Al, Cu, Au, Ti).

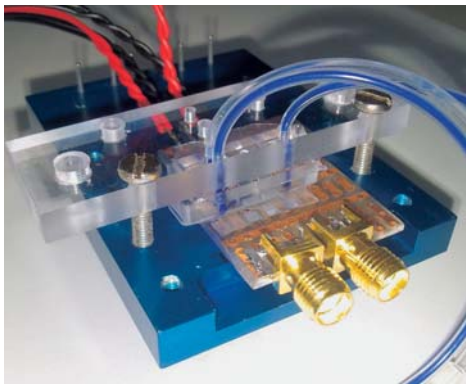

Fig. 9: Example for a modular SAW device (actuator)

Fig. 11: IFW cluster tool for the SAW material development

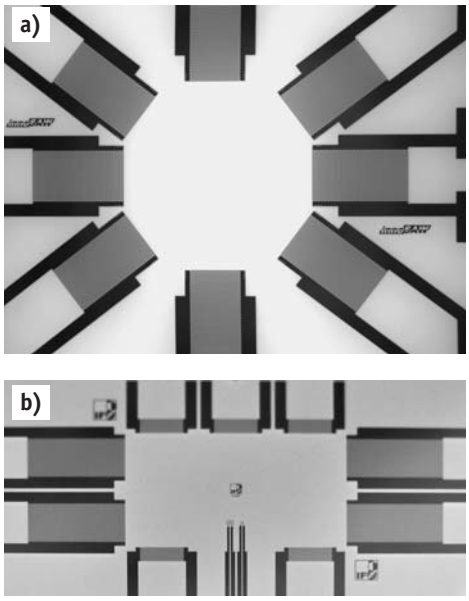

Fig. 10: Example of custom-designed SAW actuator devices, **a)** focusing IDT arrangement, **b)** device for droplet transport

Cooperation: Vectron International Teltow, TDK-EPC, SAW Components Dresden, Creavac Dresden, TU Dresden
Funding by: BMBF: InnoProfile (03IP610), BMWi: ZIM (KF2466401ED9)

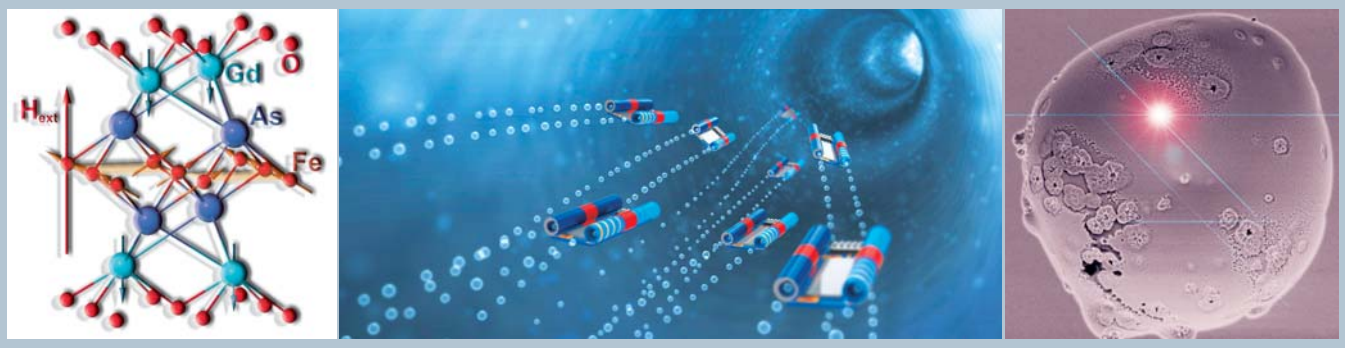

Reports from Research Areas

Research Area 1
Superconductivity and superconductors

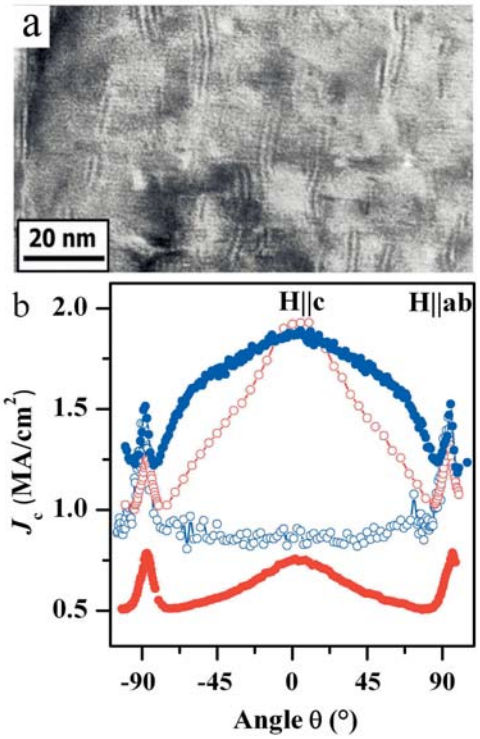

Fig. a) Moireé contrast of BZO nanoparticles and columns within the YBCO matrix. **b)** $J_c(\theta)$ at 65 K of quasimultilayers with thick (blue) and thin (red) YBCO interlayers, deposited at 810 °C (open symbols) and 850 °C (full symbols).

Nanocolumns in $BaZrO_3/YBa_2Cu_3O_{7-\delta}$ quasimultilayers

J. Hänisch, A. Kießling, T. Thersleff, E. Reich, R. Hühne, L. Schultz, B. Holzapfel

To enhance critical current densities in $YBa_2Cu_3O_{7-\delta}$ (YBCO) thin films with regard to possible applications as coated conductors in large magnetic fields, nanometre sized defects have to be introduced as flux pinning centres. $BaZrO_3$ (BZO) nanoparticles have proven to be very efficient pinning centres in YBCO thin films. We investigated the formation of these nanoparticles in YBCO-BZO quasimultilayers prepared by pulsed laser deposition. Quasimultilayers are multilayers where one component does not form closed layers, in this case BZO. The formation of BZO within the YBCO matrix is a diffusion-driven process. That means the thinner the YBCO interlayers and the higher the deposition temperature, T_{dep}, the faster is the formation of BZO. For thick YBCO interlayers and at low T_{dep} only nanoparticles are formed. For thin YBCO interlayers and high T_{dep} BZO nanocolumns parallel to the YBCO c-axis (film normal) are formed, shown in Fig. a. The density of nanoparticles and nanocolumns and their ratio determines the electrical transport properties, e.g. the angular dependence of the critical current density, $J_c(\theta)$, where θ is the angle between YBCO c-axis and applied magnetic field. That means, by varying T_{dep} and the layer architecture (here: YBCO interlayer thickness), the transport properties can be tailored as illustrated in Fig. b. The highest J_c values are observed for samples containing a mix of nanocolumns and nanoparticles. This work illustrates that a change in composition or architecture needs a readjustment of the deposition conditions for optimal transport properties.

[1] A. Kiessling et al., Supercond. Sci. Technol. 24, 055018 (2011)

Cooperation: Department of Materials Science and Metallurgy, University of Cambridge, UK

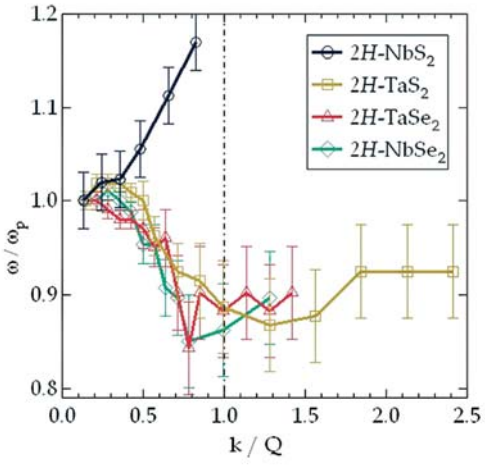

Fig.: For various related TMDCs the plasmon dispersion is negative up to a critical momentum transfer Q (except 2H-NbS2, which also shows no charge order).

Effect of Charge Order on the Plasmon Dispersion in Transition-Metal Dichalcogenides

R. Schuster, A. König, M. Knupfer, J. v. d. Brink, and B. Büchner

Many of the various polytypes of the transition-metal dichalchogenides (TMDC), consisting of hexagonal layers with weak interlayer van-der-Waals bonding, show a phase transition to a charge-density wave (CDW) phase as well as to a superconducting state at lower temperatures.

Applying Electron Energy-Loss Spectroscopy in transmission on thin films of different TMDCs, it could be proven that they show a negative dispersion of the bulk plasmon energy in the normal state and for the case of *2H*-$TaSe_2$ an even larger bandwidth of this negative dispersion in the CDW state, which is altogether not a behavior of a common metal. This being one of the clear evidences that the ability to show a CDW phase and the properties of the collective excitations are linked to each other, we presented a semiclassical Ginzburg-Landau model which accounts for these observations. It could be shown that indeed the interaction of fluctuations of the charge order and the plasma oscillations is responsible for the deviation from the usual form of the dispersion. For further details see van Wezel et al., Phys. Rev. Lett. **107,** 176404 (2011).

Cooperation: Materials Science Division, Argonne National Laboratory, Argonne, USA; Department of Physics, Univ. of Fribourg, Switzerland; Institut de Physique de la Matière Condensée, EPFL, Lausanne, Switzerland

Funded by: DFG

Suppressed superconductivity in charge-doped $Li(Fe_{1-x}Co_x)As$ single crystals

S. Aswartham, G. Behr, L. Harnagea, D. Bombor, A. Bachmann, I. V. Morozov, V. B. Zabolotnyy, A. A. Kordyuk, T. K. Kim, D. V. Evtushinsky, S. V. Borisenko, A. U. B. Wolter, C. Hess, S. Wurmehl, and B. Büchner

Among different types of Fe-based superconductors, LiFeAs has been found to be a unique representative. One reason is that the magnetically ordered spin-density wave state, which is suppressed upon doping and is considered to be obligatory for superconductivity in all Fe-As superconductors is not present in LiFeAs even after the application of pressure up to 20 GPa. Recent angle-resolved photoemission spectroscopy (ARPES) investigations on LiFeAs reveal the absence of Fermi surface nesting, high renormalization of the conduction bands, and high density of states at the Fermi level. This raises the question how superconductivity is derived in the stoichiometric superconductor LiFeAs. A recent study on this system has speculated that LiFeAs could be a triplet *p*-wave superconductor.

Single crystals of the new unconventional superconductor $LiFe_{1-x}Co_xAs$ with $x = 0$, 0.025, 0.05 were grown by a self-flux technique. The superconducting transition temperature and the superconducting volume fraction were found to decrease upon Co substitution at the Fe site. Apparently, this doping scheme suppresses superconductivity in LiFeAs, in contrast to the effects of Co doping in other Fe-As compounds, where it suppresses the spin-density wave and establishes superconductivity. Angle-resolved photoemission spectroscopy shows that the bottom of electron-like bands sinks by about 17 meV upon 5% Co doping, which indicates that the chemical substitution of Co for Fe in LiFeAs results in charge doping. In summary, this study confirms that LiFeAs is unique among the Fe-based superconductors, as charge doping in, e.g., the 122 family suppresses the spin-density wave and introduces superconductivity.

Cooperation: Department of Chemistry, Moscow State Univ., Russia

High Field Electron Spin Resonance Spectroscopy on $GdO_{1-x}F_xFeAs$ Superconductors

A. Alfonsov, F. Murányi[1], V. Kataev, G. Lang, N. Leps, L. Wang, R. Klingeler[2], A. Kondrat, C. Hess, S. Wurmehl, A. Köhler, G. Behr, S. Hampel, M. Deutschmann, S. Katrych[3], N. D. Zhigadlo[3], Z. Bukowski[3], J. Karpinski[3], and B. Büchner

The GdOFeAs compound is one of the parent compounds in the so-called 1111 family of iron pnictide high temperature superconductors. The Fe moments in the FeAs planes of GdOFeAs exhibit a long-range antiferromagnetic order of a spin density wave (SDW) type below the ordering temperature $T_{SDW} = 128$ K. The Gd^{3+} high field electron spin resonance (HF-ESR) reveals an appreciable magnetic coupling between Gd and Fe moments, through which the static magnetic order is clearly seen in the ESR spectra of GdOFeAs. The spectrum shifts, broadens inhomogeneously, and acquires a specific shape at $T < T_{SDW}$ (see Fig. (b)). This effect is caused by the interaction of the Gd spins with the uncompensated Fe moments due to the canting of SDW in the magnetic field (see Fig. (a)). Furthermore, the data suggest that due to this coupling Gd moments additionally tilt the ordered Fe moments.

Fluorine doping provides electrons to the FeAs planes giving rise to superconductivity and suppressing the bulk magnetic order. Therefore, the fluorine doped samples $GdO_{1-x}F_xFeAs$ ($x = 0.07$, and 0.14) do not show long range SDW order and are superconducting with $T_c = 20$ K ($x = 0.07$) and $T_c = 45$ K ($x = 0.14$). Surprisingly, characteristic features in the HF-ESR spectra associated with the SDW order are present also in the

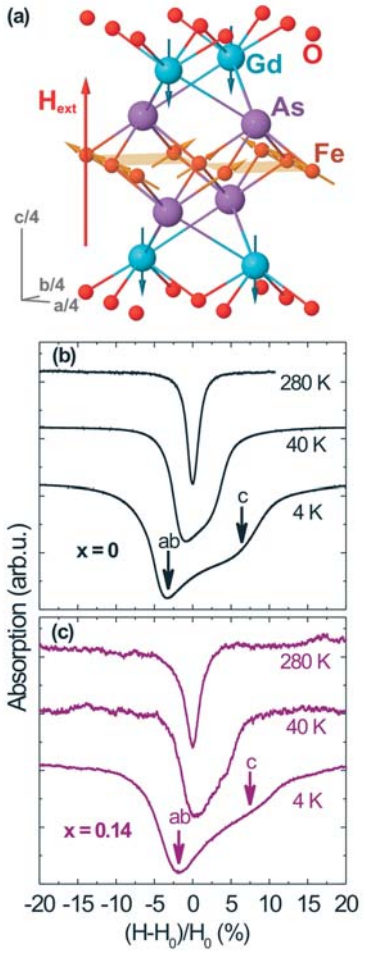

Fig.: (a) Canting of the ordered Fe moments in the applied magnetic field $H_{ext} \parallel$ c-axis. Arrows at the Fe site depict magnetic moments, whereas arrows on the Gd sites represent the internal field induced by the canting of Fe moments. **(b), (c)** Temperature evolution of the HF-ESR spectra of $GdO_{1-x}F_xFeAs$ ($x = 0$ (b), 0.14 (c)) powder samples measured at a frequency of $\nu = 328$ GHz, shown on a reduced field scale $(H - H_0)/H_0$. Here $\mu_0 H_0 = 11.7$ T is the resonance field of the signal at high temperature. Arrows labelled c and ab point at the contributions to the ESR spectrum of Gd spins experiencing the transferred internal fields in the powder grains with $H_{ext} \parallel$ c-axis (see (a)) and $H_{ext} \parallel$ ab-plane, respectively.

superconducting samples even at the optimal level of doping x = 0.14 (see Fig. (c)). This finding points to the presence of short-range static on the ESR time scale magnetic correlations in the FeAs planes, surviving up to the high doping levels. The HF-ESR data thus suggest the occurrence of an intimate interplay of magnetism and superconductivity in these materials, where on doping with fluorine there is a simultaneous increase of the superconducting critical temperature and suppression of the magnetic correlations. Details of the ESR experiments, supporting thermodynamics and transport measurements as well as the discussion of the results can be found in Ref. [1].

[1] A. Alfonsov et al., Phys. Rev. B **83**, 094526 (2011)

Cooperation: [1]Universität Zürich - Physik-Institut, Switzerland;
[2]Kirchhoff Institute for Physics, Heidelberg University, Germany
[3]Laboratory for Solid State Physics, ETH Zurich, Switzerland
Funded by: DFG

Surprising physics from local moments induced by point defects in superconducting ferropnictides

S.-L. Drechsler, V. Grinenko, G. Fuchs, F. Hammerath, G. Lang, H.-J. Grafe, S. Aswartham, S. Wurmehl, A. Wolter-Giraud, C. Hess, M. Abdel-Hafiez, B. Holzapfel, B. Büchner, L. Schultz, and J. van den Brink

Fig. 1

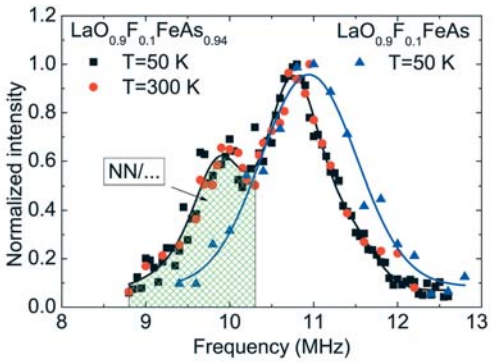

Fig. 2

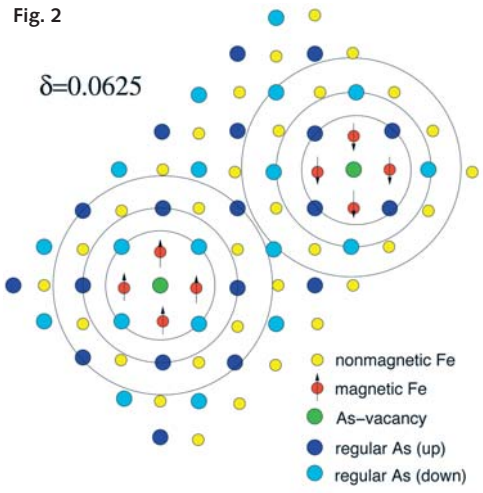

Real materials always contain some disorder and in particular, point defects. But ferropnictides are special since there even a small amount of them may have a dramatic effect on their magnetic and superconducting properties. We studied the effect of As-vacancies (AV) in $LaO_{0.9}F_{0.1}FeAs_{1-\delta}$ with $\delta \approx 0.06$ [1]. Being non-magnetic in nature, AV nevertheless polarize the surrounding Fe-sites and form local magnetic moments (LM) (see Fig. 1) which is attributed to the presence of an electronically localized state around each AV, carrying a LM of about $3.2\mu_B$/AV. AV are responsible for the strongly enhanced magnetic susceptibility and the PAULI-limiting behavior above 30 T for the upper critical field. In contrast, no PAULI-limiting behavior has been found for $LaO_{0.9}F_{0.1}FeAs$ in accord with its low spin susceptibility. Microscopically, a LM is formed when the local HUBBARD on-site repulsion exceeds a critical value of about 1eV. Surprisingly, the superconductivity at low-fields is not downgraded but *improved* due to these magnetic defect states putting constraints on the superconducting mechanism. Our model with almost homogeneously distributed As-vacancies explains the fine structure of ^{75}As-NQR spectra (see Fig. 2). Similar effects and exotic LM driven disordered magnetic phases have been observed for KFe_2As_2. Here, the LM cause non Fermi liquid behaviour in the normal state above $T_c \approx 3.8$ K, anomalies in the specific heat and in the magnetic susceptibility.

Fig. 1.: Schematic structure of an FeAs-block with 2 neighboring AV at a concen-tration of $\delta \approx 0.0625$ in the range suggested by the NQR-data shown in Fig. 2 for a typical As-deficient sample. The low-frequency spectral weight below 10.3 MHz is attributed to NN and NNN-shells around an AV whereas the high-frequency part is attributed to more distant As sites. Notice the 4 Fe-sites surrounding an AV involved in the local moment.

Fig. 2.: ^{75}As NQR spectrum at T = 50~K, together with the spectrum of a clean reference sample and measurements at 300 K. Black line: a typical fit according to an AV arrangement shown in Fig. 1.. Blue line: broad single-peak fit of the NQR-spectrum of a reference sample. NN and the shadded green area indicate schematically the low-frequency spectral weight below about 10.3 MHz suggested for the NN and NNN shells around an AV as shown in Fig. 1.

[1] R. Kuzian *et al.*, arXiv. 1201.6663
Cooperation: K. Kikoin, Tel Aviv Univ., Israel; M. Kiselev, International Centre for Theoretical Physics, Trieste, Italy; D. Efremov MPI-FKF Stuttgart, Germany
Funded by: DFG, Pakt für Forschung

Pseudogap-like phase in $Ca(Fe_{1-x}Co_x)_2As_2$ revealed by ^{75}As NQR

S.-H. Baek, H.-J. Grafe, L. Harnagea, S. Singh, S. Wurmehl, and B. Büchner

Despite a large effort in recent years in the study of the newly discovered iron-based pnictide superconductors (iron pnictides), there has been no conclusive answer as to whether the iron pnictides share the same underlying physics with the cuprates. Beyond a probably different superconducting gap symmetry, there is no consensus about the precise nature of the normal state in iron pnictides, which is crucial to understand the high temperature superconductivity. A key question is whether there exists an exotic state of matter in the normal state, equivalent to the pseudogap phase in cuprates, and where it originates from. In particular, in iron pnictides there are inconsistencies with respect to what can rightfully be called a pseudogap behavior, with contradicting experimental evidence on its presence itself, on its doping dependence, and on the region of the phase diagram where it would occur. In order to address this question, we have measured the spin lattice relaxation rate, T_1^{-1}, by means of ^{75}As NQR in $Ca(Fe_{1-x}Co_x)_2As_2$. At high temperatures, $(T_1T)^{-1}$ is independent of doping and temperature. With lowering temperature, $(T_1T)^{-1}$ as a function of x and T reveals a pseudogap behavior below a crossover temperature T* in the under- and optimally-doped region. The resulting x-T phase diagram shown in the figure shows that, after suppression of the spin-density-wave (SDW) order, T* intersects T_c falling to zero rapidly near the optimal doping regime. From the doping dependence of T*, we interpret that the pseudogap is strongly related to the SDW ordered phase at low doping, and could be a precursor state for the coherent SC phase. Moreover, the T dependence of the static susceptibility (Knight shift) is other than that of the spin lattice relaxation, which puts constraints on theoretical descriptions of the pseudogap behavior in iron pnictides.

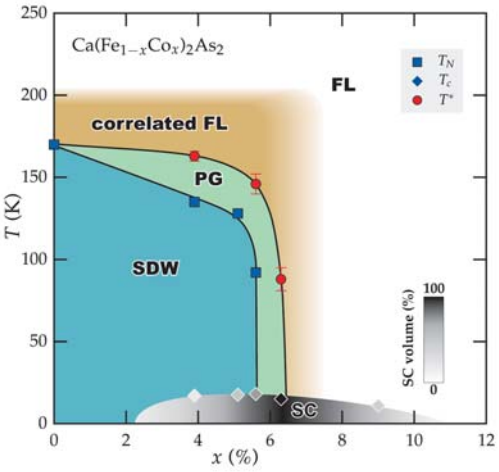

Fig.: T-x phase diagram in $Ca(Fe_{1-x}Co_x)_2As_2$ obtained by $(T_1T)^{-1}$ measurements on the ^{75}As NQR and by the uniform magnetic susceptibility χ_{DC}. FL and PG represent Fermi liquid and pseudogap, respectively. Superconducting volume fraction was estimated by the diamagnetic response of χ_{DC}.

Funded by: DFG through SPP1458 (Grants No. GR3330/2 and No. BE1749/13)

Generic buffer layers for Fe-based superconductors: Epitaxial $FeSe_{1-x}Te_x$ thin films

K. Iida, J. Hänisch, S. Haindl, E. Reich, M. Schulze, S. Aswartham, S. Wurmehl, B. Büchner, L. Schultz and B. Holzapfel

Iron chalcogenidesuperconductors are very sensitive to strain. Hence the superconducting transition temperature, T_c, of $FeSe_{1-x}Te_x$ films can be tuned by strain and even higher T_c values in films than in bulk material can be realized. The biaxial strain is usually induced by a lattice mismatch between film and substrate. However, the correlation between T_c and lattice mismatch for $FeSe_{1-x}Te_x$ is controversial. A fundamental problem is the formation of an interfacial layer between $FeSe_{1-x}Te_x$ and oxide substrates, which compromises the epitaxial growth.Therefore, we proposed the implementation of an Fe buffer layer to grow epitaxial $FeSe_{1-x}Te_x$ thin films. Similar to the Fe/Ba-122 bilayers [1], epitaxial $FeSe_{1-x}Te_x$ films with sharp out-of-plane and in-plane texture have been realized on Fe-buffered single crystalline MgO substrates [2]. These results indicate that Fe can work as generic buffer layer for epitaxial growth of Fe-based superconductors. The $Fe/FeSe_{1-x}Te_x$ bilayer with a high T_c of 17.7 K showed strong intrinsic pinning from correlated *ab*-planes, since the Se(Te)-Se(Te) interlayer distance is almost identical to the out-of-plane coherence length at low temperatures. We acknowledge J. Scheiter and E. Barbara for help with FIB cut samples and AFM observation.

[1] T. Thersleff *et al.*, Appl. Phys. Lett. **97**, 022506 (2010).
[2] K. Iida *et al.*, Appl. Phys. Lett. **99**, 202503 (2011).

Cooperation: Univ. of Jena
Funded by: DFG

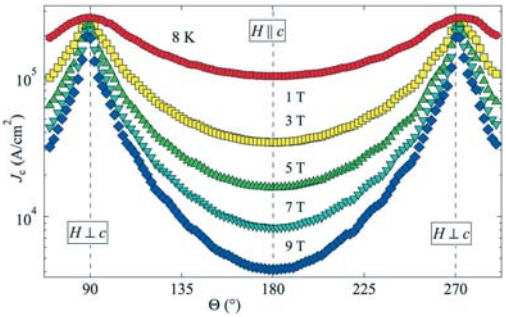

Fig.: The angular-dependent critical current densities ($J_c(\Theta)$) at 8 K measuredin several magnetic fields show a peak positioned at $\Theta = 90°$ and 270° owing mainly to intrinsic pinning.

Ab initio computation of d-level electronic structures in correlated d-metal oxides

N. Bogdanov, V. Katukuri, H.-Y. Huang, L. Siurakshina, L. Hozoi, and J. van den Brink

The vast majority of solid-state electronic-structure calculations is based nowadays on density functional theory. For strongly correlated systems, however, the wave-function-based *ab initio* methods certainly provide a viable alternative. For this class of materials, of which a typical example are the 3*d*-metal oxides, it is essential to properly describe the multiconfigurational character of the many-electron wave function. The multiconfiguration and multireference quantum chemical methods constitute here a natural choice.

With wave-function-based electronic-structure calculations we have determined the Cu *d*-level electronic structure and *d-d* excitation energies in two-dimensional (2D) and quasi-one-dimensional (1D) Cu oxides [1,2]. Complete sets of local excitations have been calculated for 1D $3d^9$ cuprates with corner-sharing (Sr_2CuO_3 and $SrCuO_2$) and edge-sharing ($LiVCuO_4$, $CuGeO_3$, $LiCu_2O_2$, and Li_2CuO_2) CuO_4 plaquettes, with corner-sharing CuF_6 octahedra ($KCuF_3$), for the ladder system $CaCu_2O_3$, for multiferroic CuO, and for layered 2D cuprates such as La_2CuO_4, $YBa_2Cu_3O_6$, and $HgBa_2CuO_4$. Excellent agreement was found with available resonant inelastic x-ray scattering (RIXS) and optical measurements for the 2D materials and for $KCuF_3$. The *ab initio* results we obtained for the other compounds should be helpful for the correct interpretation of future RIXS experiments on those anisotropic systems.

Further *ab initio* investigations are now being carried out for the correlated electronic structures of V oxide $3d^2$ perovskites, 1D Ti and V oxychlorides [3], and Os $5d^3$ and Ir $5d^5$ oxides.

[1] L. Hozoi *et al.* Nature Sci. Rep. **1**, 65 (2011)
[2] H.-Y. Huang *et al.* Phys. Rev. B **84**, 235125 (2011)
[3] N. Bogdanov *et al.* Phys. Rev. B **84**, 235146 (2011)

Funded by: DFG, EU, NSC Taiwan, MPI-PKS Dresden.

AC losses in YBCO coils

V. Grinenko, G. Fuchs, K. Nenkov and B. Holzapfel

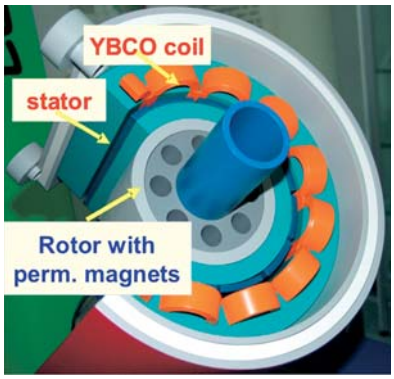

Fig.: Model of a motor with 24 race-track shaped YBCO coils as stator winding. According to this design, a compact motor was built up at Oswald Elektromotoren GmbH. The YBCO coils and the stator were cooled with liquid nitrogen. A maximum power of 40 kW was realized at 65 K. The total AC loss which is mainly determined by the magnetization AC loss of the YBCO coils was found to increase up to ~ 700 W.

Pancake coils made from YBCO high temperature superconductors (HTS) are attractive for power applications such as transformers, motors and generators. However, for most power applications, the AC losses of HTS windings are at present too high, especially if the additional efforts for the cooling equipment are taken into account. In order to realize a high transport current in YBCO pancake coils they are usually wound from parallel YBCO tapes. However, the AC losses of coils with n > 1 non-transposed parallel connected tapes are considerably higher than those of single-tape coils. This increase is related to coupling currents [1] flowing between parallel connected tapes separated by finite resistance. We investigated both AC transport current and magnetization losses in external AC magnetic field for YBCO pancake coils with different number of turns (N = 5 - 48) wound from n non-transposed parallel tapes (n = 1, 2, 4). It is shown experimentally and theoretically that the transport and magnetization AC losses of the YBCO pancake coils with n > 1 parallel connected tapes can be significantly reduced by optimizing the coils geometry and the resistance between parallel tapes. In some cases their AC losses are even comparable with the AC losses of single-tape coils.

[1] V. Grinenko, K. Nenkov, C. Stiehler, G. Fuchs, B. Holzapfel, Journal of Physics: Conference Series **234** (2010) 022011

Cooperation: Oswald Elektromotoren GmbH, Toyota Motor Europe NV/SA
Funded by: Toyota Motor Europe NV/SA

Research Area 2
Magnetism and magnetic materials

Martensite–austenite phase transition of the shape memory Heusler compound Mn_2NiGa

C. G. F. Blum, S. Ouardi, G. H. Fecher, B. Balke, X. Kozina, G. Stryganyuk, S. Ueda, K. Kobayashi, C. Felser, S. Wurmehl, and B. Büchner

Mn_2NiGa is reported to be a shape memory material with a martensite–austenite phase transition. Up to now, the driving force for the phase transition is still under discussion and may be either embossed by the band Jahn–Teller effect [1] or by Fermi surface nesting. In particular, Mn_2NiGa has generated soaring interest because of the high Curie temperature (588 K) and the martensitic transition close to room temperature [2]. Previously, few experimental and theoretical studies on Mn_2NiGa were carried out.

Crystals of Mn_2NiGa were grown by the optical floating zone method using an image furnace with vertical setup under a purified argon atmosphere, yielding a bulk sample with large grains with lateral dimensions about several millimeters. Temperature dependent measurements of the transport and magnetic properties reveal the martensitic transition close to room temperature with a thermal hysteresis of about 27 K.

The electronic structure of the valence band in both phases was studied by hard x-ray photoelectron spectroscopy. The results clearly indicate that strong changes in the electronic structure appear at the phase transition (Fig.). Band structure calculations based on the structure of Mn_2NiGa as recently revealed by neutron diffraction [3] are required and need to be compared to the valence band measured by HAXPES in order to further elucidate the origin of the phase transition [4].

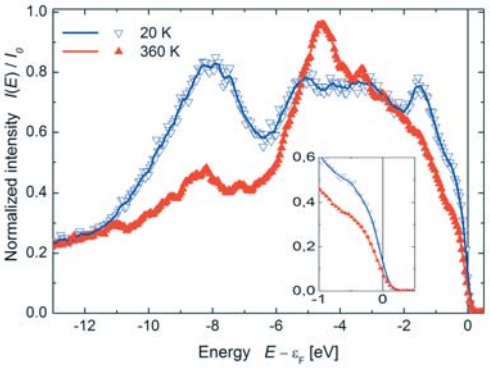

Fig.: Valence band spectra of Mn_2NiGa at different temperatures. The inset shows the valence band close to the Fermi-edge on an enlarged scale.

[1] P. J. Brown et al., J. Phys.: Condens. Matter **11**, 4715 (1999).
[2] G. D. Liu et al., Appl. Phys. Lett. **87**, 262504 (2005).
[3] P. J. Brown et al., J. Phys.: Condens. Matter **22**, 506001 (2010).
[4] C. G. F. Blum et al., Appl. Phys. Lett. **98**, 252501 (2011);

Cooperation: Institut für Anorganische Chemie und Analytische Chemie, Johannes Gutenberg-Univ. Mainz, Germany; NIMS Hyogo, Japan

Macroscopic Degeneracy and Emergent Frustration in a Honeycomb Lattice Magnet.

J. W. F. Venderbos, M. Daghofer, J. van den Brink and S. Kumar

Localized spins in strongly correlated materials, e.g. transition metal oxides, can lead to particularly fascinating properties when they form a frustrated lattice, where not all interactions can be optimized. Examples include magnetic monopoles in spin ice or large thermopower due to the presence of many nearly degenerate states. In our work we find that on the unfrustrated honeycomb lattice, geometric frustration can spontaneously emerge as a consequence of the frustration between antiferromagnetic (AF) magnetic interactions and ferromagnetism driven by itinerant electrons. For relatively weak AF exchange, ferromagnetic (FM) hexagons form that make up a triangular superlattice. Consequently, they order as would individual spins on a frustrated triangular lattice, see panel (a) of the figure.

For somewhat stronger AF interactions, smaller FM building blocks arise, namely dimers. Order between the dimers is AF, however, spins only order along one direction and remain perfectly uncorrelated along the other direction. This can be seen by noticing that the two states in panels (b) and (c) are both valid dimer coverings and yet have

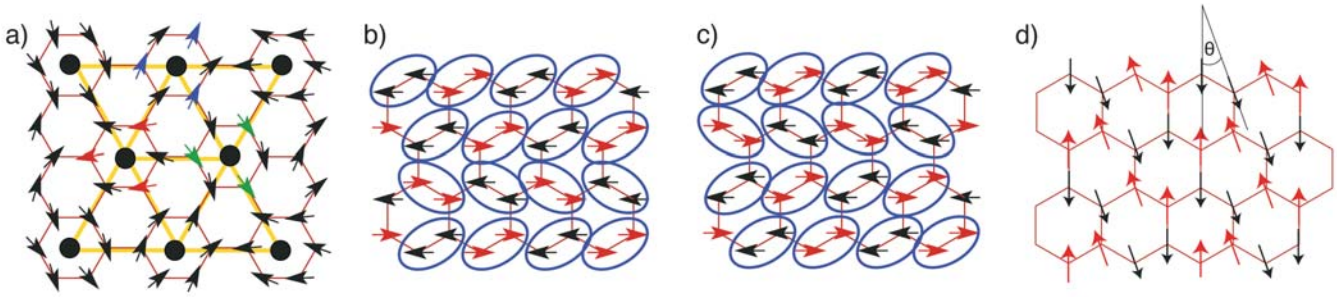

Fig.: (a) Shows the ferromagnetic hexagons making up an emergent triangular lattice (big black dots connected by yellow lines). The hexagons form the well-known so-called 120 degree state (angles between nearest neighbours are 120 degrees). **(b)** A configuration of FM dimers. **(c)** An equivalent configuration of FM dimers, obtained from (b) by "flipping" the middle two rows. **(d)** Dimer states canting towards the fully developed anti-ferromagnetic state.

different spin-spin correlation along the y-axis. Such a nematic order implies an almost macroscopic ground-state degeneracy and is related to a symmetry intermediate between local (gauge-like) and global. This exotic symmetry is not a property of the Hamiltonian, but again emerges spontaneously in the ground-state manifold. We thus find that frustration between competing charge and spin degrees of freedom can lead to exotic magnetic phases reminiscent of geometrically frustrated lattices.

[1] J. W. F. Venderbos et al., Phys. Rev. Lett. **107**, 076405 (2011).

Funded by: Emmy Noether Program of the DPG (M. Daghofer), Interphase program of the Dutch Science Foundation NWO/FOM (J. Venderbos and J. van den Brink)

Spin Gap in the Zigzag Spin-½ Chain Cuprate $Sr_{0.9}Ca_{0.1}CuO_2$

F. Hammerath, S. Nishimoto, H.-J. Grafe, A. U. B. Wolter, V. Kataev, P. Ribeiro, C. Hess, S.-L. Drechsler and B. Büchner,

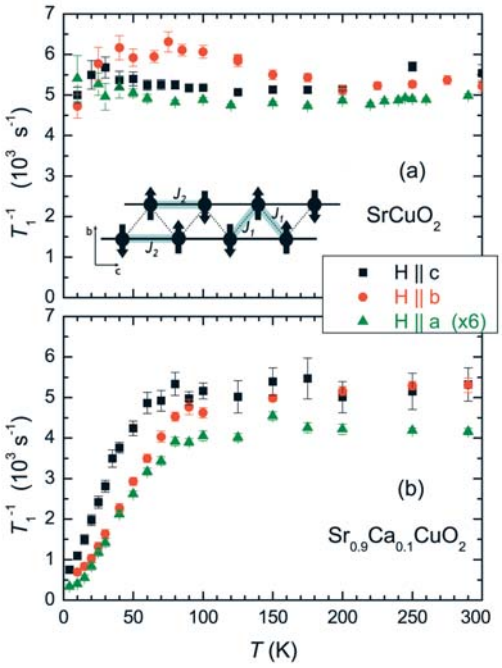

Fig.: ^{63}Cu NMR spin-lattice relaxation rate T_1^{-1} of $SrCuO_2$ **(a)** and $Sr_{0.9}Ca_{0.1}CuO_2$ **(b)** for different field directions. Inset: zigzag structure of the Cu^{2+} spins and main exchange couplings.

The spin chain compound $SrCuO_2$ is commonly considered as one of the best realizations of a one-dimensional (1D) S = ½ antiferromagnetic Heisenberg chain. Its crystal structure contains CuO_2 double chains (see inset of the figure). The intrachain exchange coupling J_2 between next nearest Cu^{2+} spins (S = ½) is large (~2000 K) and antiferromagnetic. The interchain coupling J_1 between nearest Cu^{2+} spins is much weaker (~0.1–0.2 $|J_2|$) and ferromagnetic. Due to this frustration the single chains of a given zigzag chain are magnetically decoupled and magnetic Néel-type order is absent down to $T \leq 2$ K. Nuclear Magnetic Resonance (NMR) measurements have been performed on $SrCuO_2$ and $Sr_{0.9}Ca_{0.1}CuO_2$ single crystals. For $SrCuO_2$ the spin-lattice relaxation rate T_1^{-1} is temperature independent as it is expected for a 1D Heisenberg spin chain (see upper panel of the figure). Nonmagnetic, isovalent Ca is doped on the Sr-sites outside the spin chains and should not affect the magnetic properties. But surprisingly, an exponential decrease of T_1^{-1} is observed in $Sr_{0.9}Ca_{0.1}CuO_2$ for $T < 90$ K that evidences the opening of a gap of the order of $\Delta = 50$ K in the spin excitation spectrum (see lower panel of the figure). Density Matrix Renormalization Group calculations showed that the occurrence of this spin gap can be well reproduced within a J_1-J_2 1D Heisenberg model by considering a small alternation ($\delta = 0.0027$) of the intrachain coupling J_2, regardless of the sign and the value of J_1.

[1] F. Hammerath *et al.*, Phys. Rev. Lett. **107**, 017203 (2011).

Funded by: DFG, FOR 538 and FOR 912

$Ca_2Y_2Cu_5O_{10}$: the first frustrated quasi-1D ferromagnet close to criticality

S.-L. Drechsler, R. Kuzian, S. Nishimoto, J. Málek, S. Johnston, and J. van den Brink

The title compound is build up from edge-shared CuO_4 plaquettes forming frustrated spin chain cuprates with ferromagnetic nearest neighbour (NN) and antiferromagnetic next-nearest (NNN) neighbour in-chain couplings J_1 und J_2, respectively (see Fig. 1). From inelastic neutron scattering (INS) data we analyzed its magnetic excitations in a direction where they are little affected by inter-chain couplings. We extracted $J_1 \approx -170$ K and $J_2 \approx 32$ K both significantly larger than estimated previously. The frustration ratio $\alpha = J_2/|J_1| \approx 0.19$ puts the system very close to the helical critical point $\alpha_c = 1/4$ of the J_1-J_2 chain, but in the *ferromagnetic* regime. We establish that the vicinity to criticality only marginally affects the dispersion and the coherence of the elementary, spin-wave like, magnetic excitations, but will instead result in a dramatic *T*-dependence of high-energy ZHANG-RICE singlet excitation intensities to be observed by RIXS (see Fig. 2), EELS, and optical conductivity measurements. Surprisingly it will be practically absent for the unfrustrated pure ferromagnetic case even at 300 K [1]. Thus, high-energy electron spectroscopies provide convenient tools to detect even relatively small frustrating exchange couplings which in some cases are difficult to extract from INS data without a detailed knowledge of all important in-chain and inter-chain couplings as in the present case.

[1] V. Grinenko *et al.*, Phys. Rev. B **84**, 134516 (2011)

Cooperation: M. Matsuda, Quantum Condensed Matter Division, Oak Ridge National Laboratory, USA
Funded by: DFG

Fig. 1

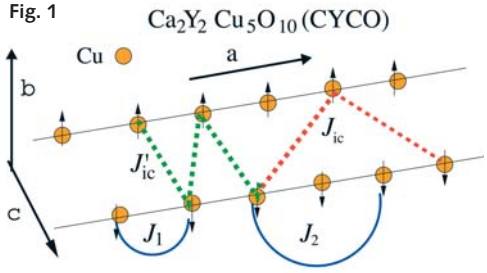

Fig. 2

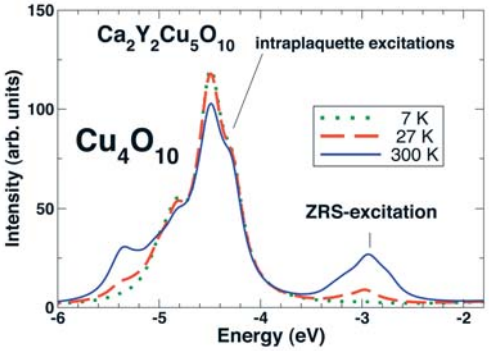

Fig. 1: Schematic structure of the CuO_2 chain layer and the main exchange pathes of $Ca_2Y_2Cu_5O_{10}$.

Fig. 2: Calculated T-dependent O-K RIXS-spectrum for in-chain xx-polarization from a Cu_4O_{10} cluster within exact diagonalization for a five-band extended HUBBARD model.

Intrinsic coupling of orbital excitations in Mott insulators

K. Wohlfeld, M. Daghofer, S. Nishimoto, J. van den Brink

If several orbitals contribute to low-energy states of a transition metal oxide and if Coulomb repulsion is strong, spin and orbital degrees of freedom become formally almost equivalent [1]. Excitations give information about the quantum dynamics, e.g., magnons in ferromagnetic manganites show that the main impact of alternating orbital order is a reduced magnon band width [2].

The analogous situation with switched roles for spins and orbitals is an orbital excitation in an orbitally polarized antiferromagnet, see the first row of the figure. The excitation can move (third and fourth rows) via virtual excitations with doubly occupied sites (second row). This situation can be mapped onto the case of a hole moving in an antiferromagnetic (AF) background, and shows a feature similar to spin-charge separation: In the fourth row, "magnetic" and "orbital" parts of the original excitations have moved apart [3].

It turns out that this reversed situation leads to fundamentally different excitation spectra than the magnon case mentioned above [3], e.g., the periodicity of the dispersion clearly reflects the doubled unit cell of the AF background and additional incoherent features arise. The decisive impact of the lowered symmetries in the orbital sector is thus revealed in the differences between magnons and orbital excitations, which can be measured in resonant inelastic x-ray scattering.

[1] K.I. Kugel and D.I. Khomskii, Sov. Phys. Usp. **25**, 231 (1982).
[2] F. Moussa *et al.*, Phys. Rev. B **54**, 15149 (1996).
[3] K. Wohlfeld *et al.*, Phys. Rev. Lett. **107**, 147201 (2011).

Cooperation: Giniyat Khaliullin, MPI für Festkörperforschung, Stuttgart
Funded by: Alexander von Humboldt Foundation, DFG (Emmy-Noether program)

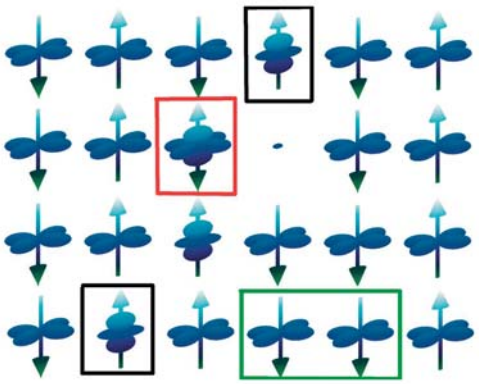

Fig.: Schematic illustration of a propagating orbital excitation separating into spin and orbital parts

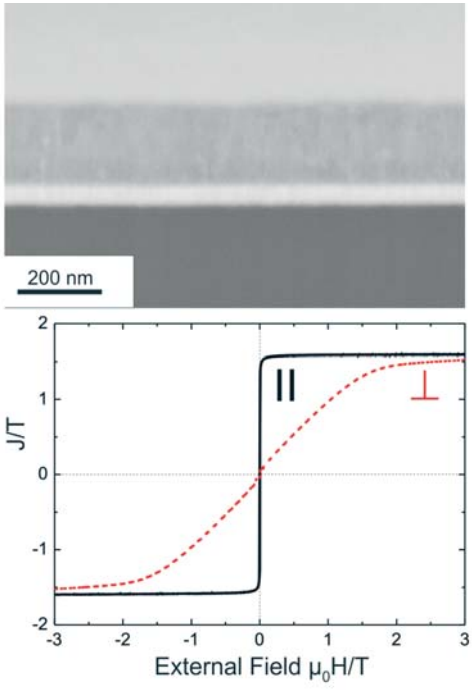

Fig.: Top: Cross sectional HR-SEM micrograph of a dense and homogeneous $Fe_{85}Ga_{15}$ film prepared by pulse plating and optimized pre-treatment conditions; **Bottom:** Hysteresis loops of the above film, measured parallel (||) and perpendicular (⊥) to the substrate.

Electrodeposition of $Fe_{80}Ga_{20}$ Alloy Films

D. Iselt, S. Neitsch, U. Gaitzsch, S. Oswald, S. Fähler, H. Schlörb, L. Schultz

Electrochemical deposition offers a simple and inexpensive method to produce functional coatings on large surfaces and in complex nanostructured geometries. Our research focusses on alloy coatings with special magnetic properties such as high magnetostriction, or the magnetic shape memory effect, which exhibit a high application potential for micro- and nano-dimensioned sensors and actuators.

Galfenol – an Fe-Ga alloy containing around 20 at.% Ga – combines high magnetostriction with good mechanical properties and is therefore promising to replace rare earth alloys such as Terfenol-D ($Tb_{0.3}Dy_{0.7}Fe_2$). However, its electrochemical deposition has been studied very little. Main challenges are the rather negative deposition potentials of the involved metals causing strong hydrogen evolution and low reproducibility and the strong tendency of gallium ions to hydrolyze and to form insoluble oxidic species, which are incorporated into the deposited films.

We have recently shown that dense and homogeneous Fe-Ga films (see fig., top) with the desired composition close to $Fe_{80}Ga_{20}$ can be successfully deposited from aqueous solutions of the simple metal salts at low pH values. By optimized pre-treatment and pulsed potential conditions the oxygen content in the films could be reduced to less than 1 at.%. The films show a (110) Fe_3Ga fibre texture and a saturation magnetization of up to 1.7 T (fig., bottom) which approaches the values for bulk single crystals of 1.75 T, confirming the high quality of the films.

[1] D. Iselt et al. Electrochim. Acta **56** (2011) 5178.

Cooperation: TU Dresden

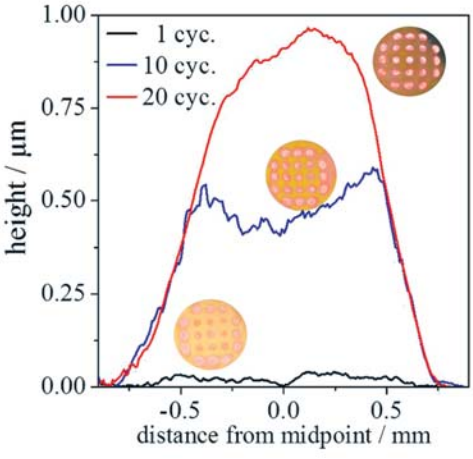

Fig.: PRP of Cu applying a **∇B**-template optical images of the **∇B**-template and obtained structures after different numbers of cycles and comparison of the height-profiles of their central spot.

Electrodeposition of free-standing 3D structures using defined magnetic field gradients

K. Tschulik, M. Uhlemann, K. Hennig, Ch. Mickel, A. Teresiak, I. Mönch, V. Hoffmann, A. Gebert

Electrochemical three-dimensional structuring of Cu even in the µm-range has been performed by pulse-reverse plating (PRP) experiments in superposed magnetic gradient fields. Magnetic gradient fields were generated by magnetized Fe-wire building blocks of Fe. Structure shapes, e.g. columnar or stripe-like, can be adjusted by the superimposed magnetic gradient fields and tailored PRP parameters. Optical images after different numbers of cycles are shown in the figure. The structure heights can be controlled by the number of pulse-reverse plating cycles (Fig.). The different structuring effects during the PRP experiments depend strongly on the action of the magnetic field gradient force. Contrary, it has been shown that the effect of the Lorentz force is almost negligible. Especially remarkable is the twofold character of the magnetic field gradient force. It induces convections towards the working electrode in regions of maximum magnetic field gradient during the deposition part of the cycle. On the contrary, it reduces the ion-dissipating convection arising during the dissolution part, enabling an enrichment of Cu^{2+} ions near the electrode at those regions. Both actions result in a locally enhanced metal deposition that explains the generation of separate deposit structures at regions of maximum magnetic gradients.

Cooperation: TU Dresden, Institute for Fluid Dynamics; HZDR, Institute for Safety Research; Universität der Bundeswehr München

Funded by: DFG / SFB 609, Studienstiftung des deutschen Volkes

Research Area 3
Molecular nanostructures and molecular solids

The role of the polymer structure on charged states in polyaniline: An *in situ* spectroelectrochemical study

E. Dmitrieva, A. Kellenberger, Y. Harima and L. Dunsch

The linear form of polyaniline (PANI) is often applied in studies of charge transfer reactions without any detailed knowledge of the real structure. The structure and stabilization of charged states during p-doping of PANI were studied by *in situ* electron spin resonance (ESR)/ultraviolet-visible-near infrared (UV-vis-NIR) and *in situ* Fourier transform infrared (FTIR) spectroelectrochemistry. The FTIR studies of "linear" PANI and in several copolymers of aniline and a phenazine derivative give evidence on the existence of phenazine units in the polymer structure. The *in situ* ESR/UV-vis-NIR spectroelectrochemistry of PANI points to preferred stabilization of a polaron pair in the charged states at the initial charge transfer reaction instead of polarons which are formed by equilibrium reaction at higher electrode potentials. The potential dependence of IR bands observed during the first redox peak in cyclovoltammogram was compared to that of the ESR intensity and the absorption data and points to the formation of diamagnetic species like π-dimers [1]. A bipolaron is detected for high doped states of the polymer film. The combination of *in situ* ESR/UV-vis-NIR and FTIR spectroelectrochemistry gives detailed information on the structure and stabilization of charged states during p-doping of PANI and allows to clarify the mechanism of the formation of charged states upon p-doping of PANI.

[1] E. Dmitrieva et al. *Phys. Chem. Chem. Phys.*, **2011,** *13*, 3411.

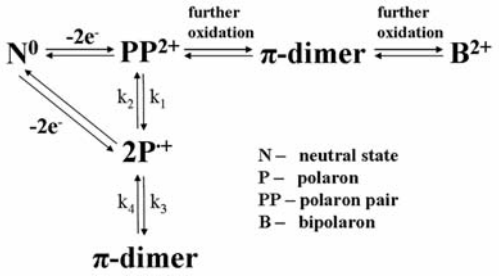

Fig.: Mechanism of the electrochemical oxidation of polyaniline.

Cooperation: University of Hiroshima, Japan, and University Politehnica of Timisoara, Romania
Funded by: BMBF

Magnetic force microscopy sensors for in-plane sensitivity measurements

T. Mühl, J. Körner, A. Leonhardt, B. Büchner

Magnetic force microscopy (MFM) is a powerful method dedicated to map stray-field distributions, or more precisely, derivatives in space of magnetic field components. Recently we developed a sensor for quantitative MFM based on an iron-filled carbon nanotube (FeCNT). The long Fe nanowire contained in the carbon nanotube can be regarded as an arrangement of two well-separated magnetic monopoles of which only the monopole nearest to the sample surface is involved in the imaging process. The monopole-like character of FeCNT MFM probes allows easy calibration [1]. Moreover, as compared to conventional coated MFM probes, FeCNT sensors show remarkable magnetic stability in external in-plane fields [2].

The figure shows our latest MFM sensor development again employing FeCNTs. By using higher order flexural vibration modes of the cantilever the new sensor provides both in-plane and perpendicular sensitivity for quantitative MFM measurements. According to Gauss's law for magnetism the divergence of the magnetic flux density is always zero, $\delta Bx/\delta x + \delta By/\delta y + \delta Bz/\delta z = 0$. Two of these terms are measured by the new sensor, e.g., the x and z terms. The remaining y term can be calculated.

[1] F. Wolny et al. Nanotechnology 21, 435501 (2010).
[2] F. Wolny et al. J. Appl. Phys. 108, 013908 (2010).

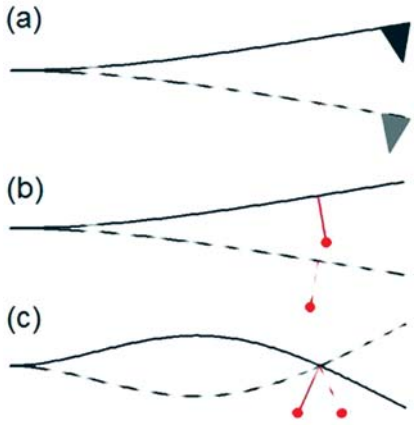

Fig.: Scheme of the envelope for vibrating cantilever beams in resonance. **(a)** Conventional MFM cantilever, **(b)** and **(c)** novel MFM sensor vibrating with the first **(b)** and the second **(c)** order flexural vibration modes. A magnetic monopole point probe (circle), e.g., a FeCNT, and a spacer are indicated in red.

Funded by: DFG

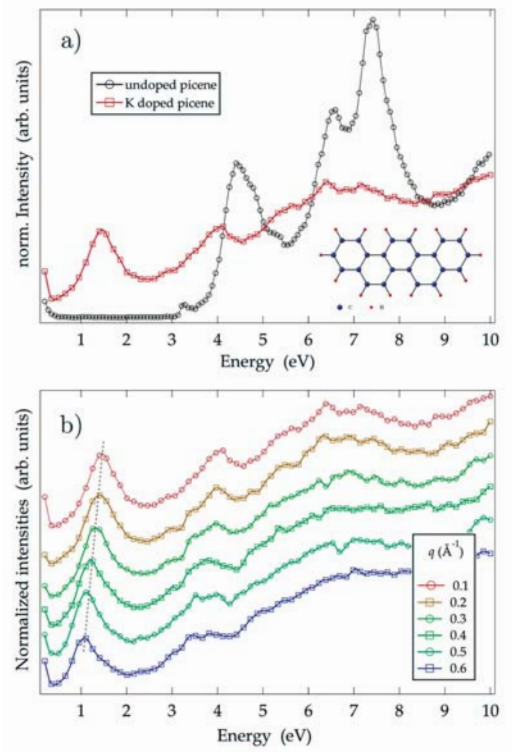

Fig.: a) Comparison of the loss function in the range of 0–10 eV for undoped and K intercalated picene (The inset shows a schematic representation of the molecular structure of picene). **b)** The momentum dependence of the EELS spectra of K_3 picene.

Electronic properties of potassium doped picene

F. Roth, B. Mahns, B. Büchner and M. Knupfer

Superconductivity is one of the most fascinating physical phenomena in solid state physics. The search for new superconducting materials is motivated by applications as well as fundamental science. Recently, a new family of organic superconductors, K-intercalated hydrocarbons, such as picene (T_c up to 18 K) or coronene (T_c up to 15 K) has been discovered. This represents a major breakthrough as it has the second highest T_c of organic solids only below the one of alkali metal intercalated fullerenes. Designing new molecular solids with higher T_c or tailored electronic response requires a detailed microscopic understanding of the electronic structure. Our electron energy-loss spectroscopy (EELS) results provide a deeper insight into the electronic properties of potassium intercalated picene. A comparison of the loss function of the undoped and doped compound shows the appearance of a new peak in the optical gap, which we attribute to the charge carrier plasmon. Furthermore, the observed negative plasmon dispersion can be seen as a result of molecular polarization and crystal local-field effects. Finally, our core level excitation data clearly signal filling of the conduction bands with electrons upon potassium addition. For details see: F. Roth *et al.*, *Phys. Rev B* **83** 144501 (2011) and Cudazzo *et al.*, *Phys. Rev. B* **84**, 155118 (2011)

Cooperation: Nano-Bio Spectroscopy group and ETSF Scientific Development Centre, Universidad del Pais Vasco, San Sebastian, Spain
Funded by: DFG

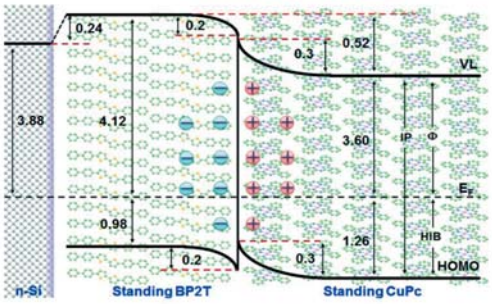

Fig.: Schematic energy level diagram of the crystalline CuPc/BP2T organic heterojunction. Energy values are given electron volt (eV).

Formation of a conductive channel at a p/p-type organic heterojunction

F. Zhu, M. Grobosch, U. Treske, M. Knupfer

We have observed a rather well conducting channel at a heterointerface between two p-type organic semiconductors, copper phthalocyanine (CuPc) and 2,5-bis(4-biphenylyl) bithiophene (BP2T) using photoelectron spectroscopy and transport studies. The energy level alignment at the interface as determined by photoelectron spectroscopy demonstrates charge transfer at this interface as schematically depicted in the Figure. The transport studies using a transistor device clearly signal a current through the transistor channel consisting of the heterostructure that is by more than two orders of magnitude larger than that for the individual materials. Our results cannot be understood in the framework of existing models and demonstrate the need for further studies of organic heterojunctions. For details see: F. Zhu *et al.*, *App. Phys. Lett.* **98,** 203303 (2011).

Cooperation: Chinese Academy of Sciences, Changchun Institute of Applied Chemistry
Funded by: DFG

The CCVD synthesis of aligned carbon nanotubes on Al foils

V. Khavrus, R. Ummethala, A. Leonhardt, B. Büchner

Supercapacitors (SCs) have attracted much attention because they satisfy desirable requirements for energy accumulation and they also possess a high specific power, a simple construction, and a long life time. A typical SC is composed of a flexible current collector, electrically connected to an inert electrode with a high surface area. Carbon nanotubes (CNTs) grown directly on thin Al foil are apparently attractive candidates for the construction of lightweight SC. Zhang et al. have mentioned that vertically aligned CNTs are more suitable and promising electrode materials for SC in terms of their fast

ionic transportation in electrolyte, compared to entangled CNTs with an irregular pore structure [1]. Analysis of the available publications shows that aligned CNTs, directly grown on Al current collector, are not investigated as a component of SC in detail till date. Apparently, the main reason is that the low melting point of Al (660 °C) prevents it from successfully withstanding the high temperatures employed in thermal catalytic chemical vapor deposition (CCVD).
CNTs on Al foil are produced using a scalable CCVD to make hybrid electrodes for SCs. It is found that surface topography of the Al foil is a governing factor for the growth of CNTs, their alignment and adhesion to the current collector. The so-prepared electrodes achieve a specific capacitance up to 11.2 F/g, which is found to be weakly sensitive to the alignment of CNTs. New catalysts based on the combinations Fe/MnO and Co/MnO for growth of aligned CNTs are proposed. Detailed thermodynamic calculations are performed to understand the correlation between the chemical state of the catalyst particles on the substrate and the morphology of the resulting nanotube arrays.
[1] L. L. Zhang, X. S. Zhao: Chem. Soc. Rev. 38 (2009) 2520-2531.

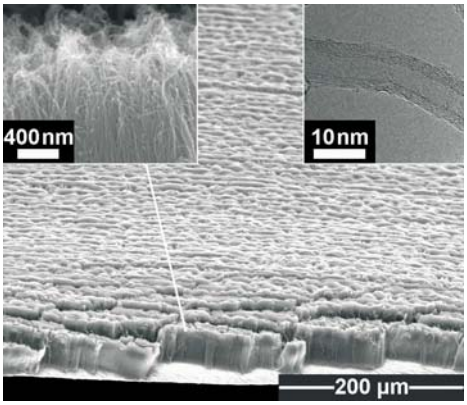

Fig.: SEM and TEM (inset) of carbon nanotubes grown on Al foil.

Cooperation: Fraunhofer Institute for Ceramic Technologies and Systems (IKTS-Dresden); TU Dresden; Univ. of Messina (Italy)
Funded by: BMBF FKZ: 03X0076C

Identification of the electronic states of manganese phthalocyanine close to the Fermi level

M. Grobosch, B. Mahns, M. Knupfer

The electronic properties of manganese phthalocyanine (MnPc) have been investigated by a joint experimental and theoretical work using photoelectron spectroscopy studies as well as density functional theory based calculations. We demonstrate that the highest occupied molecular orbital of MnPc has significant metal 3d character in contrast to other transition metal phthalocyanines. This has a direct consequence on the ionization potential which for MnPc is 0.5 eV lower as compared to other transition metal phthalocaynines. Moreover, our results also allowed the identification of the $1e_g$ symmetry of the Mn3d states near the Fermi level and they provide insight into the magnetic anisotropy of MnPc. For details see: M. Grobosch *et al.*, *Chem. Phys. Lett.* **505,** 122 (2011).

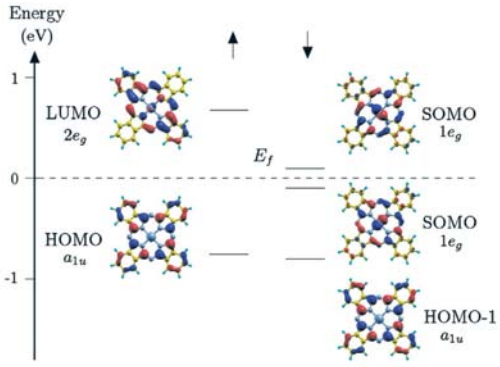

Fig.: Spin-dependent electronic structure of MnPc close to the Fermi level. In contrast to other transition metal phthalocyanines, MnPc is characterized by a singly occupied molecular orbital (SOMO) closest to the Fermi level (HOMO = highest occupied molecular orbital).

Cooperation: TU Bergakademie Freiberg, Institut für Theoretische Physik
Funded by: DFG

Room temperature magnetometry of an individual iron filled carbon nanotube

S. Philippi, U. Weißker, T. Mühl, A. Leonhardt, B. Büchner

Thorough characterization of the essential properties of individual nanoscale systems is a difficult task, because of their small size and the resulting problems in sample handling, as well as the low signal strength in any experimental application. This puts high demands to sample preparation techniques and usually requires low temperature measurements [1]. For a magnetic examination of an individual, one-side clamped iron filled carbon nanotube (CNT) at room temperature, the influence of external fields on its bending vibration has been analyzed theoretically and experimentally, with particular consideration to the changes in the resonance frequency [2]. Our model involves the application of a modified Euler-Bernoulli-beam to analyze the zero field oscillatory behaviour as well as a magnetostatic approach to determine the influence of any external

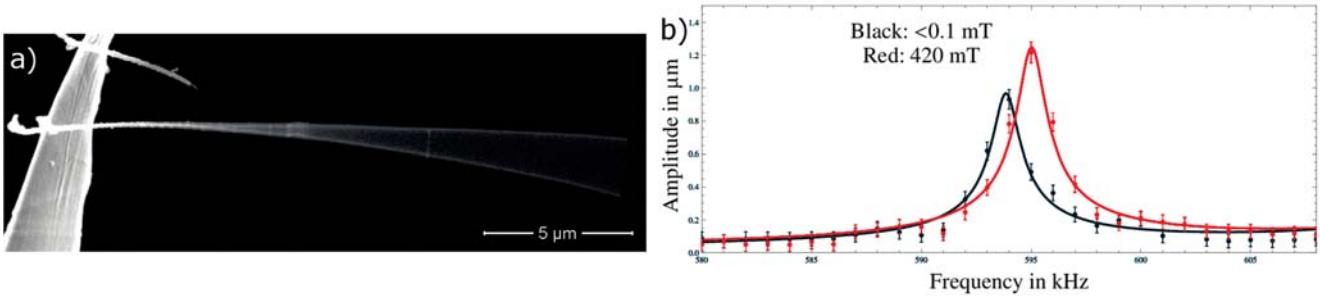

Fig.: a) Scanning electron micrograph (SEM) of a resonantly oscillating iron filled carbon nanotube at a driving frequency of 573 kHz. The high frequency movement limits the visibility in SEM to an envelope image. **b)** Typical resonance curves as observed in the experiment in zero magnetic field (black) and 420 mT (red). The shift of the resonance frequency in applied fields is proportional to the examined nanowire's magnetic moment.

field distributions present. The experiments were conducted in situ in a scanning electron microscope. The measured magnetic moment of the nanowire in the CNT at room temperature was 2.1×10^{-14} Am^2. Due to the favourable geometry of the CNT oscillator, the raw signal with this approach is significantly more favourable than state of the art cantilever magnetometry [3]. The obtained good agreement between model and experiment provides a valuable basis for the development of nanoelectromechanical systems where magnetic interactions are relevant.

[1] K. Lipert *et al.*, *Applied Physics Letters* **97**, 212503 (2010).
[2] S. Philippi *et al.*, *Journal of Applied Physics* **110**, 084319 (2011).
[3] P. Banerjee *et al.*, *Journal of Applied Physics* **96**, 252505 (2010).

Cooperation: The Ohio State University, Columbus, USA
Funded by: DFG (MU1794/6-1)

Synthesis of herringbone and platelet Carbon Nanofibers – obtaining type-pure samples by tuning the synthesis conditions

D. Maier, M. Ritschel, C. Mickel, A. Leonhardt, B. Büchner

Recently, Carbon Nanofibers(CNF) were brought into scientific focus as a starting material for the production of graphene. Due to their exposed edges they can easily be intercalated and exfoliated to nanographite with a predefined lateral dimension or graphene, respectively. One can basically distinguish two types of CNF: herringbone and platelet fibers. While in the former the graphitic 001 planes are tilted relative to the fiber axis by an angle of 30° – 70° they are arranged perpendicular to the axis in the latter.

For producing mono-fraction batches of either platelet or herringbone fibers via fixed-bed CVD optimal conditions have been developed. The optimal catalyst for herringbones consists of a Fe/Cu alloy (80 mol% Fe). In contrast a mixture of Fe and MgO (ratio 7 to 1) is needed to obtain predominantly platelets. Furthermore, the composition of the gas phase is a key parameter for the production of mono-fraction fibers. Herringbones are synthesized using a mixture of C_2H_4, H_2 and Ar, whereas platelets require the additional use of CO.

By transmission electron microscopy and selected area diffraction a preferred growth direction with respect to the Fe_3C catalyst has been revealed for each fiber type. Herringbones are characterized by a fiber axis which coincides with the [100] direction of the mostly octahedral catalysts. Carbon precipitates on the {hkl} planes which determine the tilt angle of the graphitic fiber planes. Catalysts of platelet CNF represent disc-shaped particles with a well pronounced (010) face. Thus, the graphitic planes are deposited onto its {010} planes causing a fiber axis that runs along with the [010] direction of the catalyst.

Concluding from the present results CO leads to a strong alteration of the catalyst habitus, from an octrahedral to a platelet habitus.Further research will explore the crystal-habit formation as well as the influence of Cu and CO onto it in detail. From this a synthesis mechanism is going to be formulated.

Funded by: BMBF (Inno.CNT)

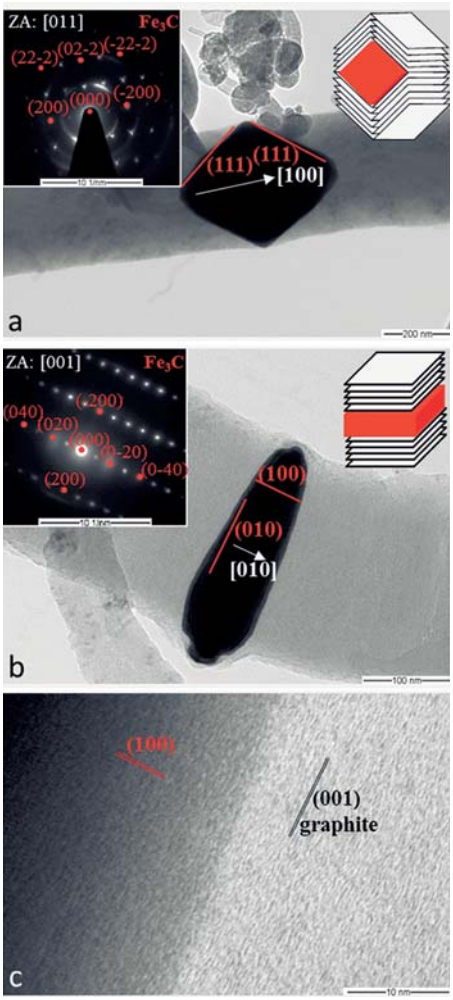

Fig.: a) TEM image of a herringbone CNF (with the white arrow pointing along the fiber axis) with the corresponding diffraction pattern (indexed as Fe_3C) and a scheme of the fiber structure
b) TEM image of a platelet CNF (with the white arrow pointing along thefiber axis) with the corresponding diffraction pattern (indexed as Fe_3C) and a scheme of the fiber structure
c) high resolution TEM image illustrating the lattice planes of the Fe_3C catalyst particle shown in b) and the graphitic planes grown on its (010) face

Paramagnetic contrast agents encapsulated in closed CNT for MRI measurements

E. Fidiani, P. M. F. J. Costa, D. Maier, A. U. B. Wolter-Giraud,
M. H. Ruemmeli, A. Leonhardt, S. Hampel, B. Buechner

The use of carbon nanotubes (CNT) for medical purposes such as drug-delivery or as active capsules for medical diagnosis has been a scientific topic of interest for the past few years. Magnetic resonance imaging (MRI) is one of the best-well known imaging methods for medical diagnosis. The most common contrast agent for MRI is Gadolinium chelate, which is very attractive because the chelate complexes reduce the toxicity and make Gd easy soluble in water. But for patients with kidney problems also these gadolinium chelates are toxic and new ideas are needed.

The concept here is the encapsulation of the gadolinium compound into CNT. The best filling strategy is a gas phase reaction with GdI_3 with filling yields of 50 % as regards the ratio of filled-to-empty CNTs. Afterwards the Gd-filled CNT are subsequently sealed by a hydrocarbon-cracking CVD method which proved to be an effective approach. So the closed CNT will work as a protective shell and reduce intensely the toxicity of the Gd. The structural and chemical features of the Gd-filled CNT were analysed with scanning and transmission electron microscopy and showed amorphous and crystalline filling types in one sample.The thermal stability of the compounds and the filling yield were evaluated with thermogravimetry. The highest filling yield with the highest crystalline filling form could be achieved at very long reaction times of 72 h. The behavior of the magnetic susceptibility of the Gd-filled CNT showed that they are paramagnetic without any magnetic impurities. The calculated effective magnetic moment around 6 μ_B is in agreement with the literature.

With all these results, the introduction of CNT into biomaterial science as MRI contrast agent has great opportunity to improve medical diagnostics.

Cooperation: Department of Urology, TU Dresden; CICECO Univ. of Aveiro Portugal
Funded by: DAAD, DKH

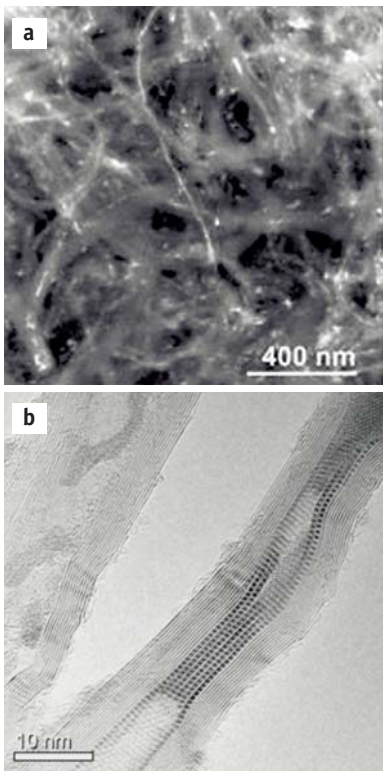

Fig.: (a) Back-scattered SEM image of GdI_3-filled CNT **(b)** TEM micrograph showing amorphous and crystalline GdI_3-filled CNT.

Nitrogen Directs Multiple CF_3 Radical Additions in $C_{59}N$ Azafullerene

N. B. Shustova,[1] A. A. Popov, L. Dunsch, Andreas Hirsch,[2] S. H. Strauss,[1] O. V. Boltalina[1]

Substitution of one carbon atom in C_{60} by nitrogen drastically affects chemical properties of the fullerene. In trifluoromethylation of azafullerene $C_{59}N$, nitrogen was found to direct addition of the first CF_3 to the carbon atom next to nitrogen and provide noticeably different addition patterns at further addition steps than in trifluoromethylated C_{60} derivatives [1]. Among several other $C_{59}N(CF_3)_x$ compounds, $C_{59}N(CF_3)_5$ with quasi C_{5v}-fold symmetry was isolated as the only compound with 5 groups and studied by ESR spectroelectrochemistry. The structure of the compound is reminiscent of the C_s-symmetric isomer of $C_{60}(CF_3)_6$ if the CF_3-bearing carbon atom in the latter is substituted by nitrogen. Since CF_3 groups completely isolate nitrogen from the rest of the fullerene π-system, reduction potentials of $C_{59}N(CF_3)_5$ and C_s-$C_{60}(CF_3)_6$ appear to be very similar. Besides, the lack of the communication between the fullerene core and the π-system of the nitrogen-bearing pentagon results in the effective C_{5v} symmetry of the former. As a result of such high symmetry, LUMO $C_{59}N(CF_3)_5$ is two-fold degenerate, which leads to the Jahn-Teller distortion in the anion-radical. Indeed, anion-radical of $[C_{59}N(CF_3)_5]^{\bullet -}$ gave broad ESR signal resembling that of C_{60} anion, whose line width was also explained by Jahn-Teller effect.

[1] N. B. Shustova et al, Angew. Chem. Int. Ed. **50** (2011) 5537.

Coopereation: [1] Colorado State University, Fort Collins (USA)
[2] Friedrich-Alexander-Universität Erlangen-Nürnberg

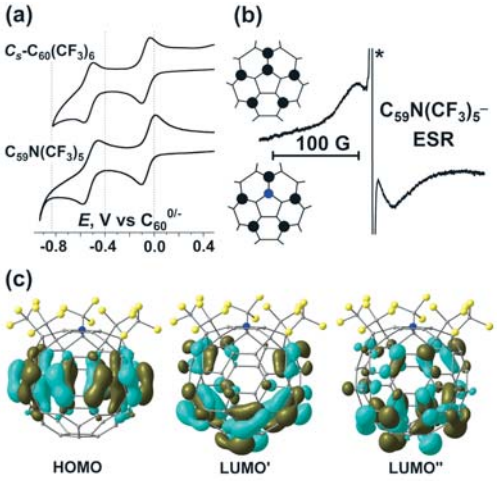

Fig.: (a) Cyclic voltammetry of C_s-$C_{60}(CF_3)_6$ and $C_{59}N(CF_3)_5$; **(b)** ESR spectrum of $C_{59}N(CF_3)_5^-$ (an asterisk marks impurity line); **(c)** HOMO and two components of quasi two-fold degenerate LUMO of $C_{59}N(CF_3)$. The insets show addition pattern of C_s-$C_{60}(CF_3)_6$ (CF_3-bearing carbon atoms are shown as black dots) and $C_{59}N(CF_3)_5$ (nitrogen position is shown as blue dot).

Research Area 4
Metastable alloys

Electrochemical micro-machining of bulk metallic glasses

J. A. Koza, R. Süptitz, M. Uhlemann, A. Gebert, L. Schultz, J. Eckert

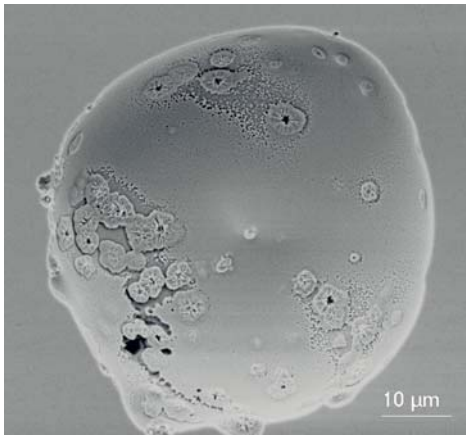

Fig. Micro-hole structure obtained by electrochemical micro-machining of a Zr-based bulk metallic glass

Advanced electrochemical micro-machining (ECMM) techniques are so far only applied to conventional crystalline metallic materials. It is expected to have a high potential for micro-structuring of bulk metallic glass surfaces, but it is also challenging due to the metastable and multi-component nature of the glassy alloys causing fast and complex dissolution processes at the micro-scale. For the first time electrochemical micro-machining of a Zr-based bulk metallic glass surface was successfully demonstrated using the micro-tool electrode technique with ultra-short voltage pulses. The selection of suitable process parameters is the key issue to reach high machining resolution and optimized structures, whereby the electrolyte chemistry is most important. Aqueous $NaNO_3$ standard machining solution is not applicable due to a formation of corrosion product layers in the surface regions machined under transpassive conditions. In contrast, when using a methanolic $HClO_4$ electrolyte micro-hole structures with significant aspect ratio can be produced. The pulse voltage has a substantial effect on the machined structure morphology. At low pulse voltages the dissolution is non-uniform and a porous morphology is obtained. As the pulse voltage increases a smoothing effect is observed. Further studies will be extended to other glassy alloy systems, e.g. Fe-based BMGs for which thermal micro-forming techniques are not applicable [1,2].

[1] J. A. Koza et al. Intermetallics 19 (2011) 437-444
[2] A. Gebert et al. Corrosion Science 52 (2010) 1711-1720

Cooperation: TU Dresden, Univ. Düsseldorf, TU Chemnitz, FhG IKTS Dresden
Funded by: DFG

Shape memory phase formation in metastable CuZr-based alloys

S. Pauly, K. K. Song, P. Gargarella, N. S. Barekar, U. Kühn and J. Eckert

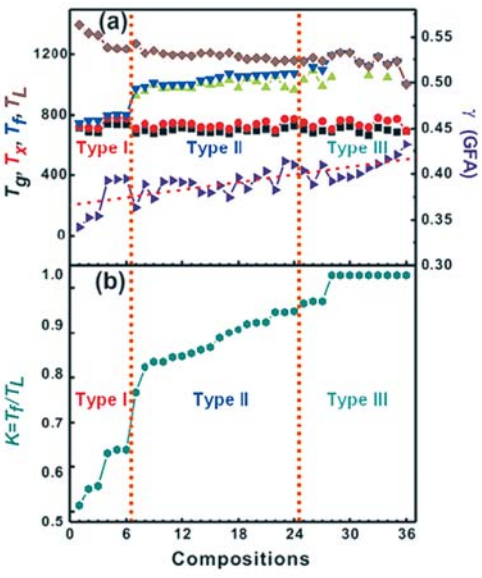

Fig.: Thermal properties of 36 CuZr-based BMGs. T_g, T_x, T_f and T_l denote the glass transition temperature, the crystallisation temperature, the temperature where the B2 CuZr is formed and the liquidus temperature, respectively. The γ parameter, $T_x/(T_g+T_l)$, characterises the glass-forming ability of the alloys. It tends to increase with decreasing thermal stability of B2 CuZr.

Rapidly quenched CuZr-based alloys offer the unique characteristic of precipitating a crystalline shape memory phase (B2 CuZr) in a metallic glass. In order to synthesise such metastable bulk metallic glass (BMG) composites, knowledge of the influence of the composition and the cooling rate on the phase selection is crucial. The systematic investigation of 36 different CuZr-based alloys suggests that they can be classified into three different types with a distinctly different thermal stability of the B2 CuZr phase (Fig.). While the thermal properties (glass transition temperature, T_g, crystallisation temperature, T_x, B2 CuZr formation temperature, T_f, and the liquidus temperature, T_l, Fig. (a) do not show strong variations, the here proposed parameter, $K = T_f/T_l$, clearly reveals the difference in these alloys (Fig. b). The parameter K basically considers the competition between vitrification, the precipitation of the metastable B2 CuZr and the low-temperature equilibrium phases [1]. It appears that the larger K, the higher the likelihood to obtain a BMG composite, which contains shape memory crystals. This new approach facilitates the search for metastable CuZr-based shape memory alloys with interesting deformation behaviour.

[1] K.K. Song et al. Acta Mater. 59, 6620 (2011).

Cooperation: Univ. Sao Paulo, Brazil; Federal Univ. Sao Carlos, Brazil; Beihang Univ., Beijing, China

Funded by: Chinese Scholarship Council (CSC), the Natural Science Foundation of Shandong Province (Z2008F08), the Excellent Youth Project of the Natural Science Foundation of Shandong Province (JQ201012), the National Basic Research Program of China (973 program 2007CB613901), the National Natural Science Foundation of China (50631010 and 50831003), DAAD and Conselho Nacional de Desenvolvimento Científico e Tecnológico (CNPq), Brazil.

Elastic constants of single crystalline β-$Ti_{70}Nb_{30}$

R. Hermann, H. Hermann, M. Calin, B. Büchner, and J. Eckert

Titanium based alloys belong to the materials currently used for biomedical applications due to high corrosion resistance and excellent biocompatibility. The combination of high strength and low Young's modulus favors this material as ultimate choice for orthopaedic implants.

β-$Ti_{70}Nb_{30}$ (at%) singles crystals were grown by magnetic field controlled floating-zone technique with two-phase radio-frequency electromagnetic heating. The Young's moduli of the crystals show pronounced anisotropy. This anisotropy is illustrated in Fig. 1. The length of a vector pointing from the origin of the coordinate system to an arbitrary point of the surface plotted in the Fig. is proportional to the Young's modulus for the corresponding crystallographic (h, k, l) direction. The lowest value is E_{100} = 39.5 GPa. Comparison of the present results with recently published data, and extrapolation to low Nb content of about 20at% shows that the preparation of binary β-TiNb alloys with $E_{100} \approx$ 20 to 30 GPa should be possible which would match the modulus of bone [4]. For details see R. Hermann et al., Scripta Materialia 2012, 66, 198 – 201.

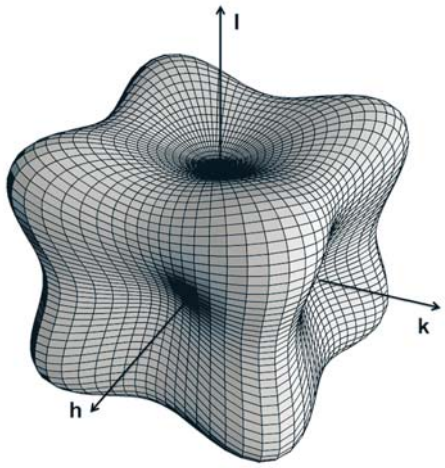

Fig.: Elastic modulus in dependence on the crystal orientation given by the (h, k, l) indices parallel to the axes.

Preparation of nano-graphene platelets by intercalation and exfoliation of graphite

H. Hermann, O. Khvostikova, H. Wendrock, Th. Gemming, J. Thomas, H. Ehrenberg, M. Ritschel, A. Leonhardt

Based on previous theoretical work and motivated by recent progress in graphene research the process of the preparation of nano-graphene platelets (NGPs) via chemical intercalation and exfoliation of graphite was studied. It was the aim of our work to find out the impact of morphology and microstructure of the graphite used as raw material on the features of the final NGPs. We showed that the success of the method of intercalation and exfoliation of graphitic material regarding the preparation of NGPs depends significantly on the microstructure of the initial material [1]. Correlations of the kinetics and the result of all process steps with the dimension of the graphite crystals and crystallites in c-direction and the lateral size were found. Fig. 1 shows a TEM image of NGPs prepared from single crystalline graphite flakes of about 50 µm thickness and 100 to 500 µm lateral size. From our observations it can be concluded that cylindrical graphite crystallites with c-axis in the direction of the cylinder axis would be most favourable for the preparation of NGPs, and single-, double-, or triple- graphene layers [1]. Graphite fibres with about 200 nm diameter and lengths of few µm, and c-axis in the direction of the fibre line will be available soon and will be used as a new raw material.

[1] O. Khvostikova et al. Mater. Sci. **46** (2011) 2422.

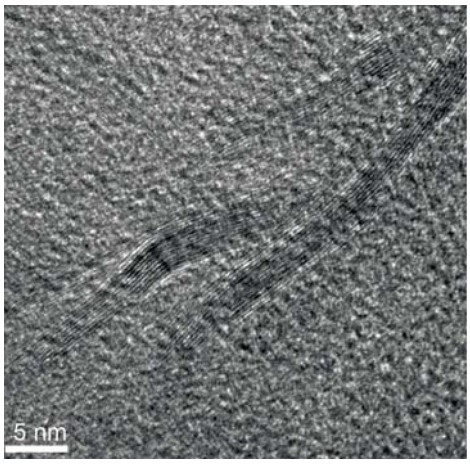

Fig.: TEM image of nano-graphene platelets with about 4 nm thickness.

Cooperation: TU Dresden, Inst. für Physikalische Chemie; Fh-IFAM Dresden
Funded by: Stiftung Energie Baden-Württemberg; ECEMP grant no: 13858/2379

Reversible Li-insertion of amorphous and partially crystalline $Al_{86}Ni_8La_6$ and $Al_{86}Ni_8Y_6$ alloys as anode materials for Li-ion batteries

F. Thoss, L. Giebeler, S. Oswald, H. Ehrenberg, J. Eckert

High-energy Li-ion batteries exceedingly depend on the high specific capacity of electrode materials. Intermetallic alloys are promising candidates to be alternative anode materials with enhanced specific capacities in contrast to state-of-the-art techniques, dominated by carbon materials. Disadvantageously the phase transitions during the charge-discharge processes, induced by the lithiation process, cause volume changes of 100 - 300 %. Due to the brittleness of intermetallic phases, the fracturing of the electrode material leads to the loss of the electrical contact. In order to overcome the huge volume changes amorphous Al-based alloys were investigated with the intension to realize the lithiation process without a phase transformation. Powders of the two alloys $Al_{86}Ni_8La_6$ and $Al_{86}Ni_8Y_6$, produced via melt spinning and subsequent ball milling, were found to be amorphous. However, only minor Li-ion transfer is observed during the electrochemical cycling process. Thus, the amorphous state does not improve the electrochemical behavior. A significant enhancement of the specific capacity is obtained for crystallized samples of the alloys. As possible origins for the observed behavior, surface oxide layers and the addition of glass formers have to be considered as minor influences. A threshold between electrochemically inactive and electrochemically active electrodes is observed by galvanostatic cycling of partially crystallized powders, which were annealed at different temperatures (Fig.). Apparently, certain crystallinity is necessary for bulk electrodes to provide sufficient possibilities for Li-insertion.

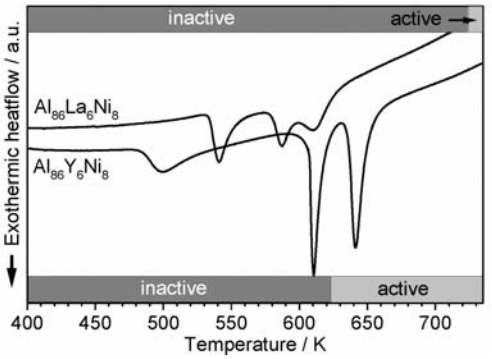

Fig.: DSC curves (heating rate 40 K min^{-1}) of $Al_{86}Ni_8La_6$ and $Al_{86}Ni_8Y_6$ amorphous ribbons.

The available free volume in amorphous materials is considered to be essential for supplying interstitial-like space as diffusion paths for additional Li-ions, because lattice site changes, as usual for diffusion in the crystalline state, are not preferential in the amorphous state. The density of the amorphous material measured by helium pycnometry was found to be just slightly lower compared with crystalline material. Therewith, the free volume of the investigated amorphous materials is insufficient for an adequate lithiation of the electrode.

Funded by: ECEMP (European Union/Free State of Saxony Grant-Nr. 13853/2379), Deutsche Bundesstiftung Umwelt (DBU)

Ti-based alloys for biomedical applications

M. Calin, A. Gebert, A. Helth, K. Zhuravleva, M. Bönisch,
S. Abdi, N. Zheng, P. Flaviu Gostin, L. Schultz, J. Eckert

For load-bearing orthopaedic applications, metallic materials have the greatest potential, owing to their excellent mechanical strength and resilience when compared to polymers and ceramics. However, major drawbacks of current Ti-based implants reducing their *in-vivo* life are the mechanical non-compatibility between bone and metal and weak interfacial bonds. Further alloy development is needed comprising strategies for reducing materials stiffness via intrinsic (Young's modulus) or extrinsic (porosity) properties and for novel surface modification techniques. In current research we explore structural and compositional options of advanced Ti-based materials [1]. In the metastable Ti-Nb system two characteristic minima of the Young's modulus at 15 - 20 and 40 - 45 wt.-% Nb exist. The first corresponds to formation of α''-martensite phase, which plays an important role in shape memory and super-elasticity effects. The second minimum is mainly related with formation of β-phase. The effect of minor alloying elements, e.g. β-stabilizers, and of processing conditions on phase formation and transformation processes is investigated. SPD processing of $Ti \geq 40$ Nb alloys was

shown to significantly increase strength and hardness, while In-additions reduce the Young's modulus. Via mechanical milling and subsequent hot consolidation with a fugitive phase porous Ti-Nb structures were obtained. Furthermore, Ti-based metallic glasses (MG) are considered as potential biomaterials. For the $Ti_{40}Zr_{10}Cu_{36}Pd_{14}$ alloy, In substitutions were found to increase the glass-forming ability and to yield increased plasticity. For the glass-forming Ti-Zr-Nb-Si system the effect of melt spinning conditions on phase formation and on the effectiveness of chemical surface modifications is studied.

[1] L. C. Zhang et al., in book 'Advances in Mechanical Engineering Research'. Vol.2., David E. Malach (Editor), Nova Science Publishers, New York, USA (2011), 233-251; ISBN 978-1-61761-984-7

Cooperation: Univ. Giessen, Univ. Heidelberg, TU Dresden, Univ. Torino (Italy), Kath. Univ. Leuven (Belgium), Univ. Wien (Austria), Univ. Aut. Barcelona (Spain), IMR Shenyang (China)
Funded by: DFG Transregio 79, EU-ITN BioTiNet, DAAD, China Scholarship Council (CSC)

Quantitative determination of the surface diffusion on Au nanoparticles with aberration-corrected HRTEM

A. Surrey, D. Pohl, L. Schultz, B. Rellinghaus

Aberration-corrected high-resolution transmission electron microscopy (HRTEM) was used to investigate the atomic diffusion at the surfaces of nanoparticles in particular during their coalescence. As the transport of material that goes along with inter-particle coalescences occurs predominantly via surface diffusion, a thorough and quantitative understanding of the latter is mandatory. Since the incident electron beam may effectively promote the sintering, possibilities of measuring the surface diffusion in situ in an electron microscope provide the general opportunity to shed some light on the interaction between the high-energy electron beam and the sample.
In the present approach, the motion of atoms (or atom columns) at the surfaces of Au nanoparticles was directly observed in the electron microscope (*FEI Titan^3 80-300*). Both, Au icosahedra on amorphous carbon substrates and single crystalline Au octahedra whose surfaces extend into the vacuum and which can thus be imaged quasi substrate-free (see figure) were studied. In order to quantitatively estimate the diffusion coefficient the temporal fluctuations of the occupation of individual columns of surface atoms were measured from time series of HRTEM images. Although (i) HRTEM only provides a 2D projection of the 3D diffusion problem and (ii) atoms are indistinguishable in the obtained micrographs, a characteristic atomic jump frequency could be measured. This was then used to calculate the coefficient of surface self-diffusion in very good agreement with results of studies utilizing atomic force and scanning tunneling microscopy.

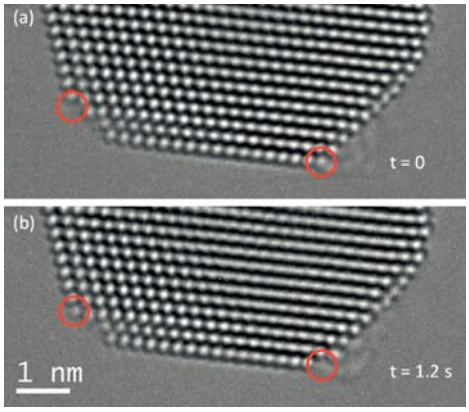

Fig.: Two out of a series of 22 subsequent HRTEM images showing one half of a Au octahedron over vacuum. The time interval between the two images is 1.2 s. Two individual surface atom columns which clearly experience changes in their occupation throughout this interval are highlighted by red circles.

Reinforced Copper Matrix Composite Thin Films

J. Gluch, S. Menzel, N. Malyar, K. Ganguly, T. Gemming, J. Eckert

The aim of the topic is to improve the mechanical properties of thin metal films as they are used in microelectronics and MEMS devices that are prone to electro- and acousto migration. One route is to strengthen the copper by using carbon nanotubes as a fiber reinforcement component of the metal matrix. To enhance their adhesion to the copper the tubes are COOH-functionalized. Our results show that the addition of carbon nanotubes to the sulphuric base bath results in pinning sites during Cu-film growth and also inhibits the self annealing of the Cu film. This results in a fine grained Cu film with

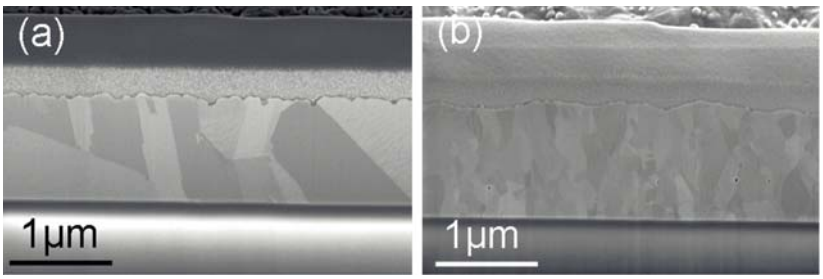

Fig.: FIB image of a Cu film **(a)** without nanotubes and **(b)** with nanotubes.

a stable microstructure (Fig.). Fracture experiments result in a typical fiber pull-out behavior and the electrical resistivity is 2 -3 µΩcm at a film thickness of 1 µm. The obtained results indicate nanotubes reinforced Cu matrix thin films as a promising candidate system for microelectronic or acousto-electronic metallizations for applications with enhanced demands on reliability and durability under high loads.

Funded by: DFG

Interactions of copper and iron in conversion reactions of nanosized oxides with large variations in iron-copper ratio

W. Gruner, J. Thomas, L. Giebeler, H. Ehrenberg, D. Wadewitz, J. Eckert

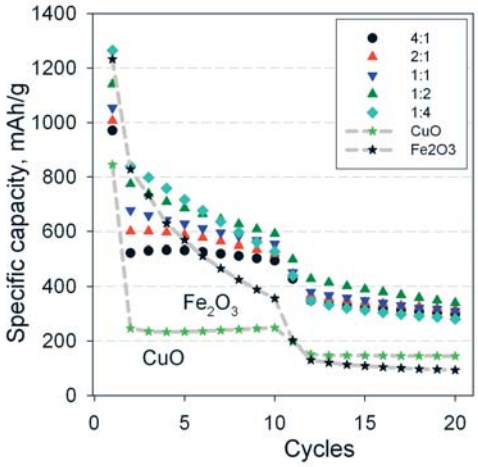

Fig.: Galvanostatic cycling stability of CFO materials with different Cu:Fe ratios (10x z/5 and 10x 1z rates, 0.2 – 3.0 V).

The ternary 3d transition metal oxide system Cu-Fe-O was investigated as conversion type electrode material to study the electrochemical interaction of both redox couples. Synthesized by the self-combustion procedure with Cu:Fe ratios from 4:1 to 1:4, the oxides have a relative homogenous distribution of copper and iron over the particles relatively to the crystallite size level. The special interest was targeted on the redox behavior of the neighbored elements copper and iron after the conversion reaction, i.e. after the first reduction step. The cyclic voltammetry measurements confirm the existence of distinct and element-specific redox couples over the following cycles but an element-specific cycling stability under the same conditions. The relative stable oxidation/reduction behavior of the copper system stabilizes the specific capacity of Cu-rich CFO electrode materials under galvanostatic cycling conditions, whereas the Fe-rich system is dominated by degradation. This effect is interpreted by the interaction of metallic Cu particles which are *in situ* formed in the near neighborhood of iron ions before the Fe^{3+}/Fe^{0} redox couple reacts.

Cooperation: Karlsruhe Institute of Technology Eggenstein-Leopoldshafen, TU Bergakademie Freiberg, Westfälische Wilhelms-Univ. Münster
Funded by: DFG-SPP 1473

Structural and Magnetic Nano-clusters in $Cu_{50}Zr_{50-x}Gd_x$ Metallic Glasses by Liquid-Liquid Phase Separation

N. Mattern , JH. Han, B. Schwarz, DH. Kim, J. Eckert

Recently, metallic alloys showing phase separation in the liquid could be frozen into phase separated metallic glasses by rapid quenching the melt [1-3]. In order to obtain phase separated glasses the strategy is to modify alloys with high glass forming ability by adding an element with large positive enthalpy of mixing to at least one other of the constituent. For $Cu_{50}Zr_{50-x}Gd_x$ alloys with low concentration of gadolinium (x = 2,5 at%), phase separated metallic glasses could be successfully prepared by melt spinning technique ($\Delta H_{Gd-Zr} = +9$ kJ/mol). Atom probe tomography and small-angle X-ray scattering

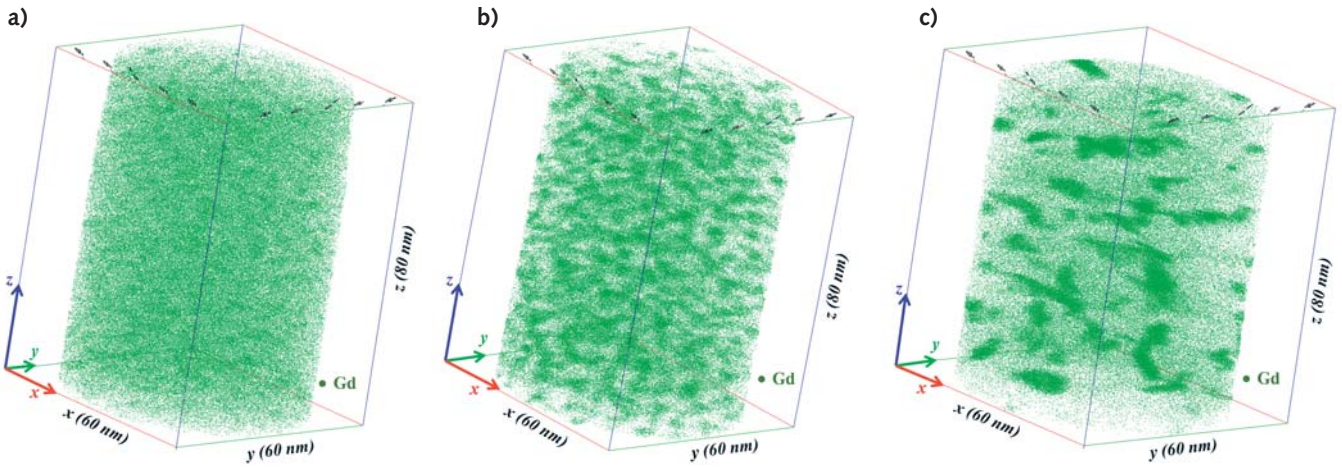

Fig.: Phase separated metallic glasses consisting of Gd-enriched clusters of 2 nm size are formed upon rapid quenching $Cu_{50}Zr_{45}Gd_5$ melt as shown by the spatial distribution of the Gd atoms measured by atom probe tomography (a). Annealing in the glassy or supercooled liquid state leads to an increase of concentration fluctuations pointing to spinodal decomposition as mechanism (b). Ostwald type ripening on a nanoscale is observed as first stage of crystallization (c).

were used to analyze the phase separation quantitatively. Figures a-c show the spatial distributions of the Gd atoms of the $Cu_{50}Zr_{45}Gd_5$ glass for the as-quenched state (a) as well as after annealing below (b) and above (c) the first crystallization event. For the as-quenched ribbon Gd-enriched clusters are detected 2 -3 nm in size. The key physical parameter to obtain such nano-clustered microstructure upon quenching is the critical temperature of liquid-liquid phase separation, which here is close to the glass transition temperature [4]. Annealing the metallic glass in the supercooled liquid state results in further accumulation of Gd within the clusters by up-hill diffusion (Fig. b). The Gd-enriched nano-clusters exhibit ferromagnetic ordering below 50 K and the cluster size regime derived from magnetization measurements is in good agreement with that obtained from atom probe tomography investigations. First stage of crystallization of $Cu_{50}Zr_{45}Gd_5$ glass is an Ostwald type ripening on a nanometer scale (Fig. c).

[1] Kündig AA, Ohnuma M, Ping DH, Ohkubo T, Hono K. Acta Mater 2004;52:2441.
[2] Park BJ, Chang HJ, Kim DH, Kim WT, Appl Phys Lett 2004; 85:6353.
[3] Mattern N., Kühn U., Gebert A., Gemming T., Zinkevich M., Wendrock H., Schultz L. Scripta Mater 2005;53:271.
[4] Mattern N, Shariq A, Schwarz B, Vainio U, Eckert J., Acta Mater (2012), doi: 101016 / j. actamat.2012.01.019

Cooperation: DESY Hamburg, Yonsey University Seoul, FhG CNT Dresden
Funded by: DFG

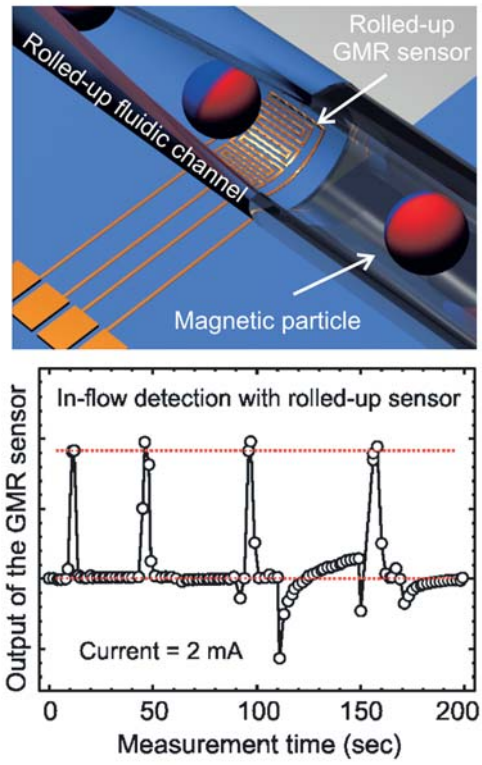

Fig.: (Top panel) Schematics revealing the main concept of rolled-up magnetic sensor for in-flow detection of magnetic objects. **(Bottom panel)** Magnetic particles detection: Time evolution of the sensor output measured while magnetic particles pass the rolled-up sensor.

Research Area 5
Stress-driven architectures and phenomena

Rolled-up magnetic sensor: Nanomembrane architecture for in-flow detection of magnetic objects

I. Mönch, D. Makarov, R. Koseva, L. Baraban, D. Karnaushenko, and O. G. Schmidt

We presented a novel concept based on rolled-up nanotech for fabrication of magnetic sensor devices, which can be straightforwardly integrated into existing fluidic architectures [1]. We applied strain engineering to roll-up a functional nanomembrane consisting of a magnetic sensor element based on $[Py/Cu]_{30}$ multilayers revealing giant magnetoresistence (GMR). The sensor's characteristics before and after the roll-up process are found to be similar, allowing for a reliable and predictable method to fabricate high quality ultra-compact GMR devices. The performance of the rolled-up magnetic sensor was optimized to achieve high sensitivity to weak magnetic fields, as required in biomedical applications. We demonstrated that the rolled-up tube, itself, can be efficiently used as a fluidic channel, while the integrated magnetic sensor provides an important functionality to detect and respond to a magnetic field. The performance of the rolled-up magnetic sensor for the in-flow detection of ferromagnetic CrO_2 nanoparticles embedded in a biocompatible polymeric hydrogel shell was highlighted (Fig.). This approach might be beneficial for efficient biodetection of protein structures, diagnostics of diseases, and sorting of living cells. The advantage of rolled-up devices is their straightforward integrability into existing on-chip technologies and the ability to combine several functions into a single architecture, possibly leading to a fully operational lab-in-a-tube system [2].

[1] I. Mönch et al., ACS Nano 5, 7436 (2011).
[2] E. J. Smith et al., Proc. SPIE 8031, 80310R (2011).

Cooperation: Claudia Kaiser and Karl-Friedrich Arndt (Physical Chemistry of Polymers, Dresden University of Technology)
Funded by: German Science Foundation (DFG) grants MO887/1-2, AR193/11-2, priority program SPP 1259, and DFG Research Unit 1713 „Sensoric Micro- and Nanosystems".

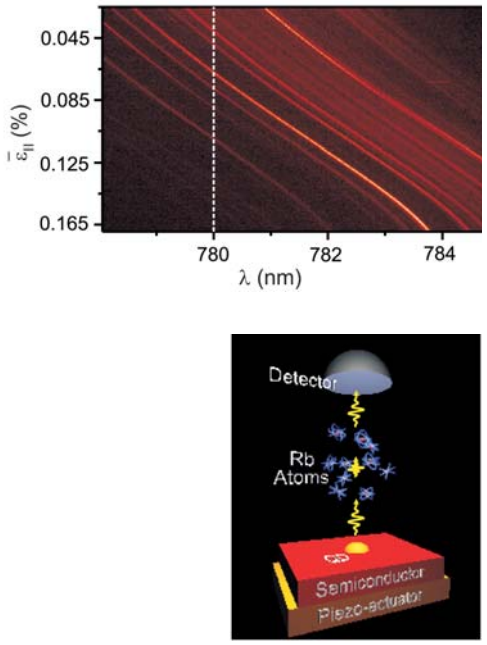

Strain-induced tuning of the emission wavelength of quantum dots in the spectral range of the ^{87}Rb D_2 lines

S. Kumar, R. Trotta, E. Zallo, P. Atkinson, A. Rastelli, and O. G. Schmidt

Optically active semiconductor quantum dots (QDs), also dubbed "artificial atoms", are currently being investigated as building blocks for future quantum communication technologies. In fact they can be used as sources of single and entangled photons on demand. A practical method to store such photons (a quantum memory) is still missing and will be essential for the realization of quantum repeaters. A possible way to realize such a memory consists in exploiting the low group velocity of light in certain media. We have now fabricated high-quality GaAs dots in AlGaAs matrix with light emission wavelength around 780 nm, corresponding to the D_2 transitions of Rubidium. In cooperation with the TU Delft, we have shown that, if the wavelength of the photons emitted by a dot

Fig.: Top: low-temperature color-coded photoluminescence spectra of GaAs quantum dots taken as a function of the measured in-plane strain $\varepsilon_{//}$. The strain in the semiconductor membrane containing the quantum dots is varied via a piezoelectric actuator. **Bottom:** schematic arrangement for slow light experiments using Rb atoms and photons with tunable wavelength emitted by quantum dots.

is precisely tuned between the two D_2 lines, photons are effectively slowed down [1]. A convenient way to achieve wavelength tuning of our artificial atoms is represented by application of reversible stress to the semiconductor heterostructure [2]. Stress modifies in fact the energy bandgap (and other electronic properties) of semiconductors. We achieve broadband and fine tuning of QD emission by integrating thin semiconductor membranes with embedded QDs on top of piezoelectric actuators made of PMN-PT.

[1] N. Akopian *et. al.*, Nat. Photonics 5, 230 (2011)
[2] S. Kumar *et. al.*, Appl. Phys. Lett. 99, 161118 (2011)

Cooperation: TU Delft
Funded by: DFG and BMBF

Tunable generation of correlated vortices in open superconductor tubes

V. M. Fomin, R. O. Rezaev and O. G. Schmidt

Advancements in fabrication of rolled-up micro- and nanotubes including superconductor layers (e.g., InGaAs/GaAs/Nb) [1] open new possibilities for investigation of the vortex matter in superconductors with curved geometries. We investigated theoretically the dynamics of superconducting vortices in the presence of transport currents in open superconductor micro- and nanotubes subject to a magnetic field orthogonal to the axis. In low magnetic fields, vortices nucleate periodically at one edge of the tube, subsequently move along the tube under the action of the Lorentz force and denucleate at the opposite edge of the tube (Fig. a). In high magnetic fields, vortices pass along rows closest to the slit (Fig. b). Characteristic times of nonequilibrium vortex dynamics (Fig. c,d) in an open tube are efficiently controlled by the tube radius (Fig. e). They are significantly different from the characteristic times in a planar film under the same magnetic field (Fig. e, upper inset). Consequently, the experimentally achievable superconductor tubes of ~ 1 μm radius act as a periodic generator of correlated vortex pairs in the tunable frequency range ~ 0.1 to 10 GHz. The frequency is tuned by changing the magnetic field. Our results demonstrate perspectives of tailoring non-equilibrium properties of vortices in curved superconductor nanomembranes and of their application as tunable superconducting flux generators for fluxon-based information technologies.

[1] D. J. Thurmer et al. *Nano Lett.* **10,** 3704–3709 (2010).

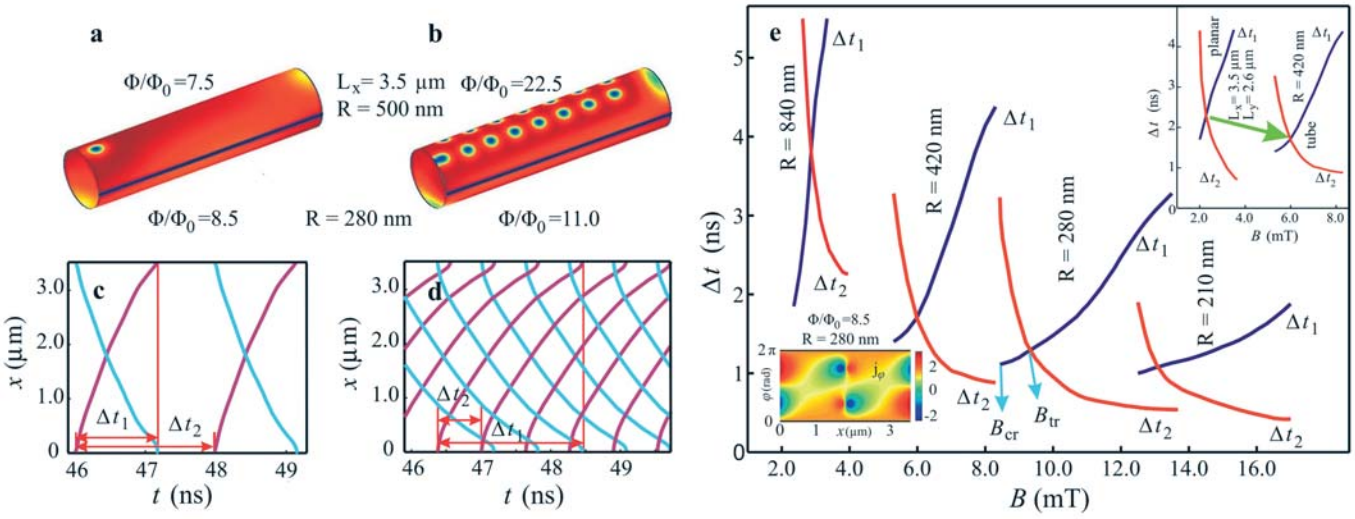

Fig.: SC order parameter **(a** and **b)** in the presence of a transport current in an open tube. The *x*-coordinates of the centers of vortex cores **(c** and **d)** as a function of time. Characteristic times of vortex dynamics Δt_1 and Δt_2 versus the magnetic field **(e)**. Upper inset: shift of the transition magnetic field by rolling up a planar film in a tube. Lower inset: pattern of the φ-component of the SC current density.

External Sources for controlling the propulsion of self-propelled microjet engines.

S. Sanchez, A. A. Solovev, E. J. Smith, C. C. Bof' Bufon,
V. M. Fomin, A. N. Ananth, M. Viehrig, O. G. Schmidt.

The control over the autonomous motion of artificial nano/micromachines and the reduction of the toxicity of the fuel are essential for real biomedical and nanotechnological applications.

We demonstrated and reported, for the first time, that both the dramatic acceleration of rolled-up microjet engines and the reduction of peroxide toxicity can be achieved by heating the fuel solution to physiological temperature (i.e. 37 °C) [1]. This temperature enables the superfast motion of the catalytic self-propelled microjets (10 mm s^{-1}, equivalent to 200 body lengths per second) using only 5% H_2O_2 as fuel. In addition, we reported on the lowest concentration of peroxide used for powering any catalytic nano- or micromotor (i.e. in 0.25% H_2O_2). Under those conditions, fibroblast cells are viable for more than 1 hour which is highly important for the not-too-distant use of artificial nanomachines in biomedical applications. The dynamics of motion of the microjets is altered while increasing the speed, i.e. the motion deviates from the linear to curvilinear trajectories which was then theoretically modelled [1].

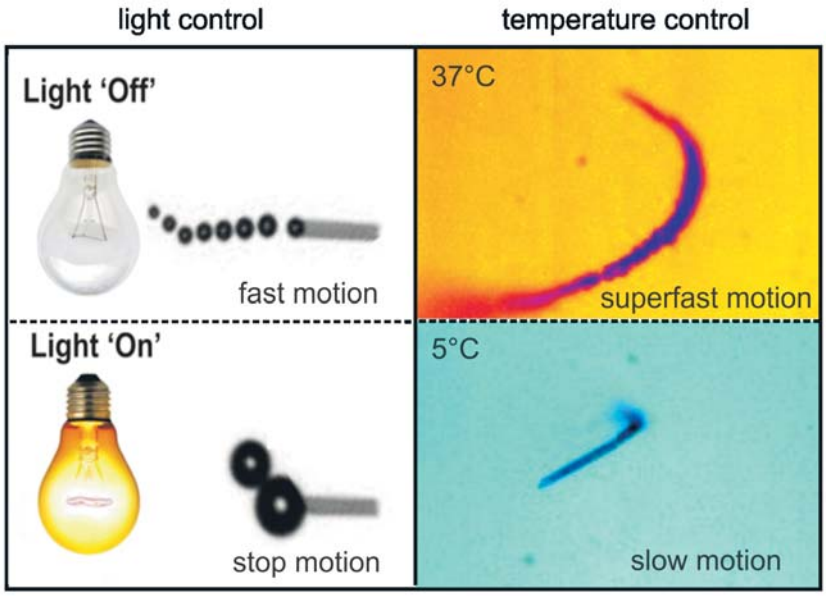

Fig.: Different ways of controlling the propulsion power of catalytic microjet engines. **Left panel:** Light control: When light illuminates the fuel solution, the fuel and surfactant concentration is reduced, slowing down the microjets. **Right panels:** Warming up the fuel solution induces the superfast motion of the microjets whereas cooling down slows their motility.

A source of white light was also used for the tuning of the propulsion power of catalytic microjets [2]. We show that light suppresses the generation of microbubbles, stopping the engines if they are fixed-to or self-propelled above a platinum-patterned surface. The microjets are reactivated by dimming the light source that illuminates the fuel solution. The illumination of the solution with visible light in the presence of Pt diminishes the concentration of hydrogen peroxide fuel and degrades the surfactant which consequently reduces the motility of the microjets. To confirm this phenomenon, electrochemical measurements and analysis of the surface tension were carried out, supporting our findings. We also studied the influence of different wavelengths over the visible spectrum (500 – 750 nm) on the formation of microbubbles showing that the sensitivity of microbubble generation is highest at shorter wavelengths. Nonetheless, it is possible to fully stop the microjets at longer wavelengths by increasing the intensity of light.

[1] S. Sanchez *et al*. J. Am. Chem. Soc. **133** (2011) 14860.
[2] A. A. Solovev *et al. Angew. Chem. Int. Edit.* **50** (2011) 10875.

Funding by: VW-Stiftung

The Institute by numbers

Personnel

In 2011, the Leibniz Institute for Solid State and Material Research Dresden employed 528 staff members, including 108 doctorate students, 40 post docs, and 20 apprentices. The quote of female staff was 35 %. Furthermore, in 2011, the IFW hosted 48 fellowship holders, that came with their own money to work at the institute. 28 diploma students worked at the IFW and 38 trainees did a practical course at the institute in 2011. Overall the total number of guest scientists was 160.

77 % of the staff belongs to the five scientific IFW institutes, 9 % to the Research Technology Division, 7 % to the Administration, 3 % to the Executive Board and Support Staff. The percentage of apprentices amounted to 4 %.

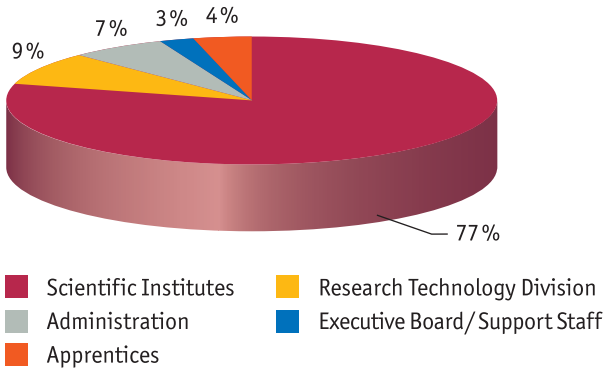

Financing

Total budget	36,544 k€
Thereof	
Federal States of Germany	13,287 k€
Free State of Saxony	13,287 k€
Third party funding spent	9,714 k€
Return on infrastructure, interest, royalties	256 k€
Third party funding	
by the DFG	3,969 k€
by the EC	1,662 k€
by the Federal States of Germany	1,902 k€
by Free State of Saxony	443 k€
by industry	1,246 k€
by foundations / others	491 k€
Total	9,713 k€

Expenditures

Remuneration costs	21,246 k€
Equipment, infrastructure and consumables	9,295 k€
Investment	6,003 k€
Total	36,544 k€

Patents

By 31 December 2011, the institute could boast of a total of 141 patents registered in Germany and 216 registered abroad. In 2011, a total of 22 inventions of the IFW were filed as patent applications in Germany.

Publications 2011

Monographs and Editorships

1) V.M. Fomin (ed.) *A Special Issue on Modern Advancements in Experimental and Theoretical Physics of Quantum Rings*, Journal of Nanoelectronics and Optoelectronics, 2011, Vol. 6, Issue 1-3.
2) M. Ruemmeli; W. Lu; J. Warner (eds.) *Fundamentals of Low-Dimensional Carbon Nanomaterials, MRS Proceedings, John J. Boeckl (ed.) ; 1284: Mark Ruemmeli, Weijie Lu and Jamie Warner (eds.), MRS 2011*, 214 S.

Journal papers

1) H.M. Abuzeid, A.M. Hashem, N. Narayanan, H. Ehrenberg, C.M. Julien, *Nanosized silver-coated and doped manganese dioxide for rechargeable lithium batteries*, Solid State Ionics 182 (2011) Nr. 3, S. 108-115.
2) N. Akopian, L. Wang, A. Rastelli, O.G. Schmidt, V. Zwiller, *Hybrid semiconductor-atomic interface: slowing down single photons from a quantum dot*, Nature Photonics 5 (2011) Nr. 4, S. 230-233.
3) A. Alfonsov, F. Muranyi, V. Kataev, G. Lang, N. Leps, L. Wang, R. Klingeler, A. Kondrat, C. Hess, S. Wurmehl, A. Koehler, G. Behr, S. Hampel, M. Deutschmann, S. Katrych, N.D. Zhigadlo, Z. Bukowski, J. Karpinski, B. Buechner, *High-field electron spin resonance spectroscopy study of GdFeAsO1-xFx superconductors*, Physical Review B 83 (2011) Nr. 9, S. 94526/1-10.
4) G.A. Almyras, D.G. Papageorgiou, C.E. Lekka, N. Mattern, J. Eckert, G.A. Evangelakis, *Atomic cluster arrangements in Reverse Monte Carlo and molecular dynamics structural models of binary CueZr metallic glasses*, Intermetallics 19 (2011) Nr. 5, S. 657-661.
5) L.J.P. Ament, G. Khaliullin, J. van den Brink, *Theory of resonant inelastic x-ray scattering in iridium oxide compounds: Probing spin-orbit-entangled ground states and excitations*, Physical Review B 84 (2011) Nr. 2, S. 20403/1-4.
6) L.J.P. Ament, M. van Veenendaal, T.P. Devereaux, J.P. Hill, J. van den Brink, *Resonant inelastic x-ray scattering studies of elementary excitations*, Reviews of Modern Physics 83 (2011), S. 705-767.
7) L.J.P. Ament, M. van Veenendaal, J. van den Brink, *Determining the electron-phonon coupling strength from resonant inelastic X-ray scattering at transition metal L-edges*, epl 95 (2011) Nr. 2, S. 27008/1-5.
8) A.V. Andreev, M.D. Kuzmin, S. Yoshii, E.A. Tereshina, K. Kindo, M. Hagiwara, F.R. de Boer, *High-field magnetization of a Dy2Fe14Si3 single crystal*, Journal of Alloys and Compounds 509 (2011) Nr. 16, S. 5042-5046.
9) A.V. Andreev, Y. Skourski, M.D. Kuzmin, S. Yasin, S. Zherlitsyn, R. Daou, J. Wosnitza, A. Iwasa, A. Kondo, A. Matsuo, K. Kindo, *Magnetic and magnetoelastic anomalies of an Er2Co17 single crystal in high magnetic fields*, Physical Review B 83 (2011) Nr. 18, S. 184422/1-9.
10) A.A. Antonysamy, S. Pauly, B.K. Dhindaw, J. Eckert, *Influence of superheat on microstructure and mechanical properties of ductile Cu47.5Zr47.5Al5 bulk metallic glass-matrix composite*, Journal of Materials Engineering and Performance 20 (2011) Nr. 7, S. 1196-1205.
11) Y.C. Arango, E. Vavilova, M. Abdel-Hafiez, O. Janson, A.A. Tsirlin, H. Rosner, S.-L. Drechsler, M. Weil, G. Nenert, R. Klingeler, O. Volkova, A. Vasiliev, V. Kataev, B. Buechner, *Magnetic properties of the low-dimensional spin-1/2 magnet alpha-Cu2As2O7*, Physical Review B 84 (2011) Nr. 13, S. 134430/1-9.
12) V.Y. Aristov, O.V. Molodtsova, M. Knupfer, *Potassium doped Co phthalocyanine films: Charge transfer to the metal center and the ligand ring*, Organic Electronics 12 (2011) Nr. 2, S. 372-375.
13) E. Arushanov, G. Fuchs, S. Levcenko, S.-L. Drechsler, B. Holzapfel, L. Schultz, *Scaling of the temperature-dependent resistivity in 122 iron-pnictide superconductors*, Superconductor Science and Technology 24 (2011) Nr. 10, S. 105004/1-6.
14) E. Arushanov, S. Levcenko, G. Fuchs, S.-L. Drechsler, *Resistivity scaling 1111 iron-pnictide superconductors*, Physica C 471 (2011) Nr. 17-18, S. 509-514.
15) E. Arushanov, S. Levcenko, G. Fuchs, B. Holzapfel, S.-L. Drechsler, L. Schultz, *Scaling of the temperature-dependent resistivity in SrFe2xNixAs2*, Physica C 471 (2011) Nr. 7-8, S. 237-241.
16) E. Arushanov, S. Levcenko, G. Fuchs, B. Holzapfel, S.-L. Drechsler, L. Schultz, *Scaling of the temperature dependent resistivity and hall effect in Ba(Fe1-xCox)As2*, Journal of Superconductivity and Novel Magnetism 24 (2011) Nr. 8, S. 2285-2292.
17) S. Aswartham, G. Behr, L. Harnagea, D. Bombor, A. Bachmann, I.V. Morozov, V.B. Zabolotnyy, A.A. Kordyuk, T.K. Kim, D.V. Evtushinsky, S.V. Borisenko, A.U.B. Wolter, C. Hess, S. Wurmehl, B. Buechner, *Suppressed superconductivity in charge-doped Li(Fe1-xCox)As single crystals*, Physical Review B 84 (2011) Nr. 5, S. 54534/1-5.
18) S. Aswartham, C. Nacke, G. Friemel, N. Leps, S. Wurmehl, N. Wizent, C. Hess, R. Klingeler, G. Behr, S. Singh, B. Buechner, *Single crystal growth and physical properties of superconducting ferro-pnictides Ba(Fe,Co)2As2 grown using self-flux and Bridgman techniques*, Journal of Crystal Growth 314 (2011) Nr. 1, S. 341-348.
19) S.M. Avdoshenko, I.N. Ioffe, G. Cuniberti, L. Dunsch, A.A. Popov, *Organometallic complexes of graphene: Toward atomic spintronics using a graphene web*, ACS nano 5 (2011) Nr. 12, S. 9939-9949.
20) A. Bachmatiuk, F. Boerrnert, V. Hoffmann, D. Lindackers, J.-H. Lin, B. Buechner, M.H. Ruemmeli, *Hydrogen-induced self-assembly of helical carbon nanostructures from ethanol over Si02 catalysts*, Journal of Applied Physics 109 (2011) Nr. 9, S. 94317/1-4.
21) S.-H. Baek, H.-J. Grafe, L. Harnagea, S. Singh, S. Wurmehl, B. Bueuchner, *Pseudogap-like phase in Ca(Fe(1-x)Co(x))(2)As(2) revealed by (75)As NQR*, Physical Review B 84 (2011) Nr. 9, S. 94510/1-5.
22) H. Bahmanpour, A. Kauffmann, M.S. Khoshkhoo, K.M. Youssef, S. Mula, J. Freudenberger, J. Eckert, R.O. Scattergood, C.C. Koch, *Effect of stacking fault energy on deformation behavior of cryo-rolled copper and copper alloys*, Materials Science and Engineering A 529 (2011), S. 230-236.

23) N. Balchev, V. Antonov, K. Nenkov, *Pinning and transport properties of undoped and Sn-doped MoSr2YCu2O8-delta*, Superconductor Science and Technology 24 (2011) Nr. 9, S. 95013/1-6.
24) N. Barekar, P. Gargarella, K. Song, S. Pauly, U. Kuehn, J. Eckert, *Effect of Al and Ag addition on phase formation, thermal stability, and mechanical properties of Cu–Zr-based bulk metallic glasses*, Journal of Materials Research 26 (2011) Nr. 14, S. 1702-1710.
25) P. Barone, S. Picozzi, J. van den Brink, *Buckling-induced Zener polaron instability in half-doped manganites*, Physical Review B 83 (2011) Nr. 23, S. 233103.
26) V. Basso, C.P. Sasso, M. Kuepferling, K.P. Skokov, O. Gutfleisch, *Er2Fe14B single crystal as magnetic refrigerant at the spin reorientation transition*, Journal of Applied Physics 109 (2011) Nr. 8, S. 83910/1-8.
27) M. Benyoucef, J.-B. Shim, J. Wiersig, O.G. Schmidt, *Quality-factor enhancement of supermodes in coupled microdisks*, Optics Letters 36 (2011) Nr. 8, S. 1317-1319.
28) M.D. Biegalski, D.H. Kim, S. Choudhury, L.Q. Chen, H.M. Christen, K. Doerr, *Strong strain dependence of ferroelectric coercivity in a BiFeO3 film*, Applied Physics Letters 98 (2011) Nr. 14, S. 142902/1-3.
29) B. Bieniek, D. Pohl, L. Schultz, B. Rellinghaus, *The effect of oxidation on the surface-near lattice relaxation in FeNi nanoparticles*, Journal of Nanoparticel Research 13 (2011), S. 5935-5946.
30) S.V. Biryukov, G. Martin, H. Schmidt, B. Wall, *Low-loss unidirectional transducer for high frequency surface acoustic wave devices*, Journal of Applied Physics 110 (2011) Nr. 7, S. 76103/1-3.
31) C.G.F. Blum, S. Ouardi, G.H. Fecher, B. Balke, X. Kozina, G. Stryganyuk, S. Ueda, K. Kobayashi, C. Felser, S. Wurmehl, B. Buechner, *Exploring the details of the martensite-austenite phase transition of the shape memory Heusler compound Mn2NiGa by hard x-ray photoelectron spectroscopy, magnetic and transport measurements*, Applied Physics Letters 98 (2011) Nr. 25, S. 252501/1-3.
32) C.C. Bof Bufon, J.D.A. Espinoza, D.J. Thurmer, M. Bauer, C. Deneke, U. Zschieschang, H. Klauk, O.G. Schmidt, *Hybrid organic/inorganic molecular heterojunctions based on strained nanomembranes*, Nano Letters 11 (2011) Nr. 9, S. 3727-3733.
33) N.B. Bogdanov, J. van den Brink, L. Hozoi, *Ab initio computation of d-d excitation energies in low-dimensional Ti and V oxychlorides*, Physical Review B 84 (2011) Nr. 23, S. 235146/1-6.
34) F. Boioli, V.A. Zinovyev, R. Gatti, A. Marzegalli, F. Montalenti, M. Stoffel, T. Merdzhanova, L. Wang, F. Pezzoli, A. Rastelli, O.G. Schmidt, L. Miglio, *Self-ordering of misfit dislocation segments in epitaxial SiGe islands on Si(001*, Journal of Applied Physics 110 (2011) Nr. 4, S. 44310/1-8.
35) C. Bonatto Minella, S. Garroni, C. Pistidda, R. Gosalawit-Utke, G. Barkhordarian, C. Rongeat, I. Lindemann, O. Gutfleisch, T.R. Jensen, Y. Cerenius, J. Christensen, M.D. Baro, R. Bormann, T. Klassen, M. Dornheim, *Effect of transition metal fluorides on the sorption properties and reversible formation of Ca(BH4)2*, The Journal of Physical Chemistry 115 (2011) Nr. 5, S. 2497-2504.
36) C. Bonatto Minella, C. Rongeat, R. Domenech-Ferrer, I. Lindemann, L. Dunsch, N. Sorbie, D.H. Gregory, O. Gutfleisch, *Synthesis of LiNH2 + LiH by reactive milling of Li3N*, RSC - Faraday Discussions 151 (2011), S. 253-262.
37) P.M.R. Brydon, M. Daghofer, C. Timm, *Magnetic order in orbital models of the iron pnictides*, Journal of Physics / Condensed Matter 23 (2011) Nr. 24, S. 246001/1-18.
38) P.M.R. Brydon, M. Daghofer, C. Timm, J. van den Brink, *Theory of magnetism and triplet superconductivity in LiFeAs*, Physical Review B 83 (2011) Nr. 6, S. 60501(R)/1-4.
39) M. Bystrzejewski, R. Klingeler, T. Gemming, B. Buechner, M.H. Ruemmeli, *Synthesis of carbon-encapsulated iron nanoparticles by pyrolysis of iron citrate and poly(vinyl alcohol): a critical evaluation of yield and selectivity*, Nanotechnology 22 (2011), S. 315606/1-10.
40) C. Cao, M. Deppe, G. Behr, W. Loeser, N. Wizent, O. Kataeva, B. Buechner, *Single crystal growth of the CeCu2Si2 intermetallic compound by a vertical floating zone method*, Crystal Growth and Design 11 (2011), S. 431-435.
41) C. Cao, W. Loeser, G. Behr, R. Klingeler, N. Leps, H. Vinzelberg, B. Buechner, *Self-flux growth of large EuCu2Si2 single crystals*, Journal of Crystal Growth 318 (2011) Nr. 1, S. 1043-1047.
42) C. Cao, W. Loeser, G. Behr, R. Klingeler, N. Leps, H. Vinzelberg, B. Buechner, *Single crystal growth of Eu2CuSi3 intermetallic compound by the floating-zone method*, Journal of Crystal Growth 318 (2011) Nr. 1, S. 1009-1012.
43) F.-F. Cao, J.-W. Deng, S. Xin, H.-X. Ji, O.G. Schmidt, L.-J. Wan, Y.-G. Guo, *Cu-Si nanocable arrays as high-rate anode materials for lithium-ion batteries*, Advanced Materials 23 (2011) Nr. 38, S. 4415-4420.
44) A. Castellero, T.A. Baser, J. Das, P. Matteis, J. Eckert, L. Battezzati, M. Baricco, *Role of crystalline precipitates on the mechanical properties of (Cu0.50Zr0.50)100-xAlx (x = 4, 5, 7) bulk metallic glasses*, Journal of Alloys and Compounds 509 (2011) Nr. Suppl. 1, S. S99-S104.
45) K. Cendrowski, X. Chen, B. Zielinska, R.J. Kalenczuk, M.H. Ruemmeli, B. Buechner, R. Klingeler, E. Borowiak-Palen, *Synthesis, characterization, and photocatalytic properties of core/shell mesoporous silica nanospheres supporting nanocrystalline titania*, Journal of Nanopartikel Research 13 (2011), S. 5899-5908.
46) P. Cendula, S. Kiravittaya, I. Moench, J. Schumann, O.G. Schmidt, *Directional roll-up of nanomembranes mediated by wrinkling*, Nano Letters 11 (2011), S. 236-240.
47) X. Chen, K. Cendrowski, M.H. Ruemmeli, R.J. Kalenczuk, E. Borowiak-Palen, *Novel method controlled synthesis of silica coated carbon nanotubes*, Physica Status Solidi A 208 (2011) Nr. 2, S. 462-465.
48) X. Chen, H. Chen, C. Tripisciano, A. Jedrzejewska, M.H. Ruemmeli, R. Klingeler, R.J. Kalenczuk, P.K. Chu, E. Borowiak-Palen, *Carbon-nanotube-based stimuli-responsive controlled-release system*, Chemistry - A European Journal 17 (2011) Nr. 16, S. 4454-4459.
49) C. Cierpka, K. Tschulik, R. Segura, M. Uhlemann, C.J. Kaehler, *Zeitaufgeloeste 3D3K Geschwindigkeitsfeldmessungen mit der fernmikroskopischen Astigmatismus PTV zur Analyse der elektrochemischen Kupferabscheidung*, tm - Technisches Messen 78 (2011) Nr. 5, S. 232-238.

50) V. Cloet, P. Lommens, R. Huehne, K. De Buysser, S. Hoste, I. Van Driessche, *A study of the parameters influencing the microstructure of thick La2Zr2O7 films*, Journal of Crystal Growth 325 (2011) Nr. 1, S. 68-75 .

51) D.Y. Cong, Q. Luo, S. Roth, J. Liu, O. Gutfleisch, M. Poetschke, C. Huerrich, L. Schultz, *Sequence of structural and magnetic transitions in Ni48Co2Mn39Sn11 shape memory alloy*, Journal of Magnetism and Magnetic Materials 323 (2011) Nr. 20, S. 2519-2523.

52) P.M.F.J. Costa, U.K. Gautam, Y. Bando, D. Golberg, *Direct imaging of Joule heating dynamics and temperature profiling inside a carbon nanotube interconnect*, nature communications 2 (2011) Nr. 429.

53) S.D. Costa, C. Fantini, A. Righi, A. Bachmatiuk, M.H. Ruemmeli, R. Saito, M.A. Pimenta, *Resonant Raman spectroscopy on enriched 13C carbon nanotubes*, Carbon 49 (2011) Nr. 14, S. 4719-4723.

54) J. Crocker, A.P. Dioguardi, N. Roberts-Warren, A.C. Shockley, H.-J. Grafe, Z. Xu, J. Wen, G. Gu, N.J. Curro, *NMR studies of pseudogap and electronic inhomogeneity in Bi2Sr2CaCu2O8-delta*, Physical Review B 84 (2011) Nr. 22, S. 224502/1-8.

55) P. Cudazzo, M. Gatti, F. Roth, B. Mahns, M. Knupfer, A. Rubio, *Plasmon dispersion in molecular solids: Picene and potassium-doped picene*, Physical Review B 84 (2011) Nr. 15, S. 155118/1-6.

56) J. Cwik, T. Palewski, K. Nenkov, O. Gutfleisch, J. Klamut, *The influence of Er substitution on magnetic and magnetocaloric properties of Dy1-xErxCo2 solid solutions*, Intermetallics 19 (2011) Nr. 11, S. 1656-1660.

57) J. Cwik, T. Palewski, K. Nenkov, J. Lyubina, O. Gutfleisch, *Magnetic properties and magnetocaloric effect in (Dy0.6Er0.4)1-xGdxCo2 multicomponent compounds*, Journal of Physics Conference Series 303 (2011) Nr. 1, S. 12025/1-7.

58) A. Das, K. Gieb, Y. Krupskaya, S. Demeshko, S. Dechert, R. Klingeler, V. Kataev, B. Buechner, P. Mueller, F. Meyer, *A new family of 1D exchange biased heterometal single-molecule magnets: Observation of pronounced quantum tunneling steps in the hysteresis loops of quasi-linear {Mn2Ni3} clusters*, Journal of the American Chemical Society 133 (2011), S. 3433-3443.

59) F. de Clippel, A. Harkiolakis, T. Vosch, X. Ked, L. Giebeler, S. Oswald, K. Houthoofd, J. Jammaer, G. Van Tendeloo, J.A. Martens, P.A. Jacobs, G.V. Baron, B.F. Sels, J.F.M. Denayer, *Graphitic nanocrystals inside the pores of mesoporous silica: Synthesis, characterization and an adsorption study*, Microporous and Mesoporous Materials 144 (2011), S. 120-133.

60) M. de Pauli, A. Malachias, H.Jr. Westfahl, J. Bettini, A. Ramirez, G.S. Huang, Y.F. Mei, O.G. Schmidt, *Study of roughness evolution and layer stacking faults in short-period atomic layer deposited Hf02/Al2O3 multilayers*, Journal of Applied Physics 109 (2011) Nr. 6, S. 63524/1-7.

61) Y. Demidenko, D. Makarov, O.G. Schmidt, V. Lozovski, *Surface plasmon-induced enhancement of the magneto-optical Kerr effect in magnetoplasmonic heterostructures*, Journal of the Optical Society of America/ B 28 (2011) Nr. 9, S. 2115-2122.

62) C. Deneke, E. Wild, K. Boldyreva, S. Baunack, P. Cendula, I. Moench, M. Simon, A. Angelo Malachias, K. Doerr, O.G. Schmidt, *Rolled-up tubes and cantilevers by releasing SrRu03-Pr0.7Ca0.3Mn03 nanomembranes*, Nanoscale Research Letters 6 (2011) Nr. 1, S. 621/1-8.

63) A. Diestel, A. Backen, U.K. Roessler, L. Schultz, S. Faehler, *Twin boundary energy of hierarchically twinned magnetic shape memory alloys*, Applied Physics Letters 99 (2011) Nr. 9, S. 92512/1-3.

64) F. Ding, B. Li, N. Akopian, U. Perinetti, Y.H. Chen, F.M. Peeters, A. Rastelli, V. Zwiller, O.G. Schmidt, *Single neutral excitons confined in AsBr3 in situ etched InGaAs quantum rings*, Journal of Nanoelectronics and Optoelectronics 6 (2011), S. 51-57.

65) E. Dmitrieva, L. Dunsch, *How linear is "linear" polyaniline?*, Journal of Physical Chemistry B 115 (2011), S. 6401-6411.

66) G.S. Dmytriv, V.V. Pavlyuk, H. Pauly, J. Eckert, H. Ehrenberg, *New real ternary and pseudoternary phases in the Li-Au-Insystem*, Journal of Solid State Chemistry 184 (2011) Nr. 5, S. 1328-1332.

67) R. Domenech-Ferrer, F. Ziegs, S. Klod, I. Lindemann, R. Voigtlaender, L. Dunsch, O. Gutfleisch, *In Situ Raman cell for high pressure and temperature studies of metal and complex hydrides*, Analytical Chemistry 83 (2011) Nr. 8, S. 3199-3204.

68) S. Dorzhieva, I. Chumak, A. Sarapulova, D. Mikhailova, J. Bazarova, H. Ehrenberg, *A tetragonal form of dysprosium orthomolybdate at room temperature*, Acta Crystallographica C 67 (2011), S. i50-i52.

69) O. Drachenko, A. Patane, N.V. Kozlova, Q.D. Zhuang, A. Krier, L. Eaves, M. Helm, *Cyclotron resonance mass and Fermi energy pinning in the In(AsN) alloy*, Applied Physics Letters 98 (2011) Nr. 16, S. 162109/1-5.

70) S.-L. Drechsler, S. Nishimoto, R.O. Kuzian, J. Malek, W.E.A. Lorenz, J. Richter, J. van den Brink, M. Schmitt, H. Rosner, *Comment on "Two-spinon and four-spinon continuum in a frustrated ferromagnetic spin-1/2 chain"*, Physical Review Letters 106 (2011) Nr. 21, S. 219701/1.

71) L. Dunsch, *Recent advances in in situ multi-spectroelectrochemistry*, Journal of Solid State Electrochemistry 15 (2011), S. 1631-1646.

72) V. Efimova, V. Hoffmann, J. Eckert, *Electrical properties of the µs pulsed glow discharge in a Grimm-type source: comparison of dc and rf modes*, Journal of Analytical Atomic Spectrometry 26 (2011), S. 784-791.

73) J. Eickemeyer, A. Gueth, J. Freudenberger, B. Holzapfel, L. Schultz, *First steps towards cube textured nickel profile wires for YBCO-coated conductors*, Physica C 471 (2011) Nr. 19-20, S. 549-552.

74) R. Essehli, B. El Bali, S. Benmokhtar, K. Bouziane, B. Manoun, M.A. Abdalslam, H. Ehrenberg, *Crystal structures and magnetic properties of iron (III)-based phosphates:Na4NiFe(PO4)3 and Na2Ni2Fe(PO4)3*, Journal of Alloys and Compounds 509 (2011), S. 1163-1171.

75) F. Fan, Y.M. Lu, L.L. Ying, Z.Y. Liu, C.B. Cai, R. Huehne, B. Holzapfel, *Epitaxial growth of Ce2Y2O7 buffer layers for YBa2Cu3O7-delta coated conductors using reel-to-reel DC reactive sputtering*, Physica C 471 (2011) Nr. 15-16, S. 471-475.

76) J. Fiedler, V. Heera, R. Skrotzki, T. Herrmannsdoerfer, M. Voelskow, A. Muecklich, S. Oswald, B. Schmidt, W. Skorupa, G. Gobsch, J. Wosnitza, M. Helm, *Superconducting films fabricated by high-fluence Ga implantation in Si*, Physical Review B 83 (2011) Nr. 21, S. 214504/1-10.

77) J. Fink, V. Soltwisch, J. Geck, E. Schierle, E. Weschke, B. Buechner, *Phase diagram of charge order in La1.8-xEu0.2SrxCu04 from resonant soft x-ray diffraction*, Physical Review B 83 (2011) Nr. 9, S. 92503/1-4.

78) V.M. Fomin, *A Special Issue on Modern Advancements in Experimental and Theoretical Physics of Quantum Rings*, Journal of Nanoelectronics and Optoelectronics 6 (2011) Nr. 1-3, S. 1-3.

79) V.M. Fomin, E.J. Smith, D. Makarov, S. Sanchez, O.G. Schmidt, *Dynamics of radial-magnetized microhelix coils*, Physical Review B 84 (2011) Nr. 17, S. 174303/1-7.

80) J. Fornell, M.D. Baro, S. Surinach, A. Gebert, J. Sort, *The influence of deformation-induced martensitic transformations on the mechanical properties of nanocomposite Cu-Zr-(Al) systems*, Advanced Engineering Materials 13 (2011) Nr. 1-2, S. 57-63.

81) F. Forte, M. Cuoco, C. Noce, J. van den Brink, *Doping dependence of magnetic excitations of one-dimensional cuprates as probed by resonant inelastic x-ray scattering*, Physical Review B 83 (2011) Nr. 24, S. 245133/1-7.

82) M. Friak, T. Hickel, B. Grabowski, L. Lymperakis, A. Udyansky, A. Dick, D. Ma, F. Roters, L.-F. Zhu, A. Schlieter, U. Kuehn, Z. Ebrahimi, R.A. Lebensohn, D. Holec, J. Eckert, H. Emmerich, D. Raabe, J. Neugebauer, *Methodological challenges in combining quantum-mechanical and continuum approaches for materials science applications*, The European Physical Journal Plus 126 (2011), S. 101/1-23.

83) R. Gaertner, R. Huehne, J. Engelmann, J. Haenisch, R. Kaltofen, S. Oswald, L. Schultz, B. Holzapfel, *High-Jc YBCO coated conductors based on IBAD-TiN using stainless steel substrates*, IEEE Transaction on Applied Superconductivity 21 (2011), S. 2920-2023.

84) W. Gang, N. Mattern, J. Bednarci, L. Xia, Q. Zhai, Y. Dong, J. Eckert, *Deformation induced structural evolution in bulk metallic glasses*, Chinese Science Bulletin- Special issue, Bulk Metallic Glasses 56 (2011), S. 3952-3959.

85) P. Gargarella, M.F. de Oliveira, C.S. Kiminami, S. Pauly, U. Kuehn, C. Bolfarini, W.J. Botta, J. Eckert, *Prediction of good glass formers in the Al-Ni-La and Al-Ni-Gd systems using topological instability and electronegativity*, Journal of Applied Physics 109 (2011) Nr. 9, S. 93509/1-7.

86) P. Gargarella, M.F. de Oliveira, C.S. Kiminami, S. Pauly, U. Kuehn, C. Bolfarini, W.J. Botta, J. Eckert, *Predicting glass-forming compositions in the Al–La and Al–La–Ni systems*, Journal of Alloys and Compounds 509S (2011) Nr. Suppl. 1, S. S170-S174.

87) D. Geissler, J. Freudenberger, A. Kauffmann, M. Krautz, H. Klauss, A. Voss, J. Eickemeyer, L. Schultz, *Appearance of dislocation-mediated and twinning-induced plasticity in an engineering-grade FeMnNiCr alloy*, Acta Materialia 59 (2011) Nr. 20, S. 7711-7723.

88) D. Geissler, K.-H. Mueller, J. Freudenberger, K. Nenkov, M. Krautz, J. Eickemeyer, L. Schultz, *Deformation induced thermoremanent magnetisation in an FeMnNiCr antiferromagnetic alloy*, Journal of Alloys and Compounds 509 (2011) Nr. 9, S. 3726-3734.

89) G. Giovannetti, S. Kumar, A. Stroppa, M. Balestieri, J. van den Brink, S. Picozzi, J. Lorenzana, *Reply to „Comment on High-Tc ferroelectricity emerging from magnetic degeneracy in cupric oxide"*, Physical Review Letters 107 (2011) Nr. 23, S. 239702/1.

90) G. Giovannetti, S. Kumar, A. Stroppa, J. van den Brink, S. Picozzi, J. Lorenzana, *High-Tc ferroelectricity emerging from magnetic degeneracy in cupric oxide*, Physical Review Letters 106 (2011) Nr. 2, S. 26401/1-4.

91) G. Giovannetti, C. Ortix, M. Marsman, M. Capone, J. van den Brink, J. Lorenzana, *Proximity of iron pnictide superconductors to a quantum tricritical point*, Nature Communications 2 (2011), S. 398/1-6.

92) J. Gluch, T. Roessler, S.B. Menzel, J. Eckert, *Microstructure and stress in High-k Hf-Y-O thin films*, Microelectronic Engineering 88 (2011), S. 561-563.

93) V. Grinenko, K. Kikoin, S.-L. Drechsler, G. Fuchs, K. Nenkov, S. Wurmehl, F. Hammerath, G. Lang, H.-J. Grafe, B. Holzapfel, J. Brink, B. Buechner, L. Schultz, *As vacancies, local moments, and Pauli limiting in LaFeAs1-delta00.9F0.1 superconductors*, Physical Review B 84 (2011) Nr. 13, S. 134516/1-10.

94) M. Grobosch, M. Knupfer, *Electronic properties of organic semiconductor/electrode interfaces: The influence of contact contaminations on the interface energetic*, The Open Applied Physics Journal 4 (2011), S. 8-18.

95) M. Grobosch, B. Mahns, C. Loose, R. Friedrich, C. Schmidt, J. Kortus, M. Knupfer, *Identification of the electronic states of manganese phthalocyanine close to the Fermi level*, Chemical Physics Letters 505 (2011) Nr. 4-6, S. 122-125.

96) P. Gruendler, L. Dunsch, *A facile route to temperature determination in hot-wire electrochemistry*, Journal of Solid State Electrochemistry online first (2011).

97) W. Gruner, J. Thomas, L. Giebeler, H. Ehrenberg, D. Wadewitz, *Interactions of copper and iron in conversion reactions of nanosized oxides with large variations in iron-copper ratio*, Journal of The Electrochemical Society 158 (2011) Nr. 12, S. A1383-A1392.

98) R.V. Gudavarthy, S. Gorantla, G. Mu, E.A. Kulp, T. Gemming, J. Eckert, J.A. Switzer, *Epitaxial electrodeposition of Fe304 on single-crystal Ni(111)*, Chemistry of Materials 23 (2011), S. 2017-2019.

99) K.H. Gudmundsson, F. Jonsdottir, F. Thorsteinsson, O. Gutfleisch, *An experimental investigation of unimodal and bimodal magnetorheological fluids with an application in prosthetic devices*, Journal of Intelligent Material Systems and Structures 22 (2011) Nr. 6, S. 539-549.

100) K. Gueth, T.G. Woodcock, L. Schultz, O. Gutfleisch, *Comparison of local and global texture in HDDR processed Nd–Fe–B magnets*, Acta Materialia 59 (2011) Nr. 5, S. 2029-2034.

101) K. Gueth, T.G. Woodcock, J. Thielsch, L. Schultz, O. Gutfleisch, *Local orientation analysis by electron backscatter diffraction in highly textured sintered, die-upset, and hydrogenation disproportionation desorption and recombination Nd–Fe–B magnets*, Journal of Applied Physics 109 (2011) Nr. 7, S. 7A764.

102) O. Gutfleisch, M.A. Willard, E. Brueck, C.H. Chen, S.G. Sankar, J.P. Liu, *Magnetic materials and devices for the 21st century: Stronger, lighter, and more energy efficient*, Advanced Materials 23 (2011) Nr. 7, S. 821-842.

103) D. Haberer, C.E. Giusca, Y. Wang, H. Sachdev, A.V. Fedorov, M. Farjam, S.K. Jafari, D.V. Vyalikh, D. Usachov, X. Liu, U. Treske, M. Grobosch, O. Vilkov, V.K. Adamchuk, S. Irle, S.R.P. Silva, M. Knupfer, B. Buechner, A. Grueneis, *Evidence for a new two-dimensional C4H-type polymer based on hydrogenated graphene*, Advanced Materials 23 (2011) Nr. 39, S. 4497-4503.

104) D. Haberer, L. Petaccia, M. Farjam, S. Taioli, S.A. Jafari, A. Nefedov, W. Zhang, L. Calliari, G. Scarduelli, B. Dora, D.V. Vyalikh, T. Pichler, C. Woell, D. Alfe, S. Simonucci, M.S. Dresselhaus, M. Knupfer, B. Buechner, A. Grueneis, *Direct observation of a dispersionless impurity band in hydrogenated graphene*, Physical Review B 83 (2011) Nr. 16, S. 165433/1-6.

105) J. Haenisch, K. Iida, S. Haindl, F. Kurth, A. Kauffmann, M. Kidszun, T. Thersleff, J. Freudenberger, L. Schultz, B. Holzapfel, *Jc scaling and anisotropies in Co-doped Ba-122 thin films*, IEEE Transactions on Applied Superconductivity 21 (2011) Nr. 3, S. 2887-2890.

106) M. Haertel, J. Richter, D. Ihle, J. Schnack, S.-L. Drechsler, *Thermodynamics of the one-dimensional frustrated Heisenberg ferromagnet with arbitrary spin*, Physical Review B 84 (2011) Nr. 10, S. 104411/1-7.

107) S. Haindl, T. Thersleff, T. Shapoval, Y.W. Lai, J. McCord, L. Schultz, B. Holzapfel, *Advanced Nb/FePt L10 hybrid thin films*, Superconductor Science and Technology 24 (2011) Nr. 2, S. 24002/1-4.

108) B.A. Hamad, M. Richter, *Exchange coupling and magnetocrystalline anisotropy of Fe/W superlattices*, Physical Review B 83 (2011) Nr. 24, S. 245135/1-7.

109) F. Hammerath, S. Nishimoto, H.-J. Grafe, A.U.B. Wolter, V. Kataev, P. Ribeiro, C. Hess, S.-L. Drechsler, B. Buechner, *Spin gap in the zigzag spin-1/2 chain cuprate Sr0.9Ca0.1CuO2*, Physical Review Letters 107 (2011) Nr. 1, S. 17203/1-4.

110) J.H. Han, N. Mattern, D.H. Kim, J. Eckert, *Phase separation and microstructure evolution of rapidly quenched Gd–Hf–Co–Al alloys*, Journal of Alloys and Compounds 509 (2011) Nr. Suppl. 1, S. S42-S45.

111) J. Hanzig, B. Abendroth, F. Hanzig, H. Stoecker, R. Strohmeyer, D.C. Meyer, S. Lindner, M. Grobosch, M. Knupfer, C. Himcinschi, U. Muehle, F. Munnik, *Single crystal strontium titanate surface and bulk modifications due to vacuum annealing*, Journal of Applied Physics 110 (2011) Nr. 6, S. 64107/1-9.

112) S.M. Harazim, P. Feng, S. Sanchez, C. Deneke, Y. Mei, O.G. Schmidt, *Integrated sensitive on-chip ion field effect transistors based on wrinkled InGaAs nanomembranes*, Nanoscale Research Letters 6 (2011) Nr. 1, S. 215/1-8.

113) L. Harnagea, S. Singh, G. Friemel, N. Leps, D. Bombor, M. Abdel-Hafiez, A.U.B. Wolter, C. Hess, R. Klingeler, G. Behr, S. Wurmehl, B. Buechner, *Phase diagram of the iron arsenide superconductors Ca(Fe1-xCox)2As2(0 x 0.2)*, Physical Review B 83 (2011) Nr. 9, S. 94523/1-4.

114) A.M. Hashem, A.M. Abuzeid, H.M. Abdel-Latif, H.M. Abbas, H. Ehrenberg, R.S. Farag, A. Mauger, C.M. Julien, *Improvement of the electrochemical performance of nanosized a-MnO2 used as cathode material for Li-batteries by Sn-doping*, Journal of Alloys and Compounds 509 (2011).

115) K. Haubner, K. Luspai, P. Rapta, L. Dunsch, *The charging of the carbon nanotube/oligothiophene interphase as studied by in situ electron spin resonance/UV-Vis-NIR spectroelectrochemistry*, Physical Chemistry Chemical Physics 13 (2011), S. 13403-13409.

116) J. He, H. Jiang, J. Zhao, N. Mattern, J. Eckert, *AlNiYCo amorphous matrix composites induced by bismuth and lead additions*, Metallurgical and Materials Transactions A 42 (2011) Nr. 13, S. 4100-4105.

117) R. Hermann, M. Uhlemann, H. Wendrock, G. Gerbeth, B. Buechner, *Magnetic field controlled single crystal growth and surface modification of titanium alloys exposed for biocompatibility*, Journal of Crystal Growth 318 (2011) Nr. 1, S. 1048-1052.

118) O. Heyer, T. Lorenz, V.B. Zabolotnyy, D.V. Evtushinsky, S.V. Borisenko, I. Morozov, L. Harnagea, S. Wurmehl, C. Hess, B. Buechner, *Resistivity and Hall effect of LiFeAs: Evidence for electron-electron scattering*, Physical Review B 84 (2011) Nr. 6, S. 64512/1-6.

119) M. Hinterstein, M. Hoelzel, H. Kungl, M.J. Hoffmann, H. Ehrenberg, H. Fuess, *In situ neutron diffraction study of electric field induced structural transitions in lanthanum doped lead zirconate titanate*, Zeitschrift fuer Kristallographie 226 (2011), S. 155-162.

120) N. Hlubek, P. Ribeiro, R. Saint-Martin, S. Nishimoto, A. Revcolevschi, S.-L. Drechsler, G. Behr, J. Trinckauf, J.E. Hamann-Borrero, J. Geck, B. Buechner, C. Hess, *Bond disorder and breakdown of ballistic heat transport in the spin-12 antiferromagnetic Heisenberg chain as seen in Ca-doped SrCuO2*, Physical Review B 84 (2011) Nr. 21, S. 214419/1-5.

121) V. Hoffmann, M. Steinert, J. Acker, *Analysis of gaseous reaction products of wet chemical silicon etching by conventional direct current glow discharge optical emission spectrometry (DC-GD-OES)*, Journal of Analytical Atomic Spectrometry 26 (2011), S. 1990-1996.

122) L. Hozoi, L. Siurakshina, P. Fulde, J. van den Brink, *Ab Initio determination of Cu 3d orbital energies in layered copper oxides*, Nature Science Reports 1 (2011), S. 65.

123) H.-Y. Huang, N.A. Bogdanov, L. Siurakshina, P. Fulde, J. van den Brink, L. Hozoi, *Ab initio calculation of d-d excitations in quasi-one-dimensional Cu d9 correlated materials*, Physical Review B 84 (2011) Nr. 23, S. 235125/1-8.

124) T. Huang, J. Zhao, M. Feng, A.A. Popov, S. Yang, L. Dunsch, H. Petek, *A molecular switch based on current-driven rotation of an encapsulated cluster within a fullerene cage*, Nano letters 11 (2011), S. 5327-5332.

125) A. Huczko, A. Dabrowska, M. Soszynski, N. Maryan, M. Bystrzejewski, P. Baranowski, H. Lange, T. Gemming, A. Bachmatiuk, M.H. Ruemmeli, *Ultrafast self-catalytic growth of silicon carbide nanowires*, Journal of Materials Research 26 (2011) Nr. 24, S. 3065-3071.

126) R. Huehne, R. Gaertner, S. Oswald, L. Schultz, B. Holzapfel, *Coated conductor architectures based on IBAD-TiN for high-Jc YBCO films*, Physica C 471 (2011), S. 966-969.

127) C. Huerrich, S. Roth, H. Wendrock, M. Poetschke, D.Y. Cong, B. Rellinghaus, L. Schultz, *Influence of grain size and training temperature on strain of polycrystalline Ni50Mn29Ga21 samples*, Journal of Physics: Conference Series 303 (2011) Nr. 1, S. 12080/1-7.

128) J. Hufenbach, U. Kuehn, L. Krueger, H. Wendrock, J. Eckert, *Transformation-induced plasticity in rapidly solidified Fe88.9Cr4.3V2.2C4.6*, Steel Research International 82 (2011) Nr. 1, S. 51-55.

129) I. Ibrahim, A. Bachmatiuk, F. Boerrnert, J. Blueher, U. Wolff, J.H. Warner, B. Buechner, G. Cuniberti, M.H. Ruemmeli, *Optimizing substrate surface and catalyst conditions for high yield chemical vapor deposition grown epitaxially aligned single-walled carbon nanotubes*, Carbon 49 (2011) Nr. 15, S. 5029-5037.

130) I. Ibrahim, A. Bachmatiuk, M.H. Ruemmeli, U. Wolff, A. Popov, O. Boltalina, B. Buechner, G. Cuniberti, *Growth of catalyst-assisted and catalyst-free horizontally aligned single wall carbon nanotubes*, Physica Status Solidi B 248 (2011) Nr. 11, S. 2467-2470.

131) K.R. Idzik, R. Beckert, E. Tauscher, P. Ledwon, P. Golba, M. Lapkowski, P. Rapta, L. Dunsch, J. Frydel, *Synthesis by stille cross-coupling procedure and electrochemical characterization of branched polymers based on substituted 1,3,5-triarylbenzenes*, Materials Science Forum 663-665 (2011), S. 876-879.

132) K. Iida, J. Haenisch, M. Schulze, S. Aswartham, S. Wurmehl, B. Buechner, L. Schultz, B. Holzapfel, *Generic Fe buffer layers for Fe-based superconductors: Epitaxial FeSe12xTex thin films*, Applied Physics Letters 99 (2011) Nr. 20, S. 202503/1-3.

133) K. Iida, J. Haenisch, S. Trommler, S. Haindl, F. Kurth, R. Huehne, L. Schultz, B. Holzapfel, *Thickness dependence of structural and transport properties of Co-doped BaFe2As2 on Fe buffered MgO substrates*, Superconductor Science and Technology 24 (2011) Nr. 12, S. 125009/1-5.

134) K. Iida, J. Haenisch, S. Trommler, V. Matias, S. Haindl, F. Kurth, I. Lucas del Pozo, R. Huehne, M. Kidszun, J. Engelmann, L. Schultz, B. Holzapfel, *Epitaxial growth of superconducting Ba(Fe1-xCox)2As2 thin films on technical ion beam assisted deposition MgO substrates*, Applied Physics Express 4 (2011), S. 13103/1-3.

135) F. Intonti, V. Matarazzo, A. Nasir, O. Makarovsky, R. Campion, A. Patane, S. Kumar, A. Rastelli, O.G. Schmidt, M. Gurioli, *Nano-sized light emitting diodes by near field laser exposure*, Applied Physics Letters 98 (2011) Nr. 18, S. 183102/1-3.

136) D. Iselt, U. Gaitzsch, S. Oswald, S. Faehler, L. Schultz, H. Schlorb, *Electrodeposition andcharacterizationofFe80Ga20 alloy films*, Electrochimica Acta 56 (2011) Nr. 14, S. 5178-5183.

137) J. J. Sirker, V.Y. Krivnov, D.V. Dmitriev, A. Herzog, O. Janson, S. Nishimoto, S.-L. Drechsler, J. Richter, *J1-J2 Heisenberg model at and close to its z=4 quantum critical point*, Physical Review B 84 (2011) Nr. 14, S. 144403/1-8.

138) P. Jakes, E. Erdem, A. Ozarowski, J. van Tol, R. Buckan, D. Mikhailova, H. Ehrenberg, R.-A. Eichel, *Local coordination of Fe3+ in Li[Co0.98Fe0.02]02 as cathode material for lithium ion batteries—multi-frequency EPR and Monte-Carlo Newman-superposition model analysis*, Physical Chemistry Chemical Physics 13 (2011) Nr. 21, S. 9344-9352.

139) F.A. Javid, N. Mattern, S. Pauly, J. Eckert, *Martensitic transformation and thermal cycling effect in Cu–Co–Zr alloys*, Journal of Alloys and Compounds 509 (2011) Nr. Suppl. 1, S. S334-S337.

140) H. Jeschke, I. Opahle, H. Kandpal, R. Valenti, H. Das, T. Saha-Dasgupta, O. Janson, H. Rosner, A. Bruehl, B. Wolf, M. Lang, J. Richter, S. Hu, X. Wang, R. Peters, T. Pruschke, A. Honecker, *Multistep approach to microscopic models for frustrated quantum magnets: The case of the natural mineral azurite*, Physical Review Letters 106 (2011) Nr. 21, S. 217201/1-5.

141) K.D. Joens, R. Hafenbrak, R. Singh, F. Ding, J.D. Plumhof, A. Rastelli, O.G. Schmidt, G. Bester, P. Michler, *Dependence of the redshifted and blueshifted photoluminescence spectra of single inxGa1xAs=GaAs quantum dots on the applied uniaxial stress*, Physical Review Letters 107 (2011) Nr. 21, S. 217402/1-5.

142) S. Johnston, A.P. Sorini, B. Moritz, T.P. Devereaux, D.J. Scalapino, *Coincidence between energy gaps and Kohn anomalies in conventional superconductors*, Physical Review B 84 (2011) Nr. 17, S. 174523/1-6.

143) P. Jovari, I. Kaban, *Local atomic order in tellurium-rich infrared optical glasses*, Inside nmi 3 2 (2011), S. 16-17.

144) I. Kaban, P. Jovari, T. Wagner, M. Bartos, M. Frumar, B. Beuneu, W. Hoyer, N. Mattern, J. Eckert, *Structural study of AsS2–Ag glasses over a wide concentration range*, Journal of Non-Crystalline Solids 357 (2011) Nr. 19-20, S. 3430-3434.

145) I. Kaban, M. Koehler, L. Ratke, W. Hoyer, N. Mattern, J. Eckert, A.L. Greer, *Interfacial tension, wetting and nucleation in Al–Bi and Al–Pb monotectic alloys*, Acta Materialia 59 (2011), S. 6880-6889.

146) H.C. Kandpal, J. van den Brink, *Calculation of magnetic exchange couplings in the S=3/2 honeycomb system (Bi3Mn4O12)NO3 from first principles*, Physical Review B 83 (2011) Nr. 14, S. 140412/1-4.

147) T. Karan, S. Ram, M. Stoica, J. Eckert, *Effect of copper additives on irreversible melting in [{(Fe0.5Co0.5)0.75B0.2Si0.05}96Nb4]100-xCux, x 3 alloys*, International Journal of Nanoscience 10 (2011) Nr. 4, S. 1013-1017.

148) A. Kario, R. Nast, W. Haessler, C. Rodig, C. Mickel, W. Goldacker, B. Holzapfel, L. Schultz, *Critical current density enhancement in strongly reactive ex situ MgB2 bulk and tapes prepared by high energy milling*, Superconductor Science and Technology 24 (2011), S. 75011/1-8.

149) D. Kasinathan, M. Schmitt, K. Koepernik, A. Ormeci, K. Meier, U. Schwarz, M. Hanfland, C. Geibel, Y. Grin, A. Leithe-Jasper, H. Rosner, *Symmetry-preserving lattice collapse in tetragonal SrFe2-xRuxAs2 (x=0,0.2): A combined experimental and theoretical study*, Physical Review B 84 (2011) Nr. 5, S. 54509/1-9.

150) G. Katsaros, V.N. Golovach, P. Spathis, N. Ares, M. Stoffel, F. Fournel, O.G. Schmidt, L.I. Glazman, S. De Franceschi, *Observation of spin-selective tunneling in SiGe nanocrystals*, Physical Review Letters 107 (2011) Nr. 24, S. 246601/1-5.

151) A. Kauffmann, J. Freudenberger, D. Geissler, S. Yin, W. Schillinger, V. Subramanya Sarma, H. Bahmanpour, R. Scattergood, M.S. Khoshkhoo, H. Wendrock, C.C. Koch, J. Eckert, L. Schultz, *Severe deformation twinning in pure copper by cryogenic wire drawing*, Acta Materialia 59 (2011) Nr. 20, S. 7816-7823.

152) A. Kauffmann, S. Yin, J. Freudenberger, L. Schultz, M.S. Khoshkhoo, H. Wendrock, J. Eckert, W. Schillinger, V. Subramanya Sarma, H. Bahmanpour, R. Scattergood, C.C. Koch, *Zwillingsbildung durch Kryoumformung*, Metall-Forschung 65 (2011) Nr. 11, S. 501-503.

153) S. Kauffmann-Weiss, M.E. Gruner, A. Backen, L. Schultz, P. Entel, S. Faehler, *Magnetic nanostructures by adaptive twinning in strained epitaxial films*, Physical Review Letters 107 (2011) Nr. 20, S. 206105/1-5.

154) S. Kaufmann, R. Niemann, T. Thersleff, U.K. Roessler, O. Heczko, J. Buschbeck, B. Holzapfel, L. Schultz, S. Faehler, *Modulated martensite: why it forms and why it deforms easily*, New Journal of Physics 13 (2011) Nr. 5, S. 53029/1-24.

155) L. Kavan, L. Dunsch, *Spectroelectrochemistry of carbon nanotubes*, ChemPhysChem 12 (2011), S. 47-55.

156) A. Kellenberger, E. Dmitrieva, L. Dunsch, *The stabilization of charged states at phenazine-like units in polyaniline under p-doping: an in situ ATR-FTIR spectroelectrochemical study*, Physical Chemistry Chemical Physics 13 (2011) Nr. 8, S. 3411-3420.

157) M.S. Khatri, H. Schloerb, S. Faehler, L. Schultz, *Correlation of crystallographic structure and magnetic properties of electrodeposited Co-rich Co-Pt films*, Physica Status Solidi A 208 (2011) Nr. 1, S. 104-108.

158) V.O. Khavrus, H. Vinzelberg, J. Schumann, A. Leonhardt, S. Oswald, B. Buechner, *On the potential of long carbon nanotube forest for sensing gases and vapors*, Physica E 43 (2011), S. 1199-1207.

159) O. Khvostikova, H. Hermann, H. Wendrock, T. Gemming, J. Thomas, H. Ehrenberg, *Effect of the microstructure on the intercalation and exfoliation behaviour of graphite*, Journal of Materials Science 46 (2011) Nr. 8, S. 2422-2430.

160) M. Kidszun, S. Haindl, T. Thersleff, J. Haenisch, A. Kauffmann, K. Iida, J. Freudenberger, L. Schultz, B. Holzapfel, *Critical current scaling and anisotropy in oxypnictide superconductors*, Physical Review Letters 106 (2011) Nr. 13, S. 137001/1-4.

161) A. Kiessling, J. Haenisch, T. Thersleff, E. Reich, M. Weigand, R. Huehne, M. Sparing, B. Holzapfel, J.H. Durrell, L. Schultz, *Nanocolumns in YBa2Cu3O7-x/BaZrO3 quasi-multilayers: formation and influence on superconducting properties*, Superconductor Science and Technology 24 (2011) Nr. 5, S. 55018/1-6.

162) K.T. Kim, J. Eckert, G. Liu, J.M. Park, B.K. Lim, S.H. Hong, *Influence of embedded-carbon nanotubes on the thermal properties of copper matrix nanocomposites processed by molecular-level mixing*, Scripta Materialia 64 (2011) Nr. 2, S. 181-184.

163) K.T. Kim, G.H. Ha, J. Eckert, *Microstructures and magnetic properties of carbon nanotube/Co-oxide nanocomposite powders*, Journal of Alloys and Compounds 509 (2011) Nr. Suppl. 1, S. S412-S415.

164) S.Y. Kim, S.S. Jee, K.R. Lim, W.T. Kim, D.H. Kim, E.-S. Lee, Y.H. Kim, S.M. Lee, J.H. Lee, J. Eckert, *Replacement of oxide glass with metallic glass for Ag screen printing metallization on Si emitter*, Applied Physics Letters 98 (2011) Nr. 22, S. 222112/1-3.

165) Y.-J. Kim, A.P. Sorini, C. Stock, T.G. Perring, J. van den Brink, T.P. Devereaux, *Probing high-energy electronic excitations in NiO using inelastic neutron scattering*, Physical Review B 84 (2011) Nr. 8, S. 85132/1-5.

166) P.D.C. King, R.C. Hatch, M. Bianchi, R. Ovsyannikov, C. Lupulescu, G. Landolt, B. Slomski, J.H. Dil, D. Guan, J.L. Mi, E.D.L. Rienks, J. Fink, A. Lindblad, S. Svensson, S. Bao, G. Balakrishnan, B.B. Iversen, J. Osterwalder, W. Eberhardt, F. Baumberger, P. Hofmann, *Large tunable rashba spin splitting of a two-dimensional electron gas in Bi2Se3*, Physical Review Letters 107 (2011) Nr. 9, S. 96802/1-5.

167) S. Kiravittaya, H.S. Lee, L. Balet, L.H. Li, M. Francardi, A. Gerardino, A. Fiore, A. Rastelli, O.G. Schmidt, *Tuning optical modes in slab photonic crystal by atomic layer deposition and laser-assisted oxidation*, Journal of Applied Physics 109 (2011) Nr. 5, S. 53115/1-3.

168) N.S. Kiselev, A.N. Bogdanov, R. Schaefer, U.K. Roessler, *Chiral skyrmions in thin magnetic films: New objects for magnetic storage technologies?*, Journal of Physics / D 44 (2011) Nr. 39, S. 392001/1-4.

169) N.S. Kiselev, A.N. Bogdanov, R. Schaefer, U.K. Roessler, *Comment on "Giant skyrmions stabilized by dipole-dipole interactions in thin ferromagnetic films"*, Physical Review Letters 107 (2011) Nr. 17, S. 179701/1-2.

170) A. Klauser, J. Mossel, J.-S. Caux, J. van den Brink, *Spin-exchange dynamical structure factor of the S=1/2 Heisenberg chain*, Physical Review Letters 106 (2011) Nr. 15, S. 157205/1-4.

171) S. Klod, N. Chen, L. Dunsch, *Changing the position of a bridged CH2 group at a fullerene cage surface in electrochemical synthesis: The case of C70 derivatives*, ChemPhysChem 12 (2011), S. 2097-2099.

172) E. Kockrick, L. Borchardt, C. Schrage, C. Gaudillere, C. Ziegler, T. Freudenberg, D. Farrusseng, A. Eychmueller, S. Kaskel, *CeO2/Pt catalyst nanoparticle containing carbide-derived carbon composites by a new In situ functionalization strategy*, Chemistry of Materials 23 (2011) Nr. 1, S. 57-66.

173) M. Koehler, L. Ratke, I. Kaban, W. Hoyer, *Heterogeneous nucleation in hypermonotectic aluminum alloys*, IOP Conference Series: Materials Science and Engineering 27 (2011) Nr. 1, S. 12005/1-7.

174) A. Koitzsch, J. Ocker, M. Knupfer, M.C. Dekker, K. Doerr, B. Buechner, P. Hoffmann, *In-gap electronic structure of LaAlO3-SrTiO3 heterointerfaces investigated by soft x-ray spectroscopy*, Physical Review B 84 (2011) Nr. 24, S. 245121/1-8.

175) V. Kokotin, H. Hermann, J. Eckert, *Computer simulation of the matrix-inclusion interphase in bulk metallic glass based nano-composites*, Journal of Physics: Condensed Matter 23 (2011), S. 425403/1-7.

176) A. Kondrat, G. Behr, B. Buechner, C. Hess, *Unusual Nernst effect and spin density wave precursors in superconducting LaFeAsO1-xFx*, Physical Review B 83 (2011) Nr. 9, S. 92507/1-4.

177) M. Kopte, S. Sawatzki, L. Schultz, V. Neu, *The nucleation of the spin spiral in epitaxial SmCo5/Fe/SmCo5 exchange spring trilayers*, IEEE Transactions on Magnetics 47 (2011) Nr. 10, S. 3736-3739.

178) A.A. Kordyuk, T.K. Kim, V.B. Zabolotnyy, D.V. Evtushinsky, M. Bauch, C. Hess, B. Buechner, H. Berger, S.V. Borisenko, *Photo-emission-induced gating of topological insulators*, Physical Review B 83 (2011) Nr. 8, S. 81303/1-4.

179) N. Korkmaz, F. Boerrnert, D. Koehler, R.G. Mendes, A. Bachmatiuk, M.H. Ruemmeli, B. Buechner, L.M. Eng, G. Roedel, *Metallization and investigation of electrical properties of in vitro recrystallized mSbsC-eGFP assemblies*, Nanotechnology 22 (2011) Nr. 37, S. 375606/1-8.

180) T. Kosub, C. Schubert, H. Schletter, M. Daniel, M. Hietschold, V. Neu, M. Maret, D. Makarov, M. Albrecht, *Coercivity enhancement in exchange biased CoO/Co3Pt bilayers*, Journal of Physics / D 44 (2011) Nr. 1, S. 15002/1-7.

181) J.A. Koza, S. Muehlenhoff, P. Zabinski, P.A. Nikrityuk, K. Eckert, M. Uhlemann, A. Gebert, T. Weier, L. Schultz, S. Odenbach, *Hydrogen evolution under the influence of a magnetic field*, Electrochimica Acta 56 (2011) Nr. 6, S. 2665-2675.

182) J.A. Koza, R. Sueptitz, M. Uhlemann, L. Schultz, A. Gebert, *Electrochemical micromachining of a Zr-based bulk metallic glass using a micro-tool electrode technique*, Intermetallics 19 (2011), S. 437-444.

183) C. Kramberger, P. Ayala, H. Shiozawa, F. Simon, A. Friedrich, X. Liu, M. Ruemmeli, Y. Miyata, H. Kataura, P. Hoffmann, T. Pichler, *Disentanglement of the unoccupied electronic structure in metallic and semiconducting C60 peapods*, Physical Review B 83 (2011) Nr. 19, S. 195438/1-5.

184) C. Kramberger, P. Ayala, H. Shiozawa, F. Simon, A. Friedrich, X. Liu, M.H. Ruemmeli, Y. Miyata, H. Kataura, P. Hoffmann, T. Pichler, *High resolution X-ray absorption on metallicity selected C60 peapods, single-, and double walled carbon nanotubes*, Physica Status Solidi B 248 (2011) Nr. 11, S. 2544-2547.
185) R. Kraus, M. Schrade, R. Schuster, M. Knupfer, A. Revcolevschi, B. Buechner, J. Geck, *Signatures of electronic polarons in La1-xSr1+xMn04 observed by electron energy-loss spectroscopy*, Physical Review B 83 (2011) Nr. 16, S. 165130/1-6.
186) A. Krause, W. Weber, A. Jahn, K. Richter, D. Pohl, B. Rellinghaus, U. Schroeder, J. Heitmann, T. Mikolajick, *Evaluation of the electrical and physical properties of thin calcium titanate high-k insulators for capacitor applications*, Journal of Vacuum Science and Technology B 29 (2011) Nr. 1, S. 1AC07/ 1-5.
187) A. Krause, W.M. Weber, U. Schroeder, D. Pohl, B. Rellinghaus, J. Heitmann, T. Mikolajick, *Reduction of leakage currents with nanocrystals embedded in an amorphous matrix in metal-insulator-metal capacitor stacks*, Applied Physics Letters 99 (2011) Nr. 22, S. 222905/1-4.
188) Y. Krupskaya, R. Zaripov, E. Vavilova, V. Miluykov, I. Bezkishko, D. Krivolapov, O. Kataeva, O. Sinyashin, E. Hey-Hawkins, V. Voronkova, K. Salikhov, V. Kataev, B. Buechner, *Electron spin coherence in antiferromagnetically coupled binuclear Mn complexes*, Physical Review B 84 (2011) Nr. 9, S. 92402/1-4.
189) U. Kuehn, J. Hufenbach, *Eisenbasislegierungen genuegen hoechsten Anspruechen*, Konstruktion (2011) Nr. 7/8, S. IW5.
190) M. Kulich, P. Kovac, H.W. Weber, W. Haessler, *SiC doped MgB2 wires in a Ti sheath prepared by stage formation*, Superconductor Science and Technology 24 (2011) Nr. 6, S. 65025/1-5.
191) P. Kumar, A. Bera, D.V.S. Muthu, A. Kumar, U.V. Waghmare, L. Harnagea, C. Hess, S. Wurmehl, S. Singh, B. Buechner, A.K. Sood, *Raman evidence for the superconducting gap and spin-phonon coupling in the superconductor Ca(Fe0.95Co0.05)2As2*, Journal of Physics / Condensed Matter 23 (2011) Nr. 25, S. 255403/1-6.
192) S. Kumar, R. Trotta, E. Zallo, J.D. Plumhof, P. Atkinson, A. Rastelli, O.G. Schmidt, *Strain-induced tuning of the emission wavelength of high quality GaAs/AlGaAs quantum dots in the spectral range of the 87Rb D2 lines*, Applied Physics Letters 99 (2011) Nr. 16, S. 161118/1-3.
193) I.V. Kuvychko, N.B. Shustova, S.M. Avdoshenko, A.A. Popov, S.H. Strauss, O.V. Boltalina, *In Search of Fullerene-Based Superacids: Synthesis, X-ray Structure, and DFT Study of C60(C2F5)5H*, Chemistry - A European Journal 17 (2011) Nr. 32, S. 8799-8802.
194) M.D. Kuzmin, *High-field low-temperature magnetisation curves of anisotropic ferrimagnets*, Journal of Magnetism and Magnetic Materials 323 (2011) Nr. 8, S. 1068-1082.
195) M.D. Kuzmin, K.P. Skokov, D.Y. Karpenkov, J.D. Moore, M. Richter, O. Gutfleisch, *Magnetic field dependence of the maximum adiabatic temperature change*, Applied Physics Letters 99 (2011) Nr. 1, S. 12501/1-3.
196) H.S. Lee, A. Rastelli, T.W. Kim, H.L. Park, O.G. Schmidt, *Optical spectroscopy of single Cd0.6Zn0.4Te/ZnTe quantum dots on Si substrate*, Thin Solid Films 519 (2011) Nr. 19, S. 6554-6556.
197) H.S. Lee, A. Rastelli, O.G., Kim, T.W. Schmidt, I.W. Lee, *Effects of SiO2 encapsulation and laser processing on single CdTe/ZnTe quantum dots grown on Si (001) substrates*, Journal of the Korean Physical Society 59 (2011) Nr. 2, S. 489-492.
198) P.V. Leksin, N.N. Garifyanov, I.A. Garifullin, J. Schumann, V. Kataev, O.G. Schmidt, B. Buechner, *Manifestation of new interference effects in a superconductor-ferromagnet spin valve*, Physical Review Letters 106 (2011) Nr. 6, S. 67005/1-4.
199) M. Li, P. Xu, J. Yang, H. Ying, K. Haubner, L. Dunsch, S. Yang, *Synthesis of pyrene-substituted poly(3-hexylthiophene) via postpolymerization and its noncovalent interactions with single-walled carbon nanotubes*, Journal of Physical Chemistry C 115 (2011) Nr. 11, S. 4584-4593.
200) S. Liang, M. Daghofer, S. Dong, C. Sen, E. Dagotto, *Emergent dimensional reduction of the spin sector in a model for narrow-band manganites*, Physical Review B 84 (2011) Nr. 2, S. 24408/1-8.
201) J.H. Lin, C.S. Chen, M.H. Ruemmeli, A. Bachmatiuk, Z.Y. Zeng, H.L. Ma, B. Buechner, H.W. Chen, *Growth of carbon nanotubes catalyzed by defect-rich graphite surfaces*, Chemistry of Materials 23 (2011), S. 1637-1639.
202) I. Lindemann, R.D. Ferrer, L. Dunsch, R. Cerny, H. Hagemann, V. D'Anna, Y. Filinchuk, L. Schultz, O. Gutfleisch, *Novel sodium aluminium borohydride containing the complex anion [Al(BH4,Cl)4]*, RSC - Faraday Discussions 151 (2011), S. 231-242.
203) S. Lindner, U. Treske, M. Grobosch, M. Knupfer, *Charge transfer at F16CoPc and CoPc interfaces to Au*, Applied Physics A 105 (2011), S. 921-925.
204) G. Liu, S. Scudino, R. Li, U. Kuehn, J. Sun, J. Eckert, *Coupling effect of primary voids and secondary voids on the ductile fracture of heat-treatable aluminum alloys*, Mechanics of Materials 43 (2011) Nr. 10, S. 556-566.
205) J. Liu, M. Krautz, K. Skokov, T.G. Woodcock, O. Gutfleisch, *Systematic study of the microstructure, entropy change and adiabatic temperature change in optimized La–Fe–Si alloys*, Acta Materialia 59 (2011), S. 3602-3611.
206) M. Loeffler, U. Weissker, T. Muehl, T. Gemming, B. Buechner, *Robust determination of Young's modulus of individual carbon nanotubes by quasi-static interaction with Lorentz forces*, Ultramicroscopy 111 (2011), S. 155-158.
207) M. Loeffler, U. Weissker, T. Muehl, T. Gemming, J. Eckert, B. Buechner, *Current-induced mass transport in filled multiwalled carbon nanotubes*, Advanced Materials 23 (2011) Nr. 4, S. 541-544.
208) W. Loeser, T.G. Woodcock, O. Shuleshova, R. Hermann, H.-G. Lindenkreuz, B. Gehrmann, S. Schneider, T. Volkmann, *Metastable solidification in undercooled liquid droplets of Fe-Ni based soft-magnetic alloys under terrestrial and microgravity conditions*, Journal of Physics: Conference Series 327 (2011) Nr. 1, S. 12005/1-6.
209) M.R. Lohe, K. Gedrich, T. Freudenberg, E. Kockrick, T. Dellmann, S. Kaskel, *Heating and separation using nanomagnet-functionalized metal-organic frameworks*, Chemical Communications 47 (2011) Nr. 11, S. 3075-3077.
210) P. Lukaszczuk, E. Borowiak-Palen, M.H. Ruemmeli, R.J. Kalenczuk, *Gel-based separation of single-walled carbon nanotubes for metallic and semiconducting fractions*, Materials Research Bulletin 46 (2011), S. 1535-1539.

211) V. Lukes, P. Rapta, K.R. Idzik, R. Beckert, L. Dunsch, *Charged states of 1,3,5-triazine molecules as models for star-shaped molecular architecture: A DFT and spectroelectrochemcial study*, Journal of Physical Chemistry B 115 (2011), S. 3344-3353.

212) Q. Luo, B. Schwarz, N. Mattern, J. Eckert, *Magnetic ordering and slow dynamics in a Ho-based bulk metallic glass with moderate random magnetic anisotropy*, Journal of Applied Physics 109 (2011) Nr. 11, S. 113904/1-3.

213) J. Lyubina, M.D. Kuzmin, K. Nenkov, O. Gutfleisch, M. Richter, D.L. Schlagel, T.A. Lograsso, K.A. Gschneidner, *Magnetic field dependence of the maximum magnetic entropy change*, Physical Review B 83 (2011) Nr. 1, S. 12403/1-4.

214) L. Ma, S. Kiravittaya, V.A.B. Quinones, S. Li, Y. Mei, O.G. Schmidt, *Tuning of optical resonances in asymmetric microtube cavities*, Optics Letters 36 (2011) Nr. 19, S. 3840-3842.

215) B. Mahns, F. Roth, M. Grobosch, D.R.T. Zahn, M. Knupfer, *Electronic excitations of potassium intercalated manganese phthalocyanine investigated by electron energy-loss spectroscopy*, The Journal of Chemical Physics 134 (2011) Nr. 19, S. 194504/1-5.

216) E.G. Maksimov, A.E. Karakozov, B.P. Gorshunov, A. S. Prokhorov, A.A. Voronkov, E.S. Zhukova, V.S. Nozdrin, S.S. Zhukov, D. Wu, M. Dressel, S. Haindl, K. Iida, B. Holzapfel, *Two-band Bardeen-Cooper-Schrieffer superconducting state of the iron pnictide compound Ba(Fe0.9Co0.1)2As2*, Physical Review B 83 (2011) Nr. 14, S. 140502/1-4.

217) T. Marr, J. Freudenberger, D. Seifert, H. Klauß, J. Romberg, I. Okulov, J. Scharnweber, A. Eschke, C.-G. Oertel, W. Skrotzki, U. Kuehn, J. Eckert, L. Schultz, *Ti-Al composite wires with high specific strength*, Metals 1 (2011) Nr. 1, S. 79-97.

218) G. Martin, S.V. Biryukov, H. Schmidt, B. Steiner, B. Wall, *Two-finger (TF) SPUDT cells*, IEEE Transactions on Ultrasonics, Ferroelectrics, and Frequency Control 58 (2011) Nr. 3, S. 658-661.

219) N. Mattern, U. Vainio, J.M. Park, J.H. Han, A. Shariq, D.H. Kim, J. Eckert, *Phase separation in Cu46Zr47-xAl7Gdx metallic glasses*, Journal of Alloys and Compounds 509 (2011) Nr. Suppl. 1, S. S23-S26.

220) Y. Mei, A.A. Solovev, S. Sanchez, O.G. Schmidt, *Rolled-up nanotech on polymers: From basic perception to self-propelled catalytic microengines*, Chemical Society Reviews 40 (2011) Nr. 5, S. 2109-2119.

221) M. Melzer, D. Makarov, A. Calvimontes, D. Karnaushenko, S. Baunack, R. Kaltofen, Y. Mei, O.G. Schmidt, *Stretchable magnetoelectronics*, Nano Letters 11 (2011), S. 2522-2526.

222) D. Mikhailova, N.N. Bramnik, K.G. Bramnik, P. Reichel, S. Oswald, A. Senyshyn, D.M. Trots, H. Ehrenberg, *Layered LixMoO2 phases with different composition for electrochemical application: Structural considerations*, Chemistry of Materials 23 (2011) Nr. 15, S. 3429-3441.

223) I. Moench, D. Makarov, R. Koseva, L. Baraban, D. Karnaushenko, D. Kaiser, K.-F. Arndt, O.G. Schmidt, *Rolled-up magnetic sensor: Nanomembrane architecture for in-flow detection of magnetic objects*, ACS nano 5 (2011) Nr. 9, S. 7436-7442.

224) I. Moench, J. Schumann, M. Stockmann, K.-F. Arndt, O.G. Schmidt, *Multifunctional nanomembranes self-assembled into compact rolled-up sensor–actuator devices*, Smart Materials and Structures 20 (2011) Nr. 8, S. 85016/1-10.

225) B. Moritz, S. Johnston, T.P. Devereaux, B. Muschler, W. Prestel, R. Hackl, M. Lambacher, A. Erb, S. Komiya, Y. Ando, *Investigation of particle-hole asymmetry in the cuprates via electronic Raman scattering*, Physical Review B 84 (2011) Nr. 23, S. 235114/1-12.

226) J.A. Morkowski, G. Chelkowska, M. Werwinski, A. Szajek, R. Troc, C. Neise, *X-ray photoemission spectrum, electronic structure, and magnetism of UCu2Si2*, Journal of Alloys and Compounds 509 (2011), S. 6994-6998.

227) C. Mueller, G.B. de Souza, A. Mikowski, O.G. Schmidt, C.M. Lepienski, D.H. Mosca, *Magnetic and mechanical properties of rolled-up Au/Co/Au nanomembranes with multiple windings*, Journal of Applied Physics 110 (2011) Nr. 4, S. 44326/1-6.

228) N.K. Mukhopadhyay, F. Ali, V.C. Srivastava, T.P. Yadav, M. Sakaliyska, K.B. Surreddi, S. Scudino, V. Uhlenwinkel, J. Eckert, *Strain-induced structural transformation of single-phase Al-Cu-Fe icosahedral quasicrystal during mechanical milling*, Philosophical Magazine 91 (2011) Nr. 19-21, S. 2482-2490.

229) F.M. Muntyanu, A. Gilewski, K. Nenkov, A.J. Zaleski, V. Chistol, *Magnetic properties and superconductivity of nano-width crystallite interfaces of bicrystals and tricrystals of Bi1-x-Sbx (x?=?0.2) alloys*, Physica Status Solidi B 248 (2011) Nr. 12, S. 2903-2907.

230) J. Nagel, K.B. Konovalenko, M. Kemmler, M. Turad, R. Werner, E. Kleisz, S. Menzel, R. Klingeler, B. Buechner, R. Kleiner, D. Koelle, *Resistively shunted YBa2Cu3O7 grain boundary junctions and low-noise SQUIDs patterned by a focused ion beam down to 80 nm linewidth*, Superconductor Science and Technology 24 (2011) Nr. 1, S. 15015/1-8.

231) Y.G. Naidyuk, O.E. Kvitnitskaya, L.V. Tiutrina, I.K. Yanson, G. Behr, G. Fuchs, S.-L. Drechsler, K. Nenkov, L. Schultz, *Peculiarities of the superconducting gaps and the electron-boson interaction in TmNi2B2C as seen by point-contact spectroscopy*, Physical Review B 84 (2011) Nr. 9, S. 94516/1-9.

232) Y.G. Naidyuk, O.E. Kvitnitskaya, K. Yanson, G. Fuchs, S. Haindl, M. Kidszun, L. Schultz, B. Holzapfel, *Point-contact study of ReFeAsO1-xFx (Re = La, Sm) superconducting films*, Superconductor Science and Technology 24 (2011) Nr. 6, S. 65010/1-7.

233) M. Nakamura, S. Nishimoto, A. O'Brian, P. Fulde, *Metal-insulator transition of spinless fermions on the Kagome lattice*, Modern Physics Letters B 25 (2011) Nr. 12-13, S. 947-953.

234) T. Namsaraeva, B. Bazarov, D. Mikhailova, N. Kuratieva, A. Sarapulova, A. Senyshyn, H. Ehrenberg, *Orthomolybdates in the Cs–FeII,III–Mo–O System: Cs4Fe(MoO4)3, Cs2Fe2(MoO4)3 and CsFe5(MoO4)7*, European Journal of Inorganic Chemistry (2011) Nr. 18, S. 2832-2841.

235) L.K. Nanver, V. Jovanovic, C. Biasotto, J. Moers, D. Gruetzmacher, J.J. Zhang, N. Hrauda, M. Stoffel, F. Pezzoli, O.G. Schmidt, L. Miglio, H. Kosina, A. Marzegalli, G. Vastola, G. Mussler, J. Stangl, G. Bauer, J. van der Cingel, E. Bonera, *Integration of MOSFETs with SiGe dots as stressor material*, Solid-State Electronics 60 (2011) Nr. 1, S. 75-83.

236) V. Narayanan, P. Lommens, K. De Buysser, R. Huehne, I. Van Driessche, *Thick lanthanum zirconate buffer layers from water-based precursor solutions on Ni-5%W substrates*, Journal of Solid State Chemistry 184 (2011), S. 2887-2896.

237) E. Nazarova, K. Nenkov, K. Buchkov, A. Zahariev, *Scaling behavior of current-voltage characteristics of Y1-xCaxBa2Cu3O7-d polycrystalline samples*, The Open Superconductors Journal 3 (2011), S. 1-6.

238) C. Neise, S. Schoenecker, M. Richter, K. Koepernik, H. Eschrig, *The effect of chemical disorder on the magnetic anisotropy of strained Fe–Co films*, Physica Status Solidi B 248 (2011) Nr. 10, S. 2398-2403.

239) A. Nicholson, W. Ge, X. Zhang, J. Riera, M. Daghofer, A.M. Oles, G.B. Martins, A. Moreo, E. Dagotto, *Competing pairing symmetries in a generalized two-orbital model for the pnictide superconductors*, Physical Review Letters 106 (2011) Nr. 21, S. 217002/1-4.

240) A. Nicholson, Q. Luo, W. Ge, J. Riera, M. Daghofer, G.B. Martins, A. Moreo, E. Dagotto, *Role of degeneracy, hybridization, and nesting in the properties of multiorbital systems*, Physical Review B 84 (2011) Nr. 9, S. 94519/1-13.

241) Z.H. Nie, D.Y. Cong, D.M. Liu, Y. Ren, M. Poetschke, S. Roth, Y.D. Wang, *Large internal stress-assisted twin-boundary motion in Ni2MnGa ferromagnetic shape memory alloy*, Applied Physics Letters 99 (2011) Nr. 14, S. 141907/1-5.

242) D.L. Nika, E.P. Pokatilov, A.A. Balandin, V.M. Fomin, A. Rastelli, O.G. Schmidt, *Reduction of lattice thermal conductivity in one-dimensional quantum-dot superlattices due to phonon filtering*, Physical Review B 84 (2011) Nr. 16, S. 165415/1-7.

243) S. Nishimoto, *Tomonaga-Luttinger-liquid criticality: Numerical entanglement entropy approach*, Physical Review B 84 (2011) Nr. 19, S. 195108/1-5.

244) S. Nishimoto, S.-L. Drechsler, R.O. Kuzian, J. van den Brink, J. Richter, W.E.A. Lorenz, Y. Skourski, R. Klingeler, B. Buechner, *Saturation field of frustrated chain cuprates: Broad regions of predominant interchain coupling*, Physical Review Letters 107 (2011) Nr. 9, S. 97201/1-4.

245) S. Nishimoto, Y. Fuji, Y. Ohta, *Spin gap of the three-leg S=3/2 Heisenberg tube*, Physical Review B 83 (2011) Nr. 22, S. 224425/1-5.

246) C.-G. Oertel, R. Schaarschuch, G.H. Cao, H.N. Tian, J. Freudenberger, H.-G. Brokmeier, W. Skrotzki, *Effect of martensitic phase transformation on the ductility of polycrystalline YCu*, Scripta Materialia 65 (2011) Nr. 9, S. 779-782.

247) A.T. Onisan, A.N. Bogdanov, U.K. Roessler, *Domain model for the magnetic shape-memory effect in non-modulated tetragonal Ni-Mn-Ga*, Journal of Physics: Conference Series 303 (2011) Nr. 1, S. 12083/1-6.

248) C. Ortix, S. Kiravittaya, O.G. Schmidt, J. van den Brink, *Curvature-induced geometric potential in strain-driven nanostructures*, Physical Review B 84 (2011) Nr. 4, S. 45438/1-5.

249) C. Ortix, J. Rijnbeek, J. van den Brink, *Defect formation preempts dynamical symmetry breaking in closed quantum systems*, Physical Review B 84 (2011) Nr. 14, S. 144423/1-6.

250) C. Ortix, J. van den Brink, *Absence of anomalous couplings in the quantum theory of constrained electrically charged particles*, Physical Review B 83 (2011) Nr. 11, S. 113406/1-3.

251) S. Oswald, D. Mikhailova, F. Scheiba, P. Reichel, A. Fiedler, H. Ehrenberg, *XPS investigations of electrolyte/electrode interactions for various Li-ion battery materials*, Analytical and Bioanalytical Chemistry 400 (2011), S. 691-696.

252) S. Oswald, F. Oswald, *A promising concept for using near-surface measuring angles in angle-resolved x-ray photoelectron spectroscopy considering elastic scattering effects*, Journal of Applied Physics 109 (2011), S. 34305/1-11.

253) S. Ouardi, G.H. Fecher, C. Felser, C.G.F. Blum, D. Bombor, C. Hess, S. Wurmehl, B. Buechner, E. Ikenaga, *Transport and thermal properties of single- and polycrystalline NiZr(0.5)Hf(0.5)Sn*, Applied Physics Letters 99 (2011) Nr. 15, S. 152112/1-4.

254) J. Paillier, C. Rongeat, O. Gutfleisch, A. Gebert, *Hydrogen and Zr-based metallic glasses: Gas/solid absorption process and structure evolution*, Journal of Alloys and Compounds 509 (2011), S. 1636-1643.

255) J.M. Park, D.H. Kim, K.B. Kim, N. Mattern, J. Eckert, *Evolution of constitution, structure, and mechanical properties in Fe–Ti–Zr–B heterogeneous multiphase composites*, Journal of Materials Research 26 (2011), S. 365-371.

256) J.M. Park, D.H. Kim, N. Mattern, K.B. Kim, E. Fleury, J. Eckert, *Microstructure and mechanical properties of Fe–Si–Ti–(Cu, Al) heterostructured ultrafine composites*, Journal of Alloys and Compounds 509 (2011) Nr. Suppl. 1, S. S367-S370.

257) J.M. Park, D.H. Kim, M. Stoica, N. Mattern, R. Li, J. Eckert, *The influence of in situ formed precipitates on the plasticity of Fe-Nb-B-Cu bulk metallic glasses*, Journal of Materials Research 26 (2011) Nr. 16, S. 2080-2086.

258) J.M. Park, G. Wang, S. Pauly, N. Mattern, D.H. Kim, J. Eckert, *Ductile Ti-based bulk metallic glasses with high specific strength*, Metallurgical and Materials Transactions A 42 (2011) Nr. 6, S. 1456-1460.

259) S. Partzsch, S.B. Wilkins, J.P. Hill, E. Schierle, E. Weschke, D. Souptel, B. Buechner, J. Geck, *Observation of electronic ferroelectric polarization in multiferroic YMn2O5*, Physical Reviwe Letters 107 (2011) Nr. 5, S. 57201/1-4.

260) G. Parzych, D. Mikhailova, S. Oswald, J. Eckert, H. Ehrenberg, *Study of the conversion reaction mechanism for copper borate as electrode material in lithium-ion batteries*, Journal of the Electrochemical Society 158 (2011) Nr. 8, S. A898-A904.

261) O. Penzin, G. Paasch, F. O. Heinz, L. Smith, *Extended quantum correction model applied to six-band valence bands near silicon/oxide interfaces*, IEEE Transactions on Electron Devices 58 (2011) Nr. 6, S. 1614-1619.

262) A. Petr, V. Kataev, B. Buechner, *First direct in situ EPR spectroelectrochemical evidence of the superoxide anion radical*, Journal of the Physical Chemistry B 115 (2011), S. 12036-12039.

263) A. Pfuetzner, C. Mickel, J. Jankowski, M. Hein, J. Meiss, C. Schuenemann, C. Elschner, A.A. Levin, B. Rellinghaus, K. Leo, M. Riede, *The influence of substrate heating on morphology and layer growth in C60:ZnPc bulk heterojunction solar cells*, Organic Electronics 12 (2011) Nr. 3, S. 435-441.

264) M. Philipp, M. Knupfer, B. Buechner, H. Gerardin, *Plasmonic excitations in ZnO/Ag/ZnO multilayer systems: Insight into interface and bulk electronic properties*, Journal of Applied Physics 109 (2011) Nr. 6, S. 63710/1-6.

265) R. Pipkorn, L. Dunsch, M. Wiessler, W. Waldeck, K. Braun, *A rare earth endo-nitrite-cluster-fullerene-conjugate useful as an intravital contrast agent in MRT?*, Biopolymers 96 (2011) Nr. 4, S. 506.

266) Y. Plevachuk, V. Sklyarchuk, R. Hermann, G. Gerbeth, *Some thermophysical properties of the intermetallic Ti40Al60 alloy in the melting-solidification temperature range*, International Journal of Materials Research 102 (2011) Nr. 3, S. 282-285.

267) J.D. Plumhof, V. Krapek, F. Ding, K.D. Joens, R. Hafenbrak, P. Klenovsky, A. Herklotz, K. Doerr, P. Michler, A. Rastelli, O.G. Schmidt, *Strain-induced anticrossing of bright exciton levels in single self-assembled GaAs/AlxGa1-xAs and InxGa1-xAs/GaAs quantum dots*, Physical Review B 83 (2011) Nr. 12, S. 121302/1-4.

268) D. Pohl, F. Schaeffel, M.H. Ruemmeli, E. Mohn, C. Taeschner, L. Schultz, C. Kisielowski, B. Rellinghaus, *Understanding the metal-carbon interface in FePt catalyzed carbon nanotubes*, Physical Review Letters 107 (2011) Nr. 18, S. 185501/1-5.

269) A.I. Popa, E. Vavilova, C. Taeschner, V. Kataev, B. Buechner, R. Klingeler, *Electrochemical behavior and magnetic properties of vanadium oxide nanotubes*, The Journal of Physical Chemistry C 115 (2011) Nr. 13, S. 5265-5270.

270) A.A. Popov, S.M. Avdoshenko, G. Cuniberti, L. Dunsch, *Dimerization of radical-anions: Nitride clusterfullerenes versus empty fullerenes*, The Journal of Physical Chemistry Letters 2 (2011), S. 1592-1600.

271) A.A. Popov, L. Dunsch, *Electrochemistry in cavea: Endohedral redox reactions of encaged species in fullerenes*, The Journal of Physical Chemistry Letters 2 (2011) Nr. 7, S. 786-794.

272) A.A. Popov, L. Dunsch, *Charge controlled changes in the cluster and spin dynamics of Sc3N@C80(CF3)2: the flexible spin density distribution and its impact on ESR spectra*, Physical Chemistry Chemical Physics 13 (2011), S. 8977-8984.

273) A.A. Popov, S. Jeon, V.M. Senyavin, L. Dunsch, S. Maragani, M. Wang, L.-S. Tan, L.Y. Chiang, *Unique ultralow 18-pi-trannulenyl HOMOLUMO energy gap of photostable emerald-green D3d-2-methylmalonato[60]fullerenes*, Journal of Physical Chemistry Letters 2 (2011), S. 2296-2299.

274) A.A. Popov, S. Schiemenz, S.M. Avdoshenko, S. Yang, G. Cuniberti, L. Dunsch, *The state of asymmetric nitride clusters in endohedral fullerenes as studied by 14N NMR spectroscopy: Experiment and theory*, The Journal of Physical Chemistry C 115 (2011), S. 15257-15265.

275) A.K. Pramanik, M. Abdel-Hafiez, S. Aswartham, A.U.B. Wolter, S. Wurmehl, V. Kataev, B. Buechner, *Multigap superconductivity in single crystals of Ba0.65Na0.35Fe2As2: A calorimetric investigation*, Physical Review B 84 (2011) Nr. 6, S. 64525/1-7.

276) A.K. Pramanik, L. Harnagea, C. Nacke, A.U.B. Wolter, S. Wurmehl, V. Kataev, B. Buechner, *Fishtail effect and vortex dynamics in LiFeAs single crystals*, Physical Review B 83 (2011) Nr. 9, S. 94502/1-5.

277) K.G. Prashanth, S. Kumar, S. Scudino, B.S. Murty, J. Eckert, *Fabrication and response of Al70Y16Ni10Co4 glass reinforced metal matrix composites*, Materials and Manufacturing Processes 26 (2011) Nr. 10, S. 1242-1247.

278) R.T. Qu, J. Eckert, Z.F. Zhang, *Tensile fracture criterion of metallic glass*, Journal of Applied Physics 109 (2011) Nr. 8, S. 83544/1-12.

279) N. Qureshi, Y. Drees, J. Werner, S. Wurmehl, C. Hess, R. Klingeler, B. Buechner, M.T. Fernandez-Diaz, M. Braden, *Crystal and magnetic structure of the oxypnictide superconductor LaFeAsO1-xFx: A neutron-diffraction study*, Physical Review B 82 (2011) Nr. 18, S. 184521/1-9.

280) D. Rall, K. Il'in, K. Iida, S. Haindl, F. Kurth, T. Thersleff, L. Schultz, B. Holzapfel, M. Siegel, *Critical current densities in ultrathin Ba(Fe,Co)2As2 microbridges*, Physical Review B 83 (2011) Nr. 13, S. 134514/1-6.

281) L. Ratkai, C. Conseil, V. Nazabal, B. Bureau, I. Kaban, J. Bednarcik, B. Beuneu, P. Jovari, *Microscopic origin of demixing in Ge20SexTe80-x alloys*, Journal of Alloys and Compounds 509 (2011) Nr. 17, S. 5190-5194.

282) L. Ratkai, A.P. Goncalves, G. Delaizir, C. Godart, I. Kaban, B. Beuneu, P. Jovari, *The Cu and Te coordination environments in Cu-doped Ge-Te glasses*, Solid State Communications 151 (2011) Nr. 21, S. 1524-1527.

283) J.L. Ren, C. Chen, G. Wang, N. Mattern, J. Eckert, *Dynamics of serrated flow in a bulk metallic glass*, AIP Advances 1 (2011) Nr. 3, S. 32158/1-6.

284) A.W. Robertson, A. Bachmatiuk, Y.A. Wu, F. Schaeffel, B. Buechner, M.H. Ruemmeli, J.H. Warner, *Structural distortions in few-layer graphene creases*, ACS nano 5 (2011) Nr. 12, S. 9984-9991.

285) A.W. Robertson, A. Bachmatiuk, Y.A. Wu, F. Schaeffel, B. Rellinghaus, B. Buechner, M.H. Ruemmeli, J.H. Warner, *Atomic structure of interconnected few-layer graphene domains*, ACS nano 5 (2011) Nr. 8, S. 6610-6618.

286) S. Roessler, D. Cherian, W. Lorenz, M. Doerr, C. Koz, C. Curfs, Y. Prots, U.K. Roessler, U. Schwarz, S. Elizabeth, S. Wirth, *First-order structural transition in the magnetically ordered phase of Fe1.13Te*, Physical Review B 84 (2011) Nr. 17, S. 174506/1-6.

287) S. Roessler, H.S. Nair, U.K. Roessler, C.M.N. Kumar, S. Elizabeth, S. Wirth, *Ferromagnetic transition and specific heat of Pr0.6Sr0.4MnO3*, Physical Review B 84 (2011) Nr. 18, S. 184422/1-10.

288) V.V. Romaka, M. Konyk, L. Romaka, V. Pavlyuk, H. Ehrenberg, A. Tkachuk, *Peculiarity of component interaction in {Y, Dy}-Mn-Sn ternary systems*, Journal of Alloys and Compounds 509 (2011) Nr. 28, S. 7559-7564.

289) C. Rongeat, I. Lindemann, A. Borgschulte, L. Schultz, O. Gutfleisch, *Effect of the presence of chlorides on the synthesis and decomposition of Ca(BH4)2*, International Journal of Hydrogen Energy 36 (2011) Nr. 1, S. 247-253.

290) C. Rongeat, N. Scheerbaum, L. Schultz, O. Gutfleisch, *Catalysis of H2 sorption in NaAlH4: General description and new insights*, Acta Materialia 59 (2011) Nr. 4, S. 1725-1733.

291) F. Roth, B. Mahns, B. Buechner, M. Knupfer, *Dynamic response and electronic structure of potassium-doped picene investigated by electron energy-loss spectroscopy*, Physical Review B 83 (2011) Nr. 14, S. 144501/1-5.

292) F. Roth, B. Mahns, B. Buechner, M. Knupfer, *Exciton character in picene molecular solids*, Physical Review B 83 (2011) Nr. 16, S. 165436/1-4.

293) M.H. Ruemmeli, A. Bachmatiuk, F. Boerrnert, F. Schaeffel, I. Ibrahim, K. Cendrowski, G. Simha-Martynkova, D. Placha, E. Borowiak-Palen, G. Cuniberti, B. Buechner, *Synthesis of carbon nanotubes with and without catalyst particles*, Nanoscale Research Letters (2011) Nr. 6, S. 303.

294) M.H. Ruemmeli, C.G. Rocha, F. Ortmann, I. Ibrahim, H. Sevincli, F. Boerrnert, J. Kunstmann, A. Bachmatiuk, M. Poetschke, M. Shiraishi, M. Meyyappan, B. Buechner, S. Roche, G. Cuniberti, *Graphene: Piecing it together*, Advanced Materials 23 (2011), S. 4471-4490.

295) H. Ryu, D. Kaelblein, O.G. Schmidt, H. Klauk, *Unipolar sequential circuits based on individual-carbon-nanotube transistors and thin-film carbon resistors*, ACS nano 5 (2011) Nr. 9, S. 7525-7531.

296) M. Samadi Khoshkhoo, S. Scudino, J. Thomas, K.B. Surreddi, J. Eckert, *Grain and crystallite size evaluation of cryomilled pure copper*, Journal of Alloys and Compounds 509 (2011) Nr. Supplement 1, S. S343-S347.
297) S. Sanchez, A.N. Ananth, V.M. Fomin, M. Viehrig, O.G. Schmidt, *Superfast motion of catalytic microjet engines at physiological temperature*, Journal of the American Chemical Society 133 (2011), S. 14860-14863.
298) S. Sanchez, A.A. Solovev, S.M. Harazim, C. Deneke, Y.F. Mei, O.G. Schmidt, *The smallest man-made jet engine*, The Chemical Record 11 (2011) Nr. 6, S. 367-370.
299) S. Sanchez, A.A. Solovev, S.M. Harazim, O.G. Schmidt, *Microbots swimming in the flowing streams of microfluidic channels*, Journal of the American Chemical Society 133 (2011) Nr. 4, S. 701-703.
300) S. Sanchez, A.A. Solovev, S. Schulze, O.G. Schmidt, *Controlled manipulation of multiple cells using catalytic microbots*, Chemical Communications 47 (2011) Nr. 2, S. 698-700.
301) T.S. Santos, B.J. Kirby, S. Kumar, S.J. May, J.A. Borchers, B.B. Maranville, J. Zarestky, S.G.E. te Velthuis, J. van den Brink, A. Bhattacharya, *Delta doping of ferromagnetism in antiferromagnetic manganite superlattices*, Physical Review Letters 107 (2011) Nr. 16, S. 167202/1-5.
302) S. Sawatzki, R. Heller, C. Mickel, M. Seifert, L. Schultz, V. Neu, *Largely enhanced energy density in epitaxial SmCo5/Fe/SmCo5 exchange spring trilayers*, Journal of Applied Physics 109 (2011) Nr. 12, S. 123922/1-7.
303) F. Schaeffel, M. Wilson, A. Bachmatiuk, M.H. Ruemmeli, U. Queitsch, B. Rellinghaus, G.A.D. Briggs, J.W. Warner, *Atomic resolution imaging of the edges of catalytically etched suspended few-layer graphene*, ACS nano 5 (2011) Nr. 3, S. 1975-1983.
304) B. Scheibe, M.H. Ruemmeli, E. Borowiak-Palen, R.J. Kalenczuk, *Separation of surfactant functionalized single-walled carbon nanotubes via free solution electrophoresis method*, Central European Journal of Physics 9 (2011) Nr. 2, S. 325-329.
305) A. Schlieter, U. Kuehn, J. Eckert, W. Loeser, T. Gemming, M. Friak, J. Neugebauer, *Anisotropic mechanical behavior of ultrafine eutectic TiFe cast under non-equilibrium conditions*, Intermetallics 19 (2011), S. 327-335.
306) F. Schmitt, B. Moritz, S. Johnston, S.-K. Mo, M. Hashimoto, R.G. Moore, D.-H. Lu, E. Motoyama, M. Greven, T.P. Devereaux, Z.-X. Shen, *High-energy anomaly in Nd2-xCexCu04 investigated by angle-resolved photoemission spectroscopy and quantum MonteCarlo simulations*, Physical Review B 83 (2011) Nr. 19, S. 195123/1-10.
307) S. Schmitz, W. Loeser, H. Klauss, B. Buechner, *Effect of elements with positive enthalpy of mixing on mechanical properties of bulk metallic glasses*, Journal of Alloys and Compounds 509 (2011) Nr. Suppl. 1, S. S131-S135.
308) J.J. Schneider, J. Khanderi, A. Popp, J. Engstler, H. Tempel, A. Sarapulova, N.N. Bramnik, D. Mikhailova, H. Ehrenberg, L.A. Schmitt, L. Dimesso, C. Foerster, W. Jaegermann, *Hybrid architectures from 3D aligned arrays of multiwall carbon nanotubes and nanoparticulate LiCoP04: Synthesis, properties and evaluation of their electrochemical performance as cathode materials in lithium ion batteries*, European Journal of Inorganic Chemistry (2011) Nr. 28, S. 4349-4359.
309) M. Schowalter, M. Tewes, K. Frank, R. Imlau, A. Rosenauer, H.S. Lee, A. Rastelli, O.G. Schmidt, M. Tavast, T. Leinonen, M. Guina, *Investigation of diffusion in AlAs/GaAs distributed Bragg reflectors using HAADF STEM imaging*, Journal of Physics: Conference Series 326 (2011) Nr. 1, S. 12035/1-4.
310) C. Schuenemann, F. Schaeffel, A. Bachmatiuk, U. Queitsch, M. Sparing, B. Rellinghaus, K. Lafdi, L. Schultz, B. Buechner, M.H. Ruemmeli, *Catalyst poisoning by amorphous carbon during carbon nanotube growth: Fact or fiction?*, ACS nano 5 (2011) Nr. 11, S. 8928-8934.
311) B. Schwarz, N. Mattern, J.D. Moore, K.P. Skokov, O. Gutfleisch, J. Eckert, *Influence of sample geometry on determination of magnetocaloric effect for Gd60Co30Al10 glassy ribbons using direct and indirect methods*, Journal of Magnetism and Magnetic Materials 323 (2011) Nr. 13, S. 1782-1786.
312) B. Schwarz, U. Vainio, N. Mattern, S.W. Sohn, S. Oswald, D.H. Kim, J. Eckert, *Combined in-situ SAXS/WAXS and HRTEM study on crystallization of (Cu60Co40)1-xZrx metallic glasses*, Journal of Non-Crystalline Solids 357 (2011) Nr. 6, S. 1538-1546.
313) A. Scott, A. Dianat, F. Boerrnert, A. Bachmatiuk, S. Zhang, J.H. Warner, E. Borowiak-Palen, M. Knupfer, B. Buechner, G. Cuniberti, M.H. Ruemmeli, *The catalytic potential of high-K dielectrics for graphene formation*, Applied Physics Letters 98 (2011) Nr. 7, S. 73110/1-3.
314) S. Scudino, B. Jerliu, S. Pauly, K.B. Surreddi, U. Kuehn, J. Eckert, *Ductile bulk metallic glasses produced through designed heterogeneities*, Scripta Materialia 65 (2011) Nr. 9, S. 815-818.
315) S. Scudino, B. Jerliu, K.B. Surreddi, U. Kuehn, J. Eckert, *Effect of cold rolling on compressive and tensile mechanical properties of Zr52.5Ti5Cu18Ni14.5Al10 bulk metallic glass*, Journal of Alloys and Compounds 509 (2011) Nr. Supplement 1, S. S128-S130.
316) C. Sekar, S. Paulraj, P. Kanchana, B. Schuepp-Niewa, R. Klingeler, G. Krabbes, B. Buechner, *Effect of rotation of feed and seed rods on the quality of Na0.75CoO2 single crystal grown by traveling solvent floating zone method*, Materials Research Bulletin 46 (2011), S. 675-681.
317) V. Senkovskyy, R. Tkachov, H. Komber, M. Sommer, M. Heuken, B. Voit, W.T.S. Huck, V. Kataev, A. Petr, A. Kiriy, *Chain-growth polymerization of unusual anion-radical monomers based on naphthalene diimide: A new route to well-defined n-type conjugated copolymers*, Journal of the American Chemical Society 133 (2011), S. 19966-19970.
318) A. Senyshyn, M. Hoelzel, T. Hansen, L. Vasylechko, V. Mikhailik, H. Kraus, H. Ehrenberg, *Thermal structural properties of calcium tungstate*, Journal of Applied Crystallography 44 (2011), S. 319-326.
319) T. Shapoval, H. Stopfel, S. Haindl, J. Engelmann, S. Inosov, B. Holzapfel, V. Neu, L. Schultz, *Quantitative assessment of pinning forces and magnetic penetration depth in NbN thin films from complementary magnetic force microscopy and transport measurements*, Physical Review B 83 (2011) Nr. 21, S. 214517/1-7.
320) A. Shariq, N. Mattern, *A study of phase separated Ni66Nb17Y17 metallic glass using atom probe tomography*, Ultramicroscopy 111 (2011), S. 1370-1374.

321) A.P. Shpak, A.G. Ilinskii, A.V. Marunyak, O.I. Slukhovskyy, Y.V. Lepeeva, A. Dekhtyar, I. Kaban, N. Mattern, J. Eckert, *Crystallization of Fe82Si2B16 and Fe82Si4B14 metallic glasses upon isothermal and non-isothermal annealing*, EPJ Web of Conferences 15 (2011), S. 1008/1-4.

322) O. Shuleshova, D. Holland-Moritz, A. Voss, W. Loeser, *In situ observations of solidification in TieAleTa alloys by synchrotron radiation*, Intermetallics 19 (2011) Nr. 5, S. 688-692.

323) N.B. Shustova, I.V. Kuvychko, D.V. Peryshkov, J.B. Whitaker, B.W. Larson, Y.-S. Chen, L. Dunsch, K. Seppelt, A.A. Popov, S.H. Strauss, O.V. Boltalina, *Chemical tailoring of fullerene acceptors: Synthesis, structures and electrochemical properties of perfluoroisopropylfullerenes*, Chemical Communications 47 (2011), S. 875-877.

324) N.B. Shustova, I.V. Kuvychko, A.A. Popov, M. von Delius, L. Dunsch, O.P. Anderson, A. Hirsch, S.H. Strauss, O.V. Boltalina, *Nitrogen directs multiple radical additions to the 9,9′-Bi-1-aza(C60-Ih)[5,6]fullerene: X-ray structure of 6,9,12,15,18-C59N(CF3)5*, Angewandte Chemie- International Edition 50 (2011) Nr. 24, S. 5537-5540.

325) N.B. Shustova, I.V. Kuvychko, A.A. Popov, M. von Delius, L. Dunsch, O.P. Anderson, A. Hirsch, S.H. Strauss, O.V. Boltalina, *Nitrogen directs multiple radical additions to the 9,9′-Bi-1-aza(C60-Ih)[5,6]fullerene: X-ray structure of 6,9,12,15,18-C59N(CF3)5*, Angewandte Chemie- German Edition 123 (2011) Nr. 24, S. 5651-5654.

326) N.B. Shustova, D.V. Peryshkov, I.V. Kuvychko, Y.-S. Chen, M.A. Mackey, C.E. Coumbe, D.T. Heaps, B.S. Confait, T. Heine, J.P. Phillips, S. Stevenson, L. Dunsch, A.A. Popov, S.H. Strauss, O.V. Boltalina, *Poly (perfluoroalkylation) of metallic nitride fullerenes reveals addition-pattern guidelines: Synthesis and characterization of a family of Sc3N@C80(CF3)n (n = 2-16) and their radical anions*, Journal of the American Chemical Society 133 (2011), S. 2672-2690.

327) G. Simha Martynkova, A. Sliva, M. Hundakova, K. Barabaszova, M. Valaskova, O. Guney, A. Bachmatiuk, M.H. Ruemmeli, *Carbonaceous nanoparticles prepared with help of silicate substrate and metal catalysts*, Advanced Science, Engineering and Medicine 3 (2011), S. 38-43.

328) Y. Skourski, M.D. Kuzmin, K.P. Skokov, A.V. Andreev, J. Wosnitza, *High-field magnetization of Ho2Fe17*, Physical Review B 83 (2011) Nr. 21, S. 214420/1-9.

329) E.P. Smirnova, A. Sotnikov, S. Ktitorov, N. Zaitseva, H. Schmidt, M. Weihnacht, *Acoustic properties of multiferroic BiFe03 over the temperature range 4.2–830 K*, European Physical Journal B 83 (2011), S. 39-45.

330) E.J. Smith, D. Makarov, S. Sanchez, V.M. Fomin, O.G. Schmidt, *Magnetic microhelix coil structures*, Physical Review Letters 107 (2011) Nr. 9, S. 97204/1-4.

331) E.J. Smith, D. Makarov, O.G. Schmidt, *Polymer delamination: towards unique three-dimensional microstructures*, Soft Matter 7 (2011), S. 11309-11313.

332) E.J. Smith, S. Schulze, S. Kiravittaya, Y. Mei, S. Sanchez, O.G. Schmidt, *Lab-in-a-tube: Detection of individual mouse cells for analysis in flexible split-wall microtube resonator sensors*, Nano Letters 11 (2011) Nr. 10, S. 4037-4042.

333) A.A. Solovev, S. Sanchez, Y. Mei, O.G. Schmidt, *Tunable catalytic tubular micro-pumps operating at low concentrations of hydrogen peroxidew*, Physical Chemistry Chemical Physics 13 (2011), S. 10131-10135.

334) A.A. Solovev, E.J. Smith, C.C. Bof Bufon, S. Sanchez, O.G. Schmidt, *Light-controlled propulsion of catalytic microengines*, Angewandte Chemie - International Edition 50 (2011) Nr. 46, S. 10875-10878.

335) K.K. Song, S. Pauly, Y. Zhang, P. Gargarella, R. Li, N.S. Barekar, U. Kuehn, M. Stoica, J. Eckert, *Strategy for pinpointing the formation of B2 CuZr in metastable CuZr-based shape memory alloys*, Acta Materialia 59 (2011), S. 6620-6630.

336) K.K. Song, S. Pauly, Y. Zhang, S. Scudino, P. Gargarella, K.B. Surreddi, U. Kuehn, J. Eckert, *Significant tensile ductility induced by cold rolling in Cu47.5Zr47.5Al5 bulk metallic glass*, Intermetallics 19 (2011), S. 1394-1398.

337) U. Stockert, M. Abdel-Hafiez, D.V. Evtushinsky, V.B. Zabolotnyy, A.U.B. Wolter, S. Wurmehl, I. Morozov, R. Klingeler, S.V. Borisenko, B. Buechner, *Specific heat and angle-resolved photoemission spectroscopy study of the superconducting gaps in LiFeAs*, Physical Review B 83 (2011) Nr. 22, S. 224512/1-5.

338) M. Stockmann, J. Naumann, J. Schumann, I. Moench, *Differential strain gauge: A sensor device for macro- and microsystems*, Strain - An International Journal for Experimental Mechanics 47 (2011), S. e104-e112.

339) M. Stoica, A. Bardos, S. Roth, L.K. Varga, L. Schultz, A. Lovas, J. Eckert, *Improved synthesis of bulk metallic glasses by current-assisted copper mold casting*, Advanced Engineering Materials 13 (2011) Nr. 1-2, S. 38-42.

340) M. Stoica, V. Kolesar, J. Bednarcic, S. Roth, H. Franz, J. Eckert, *Thermal stability and magnetic properties of partially Co-substituted (Fe71.2B24Y4.8)96Nb4 bulk metallic glasses*, Journal of Applied Physics 109 (2011) Nr. 5, S. 54901/1-6.

341) M. Stoica, R. Li, S. Roth, J. Eckert, G. Vaughan, A.R. Yavari, *[(Fe0.5Co0.5)0.75B0.20Si0.05]96Nb4 metallic glasses with small Cu additions*, Metallurgical and Materials Transactions A 42 (2011) Nr. 6, S. 1476-1480.

342) D. Stoyan, A. Wagner, H. Hermann, A. Elsner, *Statistical characterization of the pore space of random systems of hard spheres*, Journal of Non-Crystalline Solids 357 (2011) Nr. 6, S. 1508-1515.

343) A. Stoyanova, L. Hozoi, P. Fulde, H. Stoll, *Wave-function-based approach to quasiparticle bands: Insight into the electronic structure of c-ZnS*, Physical Review B 83 (2011) Nr. 20, S. 205119/1-17.

344) L. Straka, O. Heczko, H. Seiner, N. Lanska, J. Drahokoupil, A. Soroka, S. Faehler, H. Haenninen, A. Sozinov, *Highly mobile twinned interface in 10 M modulated Ni-Mn-Ga martensite: Analysis beyond the tetragonal approximation of lattice*, Acta Materialia 59 (2011), S. 7450-7463.

345) S. Strehle, S. Menzel, K. Wetzig, J.W. Bartha, *Microstructure of electroplated Cu(Ag) alloy thin films*, Thin Solid Films 519 (2011) Nr. 11, S. 3522-3529.

346) H.J. Su, J. Zhang, L. Liu, J. Eckert, H.Z. Fu, *Rapid growth and formation mechanism of ultrafine structural oxide eutectic ceramics by laser direct forming*, Applied Physics Letters 99 (2011) Nr. 22, S. 221913/1-3.

347) S. Sykora, P. Coleman, *Quasiparticle interference in an iron-based superconductor*, Physical Review B 84 (2011) Nr. 5, S. 54501/1-8.
348) J. Tan, Y. Zhang, M. Stoica, U. Kuehn, N. Mattern, F.S. Pan, J. Eckert, *Study of mechanical property and crystallization of a ZrCoAl bulk metallic glass*, Intermetallics 19 (2011) Nr. 4, S. 567-571.
349) J. Tan, Y. Zhang, B.A. Sun, M. Stoica, C.J. Li, K.K., Kuehn, U. Song, F.S. Pan, J. Eckert, *Correlation between internal states and plasticity in bulk metallic glass*, Applied Physics Letters 98 (2011) Nr. 15, S. 151906/1-3.
350) F. Tang, M. Frontzek, J. Dshemuchadse, T. Leisegang, M. Zschornak, R. Mietrach, J.-U. Hoffmann, W. Loeser, S. Gemming, D.C. Meyer, M. Loewenhaupt, *Crystallographic superstructure in R2PdSi3 compounds (R = heavy rare earth)*, Physical Review B 84 (2011) Nr. 10, S. 104105/1-16.
351) M. Taut, R. Xiao, *Ground state of graphene slabs in an external electric field*, Physical Review B 84 (2011) Nr. 23, S. 233404/1-3.
352) S. Thirupathaiah, E.D.L. Rienks, H.S. Jeevan, R. Ovsyannikov, E. Slooten, J. Kaas, E. van Heumen, S. de Jong, H.A. Duerr, K. Siemensmeyer, R. Follath, P. Gegenwart, M.S. Golden, J. Fink, *Dissimilarities between the electronic structure of chemically doped and chemically pressurized iron pnictides from an angle-resolved photoemission spectroscopy study*, Physical Review B 84 (2011) Nr. 1, S. 14531/1-7.
353) M. Toader, K. Knupfer, D.R.T. Zahn, M. Hietschold, *Initial growth of Lutetium(III) Bis-phthalocyanine on Ag(111) surface*, Journal of the American Chemical Society 133 (2011) Nr. 14, S. 5538-5544.
354) M. Toader, M. Knupfer, D.R.T. Zahn, M. Hietschold, *Initial growth at the F16CoPc/Ag(111) interface*, Surface Science 605 (2011) Nr. 15-16, S. 1507-1512.
355) J. Torrens-Serra, S. Venkataraman, M. Stoica, U. Kuehn, S. Roth, J. Eckert, *Non-isothermal kinetic analysis of the crystallization of metallic glasses using the master curve method*, Materials 4 (2011), S. 2231-2243.
356) K. Tschulik, C. Cierpka, A. Gebert, L. Schultz, C.J. Kaehler, M. Uhlemann, *In situ analysis of three-dimensional electrolyte convection evolving during the electrodeposition of copper in magnetic gradient fields*, Analytical Chemistry 83 (2011), S. 3275-3281.
357) K. Tschulik, R. Sueptitz, M. Uhlemann, L. Schultz, A. Gebert, *Electrodeposition of separated 3D metallic structures by pulse-reverse plating in magnetic gradient fields*, Electrochimica Acta 56 (2011), S. 5174-5177.
358) K. Tschulik, X. Yang, G. Mutschke, M. Uhlemann, K. Eckert, R. Sueptitz, L. Schultz, A. Gebert, *How to obtain structured metal deposits from diamagnetic ions in magnetic gradient fields?*, Electrochemistry Communications 13 (2011), S. 946-950.
359) E. van Heumen, J. Vuorinen, K. Koepernik, F. Massee, Y. Huang, M. Shi, J. Klei, J. Goedkoop, M. Lindroos, J. van den Brink, M.S. Golden, *Existence, character, and origin of surface-related bands in the high temperature iron pnictide superconductor BaFe2-xCoxAs2*, Physical Review Letters 106 (2011) Nr. 2, S. 27002/1-4.
360) J. van Wezel, R. Schuster, A. Koenig, M. Knupfer, J. van den Brink, H. Berger, B. Buechner, *Effect of charge order on the plasmon dispersion in transition-metal dichalcogenides*, Physical Review Letters 107 (2011) Nr. 17, S. 176404/1-5.
361) J.W.F. Venderbos, M. Daghofer, J. van den Brink, *Narrowing of topological bands due to electronic orbital degrees of freedom*, Physical Review Letters 107 (2011) Nr. 11, S. 116401/1-5.
362) J.W.F. Venderbos, M. Daghofer, J. van den Brink, S. Kumar, *Macroscopic degeneracy and emergent frustration in a honeycomb lattice magnet*, Physical Review Letters 107 (2011) Nr. 7, S. 76405/1-4.
363) F. Virot, R. Hayn, M. Richter, J. van den Brink, *Metacinnabar (-HgS): A strong 3D topological insulator with highly anisotropic surface states*, Physical Review Letters 106 (2011) Nr. 23, S. 236806/1-4.
364) E.S. Vlakhov, N. Kozlova, L.S. Lobanovskii, R. Wawryk, K.A. Nenkov, *High-magnetic-field study of magnetic and transport properties of hole-doped NdBaCo2O5+delta*, Physical Review B 84 (2011) Nr. 18, S. 184440/1-10.
365) S. Vock, Z. Sasvari, C. Bran, F. Rhein, U. Wolff, N.S. Kiselev, A.N. Bogdanov, L. Schultz, O. Hellwig, V. Neu, *Quantitative magnetic force microscopy study of the diameter evolution of bubble domains in a (Co/Pd)80 multilayer*, IEEE Transactions on Magnetics 47 (2011) Nr. 10, S. 2352-2355.
366) U. Vogl, A. Sass, F. Vewinger, M. Weitz, A. Solovev, Y. Mei, O.G. Schmidt, *Light confinement by a cylindrical metallic waveguide in a dense buffer-gas environment*, Physical Review A 83 (2011) Nr. 5, S. 53403/1-5.
367) M. Voronov, V. Hoffmann, W. Buscher, C. Engelhard, S.J. Ray, G.M. Hieftje, *Pressure waves generated in a Grimm-type pulsed glow discharge source and their influence on discharge parameters*, Journal of Analytical Atomic Spectrometry 505 (2011), S. 811-815.
368) T. Waechtler, S.-F. Ding, L. Hofmann, R. Mothes, Q. Xie, S. Oswald, C. Detavernier, S.E. Schulz, X.-P. Quc, H. Heinrich Lang, T. Gessner, *ALD-grown seed layers for electrochemical copper deposition integrated with different diffusion barrier systems*, Microelectronic Engineering 88 (2011), S. 684-689.
369) H. Wang, J. Luo, F. Schaeffel, M.H. Ruemmeli, A.D. Briggs, J.H. Warner, *Carbon nanotube nanoelectronic devices compatible with transmission electron microscopy*, Nanotechnology 22 (2011) Nr. 24, S. 245305/1-9.
370) W.-M. Wang, J.T. Zhang, A. Gebert, S. Roth, L. Schultz, *Casting vacuum effects on the precipitates and magnetic properties of Fe-based glassy alloys*, Journal of Non-Crystalline Solids 357 (2011) Nr. 7, S. 1657-1664.
371) Z.L. Wang, D.Y. Cong, Z.H. Nie, J. Gao, W. Liu, Y.D. Wang, *The suppression and recovery of martensitic transformation in a Ni–Co–Mn–In magnetic shape memory alloy*, Journal of Alloys and Compounds 511 (2011), S. 41-44.
372) H. Wilhelm, M. Baenitz, M. Schmidt, U.K. Roessler, A.A. Leonov, A.N. Bogdanov, *Precursor phenomena at the magnetic ordering of the cubic helimagnet FeGe*, Physical Review Letters 107 (2011) Nr. 12, S. 127203/1-5.
373) S.B. Wilkins, M.P.M. Dean, J. Fink, M. Huecker, J. Geck, V. Soltwisch, E. Schierle, E. Weschke, G. Gu, S. Uchida, N. Ichikawa, J.M. Tranquada, J.P. Hill, *Comparison of stripe modulations in La1.875Ba0.125CuO4 and La1.48Nd0.4Sr0.12CuO4*, Physical Review B 84 (2011) Nr. 19, S. 195101/1-6.
374) N. Wizent, G. Behr, W. Loeser, B. Buechner, R. Klingeler, *Challenges in the crystal growth of Li2CuO2 and LiMnPO4*, Journal of Crystal Growth 318 (2011) Nr. 1, S. 995-999.

375) K. Wohlfeld, M. Daghofer, S. Nishimoto, G. Khaliullin, J. van den Brink, *Intrinsic coupling of orbital excitations to spin fluctuations in mott insulators*, Physical Review Letters 107 (2011) Nr. 14, S. 147201/1-5.

376) K. Wohlfeld, M. Daghofer, A.M. Oles, *Spin-orbital physics for p orbitals in alkali RO2 hyperoxides: Generalization of the Goodenough-Kanamori rules*, epl 93 (2011) Nr. 2, S. 27001/1-6.

377) H. Wojcik, U. Merkel, A. Jahn, K. Richter, M. Junige, C. Klein, J. Gluch, M. Albert, F. Munnik, C. Wenzel, J.W. Bartha, *Comparison of PVD, PECVD & PEALD Ru(-C) films as Cu diffusion barriers by means of bias temperature stress measurements*, Microelectronic Engineering 88 (2011), S. 641-645.

378) M. Wolf, C. Patschureck, R. Schaefer, I. Moench, L. Schultz, J. McCord, *Array anisotropy in structured thin film arrays:Influence on the magnetodynamics*, Journal of Magnetism and Magnetic Materials 323 (2011) Nr. 12, S. 1703-1707.

379) F. Wolny, Y. Obukhov, T. Muehl, U. Weissker, S. Philippi, A. Leonhardt, P. Banerjee, A. Reed, G. Xiang, R. Adur, I. Lee, A.J. Hauser, F.Y. Yang, D.V. Pelekhov, B. Buechner, P.C. Hammel, *Quantitative magnetic force microscopy on permalloy dots using an iron filled carbon nanotube probe*, Ultramicroscopy 111 (2011) Nr. 8, S. 1360-1365.

380) L. Wondraczek, J.C. Mauro, J. Eckert, U. Kuehn, J. Horbach, J. Deubener, T. Rouxel, *Towards ultrastrong glasses*, Advanced Materials 23 (2011) Nr. 39, S. 4578-4586.

381) T.G. Woodcock, O. Gutfleisch, *Multi-phase EBSD mapping and local texture analysis in NdFeB sintered magnets*, Acta Materialia 59 (2011) Nr. 2, S. 1026-1036.

382) T.G. Woodcock, J. Wright, N. Scheerbaum, J. Liu, O. Gutfleisch, *The texture of Nd oxide grains in Nd-Fe-B sintered magnets studied by synchrotron radiation*, Journal of Applied Physics 110 (2011) Nr. 2, S. 26103/1-3.

383) S. Wurmehl, P.J. Jacobs, J.T. Kohlhepp, H.J.M. Swagten, B. Koopmans, S. Maat, M.J. Carey, J.R. Childress, *Local formation of a Heusler structure in CoFe–Al alloys*, Applied Physics Letters 98 (2011) Nr. 1, S. 12506/1-3.

384) R. Xiao, F. Tasnadi, K. Koepernik, J.W.F. Venderbos, M. Richter, M. Taut, *Density functional investigation of rhombohedral stacks of graphene: Topological surface states, nonlinear dielectric response, and bulk limit*, Physical Review B 84 (2011) Nr. 16, S. 165404/1-15.

385) W. Xu, R.B. Figueiredo, X. Wu, S. Pauly, M. Stoica, J. Eckert, T.G. Langdon, K. Xia, *Intrinsically ductile failure in a nanocrystalline beta titanium alloy*, Advanced Engineering Materials 13 (2011) Nr. 12, S. 1108-1113.

386) Y. Xu, M. Frontzek, I. Mazilu, W. Loeser, G. Behr, B. Buechner, L. Liu, *Floating zone crystal growth of selected R2PdSi3 ternary silicides*, Journal of Crystal Growth 318 (2011), S. 942-946.

387) Y. Xu, L. Liu, W. Loeser, B.M. Ge, *Precipitates identification in R2PdSi3 (R= Pr, Tb and Gd) single crystal growth*, Transactions of Nonferrous Metals Society of China 21 (2011), S. 2421-2425.

388) Y. Xu, W. Loeser, L. Liu, B. Buechner, *Solidification and crystal growth of binary Tb5Si3 intermetallics*, Journal of Crystal Growth 321 (2011), S. 45-49.

389) Y. Xu, W. Loeser, F. Tang, C.G.F. Blum, L. Liu, B. Buechner, *Crystal growth of the intermetallic compound Nd2PdSi3*, Crystal Research and Technology 46 (2011) Nr. 2, S. 135-139.

390) D. Yakhvarov, E. Trofimova, O. Sinyashin, O. Kataeva, Y. Budnikova, P. Loennecke, E. Hey-Hawkins, A. Petr, Y. Krupskaya, V. Kataev, R. Klingeler, B. Buechner, *New dinuclear nickel(II) complexes: Synthesis, structure, electrochemical, and magnetic properties*, Inorganic Chemistry 50 (2011), S. 4553-4558.

391) K. Youssef, M. Sakaliyska, H. Bahmanpour, R. Scattergood, C. Koch, *Effect of stacking fault energy on mechanical behavior of bulk nanocrystalline Cu and Cu alloys*, Acta Materialia 59 (2011) Nr. 14, S. 5758-5764.

392) O. Zaharko, N.B. Christensen, A. Cervellino, V. Tsurkan, A. Maljuk, U. Stuhr, C. Niedermayer, F. Yokaichiya, D.N. Argyriou, M. Boehm, A. Loidl, *Spin liquid in a single crystal of the frustrated diamond lattice antiferromagnet CoAl2O4*, Physical Review B 84 (2011) Nr. 9, S. 94403/1-8.

393) G.S. Zakharova, V.L. Volkov, C. Taeschner, I. Hellmann, R. Klingeler, A. Leonhardt, B. Buechner, *Synthesis, characterization and magnetic properties of hexagonal (V0)0.09V0.18Mo0.82O3·0.54H2O microrods*, Materials Letters 65 (2011) Nr. 3, S. 579-582.

394) M. Zalibera, P. Rapta, G. Gescheidt, J.B. Christensen, O. Hammerich, L. Dunsch, *Spectroelectrochemistry of dendrimers: The radical cations of low-generation PAMAM-like dendrimers with a 1,4-phenylenediamine core as studied by electron spin resonance (ESR)/UV-Vis NIR spectroelectrochemistry*, Journal of Physical Chemistry C 115 (2011) Nr. 10, S. 3942-3948.

395) J.J. Zhang, A. Rastelli, O.G. Schmidt, G. Bauer, *Role of the wetting layer for the SiGe Stranski–Krastanow island growth on planar and pit-patterned substrates*, Semiconductor Science and Technology 26 (2011) Nr. 1, S. 14028/1-5.

396) L.C. Zhang, D. Klemm, J. Eckert, Y.L. Hao, T.B. Sercombe, *Manufacture by selective laser melting and mechanical behavior of a biomedical Ti–24Nb–4Zr–8Sn alloy*, Scripta Materialia 65 (2011) Nr. 1, S. 21-24.

397) Y. Zhang, N. Mattern, J. Eckert, *Molecular dynamic simulation study of the structural anisotropy in Cu50Zr50 and Cu64.5Zr35.5 metallic glasses induced by static uniaxial loading within the elastic regime*, Journal of Alloys and Compounds 509 (2011) Nr. Suppl. 1, S. S74-S77.

398) Y. Zhang, N. Mattern, J. Eckert, *Atomic structure and transport properties of Cu50Zr45Al5 metallic liquids and glasses: Molecular dynamics simulations*, Journal of Applied Physics 110 (2011) Nr. 9, S. 93506/1-8.

399) Y. Zhang, N. Mattern, J. Eckert, *Effect of uniaxial loading on the structural anisotropy and the dynamics of atoms of Cu50Zr50 metallic glasses within the elastic regime studied by molecular dynamics simulation*, Acta Materialia 59 (2011), S. 4303-4313.

400) F. Zhu, M. Grobosch, U. Treske, L. Huang, W. Chen, J. Yang, D. Yan, M. Knupfer, *Hole transparent and hole blocking transport in single-crystal-like organic heterojunction: When rods hold up disks*, Applied Materials and Interfaces 3 (2011) Nr. 7, S. 2195-2199.

401) F. Zhu, M. Grobosch, U. Treske, M. Knupfer, L. Huang, S. Ji, D. Yan, *Interfacial energy level bending in a crystalline p/p-type organic heterostructure*, Applied Physics Letters 98 (2011) Nr. 20, S. 203303/1-3.

Contributions to conference proceedings and monographs

1) A. Bachmatiuk, F. Boerrnert, I. Ibrahim, B. Buechner, M.H. Ruemmeli, *On the carbo thermal reduction of silica for carbon nanofibre formation via CVD*, in: Fundamentals of Low-Dimensional Carbon Nanomaterials, MRS Proceedings, John J. Boeckl (ed.); 1284: Mark Ruemmeli, Weijie Lu and Jamie Warner (eds.), 214 S., MRS 2011, 1284, 19- (2011).
2) S.V. Biryukov, H. Schmidt, M. Weihnacht, *Single-mode ring waveguide resonator on SAW*, 2010 IEEE International Ultrasonics Symposium, in: Proceedings, 2099-2102 (2010).
3) F. Boerrnert, A. Bachmatiuk, B. Buechner, M.H. Ruemmeli, *Low-voltage aberration-corrected transmission electron microscopy: Progressing carbon nanostructures*, in: Microscopy: Science, Technology, Applications and Education, A. Mendez-Vilas and J. Diaz (eds.), Formatex, 2010, Vol. 1-3, 1846-1852 (2011).
4) F. Boerrnert, A. Bachmatiuk, S. Gorontla, J.H. Warner, B. Buechner, M.H. Ruemmeli, *In-situ observations of restructuring carbon nanotubes via low-volatge aberration-corrected transmission electron microscopy*, in: Fundamentals of Low-Dimensional Carbon Nanomaterials, MRS Proceedings, John J. Boeckl (ed.) ; 1284: Mark Ruemmeli, Weijie Lu and Jamie Warner (eds.), 214 S., MRS 2011, 1284, 101-105 (2011).
5) R. Bruenig, H. Schmidt, G. Guhr, M. Weihnacht, *Complex loadings on thickness shear mode resonators*, 2010 IEEE International Ultrasonics Symposium, in: Proceedings, 1886-1889 (2010).
6) J. Cwik, T. Palewski, J. Warchulska, K. Nenkov, *Magnetic properties and specitic heat of laves phase Tb1-xScxNi2(x=0.3,0.4 and 0.5) solid solutions*, 3rd International Conference on Ferromagnetic Shape Memory Alloys (ICFSMA 2011). Dresden, 18.-22.7.11, in: Proceedings (2011).
7) A. Darinskii, M. Weihnacht, H. Schmidt, *Symmetry properties of acoustic fields in piezoelectrics and their implementation in FEM simulations of the SAW propagation*, 2010 IEEE International Ultrasonics Symposium, in: Proceedings, 1894-1897 (2010).
8) G. Doerfel, *Vom geschichteten zum unsichtbaren elektrischen Licht. Der Mathematiker, Physiker und Erzieher Paul Victor Langer (1851-1925)*, in: Zeitschrift fuer Thueringische Geschichte, 65, 209-227 (2011).
9) G. Doerfel, *Im Spannungsfeld der fruehen Gluehlampentechnik - Der Geissler-Schueler Ludwig Karl Boehm (1859-?)*, in: Jahrbuch 2011 des Hennebergisch-Fraenkischen Geschichtsvereins, Kloster Vessra, Meiningen, Muennerstadt, 2011, 225-248 (2011).
10) J. Eckert, S. Scudino, M. Stoica, S. Kenzari, M. Sales, *Mechanical engineering properties of CMAs*, in: Complex metallic alloys : Fundamentals and applications, Dubois, Jean-Marie (ed.), Weinheim : Wiley-VCH-Verl., 273-316 (2011).
11) J. Freudenberger, *High strength copper-based conductor materials*, in: Copper Alloys: Preparation, properties and applications, Nova Science Publisher, Inc., 2011, Cap. 9, 160-211 (2011).
12) A. Gebert, *Corrosion of magnesium (Mg)-based bulk metallic glasses*, in: Corrosion of Magnesium Alloys, G.L. Song (ed.), Woodhead Publishing Limited, 207- (2011).
13) G. Guhr, S. Gehrisch, R. Bruenig, H. Schmidt, G. Siegert, M. Weihnacht, *Novel sensor combining impedance spectroscopy and surface acoustic waves to detect blood coagulation time and hematocrit value*, IEEE Sensors 2011, Limerick/ Ireland, 28.-31.10.11, in: Proceedings, 1413-1416 (2011).
14) D. Haase, S. Hampel, K. Kraemer, D. Kunze, A. Taylor, M. Arlt, J. Thomas, S. Oswald, M. Ritschel, R. Klingeler, A. Leonhardt, B. Buechner, *Carbon nanotubes filled with carboplatin: Towards carbon nanotube-supported delivery of chemotherapeutic agents*, in: Carbon Nanotubes for Biomedical Applications, R. Klingeler, R.B. Sim (eds.), Springer-Verl., 2011, 247-258 (2011).
15) R. Hermann, H. Hermann, M. Calin, G. Gerbeth, B. Buechner, J. Eckert, *Magnetic field controlled Ti-Nb single crystal growth and determination of elastic properties*, 8th International Pamir Conference on Fundamental and Applied MHD, Borgo/ Corsica, France, 5.-9.9.11, in: Proceedings, CD (2011).
16) V. Hoffmann, D. Klemm, V. Efimova, C. Venzago, A.A. Rockett, T. Wirth, T. Nunney, C.A. Kaufmann, R. Caballo, *Elemental distribution profiling of thin films for solar cells*, in: Advanced Characterization Techniques for Thin Film Solar Cells, Daniel Abou-Ras, Thomas Kirchartz, Uwe Rau (eds.) Weinheim: Wiley-VCH, 2011, Capter 16, 411-448 (2011).
17) V. Hoffmann, A. Quentmeier, *Glow discharge optical emission spectroscopy (GD-OES)*, in: Surface and Thin Film Analysis: A Compendium of Principles, Instrumentation, and Applications. G. Friedbacher, H. Bubert (eds.), 2. compl. rev. and enl. Ed. 2011, Weinheim: Wiley-VCH, 534 S., 329-342 (2011).
18) I. Kaban, P. Jovari, T. Petkova, P. Petkov, A. Stoilova, B. Beuneu, B. Hoyer, N. Mattern, J. Eckert, *Atomic structure of (Ge0.2Se0.8)85B15 and (Ge0.2Se0.8)85In15 glasses*, NATO Summer School on Nanotechnological Basis for Advanced Sensors, Sozopol/ Bulgarien, 30.5.-11.6.10, in: Nanotechnological Basis for Advanced Sensors, Johann Peter Reithmaier, Perica Paunovic, Wilhelm Kulisch, Cyril Popov, Plamen Petkov (eds.), NATO Science for Peace and Security Series B: Physics and Biophysics, Part 6, Dordrecht: Springer., 195-202 (2011).
19) I. Kaban, P. Jovari, T. Petkova, P. Petkov, A. Stoilova, B. Beuneu, W. Hoyer, N. Mattern, J. Eckert, *Atomic structure of (Ge0.2Se0.8)85B15 and (Ge0.2Se0.8)85In15 glasses*, in: Nanotechnological Basis for Advanced Sensors, Series: NATO Science for Peace and Security Series B: Physics and Biophysics, Reithmaier, J.P.; Paunovic, P.; Kulisch, W.; Popov, C.; Petkov, P. (eds.), Dordrecht: Springer Netherlands, 2011, Part 6, 545- (2011).
20) S. Kiravittaya, A. Rastelli, O.G. Schmidt, *Quantum dot crystals: Growth and characterization*, in: Encyclopedia of Nanoscience and Nanotechnology, H.S. Nalwa (ed.), American Scientific Publishers, 2011, 22, 23-32 (2011).
21) L. Loeber, D. Klemm, U. Kuehn, J. Eckert, *Rapid manufacturing of cellular structures of steel or titaniumaluminide*, in: Light Metals Technology V, H. Dieringa, N. Hort, K.U. Kainer (eds.), Materials Science Forum, 690, 103- (2011).
22) M.U. Lutz, K. Lipert, Y. Krupskaya, S. Bahr, A. Wolter, A.A. El-Gendy, S. Hampel, A. Leonhardt, A. Taylor, K. Kraemer, B. Buechner, R. Klingeler, *Feasibility of magnetically functionalised carbon nanotubes for biological applications: From fundamental properties of individual nanomagnets to nanoscaled heaters and temperature sensors*, in: Carbon Nanotubes for Biomedical Applications, R. Klingeler, R.B. Sim (eds.), Springer-Verl., 2011, 97-124 (2011).

23) J. Lyubina, B. Rellinghaus, O. Gutfleisch, M. Albrecht, *Structure and magnetic properties of L10-ordered Fe-Pt alloys and nanoparticles*, in: Handbook of Magnetic Materials, K. H. J. Buschow (ed.), 19, 291-407 (2011).
24) G. Martin, H. Schmidt, G. Wall, *Natural SPUDT behavior of YZ LiNbO3*, 2010 IEEE International Ultrasonics Symposium, in: Proceedings, 189-192 (2010).
25) E. Nazarova, K. Nenkov, A. Zaleski, K. Buchkov, A. Zaheriev, *Investigantions of the overdoped state in polycrystalline R1-xCaxBA2Cu3O7-delta samples (R=Y, Eu, GD, ER)*, in: Superconductivity: Theory, Materials and Applications, V.R. Romanovskii (ed.), NOVA-Science-Publishers, 2011, Chapter 5, 1-34 (2011).
26) F. Pezzoli, C. Deneke, O.G. Schmidt, *Strain engineering of SiGe micro and nanostructures*, in: SiGe Nanostructures: Materials Science, Technology and Applications, Y. Shiraki, N. Usami (eds.), Woodhead Publishing Lt., 2011, 247-295 (2011).
27) M. Poetschke, S. Roth, U. Gaitzsch, C. Huerrich, A. Boehm, L. Schultz, *Polycrystalline Ni-Mn-Ga as a potential material for magnetically driven actuators*, in: Materials Science Forum, 684, 129-137 (2011).
28) W.T. Ramsay, M. Bechu, V.A. Bolanos Quinones, Y. Mei, O.G. Schmidt, L. Paterson, *Triple beam optical trap for microsyringe construction*, SPIE 2011, Optics and Photonics, San Diego/ USA, 21.-25.8.2011, in: Proceedings, 8097, 809708/1-9 (2011).
29) C.G. Rocha, M.H. Ruemmeli, I. Ibrahim, H. Sevincli, F. Boerrnert, J. Kunstmann, A. Bachmatiuk, M. Poetschke, W. Li, S.A.M. Makharza, S. Roche, B. Buechner, G. Cuniberti, *Tailoring the physical properties of graphene*, in: Graphene: Synthesis and Applications, W. Choi and J.-W. Lee (eds.), CRC Press 2011, S.... (2011).
30) M.H. Ruemmeli, A. Bachmatiuk, A. Dianat, A. Scott, F. Boerrnert, I. Ibrahim, S. Zhang, E. Borowiak-Palen, G. Cuniberti, B. Buechner, *Low temperature CVD growth of graphene nano-flakes directly on high K dielectrics*, in: Fundamentals of Low-Dimensional Carbon Nanomaterials, MRS Proceedings, John J. Boeckl (ed.) ; 1284: Mark Ruemmeli, Weijie Lu and Jamie Warner (eds.), 214 S., MRS 2011, 1284, 19- (2011).
31) H. Schmidt, X. Kong, C. Deneke, O.G. Schmidt, *Dielectrophoretic manipulation of rolled-up microtubes by surface acoustic waves*, The 6th IEEE International Conference on Nano/Micro Engineered and Molecular Systems, Kaohsiung/ Taiwan, 20.-23.2.11, in: Proceedings, 1251-1254 (2011).
32) S. Scudino, J. Eckert, *Nanocrystalline metals and alloys prepared by mechanical attrition*, in: Nanostructured Metals and Alloys: Processing, Microstructure, Mechanical Properties and Applications. S. H. Whang (ed.) Cambridge: Woodhead Publ., 2011, Capter 3, 59-84 (2011).
33) E.J. Smith, Y. Mei, O.G. Schmidt, *Optical components for lab-in-a-tube systems*, in: Micro- and Nanotechnology Sensors, Systems, and Applications III, Thomas George, M. Saif Islam, Achyut K. Dutta (eds.), Proceedings of SPIE, 8031, 80310R/1-8 (2011).
34) A. Szytula, S. Baran, M. Balanda, L. Gondek, A. Hoser, K. Nenkov, B. Penc, *Nature of the low temperature magnetic phase transitions in ternary RT2X2(X=Si,Ge) intermetallic*, ICEC 23 - ICMC 2010, Wroclaw/ Poland, 19.-23.7.10, in: Proceedings, 1155-1159 (2011).

35) M. Weihnacht, A. Sotnikov, H. Schmidt, E. Smirnova, S. Ktitorov, *Acoustic properties of multiferroics PbFe1/2Ta1/2O3 and BiFeO3 at Neel temperature*, Applications of Ferroelectrics (ISAF/PFM)2011, International Symposium on Piezoresponse Force Microscopy and Nanoscale Phenomena in Polar Materials, Vancuver/ Canada, 24.-27.7.11, in: Proceedings, 1-4 (2011).
36) L.C. Zhang, M. Calin, J. Eckert, *High-strength titanium base alloys with multiple length-scale microstructure*, in: Advances in Mechanical Engineering Research, Vol. 2, David E. Malach (ed.), Nova Science Publishers 2011, 233-251 (2011).

Invited Talks 2011

1) A. Bachmatiuk, *Synthesizing carbon nanotubes and graphene from oxide catalysts*, Invited Talk, Merida, Yucatan/ Mexico, 9.5.11 (2011).
2) A. Bachmatiuk, *Early steps in understanding irreducible and reducible oxides as catalysts for carbon nanotubes and graphene*, Invited Talk, Wright-Patterson Air Force Base, Dayton/ USA, 25.5.11 (2011).
3) A. Bachmatiuk, *Synthesizing carbon nanotubes and graphene from oxide catalysts*, Conference NanoOstrava 2011, Ostrava/ Czech Republic, 27.-29.4.11 (2011).
4) A. Bachmatiuk, *Understanding irreducible and reducible oxides as catalysts for carbon nanotubes and graphene formation*, 7th International Conference Diffusion in Solids and Liquids, Algarve/ Portugal, 26.-30.6.11 (2011).
5) S.H. Baek, *Pseudogap-like phase in Co-doped CaFe2As2 revealed by 75As NQR*, Joint International Symposium on Heavy Electrons, SKKU Samsung Library, Sungkyunkwan University, Suwon/ Sued-Korea , 16.-18.8.11 (2011).
6) S. Bahr, *Micro-Hall sensors for ESR detection*, Workshop „Advanced EPR for Material and Solar Energy Research“, Berlin, 13.-14.10.11 (2011).
7) C.C. Bof Bufon, *3-dimensional electronics with self-rolled nanomembranes*, Seminar, Laboratorio Nacional de Nanotecnologia (LNNano), Campinas/ Brazil, 6.10.11 (2011).
8) C.C. Bof Bufon, *Fabrication and characterization of hybrid devices based on organic/inorganic nanomembranes*, Seminar, Physics Department, Universidade Federal de Sao Carlos/ Brazil, 4.10.11 (2011).
9) C.C. Bof Bufon, *3-dimensional devices based on hybrid strained nanomembranes*, Colloquium, College of Nanoscale Science and Engineering, Albany, NY/ USA, 29.4.11 (2011).
10) S. Borisenko, *Superconductivity and magnetism in iron pnictides*, Workshop on Angle-Resolved Photoemission Spectroscopy (ARPES), Diamond Light Source, Oxfordshire/ UK, 8.-9.6.11 (2011).
11) S. Borisenko, *Magnetism and superconductivity as seen by ARPES*, FAPESP School at Brazilian Synchrotron Light Laboratory, Campinas/ Brazil, 18.-22.1.11 (2011).

12) S. Borisenko, *ARPES - a tool to study nature*, FAPESP School at Brazilian Synchrotron Light Laboratory, Campinas/ Brazil, 18.-22.1.11 (2011).
13) S. Borisenko, *ARPES on density waves compounds*, Inernational Research School and Workshop on Electronic Crystals, ECRYS'11, Cargese/ France, 15.-27.8.11 (2011).
14) S. Borisenko, *Superconductivity and magnetism in iron pnictide*, Superconductivity 100 Years later: A computational Approach, Hotel Porto Conte, Alghero/ Italy, 15.-18.9.11 (2011).
15) S. Borisenko, *Superconductivity and magnetism in iron pnictides*, SUPERSTRIPES 2011, Rome/ Italy, 10.-17.7.11 (2011).
16) S. Borisenko, *New ARPES facility at BESSY*, Workshop on Novel Trends in Photoemission, ALS user's Meeting 2011, Lawrence Berkeley National Laboratory, Berkeley/ USA, 3.-6.10.11 (2011).
17) S. Borisenko, *Photoemission in new superconductors*, V Reunion Nacional de la Asociacion de Usuarios de Radiacion Sincrotron de Espana (AUSE), Valencia/ Spain, 6.-9.9.11 (2011).
18) S. Borisenko, *Magnetism and superconductivity in 111 iron pnictides*, APS March Meeting, Dallas/ USA, 21.-25.3.11 (2011).
19) S. Borisenko, *Necessary conditions for superconductivity and magnetism in iron pnictides and chalcogenides*, CORPES 2011, Berkeley/ USA, 18.-22.7.11 (2011).
20) S. Borisenko, *ARPES studies of CDW compounds*, Condensed Matter Physics Department Seminar, University of Geneva/ Switzerland, 29.3.11 (2011).
21) B. Buechner, *Phase diagram of Fe based superconductors*, MISM 2011, Moskau/ Russia, 21.-25.8.11 (2011).
22) B. Buechner, *Phase diagram of Fe based superconductors*, Contrasting Superconductivity of Pnictides and Cuprates, Aspen Center for Physics, Winter Conference 2011, Aspen/ USA, 22.-28.1.11 (2011).
23) B. Buechner, *Magnetism and superconductivity in iron pnictides*, Ringberg Symposium on High Temperature Superconductivity, MPI-FKF, Stuttgart, 16.-19.5.11 (2011).
24) B. Buechner, *Ferromagnetism and superconductivity in LiFeAs*, Invited Talk, Spin Physics, Spin Chemistry, and Spin Technology, Kazan/ Russia, 1.-2.11.11 (2011).
25) B. Buechner, *Phase diagram of Fe based superconductors*, EMRS Fall Meeting, Warschau/ Polen, 19.-22.9.11 (2011).
26) B. Buechner, *The iron age of high temperature superconductivity*, Kolloquiumsvortrag, RWTH Aachen, 30.5.11 (2011).
27) B. Buechner, *Intrinsic inhomogenities in spin correlated solids as revealed by magnetic resonance*, Invited Talk, Spin Physics, Spin Chemistry, and Spin Technology, Kazan/ Russia, 1.-2.11.11 (2011).
28) B. Buechner, *Phase diagram of Fe based superconductors*, 100th Anniversary of Superconductivity: Hot Topics and Future Directions, Lorentz Center Leiden/ The Netherlands, 4.-8.4.11 (2011).
29) M. Calin, *More women on scientific boards - why does it matter?*, DIVERSITY Workshop „Woman in European Materials Science Research Institutes", Corfu/ Greece, 19.-20.5.11 (2011).
30) M. Calin, N. Zheng, A. Helth, F. Gostin, A. Gebert, J. Eckert, *Ti-based metallic glasses and composites with improved mechanical properties*, Colloquium, Dipartimento di Chimica I.F.M., Universita di Torino, Torino/ Italy, 23.11.11 (2011).
31) M. Calin, N. Zheng, A. Helth, L.C. Zhang, A. Gebert, J. Eckert, *Phase transformations and mechanical behavior of glassy/nano-structured Ti-based alloys and their composites*, International Conference on Advanced Materials and Structures, Timisoara/ Romania, 27.-28.10.11 (2011).
32) P. Costa, U. Gautam, Y. Bando, D. Golberg, *Joule heating dynamics and electrical delivery in a hybrid carbon nanotube interconnect*, Carbon 2011 International Conference, Shanghai/ China, 24.-29.7.11 (2011).
33) M. Daghofer, *Multi-orbital models for Pnictide superconductors*, Seminar, Universitaet Augsburg, 3.5.11 (2011).
34) M. Daghofer, *Spin-polarized semiconductor induced by magnetic impurities in graphene*, APS March Meeting, Dallas/ USA, 25.3.11 (2011).
35) M. Daghofer, *Spontaneous fractional quantum-hall state in strongly correlated multiorbital systems* , Seminar, Universitaet Wuerzburg, 17.11.11 (2011).
36) M. Daghofer, *Multi-orbital models for pnictide superconductors*, Seminar, Jagiellonen- Universitaet Krakau/ Poland, 1.7.11 (2011).
37) M. Daghofer, *Multi-orbital models for Pnictide superconductors*, EMRS Fall Meeting 2011, Warschau/ Poland, 19.-21.9.2011 (2011).
38) N.M. Demspey, Y. Zhang, D. Givrod, T.G. Woodcock, O. Gutfleisch, K. Hono, *NdFeB thick films as model high performance magnets*, Intermag Conference 2011, Symposium: High Performance Motors and Magnetic Materials, Taipeh/ Taiwan, 29.5.11 (2011).
39) A. Diestel, A. Backen, S. Kauffmann-Weiss, V. Neu, L. Schultz, S. Faehler, *Martensitic and magnetic microstructure of epitaxial Ni-Mn-Ga films*, Shape Memory Seminar, Ostre/ Tschechische Republik, 1.-2.12.11 (2011).
40) K. Doerr, *Strain control of ferroic properties and switching in oxide films*, 471. WEH-Seminar, Bad Honnef, 6.1.11 (2011).
41) K. Doerr, *Strain control of electronic states in epitaxial oxide films*, Seminarvortrag, Universitaet zu Koeln, 21.1.11 (2011).
42) L. Dunsch, *Endohedrale Elektrochemie*, GOECh-Kolloquium, J. Kepler-Universitaet Linz/ Oesterreich, 10.5.11 (2011).
43) L. Dunsch, S. Yang, L. Zhang, A. Svitova, A. Popov, *Endohedral electrochemistry: New directions in metal nitride cluster fullerenes*, 219. ECS Meeting, Montreal/ Kanada, 1.-5.5.11 (2011).
44) J. Eckert, *Phase formation and microstructure development in multicomponent alloys*, Hauptvortrag im Rahmen der Fruehjahrs-tagung der Sektion Kondensierte Materie (SKM) der DPG, Symposium on „Heterogeneous Nucleation and Microstructure Formation: Steps towards a System- and Scale-bridging Understanding", Dresden, 17.3.11 (2011).
45) J. Eckert, *The role of heterogeneity for tailoring the mechanical properties of advanced metallic materials*, 2nd Symposium for the Global Research Laboratory (GRL) Program of Korea, Seoul/ Korea, 22.2.11 (2011).
46) J. Eckert, *Hybrid nanostructured materials for structural and functional applications*, 18th International Symposium on Metastable, Amorphous and Nanostructured Materials, (ISMANAM 2011), Gijon/ Spanien, 28.6.11 (2011).

47) J. Eckert, *Correlation between structure and deformation behavior in glassy materials*, 8th International Conference on Bulk Metallic Glasses (BMG VIII), Hong Kong/ PR China, 16.5.11 (2011).
48) J. Eckert, *Ti-based bulk metallic glasses and composites for structural and functional applications*, TMS Annual Meeting and Exhibition, Symposium „Bulk Metallic Glasses (VIII)", San Diego/ USA, 3.3.11 (2011).
49) J. Eckert, *Ways to improve the plasticity of bulk metallic glasses*, 2011 Taiwan Tech International Workshop on Metallic Glasses, Taiwan University of Science and Technology, Taipei/ Taiwan, 23.5.11 (2011).
50) J. Eckert, *Ti-base single- and multi-phase alloys for high strength applications*, Global Research Laboratory Germany - Korea Workshop on Bulk Metallic Glass and Nanostructured Materials, Lisbon/ Portugal, 25.8.11 (2011).
51) J. Eckert, *Present understanding of the mechanical properties of metallic glasses*, Kick-Off-Meeting of the Special Research Area 1594 „Topological Engineering of Ultrastrong Glasses" of the German Science Foundation (DFG), Erlangen, 4.10.11 (2011).
52) J. Eckert, *Development of bulk metallic glasses and composites with high plasticity*, Shanghai University, School of Materials Science and Engineering, Institute of Materials, Shanghai/ P.R. China, 13.5.11 (2011).
53) J. Eckert, *Designing ductile and tough bulk metallic glasses and composites*, 14th International Conference on Rapidly Quenched and Metastable Materials, Salvador/ Brasil, 2.9.11 (2011).
54) J. Eckert, A. Gebert, U. Kuehn, *Rare metal related issues in Germany*, 1. International Workshop on Rare Metals, KITECH, KIRAM, Incheon/ Korea, 18.-19.4.11 (2011).
55) D. Evtushinsky, V. Zabolotnyy, A. Kordyuk, T. Kim, B. Buechner, S. Borisenko, *Prerequisites and consequences of superconductivity in iron-based high temperature superconductors from ARPES*, Study of Matter at Extreme Conditions, SMEC2011, Miami/ USA, 27.3.-1.4.11 (2011).
56) S. Faehler, *Playing lego with martensite*, Institutsseminar Elektronische Festkoerpereigenschaften, Institut fuer Festkoerperphysik, TU Dresden, 11.1.11 (2011).
57) S. Faehler, *Modulated martensite: Why it forms and why it deforms easily*, TMS Spring Meeting, San Diego/USA, 27.3.-3.4.11 (2011).
58) S. Faehler, *Magnetische Formgedaechtnislegierungen: Vom Funktionsprinzip zu neuartigen Mikroaktoren*, Kolloquium Werkstofftechnik, TU Ilmenau, 10.11.11 (2011).
59) S. Faehler, *Magnetic shape memory alloy films and nanowires*, SFB459- The Final Workshop, Ruhr-Universitaet Bochum, 14.-16.9.11 (2011).
60) S. Faehler, *Playing lego with martensite*, ICOMAT, Osaka/ Japan, 4.-9.9.11 (2011).
61) J. Fink, *Stripes in high-Tc superconductors as detected by resonant soft X-ray scattering*, Seminarvortrag ALBA Synchrotron Light Source, Barcelona/ Spain, 23.6.11 (2011).
62) J. Fink, *Angle-resolved photoemission spectroscopy (ARPES)for many-body properties of solids*, Seminarvortrag ALBA Synchrotron Light Source, Barcelona/ Spain, 22.6.11 (2011).
63) J. Fink, *Angle-resolved photoemission spectroscopy (ARPES)for many-body properties of solids*, Festkoerperkolloquium, TU Muenchen, 5.5.11 (2011).
64) J. Fink, *Many-body interaction of charge carriers in solids as studied by ARPES*, Seminarvortrag, Jagiellonian University, Krakau/ Polen, 8.7.11 (2011).
65) J. Fink, *Angle-resolved photoemission, a spectroscopy for many-body properties of solids*, Wiener Physikalisches Kolloquium, Wien/ Oesterreich, 12.12.11 (2011).
66) V.M. Fomin, *Electron localization and the Aharonov-Bohm effect in non-uniform Moebius nanorings*, Condensed Matter Physics Seminar, Department of Physics and Astronomy, Northwestern University, Evanston, Illinois/ USA, 28.4.11 (2011).
67) V.M. Fomin, *Thermoelectric transport in superlattices of semiconductor quantum dots*, XV International Symposium Nanophysics and Nanoelectronics, Nizhny Novgorod/ Russia, 14.-18.3.11 (2011).
68) V.M. Fomin, *Dynamics of vortices in planar and tubular microstructured superconductors*, International Symposium NANO-2011 dedicated to the 100th Anniversary of the Discovery of Superconductivity, Chisinau/ Republic of Moldova, 6.-9.10.11 (2011).
69) V.M. Fomin, O.G. Schmidt, *Electron localization and the Aharonov-Bohm effect in 3D Moebius rings*, The 2011 Villa Conference on Interaction Among Nanostructures (VCIAN), Las Vegas, Nevada/ USA, 21.-25.4.11 (2011).
70) J. Freudenberger, *Deformation and (cold) work for an enhanced understanding of materials properties*, TU Bergakademie Freiberg, 19.8.11 (2011).
71) A. Gebert, *Korrosion von NdFeB-Magnetmaterialien und Einfluss von Magnetfeldern auf Korrosionsprozesse*, Kolloquium Fa. Vacuumschmelze, Hanau, 3.3.11 (2011).
72) A. Gebert, J. Koza, R. Sueptitz, M. Uhlemann, J. Eckert, L. Schultz, *Electrochemical micromachining of bulk metallic glasses*, International Conference on Rapidly Quenched and Metastable Materials RQ14, Salvador, Bahia/ Brasilien, 28.8.-3.9.11 (2011).
73) A. Gebert, J.A. Koza, R. Sueptitz, M. Uhlemann, J. Eckert, L. Schultz, *Utilization of electrochemical dissolution processes for micro-machining of bulk metallic glasses*, ISMANAM 2011, Gijon/ Spanien, 26.6.-1.7.11 (2011).
74) J. Geck, *Electronic polarons and nematic phases in layered manganites*, SFB Seminar, Koeln, 13.7.11 (2011).
75) D. Geissler, J. Freudenberger, A. Kauffmann, M. Krautz, J. Eickemeyer, L. Schultz, *Appearence of dislocation mediated and twinning induced plasticity in an engineering grade FeMnNiCr alloy*, Seminar des Instituts fuer Werkstoffwissenschaft, TU Bergakademie Freiberg, 6.6.11 (2011).
76) P.F. Gostin, U. Siegel, F. Mayr, J. Romberg, C. Mickel, S. Baunack, S. Oswald, A. Gebert, U. Kuehn, J. Eckert, L. Schultz, *Corrosion behaviour of amorphous iron base alloys*, Kolloquium, Vacuumschmelze Hanau, 15.9.11 (2011).
77) H.-J. Grafe, *Nuclear magnetic resonance study of pure and Ni/Co doped LiFeAs*, 477. WE-Heraeus-Seminar „Unconventional Superconductivity", Bad Honnef, 11.-13.4.11 (2011).

78) M.E. Gruner, S. Weiss, S. Faehler, L. Schultz, P. Entel, *Martensitic transformations in Fe-Pd magnetic shape memory alloys: News and views from first principles*, MSIM 2011, Moskau/ Russland, 21.-25.8.11 (2011).
79) O. Gutfleisch, *Magnetic materials in sustainable energy*, IEEE Magnetics Society Distinguished Lecture Series 2011, University of Alabama/ USA, 28.10.11 (2011).
80) O. Gutfleisch, *Li-based complex hydrides for solid state hydrogen storage and batteries*, Institutskolloquium, TU Bergakademie Freiberg, 19.8.11 (2011).
81) O. Gutfleisch, *Struktur und Funktionalitaet von magnetischen Hochleistungswerkstoffen*, Werkstoffphysikalisches Kolloquium, RWTH Aachen, 11.1.11 (2011).
82) O. Gutfleisch, *Magnetic materials in sustainable energy*, IEEE Magnetics Society Distinguished Lecture Series 2011, Imperial College London/ UK, 21.9.11 (2011).
83) O. Gutfleisch, *Magnetic materials in sustainable energy*, IEEE Magnetics Society Distinguished Lecture Series 2011, Hitachi Advanced Research Labs, Hatayama/ Japan, 1.2.11 (2011).
84) O. Gutfleisch, *Magnetic materials in sustainable energy*, IEEE Magnetics Society Distinguished Lecture, Series 2011, National Institute of Material Science (NIMS), Tsukuba/ Japan, 27.1.11 (2011).
85) O. Gutfleisch, *Magnetic materials in sustainable energy*, IEEE Magnetics Society Distinguished Lecture Series 2011, CNRS Grenoble/ France, 23.3.11 (2011).
86) O. Gutfleisch, *Permanent magnets*, Round table discussion, Intermag Conference, (mit Coey, Sagawa, Trout, Hu), Taipeh/ Taiwan, 25.5.11 (2011).
87) O. Gutfleisch, *Magnetic materials in sustainable energy*, IEEE Magnetics Society Distinguished Lecture Series 2011, University of Colorado, Colorado Springs/ USA, 4.11.11 (2011).
88) O. Gutfleisch, *Magnetic materials in sustainable energy*, IEEE Magnetics Society Distinguished Lecture Series 2011, National Tsing-Hua University, HsinChu/ Taiwan, 2.5.11 (2011).
89) O. Gutfleisch, *Magnetic materials in sustainable energy*, IEEE Magnetics Society Distinguished Lecture Series 2011, IEEE Summer School, New Orleans/ USA, 27.5.11 (2011).
90) O. Gutfleisch, *Magnetic materials in sustainable energy*, IEEE Magnetics Society Distinguished Lecture Series 2011, Institute of Physics, Chinese Academy of Science, Beijing/ China, 11.5.11 (2011).
91) O. Gutfleisch, *Magnetic materials in sustainable energy*, IEEE Magnetics Society Distinguished Lecture Series 2011, Institute of Metal Research, Chinese Academy of Science, Shenyang/ China, 10.5.11 (2011).
92) O. Gutfleisch, *Magnetic materials in sustainable energy*, IEEE Magnetics Society Distinguished Lecture Series 2011, Jiaotong University, Xian/ China, 9.5.11 (2011).
93) O. Gutfleisch, *Magnetic materials in sustainable energy*, IEEE Magnetics Society Distinguished Lecture Series 2011, Zhejiang University, Hangzhou/ China, 6.5.11 (2011).
94) O. Gutfleisch, *Magnetic materials in sustainable energy*, IEEE Magnetics Society Distinguished Lecture Series 2011, NIMTE Institute, Chinese Academy of Science, Ningbo/ China, 5.5.11 (2011).
95) O. Gutfleisch, *Magnetic materials in sustainable energy*, IEEE Magnetics Society Distinguished Lecture Series 2011, University of Colorado, Boulder/ USA, 4.11.11 (2011).
96) O. Gutfleisch, *Magnetic materials in sustainable energy*, IEEE Magnetics Society Distinguished Lecture Series 2011, Instituto de Ciencia de Materiales, Madrid/ Spain, 29.11.11 (2011).
97) O. Gutfleisch, *Magnetic materials in sustainable energy*, IEEE Magnetics Society Distinguished Lecture Series 2011, National Taiwan University, Taipeh/ Taiwan, 3.5.11 (2011).
98) O. Gutfleisch, *Magnetic materials in sustainable energy*, IEEE Magnetics Society Distinguished Lecture Series 2011, Academy of Science, Institute of Physics, Prague/ Czech Republic, 14.6.11 (2011).
99) O. Gutfleisch, *Magnetic materials in sustainable energy*, IEEE Magnetics Society Distinguished Lecture Series 2011, University of Bilbao/ Spain, 28.11.11 (2011).
100) O. Gutfleisch, *Magnetic materials in sustainable energy*, IEEE Magnetics Society Distinguished Lecture Series 2011, Department of Electrical and Electronic Engineering, Nagasaki,University, Nagasaki/ Japan, 4.2.11 (2011).
101) O. Gutfleisch, *Magnetic materials in sustainable energy*, IEEE Magnetics Society Distinguished Lecture Series 2011, University of Sheffield/ UK, 14.12.11 (2011).
102) O. Gutfleisch, *Magnetic materials in sustainable energy*, IEEE Magnetics Society Distinguished Lecture Series 2011, Hitachi Metals - Neomax, Osaka/ Japan, 3.2.11 (2011).
103) O. Gutfleisch, *Magnetic materials in sustainable energy*, IEEE Magnetics Society Distinguished Lecture Series 2011, University of California, Davis/ USA, 7.11.11 (2011).
104) O. Gutfleisch, *Material criticalities in magnetism*, EU-Japan Expert s Workshop on critical materials, (Video Talk), Tokyo/ Japan, 21.11.11 (2011).
105) O. Gutfleisch, *Magnetic materials in sustainable energy*, IEEE Magnetics Society Distinguished Lecture Series 2011, Iowa State University/Ames National Laboratory/ USA, 10.11.11 (2011).
106) O. Gutfleisch, *Magnetic materials in sustainable energy*, IEEE Magnetics Society Distinguished Lecture Series 2011, University of Birmingham/ UK, 16.12.11 (2011).
107) O. Gutfleisch, *Magnetic materials in sustainable energy*, ISMANAM Conference Keynote Lecture, Gijon/ Spain, 26.-30.6.11 (2011).
108) O. Gutfleisch, *Magnetic materials in sustainable energy*, IEEE Magnetics Society Distinguished Lecture Series 2011, Institutskolloquium, TU Ilmenau, 12.7.11 (2011).

109) O. Gutfleisch, *Magnetic materials in sustainable energy*, IEEE Magnetics Society Distinguished Lecture Series 2011, Christian-Albrechts-Universitaet Kiel, 12.12.11 (2011).
110) O. Gutfleisch, *Magnetic materials in sustainable energy*, IEEE Magnetics Society Distinguished Lecture Series 2011, University of Minneapolis, AZ/ USA, 10.11.11 (2011).
111) O. Gutfleisch, *Magnetic materials in sustainable energy*, IEEE Magnetics Society Distinguished Lecture Series 2011, Lawrence Berkeley National Laboratory, CA/ USA, 9.11.11 (2011).
112) O. Gutfleisch, *Magnetic materials in sustainable energy*, IEEE Magnetics Society Distinguished Lecture Series 2011, Western Digital, San Jose, CA/ USA, 8.11.11 (2011).
113) O. Gutfleisch, *Magnetic materials in sustainable energy*, IEEE Magnetics Society Distinguished Lecture Series 2011, University of York/ UK, 13.12.11 (2011).
114) O. Gutfleisch, *Magnetic materials in sustainable energy*, IEEE Magnetics Society Distinguished Lecture Series 2011, Spanish Club of Magnetism Annual Meeting, University of Barcelona/ Spain, 1.12.11 (2011).
115) O. Gutfleisch, M. Moore, S. Sawatzki, R. Sueptitz, A. Gebert, *Hochleistungspermanentmagnete fuer die Anwendung in leistungsstarken Elektromotoren*, E-Motive Symposium Aachen, 7.9.11 (2011).
116) O. Gutfleisch, T.G. Woodcock, S. Sawatzki, M. Moore, A. Gebert, L. Schultz, *Permanentmagnete fuer die Anwendung in leistungsstarken Elektromotoren*, 2. Dresdner Werkstoffsymposium, TU Dresden, 8.12.11 (2011).
117) D. Haberer, *Electronic properties of functionalized quasi-free-standing graphene*, Symposium Nanostructures- Future Strategies for Optoelectronics, TU Berlin, 24.-25.11.11 (2011).
118) D. Haberer, *Electronic properties of functionalized quasi-free-standing graphene and monolayer boron nitride*, Vortrag an der Chalmers University, Gothenburg/ Sweden, 3.-4.5.11 (2011).
119) D. Haberer, *Electronic properties of functionalized quasi-free-standing graphene and monolayer boron nitride*, Elettra Synchrotron, Triest/ Italy, 21.3.11 (2011).
120) D. Haberer, *Electronic properties of hydrogenated quasi-free-standing graphene*, eingeladener Seminarvortrag, Quantum Chemistry Group, Dep. of Chemnistry, Nagoya University/ Japan, 1.-8.2.11 (2011).
121) D. Haberer, *Electronic properties of hydrogenated quasi-free-standing graphene*, eingeladener Seminarvortrag, Department of Physics, Tohoku University, Sendai/ Japan, 9.-16.2.11 (2011).
122) D. Haberer, *Electronic properties of hydrogenated quasi-free-standing graphene*, 3rd GCOE International Symposium "Weaving Science Web beyond Particle Matter Hierarchy", Tohoku University, Sendai/ Japan, 17.-19.2.11 (2011).
123) S. Haindl, *Fe-based superconducting thin films: From fundamental properties to functional devices*, Seminar talk, Brookhaven National Laboratory/ USA, 17.11.11 (2011).
124) S. Haindl, *Fe-based superconducting thin films: From fundamental properties to functional devices*, Seminar talk, Ames Laboratory/ USA, 9.11.11 (2011).
125) S. Haindl, T. Thersleff, K. Iida, F. Kurth, J. Engelmann, M. Kidszun, S. Trommler, J. Haenisch, E. Reich, R. Huehne, D. Pohl, A. Hartmann, B. Rellinghaus, L. Schultz, B. Holzapfel, *New routes for epitaxial thin films of Fe-based superconductors*, ESF Exploratory Workshop, Bad Schandau, 23.-25.5.11 (2011).
126) S. Haindl, T. Thersleff, F. Kurth, J. Engelmann, M. Kidszun, S. Trommler, J. Haenisch, E. Reich, R. Huehne, *New routes for epitaxial thin films of Fe-based superconductors*, VORTEX VII Conference, Rhodos/ Greece, 10.-17.9.11 (2011).
127) S. Haindl, T. Thersleff, F. Kurth, J. Engelmann, M. Kidszun, S. Trommler, J. Haenisch, E. Reich, R. Huehne, *New routes for epitaxial thin films of Fe-based superconductors*, International Workshop on Complex Phenomena in Superconductors and Magnetic Systems, Oeystese/ Norway, 29.8.-2.9.11 (2011).
128) F. Hammerath, *Unusual NMR line broadening and spin gap in the zigzag S=1/2 spin chain compound Sr_{1-x}Ca_{x}CuO_{2}*, University of Zagreb, Department of Physics, Faculty of Science, Zagreb/ Croatia, 15.11.11 (2011).
129) C. Hess, *Probing unconventional superconductivity in LiFeAs by quasiparticle interference*, SFB 608 Colloquium, II. Physikalisches Institut, Universitaet Koeln, 11.5.11 (2011).
130) C. Hess, *Nernst effect of iron pnictide and stripe-ordering cuprate superconductors*, NATO Advances Research Workshop, New Materials for Thermoelectric Applications: Theory and Experiment, Hvar/ Croatia, 19.-25.11.11 (2011).
131) C. Hess, N. Hlubek, P. Ribeiro, B. Buechner, S. Singh, R. Saint-Martin, A. Revcolevschi, *Heat conduction of low-dimensional quantum magnets*, DPG Fruehjahrstagung, Dresden, 13.-18.3.11 (2011).
132) R. Huehne, *Supraleiter in der Energie- und Magnettechnik*, Lehrerfortbildung, Helmholtz-Zentrum Dresden-Rossendorf, 16.9.11 (2011).
133) K. Iida, J. Haenisch, S. Trommler, S. Haindl, F. Kurth, T. Thersleff, E. Reich, R. Huehne, I. Lucas del Pozo, L. Schultz, B. Holzapfel, *Epitaxial growth of superconducting Co-doped Ba-122 thin films on technical substrates*, ISS 2011, Tokyo/ Japan, 24.-26.10.11 (2011).
134) K. Iida, T. Thersleff, S. Haindl, J. Haenisch, F. Kurth, M. Kidszun, S. Trommler, I.L. Lucas del Pozo, J. Engelmann, R. Huehne, L. Schultz, B. Holzapfel, *Generic buffer layers for epitaxial superconducting Ba(Fe1-xCox)2As2 thin films*, EUCAS 2011, Hague/ Netherland, 18.-23.9.11 (2011).
135) I. Kaban, *Measurements of the surface and interfacial tension in liquid metals and alloys*, Mini-Symposium „Lorenz Force Sigmometry – LOFOS", TU Ilmenau, 24.-25.3.11 (2011).
136) V. Kataev, *High magnetic field ESR spectroscopy on FeAs-based superconductors*, International Workshop „Recent advances in broad-band solid-state NMR of correlated electronic systems", Trogir/ Croatia, 4.-9.9.11 (2011).
137) V. Kataev, *Spin polaronic states in lightly doped LaCoO3*, Transregio Seminar, Universitaet Augsburg, 7.6.11 (2011).

138) V. Kataev, *High field sub-Terahertz ESR spectroscopy on molecular magnets*, International Conference „Spin Physics, Spin Chemistry and Spin Technology“, Kazan/ Russia, 1.-6.11.11 (2011).
139) V. Kataev, *Frequency tunable ESR spectroscopy on molecular magnets in strong magnetic fields*, Colloquium of the Institute of Inorganic Chemistry, Universitaet Leipzig, 11.5.11 (2011).
140) V. Kataev, *Interplay between paramagnetism and paraelectricity in the frustrated spin chain magnet Li2ZrCu04*, „Moscow International Symposium on Magnetism“, MISM-2011, Moscow/ Russia, 21.-25.8.11 (2011).
141) V. Kataev, *Tunable sub-THz ESR spectroscopy of correlated spin systems in strong magnetic fields*, Workshop „Advanced EPR for Material and Solar Energy Research“, Berlin, 13.-14.10.11 (2011).
142) G. Katsaros, *Spin orbit effects in SiGe self-assembled quantum dots*, Helmholtz-Zentrum Dresden-Rossendorf, Institute of Ion Beam Physics and Materials Research, Dresden 15.12.11 (2011).
143) G. Katsaros, *Quantum transport through SiGe self-assembled quantum dots*, Seminar, Kavli Institute of Nanoscience, Technical University of Delft/ The Netherlands, 26.1.11 (2011).
144) G. Katsaros, *Fabrication and low temperature transport of Si based nanodevices*, Nanowires 2011, Lesvos/ Greece 14.-17.6.11 (2011).
145) G. Katsaros, *Spin orbit effects in SiGe self-assembled quantum dots*, Workshop on Quantum Spintronics, Sardinia/ Italy, 2.-6.10.11 (2011).
146) G. Katsaros, *Low temperature transport through SiGe self-assembled quantum dots*, Seminar, ICS-FORTH, Heraklion-Crete/ Greece 16.6.11 (2011).
147) G. Katsaros, *Single-ole transistors made out of SiGe self-assembled quantum dots*, Seminar, Max Planck Institute of Microstructure Physics, Halle, 12.10.11 (2011).
148) G. Katsaros, *Low temperature electronic transport through SiGe self-assembled quantum dots*, International Workshop: Epitaxial Growth and Fundamental Properties of Semiconductor Nanostructures, Traunkirchen/ Austria, 11.-16.9.11 (2011).
149) A. Kauffmann, J. Freudenberger, D. Geissler, S. Yin, W. Schillinger, V. Subramanya Sarma, H. Bahmanpour, R. Scattergood, M.S. Khoshkhoo, H. Wendrock, C.C. Koch, J. Eckert, L. Schultz, *Zwillingsbildung durch Kryoumformung*, Seminar des Instituts fuer Werkstoffwissenschaft, TU Bergakademie Freiberg, 14.12.11 (2011).
150) S. Kauffmann-Weiss, L. Schultz, S. Faehler, *Controlling magnetic properties of the magnetic shape memory system Fe-Pd-X*, Shape Memory Seminar, Ostre/Tschechische Republik, 1.12.-2.12.11 (2011).
151) M. Kidszun, *Superconducting thin films*, University of Stanford/ USA, 29.4.11 (2011).
152) M. Kidszun, S. Haindl, *Oxypnictide thin films: Vortex glas transition*, Ames Laboratory, Iowa/ USA, 10.11.11 (2011).
153) M. Kidszun, S. Haindl, *Oxypnictide thin films: Vortex glas transition*, Brookhaven National Laboratory, New York/ USA, 18.11.11 (2011).
154) M. Kidszun, S. Haindl, T. Thersleff, K. Iida, F. Kurth, E. Reich, J. Haenisch, A. Kauffmann, J. Freudenberger, J. Werner, L. Schultz, B. Holzapfel, *Critical current density and scaling behavior of oxypnictide thin films*, MRS-Spring Meeting, San Francisco/ USA, 25.-29.4.11 (2011).
155) D. Klemm, L. Loeber, R. Petters, U. Kuehn, J. Eckert, *3D Laserstrahlschmelzen - Anwendung in der Materialwissenschaft und in der Medizintechnik*, Institutskolloquium IFOM, Prof. Fuessel, Westsaechsische Hochschule Zwickau, 1.6.11 (2011).
156) M. Knupfer, *Electronic properties of picene molecular solids*, Seminar der Forschergruppe 1162, Universitaet Wuerzburg, 7.4.11 (2011).
157) M. Knupfer, *Electronic properties of condensed aromatic hydrocarbons: Undoped and doped picene*, Seminar, Institut fuer Materialphysik, Universitaet Wien/ Oesterreich, 16.6.11 (2011).
158) M. Knupfer, *Energy level alignment at highly ordered organic heterointerfaces*, Electronic Structure and Processes at Molecular-Based Interfaces (ESPMI-VI) Workshop, KIT Karlsruhe, 25.-29.9.11 (2011).
159) M. Knupfer, *Electronic properties of organic semiconductor interfaces*, Antrittsvorlesung, TU Bergakademie Freiberg, 29.9.11 (2011).
160) M. Knupfer, *Electronic properties of organic semiconductor interfaces*, Prague-Dresden Electrochemical Seminar 2011, Oybin, 24.-26.11.11 (2011).
161) M. Knupfer, *Electronic properties of condensed aromatic hydrocarbons: Insulators, semiconductors, superconductors*, Kolloquium, Institut fuer Festkoerperphysik, Universitaet Jena, 27.5.11 (2011).
162) M. Kohl, S.R. Yeduru, V. Pinneker, A. Backen, S. Faehler, Y. Ezer, A. Sozinov, B. Krevet, *Development of ferromagnetic shape memory microdevices*, 3rd International Conference on Ferromagnetic Shape Memory Alloys, Dresden, 18.-22.7.11 (2011).
163) A. Kordyuk, *Electronic structure of ferro-pnictides from ARPES experiment*, Fundamental Problems of High-Temperature Superconductivity (FPS'11), Moscow-Zvenigorod/ Russia, 3.-7.10.11 (2011).
164) P. Kratzer, V.M. Fomin, *Theoretical studies of electrical cross-plane transport in semiconductor multilayer heterostructures*, Spring Meeting of the German Physical Society, DPG, Dresden, 14.-18.3.11 (2011).
165) L. Loeber, *Selektives Laserschmelzen von Titanaluminiden*, Firmenvortrag, Muenchen, 5.5.11 (2011).
166) L. Ma, *Asymmetric rolled-up microtube cavity: Applications and elliptically polarized resonant light*, Seminar, Max Planck Institute for the Science of Light, Erlangen, 12.9.11 (2011).
167) D. Makarov, *Shapeable magnetoelectronics in research and technology*, Seminar, Institute Jean Lamour, University Nancy/ France, 12.12.11 (2011).
168) D. Makarov, M. Melzer, I. Moench, O.G. Schmidt, *Shapeable magneto-electronics*, XLVI Zakopane School of Physics, Breaking Frontiers: Submicron Structures in Physics and Biology Zakopane/ Poland, 16.-21.5.11 (2011).

169) N. Mattern, *Phase-separated metallic glasses*, Institutsseminar, 1. Physikalisches Institut, Universitaet Goettingen, 5.12.11 (2011).
170) N. Mattern, *Structure formation and properties of phase separated metallic glasses*, Taiwan Tech Workshop on Metallic Glasses, National Taiwan University of Science and Technology, Taipei/ Taiwan, 23.5.11 (2011).
171) N. Mattern, *Phase separation in liquid and amorphous metallic alloys*, Institute Seminar, Shanghai University, Shanghai/ China, 13.5.11 (2011).
172) N. Mattern, *Heterogeneous metallic glasses studied by anomalous small angle X-ray scattering and atom probe tomography*, ASAXS in Condensed Matter Science, Helmholtzzentrum fuer Materialien und Energie, Berlin, 24.-25.11.11 (2011).
173) J. Moore, J. Liu, M. Krautz, K. Skokov, C. Teixeira, O. Gutfleisch, *La-Fe-Si alloys: from fundamentals to application*, Delft Days on Magnetocalorics Workshop, Delft/ Netherlands, 24.-25.10.11 (2011).
174) T. Muehl, *Magnetische und mechanische Eigenschaften von eisengefuellten Kohlenstoff-Nanoroehren sowie vielversprechende Anwendungen dieser stabilen Nanomagnete*, Eingeladener Vortrag, TU Chemnitz, Institut fuer Physik, 10.5.11 (2011).
175) G. Paasch, *The influence of gausslan disorder on the performance of organic devices*, Seminar des Weierstrass-Institut Berlin, 1.12.11 (2011).
176) R. Pfrengle, *Regionale Schwerpunktbildung in Kooperation mit Hochschulen und anderen Forschungseinrichtungen*, Leibniz-Fuehrungskolleg, Schloss und Gut Liebenberg, 16.-19.6.11 (2011).
177) R. Pfrengle, *Impulsvortrag zur Abschlusstagung: Fachkraeftebedarf aus Sicht der Unternehmen und Forschungseinrichtungen*, MINT-Aktivitaeten im Freistaat Sachsen am Beispiel des TU-Projektes FINA , Abschlusstagung, TU Dresden, 29.4.11 (2011).
178) A. Popov, L. Dunsch, *Molecular and spin dynamics of pristine and charged endohedral metallofullerenes and the impact of dynamics on the spectroscopic properties*, 219th ECS Meeting, Montreal/ Canada, 1.-6.5.11 (2011).
179) A. Rastelli, *Piezoelectric control of excitons in single quantum dots*, Seminar, Institut fuer Physik, University of Augsburg, 9.11.11 (2011).
180) A. Rastelli, *Strain-tunable quantum dot devices*, German-Moldovan Workshop on Novel Nanomaterials for Electronic, Photonic and Biomedical Applications, Chisinau/ Moldova, 7.-8.7.11 (2011).
181) A. Rastelli, *Investigating the shape and composition of semiconductor quantum dots by scanning probe microscopy and selective wet chemical etching*, 18th Interdisciplinary Surface Science Conference (ISSC-18), Warwick/ UK, 4.-7.4.11 (2011).
182) A. Rastelli, *Strain-tunable quantum dot devices*, International Workshop: Epitaxial Growth and Fundamental Properties of Semiconductor Nanostructures, Traunkirchen/ Austria, 11.-16.9.11 (2011).
183) A. Rastelli, *Electro-elastic control of excitons in single quantum dots*, Seminar, Institute of Semiconductor and Solid State Physics, University of Linz/ Austria, 21.11.11 (2011).
184) A. Rastelli, *Reversible control of optically active quantum dots by strain*, Seminar, School of Physics and Astronomy, Cardiff University, Cardiff/ United Kingdom, 15.6.11 (2011).
185) A. Rastelli, *Strain-tunable quantum dot devices*, Seminar, Kavli Institute of Nanoscience, Technical University of Delft/ The Netherlands, 11.5.11 (2011).
186) B. Rellinghaus, D. Pohl, A. Surrey, E. Mohn, B. Bieniek, L. Schultz, *Segregation tendencies in binary metal nanoparticles*, Seminar, National Center for Electron Microscopy, NCEM, Berkeley/ USA, 3.5.11 (2011).
187) M. Ruemmeli, *Evolving catalytic routes for carbon nanotube and graphene growth*, Invited Talk, Al Quds/ Palestine, 4.-6.6.11 (2011).
188) M. Ruemmeli, A. Bachmatiuk, I. Ibrahim, *Evolving catalytic routes for carbon nanotube and graphene growth*, Invited Talk, Nablus/ Palestine, 1.-2.6.11 (2011).
189) S. Sanchez, *Microbots and biosensing applications of nanomembranes*, Conference for the International Year of Chemistry 2011, Mexico/ Mexico, 18.4.11 (2011).
190) S. Sanchez, *Nanorobots*, Sci | Art NanoLab 2010, UCLA, Los Angeles/ USA, 29.6.11 (2011).
191) S. Sanchez, *Nanorobots and their applications in Nanobiotechnology*, Special Seminar, Tecnologico de Monterrey, Monterrey/ Mexico, 8.4.11 (2011).
192) S. Sanchez, *Catalytic and biocatalytic microbots*, ICYS Workshop, Manza/ Japan, 19.-21.1.11 (2011).
193) S. Sanchez, *Self-propelled nanomachines: Spherical particles and nanojets*, Seminar, Max Planck Institute for Intelligent Systems, Stuttgart, 1.9.11 (2011).
194) S. Sanchez, O.G. Schmidt, *Nanomembranes in good shape: From nanorobotics to lab-in-a-tube applications*, Soft Matter at Interfaces 2011 Schloss Ringberg, Tegernsee, 2.-5.3.11 (2011).
195) S. Sawatzki, O. Gutfleisch, M. Moore, R. Sueptitz, A. Gebert, L. Schultz, *Definition und Auswahl von spezifikationsrelevanten Pruefungen fuer die Entwicklung und Serienueberwachung von Hochleistungspermanentmagneten*, FVA-Informationstagung zur Elektromobilitaet, Wuerzburg, 24.11.11 (2011).
196) R. Schaefer, *Kerr microscopy*, Seminarvortrag, King Abdullah University of Science and Technology, Jeddah/ Saudi Arabia, 14.2.11 (2011).
197) R. Schaefer, *Magnetismus*, Seminarvortrag anlaesslich der Saechsischen Physik-Olympiade am Martin-Andersen-Nexoe-Gymnasium Dresden, 9.3.11 (2011).
198) H. Schmidt, X. Kong, C. Deneke, O.G. Schmidt, *Dielectrophoretic manipulation of rolled-up microtubes by surface acoustic waves*, IEEE NEMS 2011, Kaohsiung/ Taiwan, 20.-23.2.11 (2011).
199) O.G. Schmidt, *Flexible nanomembranes*, Colloquium, Leibniz-Institut fuer Oberflaechenmodifizierung, Leipzig, 18.11.11 (2011).
200) O.G. Schmidt, *Ultra-thin membranes: Shaping a new nanoworld*, Seminar, Bio Innovations Center Dresden, 14.11.11 (2011).
201) O.G. Schmidt, *Nanostructures under stress: From artificial atoms to engines*, Edgar Luescher Seminar, Klosters/ Switzerland, 12.-18.2.11 (2011).

202) O.G. Schmidt, *Entwurf und Entwicklung der kleinsten Duesenantriebe der Welt*, Festvortrag, Jahresauftaktveranstaltung des VDI 2011, Dresden, 3.2.11 (2011).
203) O.G. Schmidt, *Strained nanomembranes for interdisciplinary research*, Seminar, Kavli Institute of Nanoscience, TU Delft/ The Netherlands, 28.9.11 (2011).
204) O.G. Schmidt, *Fundamental concepts and potential applications of strainable and shapeable nanomembranes*, CeNS Workshop 2011: Nanosciences – From Molecular Systems to Functional Materials, Venice/ Italy, 19.-23.9.11 (2011).
205) O.G. Schmidt, *Magnetic and hybrid nanomembranes: From fundamental conceptions to integrative applications*, XVIII International Summer School "Nicolas Cabrera" Frontiers in Science and Technology, Madrid/ Spain, 12.-16.9.11 (2011).
206) O.G. Schmidt, *Straining and shaping hybrid material nanomembranes*, Seminar, Institute of Materials, Ecole Polytechnique Federale de Lausanne/ Switzerland, 26.9.11 (2011).
207) O.G. Schmidt, *Engineering artificial engines at the micro-/nanoscale*, 85th ICYS Special Seminar, NIMS Tsukuba/ Japan, 18.1.11 (2011).
208) O.G. Schmidt, *Rolled-up multifunctional materials*, LOTHERM Summer School on Emergent Materials for Technical Applications, Dresden, 27.-28.6.11 (2011).
209) O.G. Schmidt, *Nanomembranes: Shaping a new nanoworld*, Colloquium, Max-Planck-Institute for Solid State Research Stuttgart, 13.12.11 (2011).
210) O.G. Schmidt, *Ultra-compact optofluidic components from rolled-up nanomembranes*, 1st EOS Conference on Optofluidics, Muenchen, 23.-25.5.11 (2011).
211) O.G. Schmidt, *Towards multifunctional lab-in-a-tube systems and artificial micromachinery*, Saxon Biotechnology Symposium 2011, Dresden, 2.5.11 (2011).
212) O.G. Schmidt, *Photonics and transport with Si and SiO based nanomembranes*, E-MRS Spring Meeting, Nice/ France, 9.-13.5.11 (2011).
213) O.G. Schmidt, *Nanomembranen als neue Komponenten fuer elektronische und photonische Anwendungen*, Fachtagung Trends in der Materialforschung fuer die Mikro- und Optoelektronik, Berlin, 11.4.11 (2011).
214) O.G. Schmidt, *Nanomembrane materials for new physical, chemical and biophysical concepts and applications*, Colloquium, Fudan University, Shanghai/ China, 8.4.11 (2011).
215) O.G. Schmidt, *Nanophotonics and nanomembranes*, Seminar, Shanghai Institute of Technical Physics of the Chinese Academy of Sciences, Shanghai/ China, 7.4.11 (2011).
216) O.G. Schmidt, *Hybrid nanomembranes*, IRTG Summer School Shanghai, Shanghai/ China, 7.4.11 (2011).
217) O.G. Schmidt, *Nanomembranes for optofluidic and autonomous systems*, SPIE, Defense, Security and Sensing, Orlando, Florida/ USA, 25.-29.4.11 (2011).
218) O.G. Schmidt, *Nanostructures under stress: Quantum dots and smart tubes*, ICYS Workshop, Manza/ Japan, 19.-21.1.11 (2011).
219) O.G. Schmidt, *Nanomembranes in good shape*, The 2011 Villa Conference on Interaction Among Nanostructures (VCIAN), Las Vegas, Nevada/ USA, 21.-25.4.11 (2011).
220) O.G. Schmidt, *Flexible, shapeable and stretchable nanomembranes for on and off-chip applications*, Seminar, Fraunhofer Institute for Photonic Microsystems, Dresden, 28.4.11 (2011).
221) O.G. Schmidt, *Flexible, stretchable and shapeable nanomembranes*, Seminar, University Nancy/ France, 19.12.11 (2011).
222) O.G. Schmidt, *Quantum dots and smart tubes for interdisciplinary research*, Kolloquium, TU Chemnitz, 12.1.11 (2011).
223) R. Schoenfelder, *Sintesis, purificacion y caracterizacion de los nanotubos de carbono y sus aplicaciones*, Seminarvortrag, Universitaet Cauca, Popayan/ Kolumbien, 26.4.11 (2011).
224) L. Schultz, *SupraTrans II: Research facility for large scale HTS applications*, European Conference on Applied Superconductivity 2011 (EUCAS-ISEC-ICMC), Den Haag/ Netherlands, 22.9.11 (2011).
225) L. Schultz, *Supraleitendes Schwebesystem fuer den spurgebundenen Individualverkehr - die wundersame Welt der Supraleiter*, Karlsruher Werkstoffkolloquium, KIT Karlsruhe, 7.6.11 (2011).
226) L. Schultz, *Voellig losgeloest - vom Schweben auf Magneten - Die wundersame Welt der Supraleitung*, Physik im Kaufpark, Dresden, 7.3.11 (2011).
227) L. Schultz, *SupraTrans II - Research facility for large scale superconducting levitation systems*, International Seminar on Advanced Materials for Green Growth, University of Ulsan/ Russland, 15.11.11 (2011).
228) L. Schultz, *SupraTrans - ein supraleitendes Schwebesystem fuer den spurgebundenen urbanen Individualverkehr*, Industriepartner-Symposium 2011 der Fakultaet Elektrotechnik und Informationstechnik, TU Dresden, 6.10.11 (2011).
229) L. Schultz, *From supra trans to trackbound individual traffic*, 22. Edgar-Luescher-Seminar, Klosters/ Schweiz, 14.2.11 (2011).
230) L. Schultz, *Schweben auf Magnetfeldern - die wundersame Welt der Supraleiter*, DGM-Tag 2011, TU Dresden, 15.6.11 (2011).
231) L. Schultz, *SupraTrans - ein supraleitendes Schwebesystem fuer den spurgebundenen urbanen Individualverkehr*, Industriepartner-Symposium 2011 der Fakultaet Elektrotechnik und Informationstechnik, TU Dresden, 6.10.11 (2011).
232) L. Schultz, A. Kirchner, *Vom Schweben auf Magnetfeldern - die wundersame Welt der Supraleiter*, Senatssitzung der Leibniz-Gemeinschaft, Hotel Schweizerhof (Pullman), Berlin, 12.7.11 (2011).
233) L. Schultz, A. Kirchner, *Vom Schweben auf Magnetfeldern - die wundersame Welt der Supraleiter*, Hochschulvortragsreihe 2011, VDE/VDI Ulm, 12.1.11 (2011).
234) L. Schultz, A. Kirchner, K. Clausnitzer, S. Fleischer, *Schweben auf Magnetfeldern - die wundersame Welt der Supraleiter*, Kinder-Universale, Hohenstein-Ernstthal, 9.3.11 (2011).

235) L. Schultz, E. Reich, *SupraTrans II- neuer Demonstrator fuer ein supraleitendes Schwebesystem*, Fachtagung 20 Jahre ELBAS, Congress Center Dresden, 5.5.11 (2011).
236) L. Schultz, H. Schloerb, *Supraleitendes Schwebesystem fuer den spurgebundenen urbanen Individualverkehr - die wundersame Welt der Supraleiter*, Kolloquium, Institut fuer Mikro- und Nanotechnologie, TU Ilmenau, 7.12.11 (2011).
237) L. Schultz, J. Thielsch, *Supraleitendes Schwebesystem fuer den innerstaedtischen spurgebundenen Individualverkehr von morgen - die wundersame Welt der Supraleiter*, Berliner Industriegespraech der DPG, Magnus-Haus Berlin, 13.4.11 (2011).
238) L. Schultz, J. Thielsch, *Riding on magnetic fields - The magic world of superconductors*, Ceremonial Talk, New Year's Meeting, Faculty of Materials Science and Technology, Slovak University of Technology Bratislava, Trnava/ Slovakia, 20.1.11 (2011).
239) L. Schultz, J. Thielsch, *Supraleitendes Schwebesystem fuer den innerstaedtischen spurgebundenen Individualverkehr von morgen*, Berliner Industriegespraech (Deutsche Physikalische Gesellschaft), Magnus-Haus, Berlin, 13.4.11 (2011).
240) E.J. Smith, *Ultra-compact optofluidic components for lab-in-a-tube applications*, Edgar Luescher Seminar, Klosters/ Switzerland, 12.-18.2.11 (2011).
241) E.J. Smith, *Polymer delamination: A method for creating unique 3D microstructures*, Seminar, Institute for Applied Physics, University of Hamburg, 1.11.11 (2011).
242) M. Stoica, *Thermal stability and phase evolution of Cu-added Fe-based bulk metallic glasses*, The 14th International Conference on Rapidly Quenched and Metastable Materials, RQ14, Salvador/ Brazil, 28.8.-3.9.11 (2011).
243) A. Svitova, A. Popov, S. Yang, L. Zhang, L. Dunsch, *Large ions in mixed metal nitride clusters*, 219. ECS Meeting Montreal, Canada, 1.-6.5.11 (2011).
244) J. Thomas, J. Ramm, T. Gemming, *Elektronenbeugung zur Analyse duenner Funktionsschichten - ein Ueberblick*, Workshop EFDS „Moderne Methoden der Oberflaechen- und Duennschichtanalytik", Dresden, 29.-30.11.11 (2011).
245) J. Thomas, J. Ramm, T. Gemming, *Elektronenbeugung zur Analyse duenner Funktionsschichten: Eine moderne Methode?*, 16. Tagung Festkoerperanalytik, Wien/ Oesterreich, 4.-6.7.11 (2011).
246) M. Uhlemann, *Magnetoelectochemistry - Structured electrodeposition in magnetic gradient fields*, 8th International PAMIR Conference - GAMAS School, Borgo/ France, 5.-9.9.11 (2011).
247) N. Van Steenberge, D. Ruiz Romera, M. Stoica, G. De Vos, S. Claessens, *Towards the industrial upgrade of bulk metallic glasses: challenges to overcome*, The European Congress and Exhibition on Advanced Materials and Processes (EUROMAT 2011), Symposium C13: Metallic Glasses and Related Composites: New Routes for Functional and Strong Materials, Montpellier/ France, 12.-15.9.11 (2011).
248) S. Wege, H. Wendrock, J. Eckert, *Method for measuring local strains in polycrystals using EBSD or KOSSEL*, RMS EBSD Tagung 2011, Duesseldorf, 28.-30.3.11 (2011).
249) S. Wege, H. Wendrock, J. Eckert, *Method for measuring local strains in polycrystals using EBSD or KOSSEL*, RMS EBSD Tagung 2011, Duesseldorf, 28.-30.3.11 (2011).
250) S. Wege, H. Wendrock, J. Eckert, *A new concept of strain determination by precision EBSD*, Workshop, Leipzig, 1.3.11 (2011).
251) U. Wolff, *Imaging of magnetic structures on a nanometer scale by MFM*, 1st BIT-Conference on Nanoscience and -technology, Dalian/ China, 23.-26.10.11 (2011).
252) A. Wolter, *Magnetic properties and revisited exchange integrals of the frustrated chain cuprate PbCuSO4(OH)2 - linarite*, Vortrag am HZDR, Dresden-Rossendorf, eingeladen von Prof. Wosnitza, Dresden, 5.8.11 (2011).
253) T.G. Woodcock, G. Hrkac, T. Schrefl, O. Gutfleisch, *Characterisation and modelling of interfaces in Nd-Fe-B permanent magnets*, Internationale Tagung: Magnetism and Magnetic Materials (MMM), Scottsdale, Arizona/ USA, 31.10.-4.11.11 (2011).
254) T.G. Woodcock, G. Hrkac, T. Schrefl, S. Zaefferer, O. Gutfleisch, *Novel approaches to microstructural characterisation in NdFeB materials*, TMS Annual Meeting, Symposium on Magnetic Materials for Energy Applications, San Diego/USA, 27.2-3.3.11 (2011).

Patents 2011

Issues of Patents

DE 10 2008 001 005 Verfahren zur Herstellung eines Schichtverbundes mit epitaktisch gewachsenen Schichten aus einem magnetischen Formgedächtnis-Material und Schichtverbund mit epitaktischen Schichten aus einem magnetischen Formgedächtnis-Material sowie dessen Verwendung
Inventors: J. Buschbeck, S. Fähler, O. Heczko et al.

DE 10 2008 040 087 Elektrisch leitfähiger Hochtemperatur-Supraleiter-Schichtaufbau und Verfahren zu seiner Herstellung
Inventors: R. Hühne, K. Güth, R. Kaltofen

DE 10 2008 026 008 Verfahren zur Bestimmung der Viskosität und Elastizität von viskoelastischen Medien
Inventors: M. Weihnacht, R. Brünig, H. Schmidt, G. Martin

DE 10 2009 002 497 Verfahren zur Ermittlung elektrischer und mechanischer Materialeigenschaften
Inventors: G. Guhr, R. Brünig, M. Jäger

DE 10 2010 062 011 Verfahren zur Wärmebehandlung von hochfesten Eisenlegierungen
Inventors: J. Hufenbach, J. Eckert, U. Kühn, S. Kohlar

Patent Applications

11102 Verfahren zur Herstellung von Halbzeugen auf der Basis intermetallischer Verbindungen
Inventors: J. Freudenberger, T. Marr

11103 Magnetoelektronisches Bauelement und Verfahren zu seiner Herstellung
Inventors: D. Makarov, O. G. Schmidt

11105 Verfahren zur Herstellung eines Anodenmaterials
Inventors: J. Freudenberger, T. Marr, L. Giebeler

11106 Verfahren zur Ermittlung von Dehnungstensor, Gitterparametern und/oder Orientierungsmatrix von Kristalliten in polykristallinen Materialien
Inventors: S. Wege, H. Wendrock

11107 Synthese wasserfreier, stabilisierter und monodisperser Nanopartikel mittels inverser Mikroemulsionstechnik
Inventors: T. Freudenberg, B. Holzapfel et al.

11108 YBCO-Pancake-Spulen mit reduzierten AC-Verlusten
Inventors: V. Grinenko, G. Fuchs, K. Nenkov, B. Holzapfel

11109 Mehrspur-Unidirektionalwandler
Inventors: S. Biryukov, G. Martin et al.

11110 Akustisches Oberflächenwellenbauelement und Verfahren zu seiner Herstellung
Inventors: S. Menzel, A. Winkler

11111 Verbundwerkstoff und Verfahren zu seiner Herstellung
Inventors: J. Romberg, S. Roth, M. Pötschke, C. Hürrich, S. Weiß, U. Gaitzsch, L. Schultz

11112 Dünnschichtbauelement und Verfahren zu seiner Herstellung
Inventors: I. Mönch, D. Makarov, M. Melzer, O. G. Schmidt

11113 Verfahren zur Herstellung von gedruckten magnetischen Funktionselementen für Widerstandssensoren und gedruckte magnetische Funktionselemente
Inventors: D. Karnaushenko, D. Makarov, O. G. Schmidt

11115 Verwendung eines elastischen magnetischen Sensorelementes, Verfahren zu seiner Herstellung, und elastisches magnetisches Sensorelement
Inventors: M. Melzer, D. Karnaushenko, L. Baraban, D. Makarov, O. G. Schmidt

11118 Verfahren und Vorrichtung zur Messung von Kraftgradienten bei der Kraftmikroskopie
Inventors: T. Mühl, J. Körner

11119 Verfahren zur Herstellung von Titaniumdioxidpartikeln
Inventors: G. Zakharova, C. Täschner, A. Leonhardt

11125 Magnetisches Material und Verfahren zu dessen Herstellung
Inventors: O. Gutfleisch, K. Güth

11127 Massive wasserstoffhaltige vakuumdichte Proben, Verfahren zu ihrer Herstellung und Verwendung
Inventors: V. Hoffmann

11128	Verwendung von flexiblen magnetischen Dünnschicht-sensorelementen *Inventors:* D. Makarov, M. Melzer, I. Mönch, O. G. Schmidt et al.
11129	Magnetisches Material und Verfahren zu dessen Herstellung *Inventors:* O. Gutfleisch, K. Güth
11131	Lithium enthaltendes amorphes Elektrodenmaterial und Verfahren zu seiner Herstellung *Inventors:* F. Thoss, L. Giebeler, H. Ehrenberg, J. Eckert
11132	Vorrichtung zur Qualitätssicherung von mittels Laserbearbeitung hergestellten Produkten *Inventors:* V. Hoffmann et al.
11134	Resonanzdedektor *Inventors:* D. Karnaushenko, D. Makarov, L. Baraban, O. G. Schmidt
11137	Supraleitendes Magnetlager-Ring-Drallelement-System für Ringspinn- bzw. Ringzwirnmachinen *Inventors:* L. Schultz, D. Berger et al.

PhD and diploma theses 2011

PhD theses

Alexey Alfonsov	High-field electron spin resonance study of electronic inhomogeneities in correlated transition metal compounds
Yulieth Arango	Electron spin resonance (ESR) spectroscopy of low-dimensional spin systems
Danny Baumann	Aufbau eines ultrahochauflösenden Tieftemperatur-Rastertunnelmikroskops
Raimund Brünig	Modellierung von akustischen Dickenscherschwingern im Frequenzbereich
Varvara Efimova	Study in analytical glow discharge spectrometry and ist application in material science
Ahmed El-Gendy	Carbon coated nanomagnets: synthesis, characterization and feasibility for magnet hyperthermia
Jürgen Gluch	Untersuchung von yttriumstabilisiertemHafniumoxid als Isolatorschicht für DRAM-Kondensatoren
Flavio Gostin	Corrosion behaviour of advanced Fe-based bulk metallic glasses
Diana Haase	Kohlenstoffnanoröhren als potentielle Wirkstofftransporter
Franziska Hammerath	Magnetism and Superconductivity in Iron-based Superconductors as probed by Nuclear Magnetic Resonance
Nikolai Hlubek	Magnetic heat transport in one-dimensional quantum antiferromagnets
Marko Kaiser	Thermoplastische Umformung des metallischen Glases Zr48Cu36Al8Ag8
Anna Kario	High Energy Milled Ex situ MgB2 for Tapes and Wires
Olga Khvostikova	Untersuchung der Physisoption von Wasserstoff in porösen Materialien mit einer neuartigen volumetrischen Apparatur
Yulia Krupskaya	Magnetic Properties of Molecular and Nanoscale Magnets
Kamil Lipert	Development of a Micro-Hall-Magnetometer and Studies on Inividual Fe-filled Carbon Nanotubes
Ferdinand Lipps	Electron spin in reduced dimensions: ESR spectroscopy on semiconductor heterostructures and spin chain compounds
Wolfram Lorenz	On the Spin-Dynamics of the Quasi-One-Dimensional, Frustrated Quantum Magnet Li2CuO2
Norbert Martin	Herstellung und Charakterisierung von magnetisch heterogenen Schichten und Elementen
Carsten Neise	Magnetic Properties Studied by Density Functional Calculations Including Orbital Polarisation Corrections
Anupama Parameswaran	Magnetic properties of Mn, Ni and Fe based metal-organic complexes
Martin Philipp	Electrical Transport and Scattering Mechanisms in Thin Silver Films for Thermally Insulating Glazing“
Martin Pötschke	Herstellung und Charakterisierung von texturiertem Ni-Mn-Ga als magnetisches Formgedächtnismaterial
Elke Reich	Schichtwachstum und Supraleitung von kupratbasierten Quasimultilagen und Oxipniktiden
Carine Rongeat	Mechano-chemical synthesis and characterisation of complex hydrides for solid state hydrogen storage
Miroslava Sakaliyska	Production and characterization of microstructure and mechanical behavior of Al-Mg based Complex Metallic Alloys and their composites
Stephan Schönecker	Theoretical Studies of Epitaxial Bain Paths of Metals
Elliot Smith	Self-assembled rolled-up devices: towards on-chip sensor technologies
Ralph Süptitz	Einfluss homogener und inhomogener Magnetfelder auf die Korrosion ferromagnetischer Elektroden
Kumar Babu Surreddi	Production of high strength Al-based alloys by consolidation of amorphous and partially amorphous powders
Thomas Thersleff	The nanoscale characterization of functional superconducting thin film
Dominic Thurmer	Nanomembrane-based hybrid semiconducto –superconductor heterostructures
Andreas Winkler	SAW-basierte modulare Mikrofluidiksysteme hoher FlexibilitätVarvara Efimova
Franziska Wolny	Magnetic properties of individual iron filled carbon nanotubes and their application as probes for magnetic force microscopy
Daniil Yevtushynsky	Physical properties of layered superconductors from angle-resolved photoemission spectroscopy (ARPES)
Orkidia Zeneli	Strain-dependent magnetism and electrical conductivity of La1-xSrxCoO3 films

Diploma, master and bachelor theses

Adithy N. Ananth	Self-propelled Catalytic and bio-catalythic Microjet engines
Anne Bachmann	Transporteigenschaften von Pniktid-Supraleitern
Martin Bauch	Elektrische Transporteigenschaften der topologischen Isolatoren Bi2Se3 und Be2Te3
Judith Ventayol i Boada	Platinum filled CNTs as temperature sensor for biomedical applications
Erik Brachmann	Entwicklung eines Ansteuermoduls für SAW-Aktorikbauelemente
Anett Diestel	Martensitisches Gefüge und magnetische Domänen von epitaktischen Ni-Mn-Ga Schichten
Elok Fidiani	Synthesize of Carbon Nanotube Filled with Contrast Agent
Andreas Gang	Magnetostriktionsmessungen an magnetischen dünnen Schichten
Markus Gellesch	Carbon nanotubes filled with intermetallic ferromagnetic compounds
Anja Grohme	Darstellung und Charakterisierung von Ce-basierten Nitridclusterfullerenen
Christian Jähnichen	Untersuchungen zum Einfluss einer interdendritischen Ti-Cu-Ni-Phase auf die mechanischen Eigenschaften einer rascherstarrten Beta-Titanlegierung
Andreas Jost	Thermischer Transport in niedrigdimensionalen Spinsystemen
Konrad Kosiba	Microstructurtal evolution and mechanical behavior of Cu-Zr-Co alloys
David Kuhnhardt	Synthese von Cer-basierten Clusterfullerenen
Norman Lange	Änderung magnetischer Eigenschaften ultradünner Eisen-Platin-Schichten in einem Elektrolyten
Runshuang Lu	Synthesis, Separation and Charaterization of Endohedral Fullerenes
Ignacio G. G. Martinez	Synthesis and characterization of boron- and aluminium-based nanostructures
Polyxeni Nikolakopoulou	Electron Spin Resonance Spectroscopy of Molecular Magnetic Complexes
Patrick Pahlke	Herstellung und Untersuchung von supraleitenden YBCO-Schichten auf piezoelektrischen Substraten
Romy Petters	Untersuchungen zur Herstellung amorpher Bauteile mit dem Lasterstrahlschmelzverfahren am Beispiel einer Fe-Basislegierung
Thomas Prestel	Classical spin model with quantum mechanically treated electrons for pnictides
Kamsanipally Raghunandan	Synthesis and Biocompatibility of functionalised magnetic particles
Ludwig Reichel	Ultradünne L10-COPt-Schichten und deren magnetische Eigenschaften bei elektrischer Beladung in einem Elektrolyten
Tobias Ritschel	Druckabhängikeit der Ladungsdichtewelle in 1T-TaS2
Martha Scheffler	Aufbau eines Rastertunnelmikroskops und Untersuchungen von magnetischen Molekülen
Robert Sommer	Fabrication and characterization of electrostatic energy storage elements based on high-k oxides
Rico Staude	Weiterentwicklung eines Ansteuermoduls für SAW-Aktorikbauelemente
Henry Stopfel	Quantitative magnetische Kraftmikroskopie zur Untersuchung von Flusslinienanordnung und deren Eigenschaften
Frank Streller	Development and Characterization of Pt-Silicides as Contact Material on NEMS Switches
Alexander Surrey	Atomare Charakterisierung der Oberflächen von Nanopartikeln mittels aberrationskorrigierter Transmissionselektronenmikroskopie
Bezuayehu Teshome	Hybrid organic/inorganic molecular heterojunctions based onnanomembranes
Jens Trommer	Optimization of SiO2 optical Microtube Ringresonators
Xiaorui Wang	Hochfeste Al-Basis-Verbundwerkstoffe hergestellt durch Pulvermetallurgie
Richard Zahn	Hochfeld-Electronenspin-Resonanz-Spektroskopei an den Eisenarsenid-basierten Supraleitern

Calls and Awards

Calls on Professorships

Prof. Dr. Oliver Schmidt	Univ. Utah
Dr. Oliver Gutfleisch	Univ. Darmstadt

Appointments as Guest and Honorary professorships

Prof. Dr. Oliver Schmidt	Fudan Univ. China (Honorary Professorship)
Dr. Martin Knupfer	TU Bergakademie Freiberg (Honorary Professorship)

Awards

SciDre Scientific Instruments GmbH und IFW Dresden: Sonderpreis im Wettbewerb „wissen.schafft.arbeit“

Michael Melzer	Dresdner Barkhausen-Poster-Preis für den Poster-Beitrag „Towards Flexible and Stretchable Magnetoelectronics"
Mohsen Samadi Khoshkhoo	Best Junior Researcher Award – 2nd Place, TMS 2011Can Diego, California
Jin Young Kim et al.	Best Paper Award of the 7th International Conference on porous Metals and Metallic Foams

IFW Awards

Dr. Oliver Gutfleisch	IFW Research Award 2011
Dr. Daniil Yevtushynsky	Deutsche Bank Junior Award 2011 for the best PhD thesis
Dr. Vladislav Kataev	IFF Research Award 2011
Dr. Stefan Roth	IMW Research Award 2011
Dr. Mihai Stoica	IKM Research Award 2011
Dr. Samuel Sanchez	IIN Research Award 2011

Tschirnhaus-Medal of the IFW for excellent PhD theses 2011

Dr. Franziska Wolny
Dr. Petre Flaviu Gostin
Dr. Elliot Smith
Dr. Stephan Schönecker
Dr. Ferdinand Lipps
Dr. Norbert Martin
Dr. Daniil Yevtushynsky
Dr. Franziska Hammerath
Dr. Elke Reich

Scientific conferences and IFW colloquia

Conferences

Kick-Off Meeting „Hochtemperatursupraleitung in Eisenpniktiden“
DFG SPP 1458
24. - 25. Februar 2011, IFW Dresden

DPG Frühjahrstagung der Sektion Kondensierte Materie gemeinsam mit der Sektion Atom- und Molekülphysik
March 2011, Dresden, Germany
Chairman: Prof. L. Schultz (IFW Dresden)
6000 participants

477. Heraeus-Seminar: „Unconventional Superconductivtiy“
11. – 13. April 2011, Bad-Honnef, Germany

LOTHERM Summer School: Emergent materials for technical applications
27. – 28. Juni 2011, IFW Dresden

Summer School in Spectroelectrochemistry
26. August – 02. September 2011, IFW Dresden

E - MRS 2011 Fall Meeting
19. – 23. September 2011, Warsaw, Poland

International workshop: Polymers at Electrodes. A Quarter of a Century later
6. – 9. November 2011, Bad Schandau, Germany

IFW colloquia

Prof. Dr. Hannes Lichte, TU Dresden, Electron Holography for Nano-Measurements, 06.01.2011

Prof. Dr. George Sawatzky, Univ. British Colombia Vancouver, The strongly varied role of anions in the properties of strongly correlated electron systems, 07.01.2011

Prof. Dr. Bradley Nelson, ETH Zürich, MicroRobotics and NanoMedicine, 13.01.2011

Prof. Dr. Klaus Ensslin, ETH Zürich, Single electron control in quantum materials, 20.01.2011

Prof. Dr. Ralf Riedel, TU Darmstadt, Polymer-Derived Ceramics – 40 years of Research and Innovation in Advanced Ceramics, 27.01.2011

Prof. Dr. Roberta Sessoli, Univ. Florence, Single Molecule Magnets on magnetic and metallic surfaces, 03.02.2011

Prof. Helena Van Swygenhoven-Moens, Paul Scherrer Institut Villingen, Micromechanics and Microstructures:Xrays, Neutrons and Compatation, 10.02.2011

Prof. Dr. Henning Riechert, Humboldt Univ. Berlin, GaN nanowires – a new approach for visible light emitting LEDs, 14.04.2011

Prof. Dr. Adrian Bachtold, ICN Barcelona, NEMSs based on Nanotubes: From Thermal Motors to Resonators, 05.05.2011

Prof. Dr. Caspar van der Wal, Univ. of Groningen, Quantum optics with semiconductor spin ensembles, 26.05.2011

Prof. Dr. Andrea Cavalleri, Univ. of Hamburg, Light Control of Superconductivity, 09.06.2011

Prof. Dr. Manfred Sigrist, ETH Zürich, Sr2Ru04 – Chiral p-wave Pairing under a Stresstest, 07.07.2011

Prof. Dr. Jerome Bibette, ESPCI Paris, Hydrogel Sacs and Tissue Growth, 14.07.2011

Prof. Dr. Victor Puntes, ICN Barcelona, Toxicology of engineered nanoparticles, 01.12.2011

Prof. Dr. Michael Siegel, KIT Karösruhe, Detectors for visible, infrared and THz radiation with superconducting nanostructures, 15.12.2011

IFW Winterschool on “Surfaces and Interfaces” in Oberwiesenthal, Jan. 16 –19, 2011

Honorary colloquium on the occasion of the 80th birthday of Prof. Dr. Hans Warlimon, Oct. 20, 2011

Opening of the IFW Colloquium in the winter terms with talks of the prize winners of the Research Awards 2011 of the IFW’s Institutes, Oct. 20, 2011

Guests and Scholarships

Guest scientists (stay of 4 weeks and more)

Name	Home Institute	Home country
Aliabadi Azar	Sharif University of Technology	Iran
Prof. Dr. Aristov Victor	Institute of Solid State Physics, Moscow	Russia
Assfour Bassem		Syria
Bautista Quijano Jose Roberto	Investigacion Cientifica de Yucatan	Mexico
Dr. Belesi Maria Eleni	EPFL (Switzerland)	Greece
Bentaleb Yassine		Morocco
Buljan Hrvoje	University of Zagreb	Kroatia
Prof. Cao Chongde	Northwestern Polytechnical Univ. Xi'an	China
Chareev Dmitriy	International University of the Nature Dubna	Russia
Chen Chuanbao	Univ. of Science and Technology Hefei	China
Cui Jun-Wie	Chinese Academy of Science Shenyang	China
Dr. Darinskiy Alexander	Institute for Crystallography Moscow	Russia
Dmytriv Hryhoriy	Ivan Franko Lviv National Univ.	Ukraine
Fan Feng	Univ. Shanghai	China
Prof. Dr. He Jie	Chinese Academy of Sciences Shenyang	China
Dr. Holovach Vitaily	CEA Grenoble	Ukraine
Hosko Jozef	Fyzikalny ustav SAV, Bratislava	Slovakia
Huo Yongheng	Chinese Academy of Sciences, Beijing	China
Prof. Dr. Kikoin Konstantin	Tel-Aviv Univ. (Israel)	Russia
Dr. Kivelä Henri Mikael	Univ. of Turku	Finland
Klauser Antoine	FOM, Lorentz-Institute, Leiden Univ.	Netherlands
Kursun Celal	Cahramanmaras Sutcu Imam Univ.	Turkey
Dr. Kuzian Roman	Institute for Materials Science	Ukraine
Leksin Pavel	Kazan Physical Technical Institute	Russia
Li Caiju	Kunming Uni. Of Science and Technology	China
Dr. Lu Yuming	Shanghai Univ.	China
Mukhopadhyay Nilay Krishna	Banaras Hindu Univ.	India
Omar Ahmad	Indian Institute of Technology Madras	India
Otsuka Tomofumi	Niigata University	Japan
Packalen Anna Lea	Abo Akademie Univ. Turku	Russia
Dr. Park Jin Man	Yonsei Univ.	Korea
Pecko Darja	Jozef Stefan Institute Ljubljana	Slovenian
Pinedo Ricardo	Univ. of Basque Country	Spain
Dr. Pramanik Ashim Kumar	UGC-DAE Consortium for Scientific	India
Prashanth Konda Gokuldoss	Helmholtz Zentrum Berlin	India
Qu Ruitao	Chinese Academy of Sciences Shenyang	China
Ramachandran Ganesh	McLennan Physical Laboratories (Canada)	India
Roslova Mariia	Lomonossow Univ. Moscow	Russia
Salazar Enriquez Christian David	Univ. National de Colombia	Columbia
Samadi Khoshkhoo Mahdi	Amirkabir Univ. of Technology, Tehran	Iran
Shakur Shahabi Hamed	Iran Univ. of Science & Technology	Iran
Singh Surjeet	Indian Institute of Science Maharashtra	India
Dr. Smirnova Elena	Ioffe Institute	Russia
Sun Baoan	Institute of Physics, Chinese Academy of Science Beijing	China
Taghvaei Amir Hossein	Shiraz Univ.	Iran
Tkachenko Dmitry	Taras Shevchenko Transnistria State Univ.	Rep. Moldavia

Vakaliuk Oleksii	Institute for Metal Physics NASU Kiev	Ukraine
Yang Liping	FOM, Lorentz-Institute, Leiden Univ.	China
Yu Chunlin	Lund Univ. (Sweden)	China
Dr. Zakharova Galina	Institute of Solid State Chemistry Yekaterinburg	Russia
Zhu Xiaoxi	Beijing Univ. of Aeronautics and Astronautics	China

Scholarships

Name	Home country	Donor
Dr. Bachmatiuk Alicja	Poland	Alexander von Humboldt-Stiftung
Dr. Cong Daoyong	China	Alexander von Humboldt-Stiftung
Prof. Dr. Gracias David	USA	Alexander von Humboldt-Stiftung
Dr. Wohlfeld Krzysztof	Poland	Alexander von Humboldt-Stiftung
Dr. Rapta Peter	Slovakia	Alexander von Humboldt-Stiftung
Dr. Luo Qiang	China	Alexander von Humboldt-Stiftung
Dr. Kuzhichalil Peethambharan Surendran	India	Alexander von Humboldt-Stiftung
Chaubey Anil Kumar	India	DAAD
Fedorov Fedor	Russia	DAAD
Chang Hung-Tai	China	DAAD
Dimitrakopoulou Maria	Greece	DAAD
Makharza Sami Atallah Mahmoud	Palestine	DAAD
Pal Santosh Kumar	India	DAAD
Dr. Bisogni Valentina	Italy	DAAD
Parzych Grzegorz	Poland	ECEMP
Romberg Jan	Germany	ECEMP
Bogdanov Nikolay	Russia	Erasmus Mundus
da Silva Teixeira Cristiano	Brazil	Erasmus Mundus
Niyomsoan Saisamorn	Thailand	Erasmus Mundus
Chivu Adriana-Elena	Rumania	EU Fellowship
Stoica Emanuela-Daniela	Rumänien	EU Fellowship
Vock Silvia	Germany	Cusanuswerk
Patschureck Claudia	Germany	Studienstiftung des deutschen Volkes
Seifert Marietta	Germany	Studienstiftung des deutschen Volkes
Thoss Franziska	Germany	Deutsche Bundesstiftung Umwelt
Malyar Natalia	Russia	Agricola-Stipendium
Elgendy Ahmed Aboud Mahmoud	Egypt	Egypt
Hassan Abdelwahab Hamdy	Egypt	Egypt
Dr. Grüneis Alexander	Austria	APART Austria
Dr. Mohamed Mahmoud Abdel-Hafez	Egypt	Arabic Republic
Holcombe Alexanne	USA	Center for Emergent Materials
Zhang Jiaxiang	China	China Scholarship Council
Tan Jun	China	China Scholarship Council
Cui Jun-Wie	China	China Scholarship Council
Song Kaikai	China	China Scholarship Council
Li Kefeng	China	China Scholarship Council
Zheng Na	China	China Scholarship Council
Qu Ruitao	China	China Scholarship Council
Li Shilong	China	China Scholarship Council
Zhang Yang	China	China Scholarship Council
Wang Zhi	China	China Scholarship Council
Prof. Fu Lei	China	Chinese-German Centre

Guest stays of IFW members at other institutes

Mohan Ashwin	Univ. Paris Sued, 13.01.2011-13.04.2011, Guest scientist in the LOTHERM Project
Jorge E. Hamann Borrero	Univ. of British Columbia, Vancouver, Canada, 01.10.2011-03.12.2011, measuring time
Dr. Uwe Gaitzsch	Boise State Univ., Idaho, USA, 30.09.2010-28.02.2011, DAAD Research Fellowship
Alexander Grüneis	ELLETRA Trieste, Italy, 11.10.2011-31.10.2011
Danny Haberer	Univ. Nagoya, Harima, Sendai, Japan, 20.01.2011-20.02.2011; 13.03.2011- 04.04.2011 measuring time, invited talks
Veronika Hähnel	Univ. of Bristol, UK 01.06.2011-31.08.2011, Guest scientist
Alexander Kordyuk	Moscow, Russia, 13.09.2011-08.10.2011, invited talks
Oleg Mityashkin	Univ. of Groningen, 04.09.2011-04.10.2011, measuring time
Ronny Schlegel	Ohio State Univ., 06.04.2011-30.09.2011, research exchange
Laura Steller	Univ. of Crete, Heraklion, 15.03.2011-14.06.2011, Guest scientist

Board of trustees

Joachim Linek, Saxonian Ministry of Science and Art - Head -
Dr. Herbert Zeisel, Federal Ministry of Education and Research
Prof. Dr. Bernd Kieback, TU Dresden
Prof. Dr. Konrad Samwer, Univ. Göttingen

Scientific Advisory Board

Prof. Dr. Reiner Kirchheim, Univ. Göttingen, Germany - Head -
Prof. Dr. Dominique Givord, Laboratoire Louis Néel, Grenoble, France
Prof. Dr. Alan Lindsay Greer, Univ. of Cambridge, U.K.
Prof. Dr. Rudolf Gross, Walter Meißner Institute Garching, Germany
Prof. Dr. Rolf Hellinger, Siemens AG Erlangen, Germany
Prof. Dr. Max Lagally, Univ. of Wisconsin-Madison, U.S.A.
Prof. Dr. Xavier Obradors Berenguer Univ. Autònoma de Barcelona, Spain
Prof. Dr. Stuart Parkin, IBM Almaden Research Center, San Jose, USA
Prof. Dr. Eberhardt Umbach, Karlsruhe Institute of Technology, Germany
Prof. Dr. Gertrud Zwicknagl, TU Braunschweig, Germany

IFW's Research Program 2012

1. Superconductivity and superconductors
1.1 Electronic structure and fundamentals
1.2 Superconducting materials
1 P1 Superconducting transport systems and magnetic bearings
1 P2 YBCO tape conductors
1 P3 Nanoscaled inhomogeneities in superconductors (Pakt 2009)

2. Magnetism and magnetic materials
2.1 Theoretical and experimental fundamentals
2.2 Magnetic materials
2.3 Magnetic microstructures
2 P1 Pulsed high magnetic fields
2 P2 Magnetic shape memory alloys
2 P3 Energy efficient cooling with magnetocaloric materials (Pakt 2010)

3. Molecular nanostructures and molecular solids
3.1 Fullerenes, nanotubes and graphene
3.2 Conducting polymers and organic molecular solids
3.3 Molecular Magnets

4. Metastable alloys
4.1 Phase formation in complex systems
4.2 Corrosion and hydrogen
4.3 Bulk amorphous metals and composite materials
4.4 Electrochemical energy storage systems / Lithium-ion batteries
4 P1 Electrochemical energy storage in autonomous microsystems (Pakt 2011)

5. Stress-driven architectures and phenomena
5.1 3D micro/nanoarchitectures
5.2 Quantum dots
5.3 SAW systems